International Symposium on

Quantitative Feedback Theory and Robust Frequency Domain Methods

26 and 27 August 1999
University of Natal, Durban, South Africa

Edited by
Edward Boje and Eduard Eitelberg

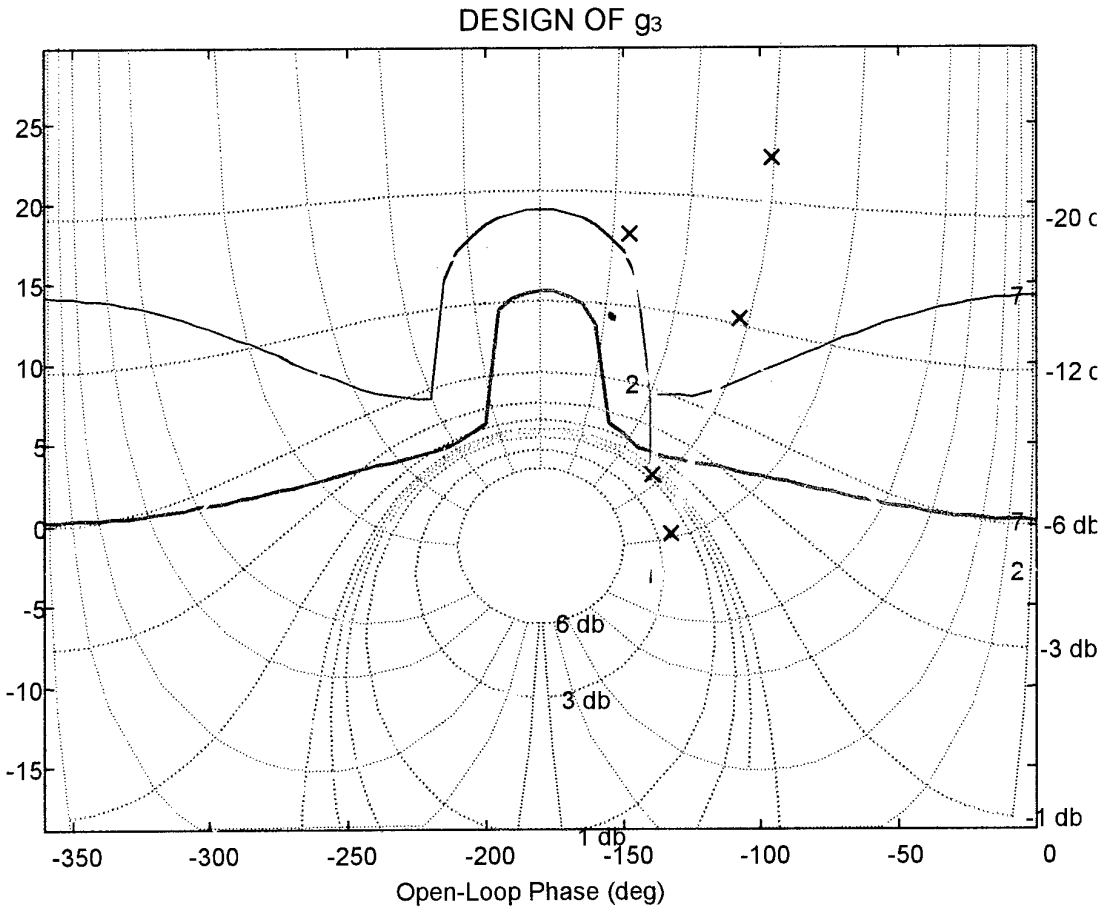

Co-Sponsors: European Office of Aerospace Research and Development
South African Council for Automation and Computation
IEEE Control Systems Society
Natal University

REPORT DOCUMENTATION PAGE

Form Approved OMB No. 0704-0188

1. AGENCY USE ONLY (Leave blank)	2. REPORT DATE	3. REPORT TYPE AND DATES COVERED
	30 August 1999	Conference Proceedings

4. TITLE AND SUBTITLE

1999 Quantitative Feedback Theory (QFT) Symposium

5. FUNDING NUMBERS

F61775-99-WF011

6. AUTHOR(S)

Conference Committee

7. PERFORMING ORGANIZATION NAME(S) AND ADDRESS(ES)

Natal University--Electrical Engineering
King George V Avenue
Durban 4041
South Africa

8. PERFORMING ORGANIZATION REPORT NUMBER

N/A

9. SPONSORING/MONITORING AGENCY NAME(S) AND ADDRESS(ES)

EOARD
PSC 802 BOX 14
FPO 09499-0200

10. SPONSORING/MONITORING AGENCY REPORT NUMBER

CSP 99-5011

11. SUPPLEMENTARY NOTES

12a. DISTRIBUTION/AVAILABILITY STATEMENT

Approved for public release; distribution is unlimited.

12b. DISTRIBUTION CODE

A

13. ABSTRACT (Maximum 200 words)

The Final Proceedings for 1999 Quantitative Feedback Theory (QFT) Symposium, 27 August 1999 - 28 August 1999

This is an interdisciplinary conference. Topics include: Quantitative Feedback Theory and Robost Frequency Domain Methods.

14. SUBJECT TERMS

EOARD, Control, Quantitative Feedback Theory (QFT)

15. NUMBER OF PAGES

239

16. PRICE CODE

N/A

17. SECURITY CLASSIFICATION OF REPORT	18. SECURITY CLASSIFICATION OF THIS PAGE	19. SECURITY CLASSIFICATION OF ABSTRACT	20. LIMITATION OF ABSTRACT
UNCLASSIFIED	UNCLASSIFIED	UNCLASSIFIED	UL

International Symposium on Quantitative Feedback Theory and Robust Frequency Domain Methods

26 and 27 August 1999

University of Natal, Durban, South Africa

Edited by

Edward Boje and Eduard Eitelberg

Proceedings of the International Symposium on Quantitative Feedback Theory and Robust Frequency Domain Methods.
University of Natal, Durban, South Africa, 26 and 27 August 1999.

ISBN 1-86840-330-0

Editors: Prof. Edward Boje and Prof. Eduard Eitelberg

Copies may be ordered from Prof. Edward Boje
Electrical and Electronic Engineering
University of Natal
Durban 4041
South Africa

International Symposium on Quantitative Feedback Theory and Robust Frequency Domain Methods

26 and 27 August 1999

University of Natal, Durban, South Africa

CONTENTS

4 Cascade Control

5 Multivariable Control

6 Non-linear Control

International Symposium on Quantitative Feedback Theory and Robust Frequency Domain Methods
Wright Patterson Airforce Base, Dayton, Ohio, August 1992
Purdue University, West Lafayette, Indiana, August 1995
University of Strathclyde, Glasgow, Scotland, August 1997
University of Natal, Durban, South Africa, August 1999

International Symposium on Quantitative Feedback Theory and Robust Frequency Domain Methods

26 and 27 August 1999

University of Natal, Durban, South Africa

Introduction

This symposium is the fourth in series of specialist conferences on quantitative feedback theory (QFT) and other robust frequency domain design methods. Its purpose is to bring together practitioners and researchers in the field and to promote the development and teaching of these methods, and their practical application. This symposium is indeed fortunate to have two eminent QFT practitioners as plenary speakers. Neither is likely to need introduction to the readers of these proceedings:

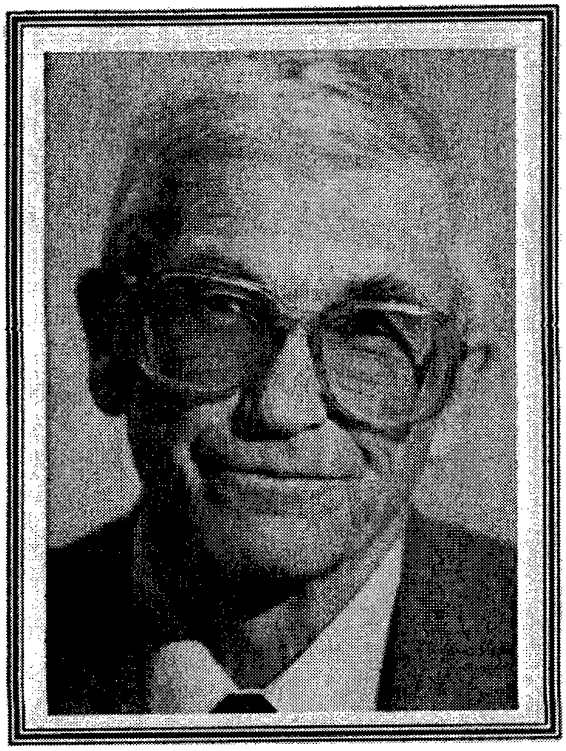

Dr Isaac Horowitz, the father of QFT, is Professor Emeritus, Weizmann Insitute of Science and of the University of California, Davis. He has steadily championed the cause of robust frequency domain design for more than half a century, during which time many control fashions have come and gone. Frequency domain techniques have returned to the academia with the norm-based theories. It still remains to be seen how this will affect undergraduate teaching or everyday control engineering and instrumentation in such places as automotive or chemical process industries. Time will tell if a synergy between powerful computer based tools of "modern control" and the deep engineering insight of real quantitative "classical" control system design theory will be found. Prof Horowitz' contribution to the philosophy of control engineering design-to-specification has been enormous.

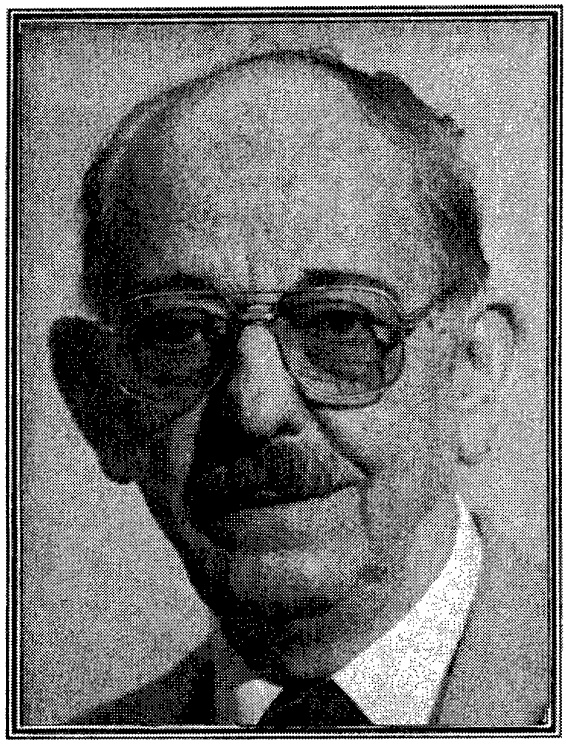

Dr Dino Houpis is Professor Emeritus of Electrical Engineering at the US Air Force Institute of Technology and Senior Research Associate Emeritus, Air Force Research Laboratory. In addition to his scientific contribution to QFT, he has been a constant champion of QFT within the Air Force and his teaching and influence have vastly helped the field.

Dr Osita DI Nwokah

It is with great sadness that we must report the sudden death of Dr Osita Nwokah on April 20, 1999. Dr Nwokah was Professor and Chairman of Mechanical Engineering at Southern Methodist University, Dallas, Texas. Born in Nigeria, Dr. Nwokah graduated with honours from the University of Leeds. He earned advanced degrees from the Universities of Manchester, Toronto and from Imperial College. He served on the faculties of University of Nigeria, Manchester Polytechnic, University of Manchester, University of Notre Dame, and Purdue University before moving to Dallas in 1994. He made several important contributions to the theory of quantitative feedback design. He was very enthusiastic about the prospect of having this conference in Africa!

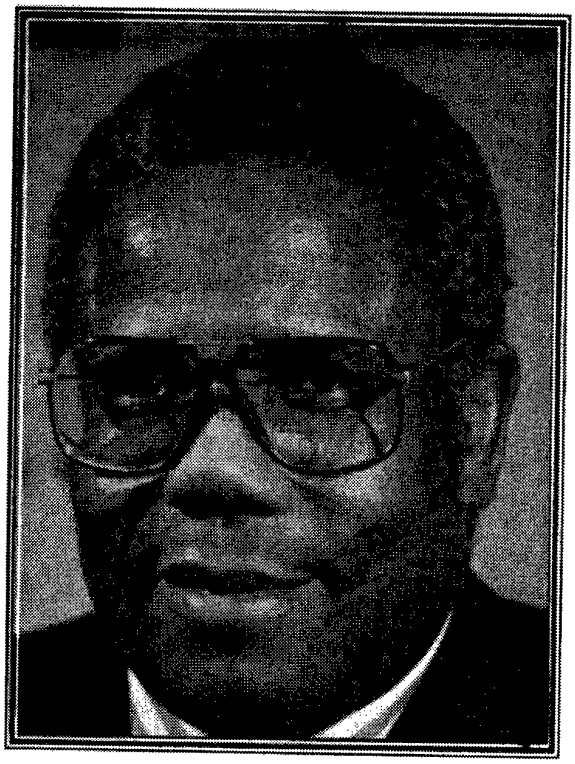

Dr. Nwokah is survived by his wife, Eva Nwokah; a daughter, Orlena Blanchard; and three sons, Ekechi , Zibbie and Etugo.

International Symposium on Quantitative Feedback Theory and Robust Frequency Domain Methods

26 and 27 August 1999, University of Natal, Durban, South Africa
Technical Programme

WEDNESDAY 25th August
Technical tour to South African Breweries.
Reception and South African braai on the roof of Electrical and Electronic Engineering Building.

THURSDAY 26th August
Opening and Welcome: Prof. AC Bawa, Deputy Vice Chancellor, University of Natal

Plenary 1: *"Unmanned research vehicle: development, implementation, & flight test of a MIMO digital flight control system designed using quantitative feedback theory"*, Dr H C Houpis, Professor Emeritus of Electrical Engineering, Air Force Institute of Technology and Senior Research Associate Emeritus, Air Force Research Laboratory.

Session 1 - Process Applications
Session 2 - Norm Based Methods
Session 3 - QFT theory and computation
Banquet at Killie Campbell Museum

FRIDAY 27th August
Plenary 2: *"A life in the frequency domain"*, Dr I Horowitz, Professor Emeritus, Weizmann Insitute of Science and University of California, Davis.

Session 4 - Cascade Control
Session 5 - Multivariable Control
Session 6 – Non-linear Control

International Organising Committee

General Chair	N Munro
Local Chair	E Boje
Members	Y Chait, E Eitelberg , M Grimble, P Gutman, C Houpis, O Nwokah

Local Organising Committee

E Boje, E Eitelberg

Reviewers

V Bajic, D Balance, E Boje, Y Chait, I Craig, E Eitelberg, M Grimble, Y Hürmüzlü, M Mulholland, D Thompson, B Wigdorowitz, O Yaniv.

Technical Co-Sponsors

Electrical and Electronic Engineering, University of Natal, Durban, South Africa
South African Council for Automation and Computation
IEEE Control Systems Society

Thanks

We wish to thank the following for their contribution to the success of this conference:
European Office of Aerospace Research and Development, Air Force Office of Scientific Research, United States Air Force Research Laboratory,
United States Army Research Development and Standardisation Group (UK).

1999 International Symposium on
Quantitative Feedback Theory and Robust Frequency Domain Methods

Presented at the NATO/RTA Symposium in Ankara, Turkey, April 26-28, 1999

UNMANNED RESEARCH VEHICLE (URV): DEVELOPMENT, IMPLEMENTATION, & FLIGHT TEST OF A MIMO DIGITAL FLIGHT CONTROL SYSTEM DESIGNED USING QUANTITATIVE FEEDBACK THEORY

By

C. H. Houpis, Professor Emeritus, Air Force Institute of Technology
Senior Research Associate Emeritus, Air Force Research Laboratory

S. J. Rasmussen, Research Associate, Air Force Institute of Technology

Air Force Institute of Technology/ENG, Bldg 642, 2950 P Street
Wright-Patterson Air Force Base, OH 45433-7765, U.S.A.

Abstract

The Quantitative Feedback Theory (QFT) design technique, which has the ability to bridge the gap between theory and the real-world control design problem, is utilized in the design of a MIMO digital flight control system for an unmanned research vehicle (URV) that is presented in this paper. The design illustrates how the "real-world" knowledge of the plant to be controlled and the desired performance specifications can be utilized in trying to achieve a successful robust design for a nonlinear control problem. This paper presents some of the issues involved in developing, implementing, and flight testing a flight control system (FCS) designed using QFT. Achieving a successful FCS involves a number of steps: specification of the control problem, aircraft model data, theoretical flight control system design, implementation, ground testing, and flight test. The last three steps embody the "practical engineering" aspects that are vital to achieving a successful FCS. The main emphasis of this paper is on these steps. First, there is a brief explanation of the MIMO design QFT process. This is followed by a description of the steps involved in the implementation and testing of a QFT designed FCS. Thus, this presentation provides an overview of "using robust control system design to increase quality" in attempting to demonstrate the "Bridging the Gap" between control theory and the realities of a successful control system design. In facing the technological problems of the future, it is necessary that engineers of the future must be able to *bridge the gap*, i.e., this "Bridging the Gap" must be addressed to better prepare the engineers for the 21st century.

I INTRODUCTION

In facing the technological problems of the 21st century, it is necessary that engineers of the future must be able to *bridge the gap* between the scientific and engineering methods. Developing a set of Engineering Rules (E.R.) is a first step towards achieving this goal (see Chap. 9 of ef. 1). This paper provides the next step in enhancing this goal: overcoming problems encountered during design, implementation, and achieving a successful real world QFT designed FCS control system. The QFT technique is a design method that has the inherent capability to assist in bridging the gap between the scientific and engineering methods. Thus, a discussion of the development, implementation, and successful flight test of a flight control system, designed using QFT techniques, is presented in this paper. The robust flight control system was designed for and flown on the Lambda Unmanned Research Vehicle (URV. Lambda is a remotely piloted aircraft that is operated by the Air Force Research Laboratory at Wright-Patterson AFB, OH for research in flight control technology.

Control design problems generally involve real world nonlinear plants. In utilizing control system design techniques, which require linear plant models, it is necessary that assumptions be made that allow simplification of these nonlinear plants, i.e., "assume linear behavior" that result in obtaining linear plant models. Thus, it is important for the designer to follow a design and implementation process that allows the testing of the assumptions as early in the process as possible so the control system can be redesigned, for example, to take into account unmodeled effects. As detailed in this paper, the control design process should include simulation of the control system on increasingly realistic models which helps transition to implementation on real world applications. Most of the real world implementation problems are the result of assumptions made during the design process.

II OBJECTIVE

The objective of this project was twofold. First, develop a robust flight control system using QFT, and take the design through a flight test. Second, implement an inner loop FCS on the Lambda URV that would be part of an autonomous flight control system. During the project the first objective was accomplished and then, because of hardware improvements, a second design was developed and flight tested. This second design was accomplished to better meet the requirements of the second objective. The FCS design process used is shown in Fig. 1. As indicated by the arrows in the one complete FCS design cycle covers the process through the flight test and then back to the redesign stage. During this project there were four cycles around this loop. Two of the cycles produced unsuccessful flight tests and two produced successful flight tests.

III. QFT DESIGN PROCESS[1-4]

The QFT technique requires that $\iota = 1,2,3,\ldots,J$ LTI models be determined that represent the dynamical model over its operating scenario in order to achieve a robust design. These LTI plants determine the template contours which represent the region of plant parameter uncertainty and are used in the QFT design technique. The robust digital flight control system design was performed as a psuedo-continuous-time (PCT) control system. Upon completion of the design the compensators and prefilters are transformed into the z-domain controllers and prefilters by use of the Tustin transformation.

IV CONTROL SYSTEM DESIGN PROCESS (FIG. 1)

In order to design a control system for a real world control problem, the designer must follow a design process such as that shown in Fig. 1. This figure represents a design process that moves the designer from the problem definition stage to the successful control system implementation in steps of increasing reality. If the control system does not meet performance specifications at any stage of the process, the control system is redesigned and retested. In general, as the simulations become more realistic, they also become more expensive both in cost and time. Therefore, it is very important to be able to find potential problems early in the design process for the control system. The ovals inside the circle in Fig. 1 indicate the features of the QFT technique that assist in the design of control systems and can best meet performance specifications and be implemented on the real world system. The following sections describe the individual stages of the control design and implementation process. Indicated in the following sub-section titles is a number that refers to the block number in Fig. 1 to which the sub-section applies.

III-1 FUNCTIONAL REQUIREMENTS (#1)

The designer, at the onset, must have a clear understanding of the problem that needs to be solved. That is, the designer must understand what the controlled system is required to do and what are its operational requirements. The designer must also understand the environment in which the system is required to operate, i.e., the environmental requirements. Together these two requirements make up what is referred to as the *functional requirements*. If the designer does not start with a clear understanding of the functional requirements, costly time can be wasted in the design-test-redesign cycle. If during the design process, it becomes clear that the functional requirements cannot be met, the designer might be called upon to use engineering judgement and the knowledge of the goals of the controlled system to modify these requirements. Note, this is not a step that a control designer normally takes on his own.

III-2 PERFORMANCE SPECIFICATIONS (#2)

Performance specifications[1,2] are essentially mathematical models developed from the functional requirements and are utilized during the design process in order to achieve the desired system performance robustness. Since performance specifications are normally only interpretations of the functional requirements, the designer must be aware of how the specifications and requirements relate and what tradeoffs need to be made. During the design process, the designer might need to apply engineering judgement in order to make the necessary modifications to the specifications that, while still meeting the requirements, enables achieving a robust control system design.

III-2.3 DYNAMICS MODEL (#3)

A *dynamic model* is a mathematical model of the system to be controlled and is developed from a knowledge of the system and its operating requirements. This model can be as simple as a linear-time-invariant (LTI) transfer function or a complicated set of nonlinear differential and algebraic equations with time varying parameters. In many cases, a simplified model of the dynamical system can be used to represent the system in the control design process. In fact, the designer should try to use as simple a model as possible that represents the important system dynamics in the design process. For example, from an analysis of the LTI transfer functions a designer may be able to determine their nondominating poles and zeros, i.e., those which have a negligible effect on the system's performance (those that lie outside the system's bandwidth). Thus, by deleting the nondominating poles and zeros from these LTI transfer functions reduced order models are obtained. Not only does a reduced order model simplify the design process, but also reduces the risk of introducing numerical inaccuracies in the design process. But remember, an oversimplified model can lead to trouble as in the case of bending modes as discussed in Sec. IX

III-2.4 CONTROL AUTHORITY ALLOCATION (#4)

An important part of the design process is the *control authority allocation* assigned to each of the control effectors. Depending on the dynamical system, there may be redundant control effectors, i.e. the number of control effectors available to the controller may be greater than the number of controlled variables. Also, the control effectors available may induce cross-coupling in the dynamical system and do not clearly control any one variable. In these cases, judgement must be exercised by the designer, based upon knowledge of the real-world operating characteristics of the plant, in determining the percentage of the control authority that is allocated to the various controlled variables. That is, a method for determining the percentage of control power available from each control effector to each controlled variable must be determined. The optimization of the control effectors' control authority allocation can be used to help decouple the system and assist in achieving the desired robust system performance. This control authority allocation is accomplished by the proper selection of the w_{ij} elements of the weighting matrix W.

III-2.5 QFT CONTROL SYSTEM DESIGN (#5)

The QFT design process is used to develop mathematical algorithms that can be implemented in order to achieve the desired control system performance. Implementation issues and insights provided by the QFT process to the designer are discussed in the following sections. A QFT design can be accomplished by use of the MIMO QFT CAD package[5] which greatly simplify the design process.

III-2.6 LINEAR SIMULATION (#6)

Once the control algorithms have been designed, they are implemented along with linear representations of the dynamical system. These systems are simulated and the results are compared to the specifications. Since QFT design involves linearizing non-linear equations, the control system must be simulated for each of the J LTI transfer functions to check the result against the specifications. If some or all of the specifications have not been met, the designer can either redesign the control system or reexamine the requirements. In some cases, the initial specified requirements may not be realistic. For designs that involve control effector damage, the designer must ensure that the assumed percentage of effector damage is realistic with respect to its associated remaining control authority available to satisfy the control system performance requirements; for example, to still be able to fly the aircraft. Also, the designer must ensure that the system performance is close enough to the specifications to meet the overall functional requirements.

III-2.7 NONLINEAR SIMULATION (#7)

Once the control system has passed the linear simulation testing phase, the simulation complexity is increase by adding nonlinear components and any other components that are removed to simplify the simulation. As with the linear simulations it may be necessary to accomplish a redesign or a revaluation of the specifications (performance specifications, control authority allocation, and/or the percentage of control effector failure).

III-2.8 ENGINEERING VISUALIZATION (#8)

After each of the simulations it is valuable to animate, by a computer simulation, the dynamics data to better understand exactly what occurs during the simulation. Note that the three dimension engineering visualizations integrate all of the dynamics of the simulation. For example, in the case of an aircraft (A/C) this means that the designer can view the angle of attack, pitch rate, pitch attitude, forward velocity, vertical velocity, and altitude simultaneously. Instead of trying to decipher the position and attitude of the A/C from six two dimensional plots, the designer can obtain a clearer understanding from watching the computer animation of the maneuver. For more specific details of the maneuver the designer can then return to the data plots.

III-2.9 ENGINEERING INTERACTIVE SIMULATION (#9)

When there is an operator involved in the controlled system, for example, a pilot flying an A/C, it is often useful for the designer to use an interactive simulation in order to obtain a better understanding of the operation of the system. It should be noted in reality that the pilot is a part of the overall flight control system, i.e., he forms the "outer loop" of the control system. Thus, this type of control system is referred as a *manual flight control systems*. An interactive simulation provides the designer with the ability to implement the control system in the same fashion that it will be implemented on the dynamical system. The interactive simulation also gives the designer the ability to test the system continuously throughout the operating environment. In the case of a control system designed for an A/C, the interactive simulation involving a pilot gives the designer the ability to perform a simulated flight test before the design leaves her/his desk. Such simulations, for a specified A/C, are often performed by a pilot, for example, at the Wright-Patterson AFB Lamars simulator.

III-2.10 HARDWARE-IN-THE-LOOP SIMULATION / IMPLEMENTATION (#10)

At this stage of design and implementation the control system algorithms are implemented on the same type of hardware systems as those that control the dynamical system. Other hardware components such as actuators and sensors are also connected to the system. This allows simulation of real-time operation of control algorithm, noise corrupted measurements for feedback, and computation cycle time/sampling rate quantization errors. A hardware-in-the-

loop-simulation is also useful to ensure that commands issued from the control system move the effectors in the correct directions and the outputs of the feedback sensors have the correct polarity.

III-2.11 OPERATOR-IN-THE-LOOP SIMULATION (#11)

In order to insure the controlled system meets the requirements of the human operator a simulation is set up to allow the operator to interact with a simulation of the system. Many of these simulations surround the operator with visual cues and some, inject motion into the simulation. These types of simulations are used to improve the handling qualities of the controlled system by giving the operator a chance to try out the controlled system and then using his or her responses to help shape a redesign.

III-2.12 SYSTEM TEST (#12)

The final testing of the control system involves implementation on the dynamical system and operational testing. Once the controlled system has been shown to meet the performance specifications for the operating environment, a successful control design has been achieved.

III-2.13 REDESIGN (#13)

At every stage of the control system design and implementation process the designer makes a decision to move to the next stage or to redesign (modify) the control system. Once the control system is modified the simulation testing is repeated.

IV DESIGN PROCESS EXAMPLE

The Lambda Unmanned Research Vehicle (URV) shown in Fig. .2 is a remotely piloted A/C with a wingspan of *14 ft* and is operated by the US Air Force for research in flight control technology. The objectives of the project described in this section are as follows:

1. To design robust flight control systems using the QFT design technique
2. To flight test these designs
3. To implement an inner loop FCS on the Lambda URV that would be part of an autonomous flight control system
4. To illustrate some of the real-world problems that are encountered in performing the control system design process shown in Fig. 1.

In accomplishing this design project required four cycles around the control design process loop. These four design cycles are:

Cycle 1 – This cycle involved the satisfaction of only the first two of the project objectives.
Cycle 2 – Cycle 1 was repeated but involved the design of an improved integrator wind-up limiter.
Cycle 3 – A redesign of the FCS was accomplished to satisfy requirements 1 through 3.
Cycle 4 – A refinement of the plant model was made in order to take into account a bending mode that was neglected in the previous designs.

Cycles 1 and 3 were unsuccessful and cycles 2 and 4 produced successful flight tests.

IV-1 FIRST DESIGN CYCLE

Requirements

There were two major design requirements for this project. The first was a desire to develop a robust flight control system using QFT, and take the design through flight test. The second was a need for an inner loop FCS on Lambda that would interface with an autonomous waypoint directed autopilot.

Specifications

The time response specifications were selected base on the open-loop response of Lambda. The pitch rate was an underdamped response that settled fairly quickly. Overshoot and settling time were chosen to be *25%* and *1 sec.*, respectively, for pitch rate response. Roll rate was an overdamped response that settled quickly, and the settling time was chosen to be one second. Yaw rate was also underdamped, but it did not reach steady state as fast as the other two. Yaw rate overshoot and settling time were chosen to be *15%* and *2 secs.*, respectively. These specifications were transformed into LTI transfer functions for use in the QFT design.

Aircraft (A/C)Model

The A/C model developmental process began with the use of Digital Datcom, a computer program which predicts stability and control derivatives for aerospace vehicles based on the physical characteristics of the vehicle. Datcom information forms the baseline model of the A/C. This baseline model was refined by using system identification software to estimate the aerodynamic derivatives from actual flight test data[6]. Maximum likelihood identification was used to identify the natural frequency and damping ratios of the short period and roll modes. This information combined with the Datcom information provided a working model for the flight control system design.

FCS Design

There were two QFT designs accomplished at the Air Force Institute of Technology[7,8] (AFIT) The first was based on the

DATCOM model of Lambda alone. The second design was based on the DATCOM model with the refinements made with system identification. This second design used linearized transfer functions to represent Lambda in various flight conditions, covering the entire proposed flight envelope, to accomplish the design and for linear simulations.

Linear Simulations and Nonlinear Simulations

All FCS designs were simulated using $Matrix_x$ and LTI state space models representing the full flight envelope of Lambda. After successful linear simulations, nonlinearities such as control surface travel limits were introduced into the linear simulation. A nonlinear simulation was developed at the Air Force Research Laboratory (formerly the Wright Laboratory) that incorporated a six degree of freedom simulation, automatic trim calculation, air vehicle kinematics, and control surface saturation. While this design produced the desired responses in the linear simulation, when implemented in the nonlinear simulation the original control system exhibited undesirable behavior due to the initial assumptions about allowable gain being incorrect. Thus, the allowable gain was modified to achieve a redesigned controller.

Hardware-in-the-Loop Simulation

Software from the nonlinear simulation were used to develop a hardware-in-the-loop simulation[9]. This simulation allowed the implemented FCS, which is programmed on a EPROM chip, to be tested in the A/C. When the FCS was implemented in this simulation, it was discovered that the angular rate sensors had high levels of noise, with peak values on the order of *0.5 deg/sec.* The FCS amplified this noise and this effectively masked any control command signal. The noise was recorded and was incorporated into the nonlinear simulation. The MIMO QFT CAD[1,2,5] for designing control systems allows for a rapid redesign. The noise problem was minimized by lowering the loop transmission gain and then testing the resulting FCS in the nonlinear simulation. This remedy was an "engineering decision" in order to obtain a satisfactory design. In the Third Design Cycle a more satisfactory resolution of the noise problem was achieved. Once simulations of the redesign were satisfactory, the FCS was flight tested (Flight Test #1).

Flight Test #1

Two major difficulties caused the first flight test to fail; the first was reversed polarity on an angle sensor and the second was an integrator wind-up limiter scheme that did not work. Since the inner loop FCS was to be implemented as a part of an autonomous system, turn coordination logic was implemented around the inner loop FCS that relied on the roll angle. Post flight analysis of the flight test video and data showed that the polarity of the roll angle sensor was backward, thus, when the A/C was commanded to bank, the rudder was commanded to deflect in the wrong direction. The FCS was thus turned off and the testing involving the lateral control channel was terminated. Later, during the same flight test, when the FCS pitch channel was turned on, the aircraft developed a high pitch rate. This test was also terminated and post analysis revealed that the scheme used to limit integrator wind-up had caused a numerical instability.

IV-2 SECOND DESIGN CYCLE

Requirements and Specifications and Aircraft Model

The requirements for the second design cycle did not change from the original requirements. An additional requirement was incorporated for the second design cycle that involved the design of an improved integrator wind-up limiter. The specifications and the A/C model for the second design cycle did not change from the original requirements.

FCS Design

Since the problems encountered in the first test had nothing to do with the QFT designed FCS, the same QFT FCS designed for the first flight test, was used in the second flight test. During the second flight test, there was no attempt to use a turn coordination algorithm. The insertion of an integrator wind-up limiter involved a different form of the controller implementation for the second design cycle. In this cycle instead of each of the controllers being implemented by a single software algorithm relating their respective outputs to their respective inputs, they were implemented in the manner described by E.R.12 of Chap. 9 of Ref. 1. That is, the continuous time domain transfer functions were factored into poles and zeros in order to create first order cascaded blocks (transfer functions) that were individually transformed into the discrete time domain. The individual transfer functions were then implemented, by their own respective software algorithm.. This implementation allowed limitations to be placed only on those pieces of the FCS that contained pure integrators and provided the required controller accuracy.

Linear, Nonlinear, Hardware-in-the-Loop Simulation

All simulations consisted of checking out the new implementation of the FCS. There were no problems encountered during any of these simulations.

Flight Test #2

On 20 Nov 92, the temperature was in the *60°F+* with winds at *5* to *7 mph.* Lambda was flown in manual mode for takeoff, setup, and landing. Due to problems with the first flight test the FCS was engaged only during the test maneuvers. The maneuvers performed consisted of unit step commands in all three axes. This set of maneuvers was first performed with the QFT FCS and then with the open loop A/C. As shown in Fig. 3, the QFT FCS performed as it was designed.

The figure shows the responses of Lambda to a step pitch down command. The dotted lines in the plot represent the specified T_{R_U} *and* T_{R_L}. It is important to note that during this maneuver the A/C covered a large portion of its dynamics envelope by varying in forward airspeed from *75 kts* to *110 kts*.

IV-3 THIRD DESIGN CYCLE

Requirements

The requirements for the third design cycle had not changed from the original requirements. This cycle involved the design of an inner loop FCS that had intrinsic turn coordination. Also, the sensor noise problem was reduced by an order of magnitude by the addition of a hardware noise filter on the output of the sensors. It was determined that the noise originated from a motor on the sensor; the noise was a high frequency noise that was being sampled at a lower frequency. Thus, this aliased noise had a relatively high bandwidth. The remedy was to place a filter at the sensor output before the sampler. This allowed a redesign of the FCS to improve the system performance.

Specifications

For this iteration of the design a *sideslip angle command* was incorporated as part of the inner loop controller. Since Lambda has a sideslip sensor, a sideslip command was used to cause the A/C to intrinsically fly coordinated turns. That is, the goal of turn coordination is to reduce the sideslip angle to zero during a turn by using the proper amount of rudder deflection during the turn. Changing to sideslip command allowed the use of the yaw rate sensor to implement a *yaw damper* to reduced the dutch roll mode oscillations. This yaw damper was implemented by adding a washout filter, designed through the use of a root locus plot. The yaw damper was designed and then incorporated in the A/C model for a FCS design. During the second flight test the pilot felt that the aircraft's roll rate response was too slow. Therefore, the roll rate response specification was change to match that of the pitch rate. After this change the roll specifications for overshoot and settling time were *2.5%* and *1 sec*, respectively.

Aircraft Model

The sensor improvement, mentioned above, was included in the nonlinear aircraft model by recording actual noise and inserting it as a block in the model. During the system identification work for the second A/C model, some of the parameters had been scaled incorrectly. This caused some modeling errors. After the second flight test these errors were corrected through the use of system identification applied to flight test data that resulted in a refinement of the A/C model.

FCS Design

$Matrix_x$ was used to develop linearized plant models about flight conditions in the flight envelope. An attempt was made to choose flight conditions in such a way as to fully describe the flight envelope with the templates. To do this a template expansion process was developed and is explained in Sec. V.

Linear, Nonlinear, and Hardware-in-the-Loop Simulations

The refined Lambda model was implemented in all three simulations. The FCS was implemented in the cascaded method outlined previously. All simulations produced the desired responses to given stimulus.

Flight Test #3

During the third flight test, when the FCS was engaged, the A/C exhibited an uncontrolled pitching, or porpoising, behavior. While the post flight test analysis was inconclusive, a longitudinal bending mode at *13.2 rad/sec* seemed to be the likely cause.

IV-4 FOURTH DESIGN CYCLE

Requirements and Specifications

The requirements for the fourth flight test had not changed from the original requirements, but involved a refinement in the aircraft model to incorporate effects of the bending mode discovered in Flight Test #3. The specifications for the fourth design cycle were the same as those for the third cycle.

Aircraft Model

A model of the porpoising behavior encountered in the third flight test was identified by assuming that the behavior was caused by an unmodeled effect. Various models were incorporated into the nonlinear model and simulated. This simulation used the identical flight test inputs as simulation inputs and compared the simulated outputs to the flight test data. Using this procedure, see Sec. VIII, a violation of the gain margin was ruled out by increasing the inner loop gain in the model and observing the response. Instability caused by actuator rate limiting was ruled out by inserting severe rate limited actuator models in the nonlinear simulation. When a bending mode, modeled as a lightly damped pair of poles, was inserted in the model, the simulated responses were very similar to the flight test results.

FCS Design

$Matrix_x$ was used to develop linearized plant models about the given flight conditions and the FCS was redesigned based on the model containing the bending mode. Note, when the FCS from design cycle three, using the A/C model with the bending mode, there were violations of stability

criteria in the frequency domain and, as expected, the porpoising behavior occurred.

Linear, Nonlinear, and Hardware-in-the-Loop Simulation

A fourth design cycle was accomplished using the new model. This design was implemented and all three simulations were run and tested. This FCS design simulation responded within specifications and, as expected, the porpoising effect was eliminated.

Flight Test #4

The fourth flight test occurred in September 1993. The field conditions were a little gusty, but within acceptable limits for the flight test. During the flight the FCS was engaged and then left engaged for the entire series of tests. The FCS performed as designed. The intrinsic turn coordination scheme worked as designed. The pilot was pleased with the handling qualities and felt comfortable flying with the FCS engaged at all times. His one criticism was that the roll rate was too slow. Since the roll rate was limited by the maximum roll rate detectable by the roll rate gyro, the problem was unavoidable. When the data was examined, it was found that all of the *60 Hz* data had been lost, but much of the *10 Hz* data had been captured. Analysis of this data showed that the FCS did cause Lambda to respond within the specified envelope, during onset of the command, but, in some cases, Lambda's response exhibited more overshoot and longer settling time than specified. These problems could be attributable to the gusty conditions, since no gust disturbance was specified during the design process. More flight testing of this FCS will be required to answer this question.

V SELECTION OF DESIGN ENVELOPE

At the onset of a QFT design, the designer must select a set of operating conditions in order to obtain the LTI transfer functions that represent the dynamical system and which are used to obtain the templates that are required for the design. The problem is which operating conditions to choose. Only those operating conditions that yield points that lie on the contour of the templates, for all frequencies of interest, are necessary. Choosing too many LTI plants may yield points that lie inside the template contours and can lead to computational problems during the design. Note by applying engineering insights it is readily determined that the template contours and not the LTI plants which lie within the template's contour determine the performance bounds that need to be satisfied by the synthesized functions. Thus, the computational workload and associated problems may be minimize by reducing the number of plants to be utilized in the design process to only those plants that lie on the template contours.

Through engineering knowledge of the problem the designer is able to determine the particular parameters that effect the operating conditions and the physical limits of these parameters. In the case of Lambda the parameters that were varied to set the operating conditions were airspeed, altitude, weight, and center of gravity. Gross limits were set for these values from knowledge of the A/C and the possible flight envelope. Next, the template expansion process was used to find the set of operating conditions that fully described the flight envelope. The template expansion process, shown in Fig. 5, is a graphical process that tracks the effect of variations of the parameters which are involved in selecting the operating conditions and determine the resulting LTI plants. The process is as follows:

1. Determine the important parameters that describe the operating condition and their minimum, maximum, and nominal values.
2. Choose a template frequency for the expansion process. This frequency should be representative of the dynamic system in the bandwidth of interest. At the end of the process, other template frequencies should be checked to insure that a complete set of operating conditions have been chosen.
3. For the template frequency of step 2, plot the dB vs phase values of the nominal operating condition.
4. On this same graph, plot the results of varying each parameter through its maximum and minimum while holding the rest of the parameters at their nominal values. This forms an initial template.
5. Identify the variations caused by each parameter. This can be accomplished by connecting the points on the template due to each parameter variation.
6. Choose the two parameters that cause the largest variations and use these to expand the template. This is accomplished by holding the remaining parameters at their nominal values and plotting the four points of the templates resulting from the extremes of the two parameters.
7. Use the outside points, on this expanded template, as nominal points for further expansion with other parameters.
8. Choose other frequencies in the bandwidth of interest to ensure that the operating envelope is completely defined.

For Lambda, a nominal flight condition was chosen to be *50 kts,* velocity, *1,000 ft* altitude, a weight of *205 lbs*, and center of gravity at *29.9%* of the mean aerodynamic cord. From this nominal trim flight condition, each parameter was varied, in steps, through maximum and minimum values, while holding the other parameters at their nominal trim values. These variations produced an initial set of templates. On these templates, the variation corresponding to each parameter was identified. Each variation when translated, on the template, identified an expanded template area of the flight envelope that required more plants for better definition.

VI CONTROL SYSTEM IMPLEMENTATION ISSUES

An implementation problem that can cause stability and performance problems is integrator wind-up. This is the situation that occurs when the controlled system cannot respond quickly enough to the commands from the controller and the commanded values keep increasing due to integrator action. A situation like this occurs when a control effector has reached its limits. The longer the system is in this state the more the commanded value increases. The problem occurs when the controller tries to reverse the command, the commanded value must be "integrated" back down to the operational range before it becomes effective. In order to prevent integrator wind-up, anti-windup algorithms must be applied to integrators during implementation. During the QFT design process the controller is in the form of transfer functions that can be of any order. For implementation, these transfer functions can be separated into first and second order transfer functions (see E.R. 12 of Chap. 9[1]). With the transfer functions separated in this manner individual integrators can be limited.

VII HARDWARE/SOFTWARE CONSIDERATION

During the modeling and development of the control system, assumptions were made as to the polarity of feedback and command signals. During implementation these assumptions must be tested. This is one of the reasons to use a hardware-in-the-loop simulation. With this type of simulation the control algorithms can be implemented and the control effectors can be monitored during simulated operation. Feedback signals can be checked by moving sensors by hand, if possible.

The other phenomena that a hardware-in-the-loop simulation can identify is the effects of feedback noise on the controlled system. If the feedback noise is within the bandwidth of the control system, and the noise has not been included in the modeling or simulation, the controller may need to be redesigned to account for the noise. This might result in a trade off between performance and noise rejection. Sometimes it is possible to implement a hardware filter after the sensor, but before the sampler too reduce the noise in the bandwidth of interest.

VIII BENDING MODES

During the design of a control system, the effects of higher frequency modes on stability and performance must be considered. In A/C, one source of higher frequency modes is structural bending. A control system that excites a bending mode in a flying A/C can produce disastrous consequences. During the modeling process it is very important to include the effects of these higher frequency modes so they can be minimized during the design process. In the case of Lambda, the existence of a bending mode was discovered during a flight test.

VIII-1 Lambda Bending Example

Following the initial flights, the A/C operators decided that they would prefer a different feedback structure in the FCS that included turn compensation. Thus, to implement turn compensation, a sideslip angle command was incorporated as part of the inner loop controller. The goal of turn coordination is to reduce the amount of sideslip angle during a turn by using the proper amount of rudder deflection during the turn. Since Lambda has a sideslip sensor, sideslip feedback was used to cause the A/C to intrinsically fly coordinated turns. Changing to sideslip command also allowed the use of the yaw rate sensor to implement a yaw damper to reduced the dutch roll mode oscillations. This yaw damper was implemented by adding a washout filter, designed through the use of a root locus plot. The yaw damper was designed and then incorporated in the A/C model for a FCS design.

When this design was finally flight tested, a porpoising behavior was observed. To ensure flight safety, Lambda was flown to a safe altitude by the pilot before the QFT FCS was engaged. The pilot had Lambda flying in level flight when the longitudinal portion of the QFT FCS was engaged. At this point Lambda began oscillations in the pitch axis and the QFT FCS was disengaged immediately. In order to collect sensor data on this behavior, Lambda was flown back to level flight, the longitudinal portion of the QFT FCS was engaged and the sensor data was recorded for further analysis. Pitch attitude data from this flight is shown in Fig. 5 whose high resolution data was at a 60Hz sample rate.

VIII-2 Unmodeled Behavior

A model of the porpoising behavior was identified by assuming that the behavior was caused by an unmodeled effect. Various proposed models were incorporated into a nonlinear model of Lambda and simulated. This simulation used the actual flight test inputs as simulation inputs and compared the simulated outputs to the flight test data. Using this procedure, a violation of the gain margin was ruled out by increasing the inner loop gain in the model and observing the response. Instability caused by actuator rate limiting was ruled out by inserting severe rate limited actuator models in the nonlinear simulation. Upon reviewing the video record of the flight, it was suggested that the A/C appeared to have a second-order bending mode in the longitudinal axis. It was possible to excite and observe such a mode by tapping rhythmically on the tail of the A/C.

A bending mode modeled as a lightly damped pair of poles at *13.2 rad/sec*, just within the bandwidth of the FCS, was inserted in the nonlinear simulation as shown in Fig. 6. This model generated a pitch acceleration signal from elevator deflection which was passed through the second order filter:

$$\dot{q} = \frac{-20}{s^2 + 5.28s + 174.2}\delta_{elev}$$

The simulated response was very similar to the flight test results. Matrix$_X$ was used subsequently to develop new linearized plant models containing the bending mode about the given flight conditions. The Bode plots of these models are shown in Fig. 7

The new plant models were entered in to the MIMO QFT CAD software. The FCS was redesigned based on the new models using the FCS from the previous design cycle as a baseline. The previous controller was:

$$g_{11}(s) = \frac{1093(s+8.5)(s+11)(s+3.9 \pm j2)}{s(s+2)(s+80)(s+36 \pm j48)}$$

The MIMO QFT CAD software showed that, with the old controllers, there were violations of stability criteria on the Nichols chart.

The standard method of design would be to add a notch filter to keep the mode from becoming excited. The bending mode is close enough in frequency to the performance bandwidth of Lambda that care needs to be taken to design a controller that will be able to take advantage of the available bandwidth to deliver performance, stability, and disturbance rejection without exciting the bending mode. A standard notch filter would not take advantage of any beneficial dynamics at frequencies nearv the bending mode. It would also increase the order of the compensator. As an alternative, the inner loop filter was revised to compensate for the new information. It was also possible to design a fourth-order controller to replace the earlier fifth-order design, lowering the complexity of the controller instead of increasing it. The new controller was determined to be .

$$g_{11}(s) = \frac{125(s+1)(s+2.5 \pm j9.4)}{s(s+10)(s+35 \pm j35.7)}$$

A characteristic of a bilinear transformation is that, in general, it transforms an unequal-order transfer function ($n_s \neq w_s$) in the s-domain into one for which the order of the numerator is equal to the order of its denominator ($n_z = w_z$) in the z-domain. This characteristic must be kept in mind when synthesizing $g_i(s)$and $f_{ii}(s)$. Therefore, a nondominating s-domain zero at -150 is inserted in f_{11}.

With the MIMOQCAD program it was possible to shape the loop so that at *5 rad/sec* the loop intersected a point on the Nichols chart where the stability boundary and the performance boundary met. This was an optimal point for the loop to pass through given Lambda's performance bandwidth. The new A/C model was implemented in the nonlinear simulations and tested with both filters. As expected, the resonance occurred with the FCS that was designed in Design Cycle #3. The FCS resulting from Design Cycle #4 responded within specifications. The new FCS passed a hardware-in-the-loop simulation and was scheduled for a flight test. During the next flight test, the field conditions were gusty, but within acceptable limits for the experiment. The QFT FCS was engaged and there was no noticeable oscillation. The pilot was very pleased with the handling qualities and felt comfortable flying with the FCS engaged for the entire series of tests. The only problems encountered were some roll performance problems which could be attributed to the windy conditions. Pitch response during this flight is shown in Fig. 8. Unfortunately, the test data recording function failed during the flight so that the only data available is low resolution data ($\pm 0.5^\circ$) recorded at *10Hz*.

IX SUMMARY

Control design and implementation in the real world is an iterative process. Initial steps are performed with linear models that have been formulated with simplifying assumptions. After successful testing of the designed control system, based upon these simplified models, it is tested on increasingly realistic (nonlinear) models. At any point in the design process, if the control system does not meet performance and stability specifications, the control system must be redesigned and retested on the simplified models. This redesign is followed, once again, by testing on the nonlinear model (see Fig. 1). At every point of the design process the designer must be aware of test assumptions so engineering judgement can be use to help guide the design to a successful implementation and operation. The bottom line is that the controlled system must meet the requirements set out at the beginning of the process.

REFERENCES

1. Houpis, C. H. and S. Rasmussen, "Quantitative Feedback Theory (QFT): Theory & Application," Marcel Dekker, Inc., New York, 1999.
2. D'Azzo, J.J., and C. H. Houpis, "Linear Control System Analysis and Design," McGraw-Hill, NY, 4th Ed. 1995.
3. Horowitz, I. M., "Quantitative Feedback Theory." Proceeding of the IEE, Vol. 129, Pt D, No. 6, 1982.
4. Horowitz, I. M., "Quantitative Synthesis of Uncertain Multiple Input-Multiple Output Feedback Systems," Int. J. of Control, Vol. 30, No. 1, 1979.
5. Sating, R. R., "Development of an Analog MIMO Quantitative Feedback Theory (QFT) CAD Package," MS Thesis, AFIT/GE/ENG/92J-04, Graduate School of Engineering, Air Force Institute of Technology, Wright Patterson AFB, OH, 1992.
6. Swift, Gerald A. Model Identification and Control System Design for the Lambda Unmanned Research Vehicle. MS Thesis, Air Force Institute of Technology, Wright-Patterson AFB, OH, Sept. 1991.
7. Lacey, D. J., Jr., "A Robust Digital Flight Control System for an Unmanned Research Vehicle Using Discrete Quantitative Feedback Theory," MS Thesis, AFIT/GE/ENG/91D, Graduate School of Engineering,

Air Force Institute of Technology, Wright-Patterson AFB, OH, Dec. 1991.

8. Wheaton, David G., Automatic Flight Control System for an Unmanned Research Vehicle Using Discrete Quantitative Feedback Theory. MS Thesis, Air Force Institute of Technology, Wright-Patterson AFB, OH, Dec. 1990.

9. Robertson, Scott D., A Real-time Hardware-in-the-Loop Simulation of an Unmanned Aerial Research Vehicle. Technical Report WL-TR-93-9005, Wright Laboratory-Wright-Patterson AFB, OH, Aug. 1992.

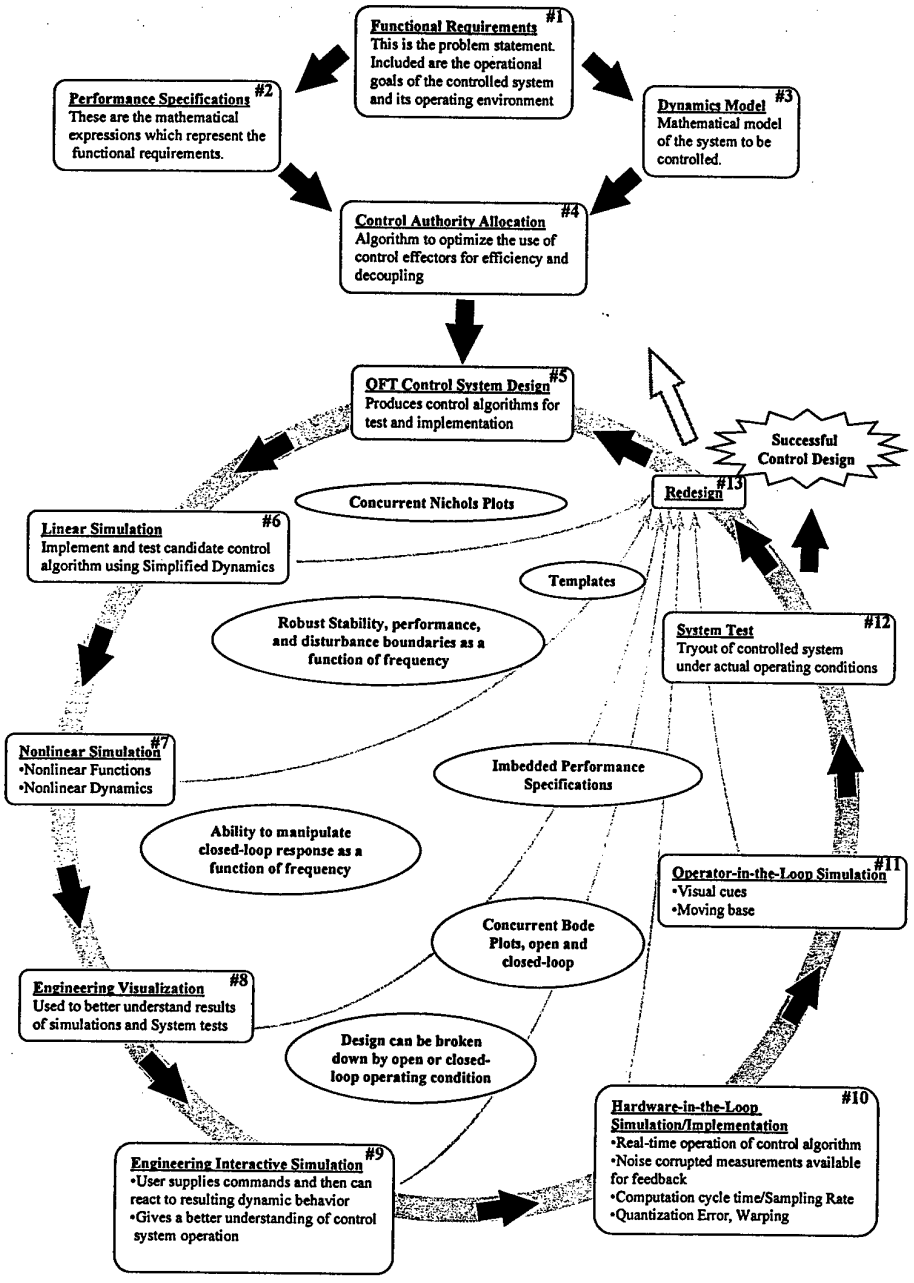

Fig. 1 The QFT control system design process: Bridging the Gap.

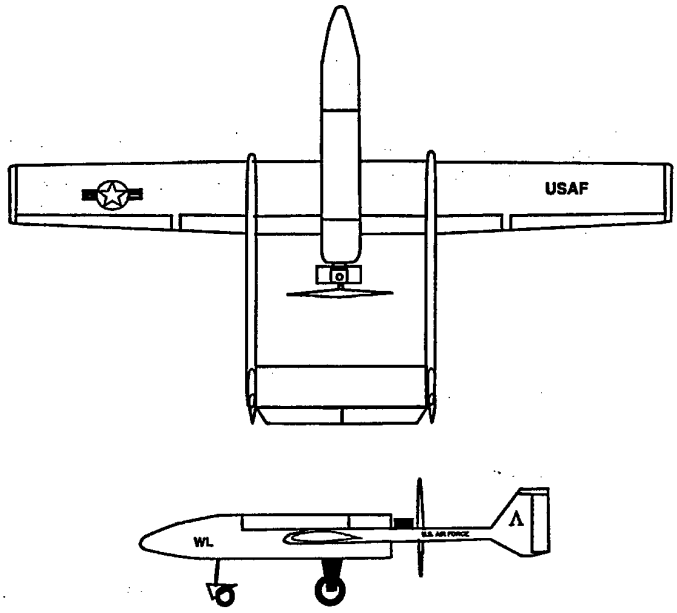

Fig. 2 Lambda Unmanned Research Vehicle (URV).

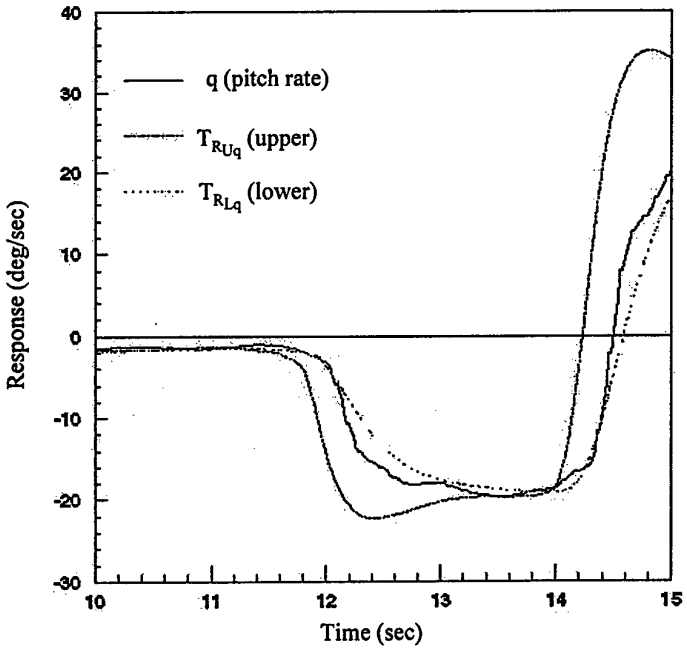

Fig. 3 Response to pitch-down command.

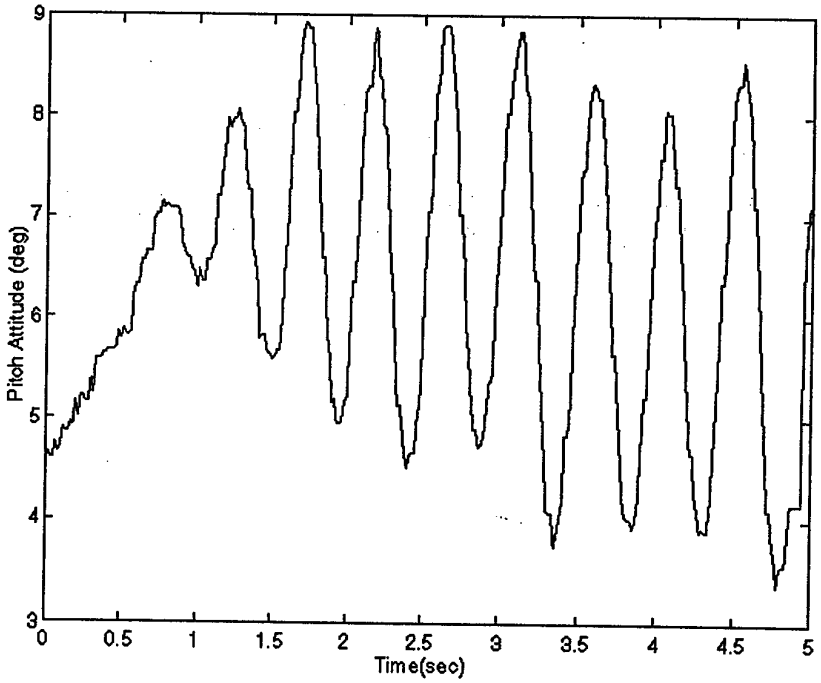

Fig. 4. Pitch resonance during flight.

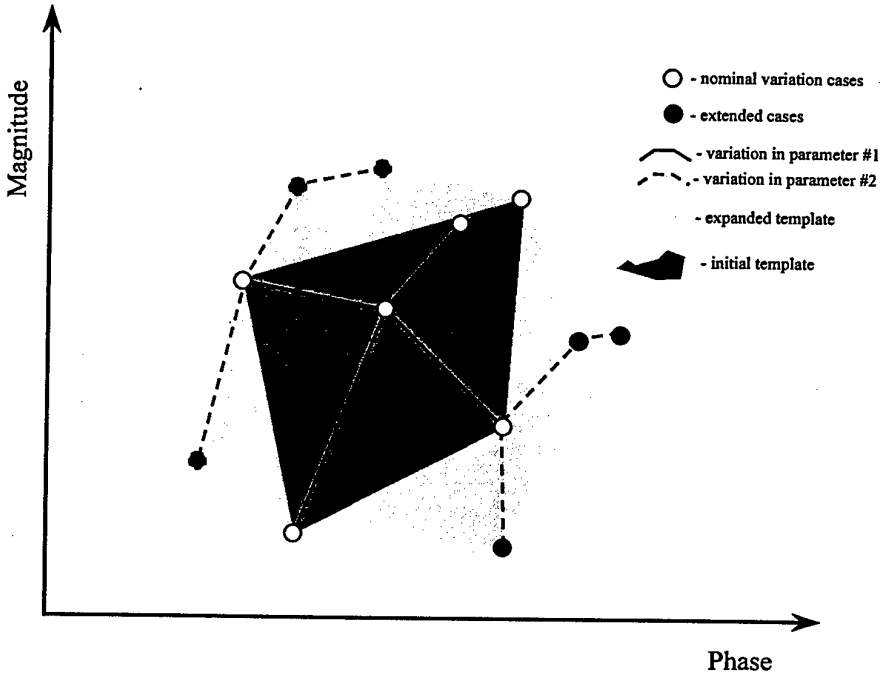

Fig. 5. Template expansion process.

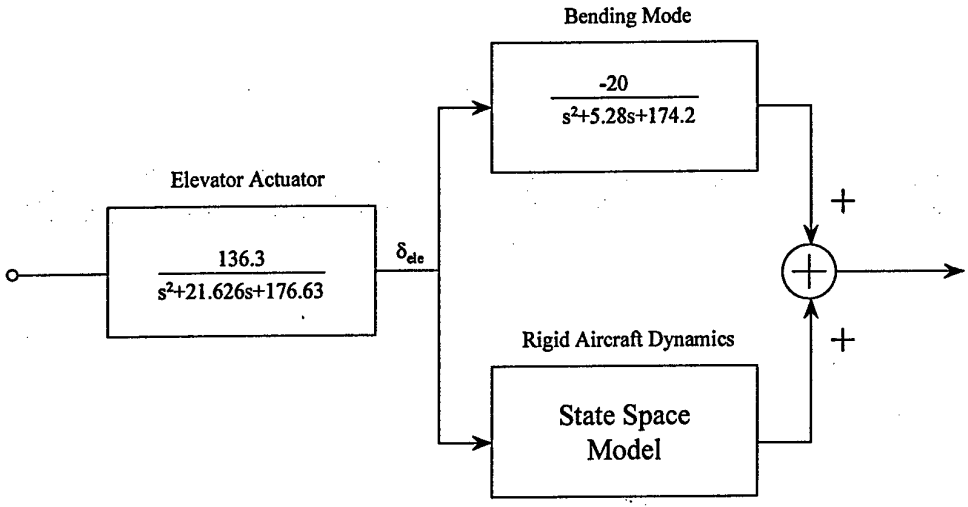

Fig. 6. Lambda bending model structure.

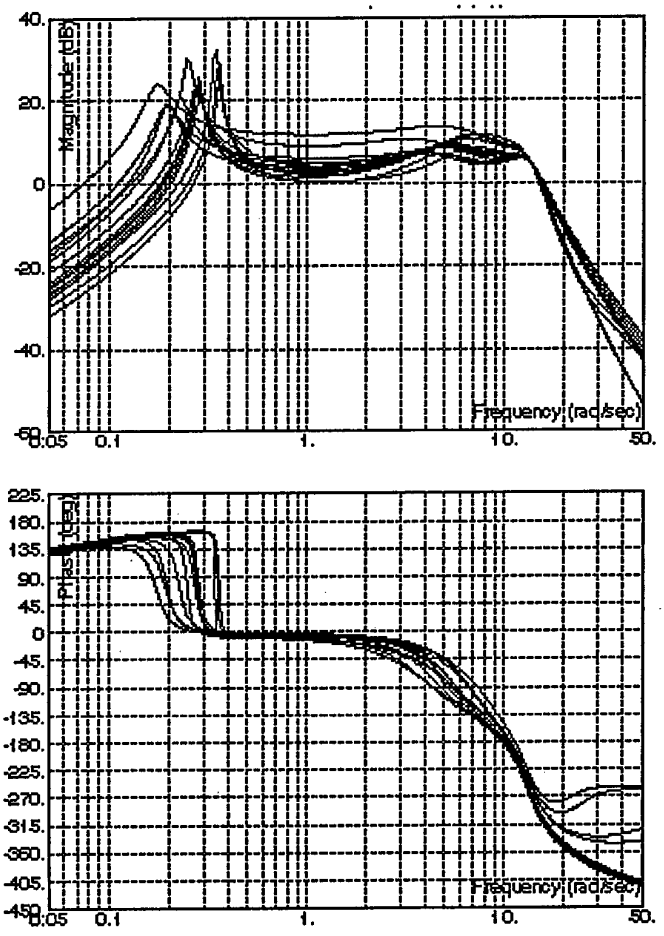

Fig. 7 Lambda bending models.

1999 International Symposium on
Quantitative Feedback Theory and Robust Frequency Domain Methods

Design of a Robust Decentralized Controller for a Non-Minimum-Phase Continuous Stirred-Tank Reactor

W. Wang and S. Engell

Process Control Laboratory, Department of Chemical Engineering
University of Dortmund, D-44221 Dortmund, Germany
e-mail: wangwei@ast.chemietechnik.uni-dortmund.de
s.engell@ct.uni-dortmund.de
Tel.: ++49/(0)231-755-5126, Fax:++49/(0)231-755-5129

Abstract

This paper proposes a procedure to design robust decentralized controllers for linear systems. The design procedure combines a robust frequency domain design procedure (Wang, Trierweiler and Engell, 1997) with the sequential closure of the loops (Mayne, 1973; Hovd and Skogestad, 1994). In each step of the sequential design, an individual controller is designed by the robust design procedure. To reduce the complexity of the controller, the order of the elements of the individual controller in each step is reduced by frequency response approximation (Engell and Müller, 1993). The approach is demonstrated for a non-minimum-phase continuous stirred tank reactor (CSTR).

Keywords: process control, decentralized control, robust control, reactor control, order reduction, loop shaping

1 Introduction

Decentralized controllers are usually preferred because they can be easily implemented, simply designed and individually tuned. Furthermore it is easy to make the closed-loop system failure-tolerant by decentralized control. In chemical processes, restrictions on the feedback compensator structure are often encountered. When several control stations are provided only with local measurements, decentralized controllers must be used. The commonly used methods for the design of decentralized controllers can be arranged in the following three groups: independent design (Skogestad and Morari, 1989), sequential design (Mayne, 1973; Chiu and Arkun, 1992) and direct parameter optimization (e.g. Sandell et al., 1978; Davison and Ferguson ,1981).

In this paper the decentralized control design is conducted by combing a robust controller design procedure (Wang, Trierweiler and Engell, 1997) with the sequential design approach. As the robust controller design procedure usually yields a high order controller, in each step a single loop controller is first computed and order reduction is performed using frequency response approximation method (Engell and Müller, 1993). With the resulting low order controllers the loops are closed one after another.

In Chiu and Arkun (1992), a general analysis of the robustness of sequentially designed decentralized control systems was proposed. With the results of the analysis the robust stability or robust performance obtained using H_∞ methods can be incorporated in the sequential design. The main results of their work can be stated as follows: If certain robustness constraints on the individual decentralized controllers are satisfied, the closed-loop system is guaranteed to possess prespecified robustness properties if and only if the overall system is nominally stable as well. The robustness of the individual loops can lead to the robustness of the coupled system if certain constraints on individual decentralized controllers are satisfied. In the design procedure of decentralized controllers discussed in this paper the robustness of the overall system is guaranteed by adjusting the robustness of the individual loops. The application of the above design procedure to a CSTR shows that the design strategy is viable.

2 The sequential design procedure

Sequential design is the most popular design method for decentralized control of real multivariable processes. In the sequential design, each step in the design procedure involves designing one individual controller. Because at each step one utilizes the information about controllers designed in the previous steps, the method can be less

conservative than independent design. In sequential design, if stability has been achieved after the design of each loop, then the system will remain stable if loops fail or are taken out of service in the reverse order of how they were designed. Similarly, during startup the system will be stable if the loops are brought into service in the same order as they had been designed.
In a sequential design the final controller depends on the order in which the controllers in the individual loops are designed. Usually the fast loops are closed first, because the loop gain and phase in the bandwidth region of the fast loops is relatively insensitive to the tuning of the lower loops. Since the closing of subsequent loops may change the response of previously designed loops, an iterative design may be necessary.

3 A new robust design procedure

Our new robust design procedure is a combination of the Frequency Response Approximation (FRA) method (Engell and Müller, 1993) and the Loop Shaping Design Procedure (LSDP) (McFarlane and Glover, 1990).

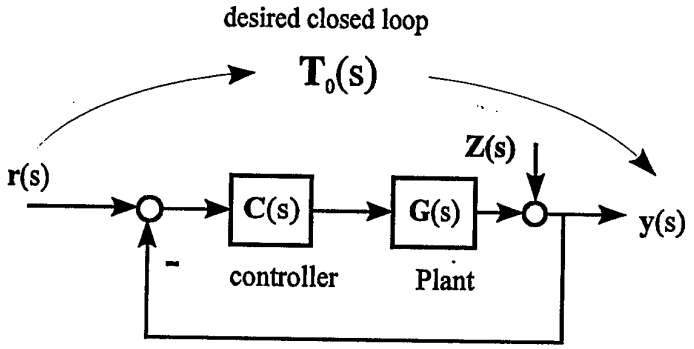

Figure 1 The standard feedback control loop for FRA

In the FRA method the classical frequency compensation technique is understood as the approximation of an ideal controller

$$\mathbf{C}_0(j\omega) = \mathbf{G}^{-1}(j\omega)(\mathbf{T}_0^{-1}(j\omega) - \mathbf{I})^{-1} \tag{1}$$

which achieves a desired closed-loop system $\mathbf{T}_0(j\omega)$, where $\mathbf{G}(j\omega)$ is the nominal plant. In LSDP, the plant is premultiplied by a loop shaping precompensator (weighting function) $\mathbf{C}(s)$. The feedback controller $\mathbf{K}_\infty(s)$ is then optimized for $\mathbf{G}(s)\mathbf{C}(s)$ instead of $\mathbf{G}(s)$. A disadvantage of the LSDP is that there is no clear methodology for the selection of the weighting function $\mathbf{C}(s)$. In the combined robust design procedure (Wang, Trierweiler and Engell, 1997), the weighting function which insures the desired closed-loop behavior is optimized by the FRA procedure, avoiding the "trial and error" process in the weighting function selection. This reduces the design time considerably.

Figure 2 shows the control structure for the robust control design. The detailed design procedure proceeds as follows:

1. Choose a nominal plant $\mathbf{G}(s)$. For the computation of $\mathbf{C}(s)$, select a desired closed-loop reference-to-output transfer matrix $\mathbf{T}_0(s)$.

2. For the nominal plant model $\mathbf{G}(s)$, the weighting function $\mathbf{C}(s)$ is optimized by the FRA procedure. It consists of two steps:
   a.) Use the column-by-column least squares optimal frequency response approximation to calculate a transfer function $\mathbf{C}(s)$ which achieves good model-matching.
   b.) Using $\mathbf{C}(s)$ from a. as a starting point, the non-linear optimization of the weighting function $\mathbf{C}(s)$ is performed such that

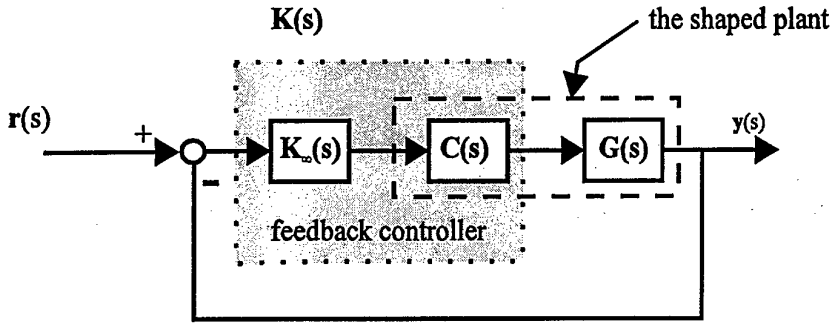

Figure 2 Control structure for the robust control design

$$J = \rho \sum_{l=1}^{N} \left\| \frac{[\mathbf{I} + \mathbf{L}(j\omega_l)]^{-1}\mathbf{L}(j\omega_l) - \mathbf{T}_0^1(j\omega_l)}{j\omega_l} \right\|_F^2 + \varepsilon_{\max}^{-1}[\mathbf{G}_n(s), \mathbf{C}(s)] \qquad (2)$$

is minimized, where $\mathbf{L}(s)=\mathbf{G}(s)\mathbf{C}(s)$. Here ε_{max} is the design indicator in the LSDP which represents the maximum achievable stability margin of the compensated closed-loop system. In the cost function the first term is for good model-matching. The second term maximizes the maximum achievable stability margin ε_{max} for the shaped plant $\mathbf{G}_n(s)\mathbf{C}(s)$. The constant ρ controls the compromise between the model-matching and the robust stability of the closed-loop.

3. For ensuring robust stability of the closed-loop system, a feedback controller $\mathbf{K}_\infty(s)$ is computed for $\varepsilon = 0.95\ \varepsilon_{max}$. The final feedback controller is $\mathbf{K}(s) = \mathbf{C}(s)\mathbf{K}_\infty(s)$. If robust stability of the closed-loop system can not be achieved by $\mathbf{K}(s)$, adjust ρ and return to step 2.b.

The structure and the orders of the elements of the weighting matrix $\mathbf{C}(s)$ can be chosen freely by the designer. $\mathbf{K}_\infty(s)$ can be computed by a standard algorithm (McFarlane and Glover, 1990).

4 Sequential design of robust decentralized controllers

Combining the new robust design procedure in the SISO case with the sequential design method, we have the following sequential design procedure of robust decentralized controllers:

Step 1: Determine the order of loop-closing by estimating the desired bandwidth in each loop.

Step 2: Design the controller $K_1(s) = C_1(s)K_{1\infty}(s)$ using the new robust design procedure in the SISO case considering only the transfer function $Q_1(s)$ from u_1 to y_1.

Step 3: Calculate the transfer function $Q_2(s)$ from u_2 to y_2 by which the first loop is closed by the controller $K_1(s)$. For the transfer function $Q_2(s)$, design the controller $K_2(s)=C_2(s)K_{2\infty}(s)$.

...

Step k: Design the controller $K_k(s) = C_k(s)K_{k\infty}(s)$ for $Q_k(s)$ which is the transfer function from $u_k(s)$ to $y_k(s)$ after closing the first (k-1) loops with the designed controllers $K_1(s)$, $K_2(s)$, ..., $K_{k-1}(s)$.

...

Step r: Design the last controller $K_r(s) = C_r(s)K_{r\infty}(s)$ via Qr(s).

Here r is the number of the inputs and outputs of the system. The new robust controller design procedure usually yields a high order controller. Therefore in each step a high order SISO controller is first designed, and then order reduction is performed using the frequency response approximation method again to reduce the controller

complexity. With the resulting low order controllers the loops are closed. If the performance of the closed-loop system is not satisfactory, an adjustment of the design parameter ρ_i in each design step and a different design sequence may be necessary.

5 Example

Here we consider the control problem of a continuous stirred-tank reactor (CSTR) which was used as a benchmark problem for controller design for nonlinear processes by Engell and Klatt (1993), Amann and Allgöwer (1994) and others. The plant is non-minimum-phase and exhibits significantly nonlinear behaviour, thus robustness plays an essential role when a linear controller is designed for a range of operating points.

5.1 The control problem

The CSTR considered here is an example for the Van de Vusse reaction scheme (Kantor, 1986). The abstract reaction scheme is

$$A \xrightarrow{k_1} B \xrightarrow{k_2} C \tag{3}$$

$$2A \xrightarrow{k_3} D \tag{4}$$

where A is the educt, B the product and C and D are unwanted byproducts. The dynamics of the system considered here are described by four nonlinear differential equations which can be derived from mass and energy balances (Engell and Klatt, 1993):

$$\frac{dc_A}{dt} = \frac{\dot{V}}{V_R}(c_{A0} - c_A) - k_1(\theta)c_A - k_3(\theta){c_A}^2 \tag{5}$$

$$\frac{dc_B}{dt} = -\frac{\dot{V}}{V_R}c_B + k_1(\theta)c_A - k_2(\theta)c_B \tag{6}$$

$$\begin{aligned}\frac{d\theta}{dt} = &\frac{\dot{V}}{V_R}(\theta_0 - \theta) + \frac{k_w A_R}{\rho C_P V_R}(\theta_K - \theta) \\ &- \frac{1}{\rho C_P}[k_1(\theta)c_A\Delta H_{R_{AB}} + k_2(\theta)c_B\Delta H_{R_{BC}} + k_3(\theta){c_A}^2\Delta H_{R_{AD}}]\end{aligned} \tag{7}$$

$$\frac{d\theta_K}{dt} = \frac{1}{m_K C_{PK}}[\dot{Q}_K + k_W A_R(\theta - \theta_K)] \tag{8}$$

where c_A is educt concentration, c_B is product concentration, θ is reactor temperature and θ_K is the temperature of the coolant medium. V_R is the volume of the reactor, and $\dot{V}$ is the volume flow through the reactor. $\Delta H_{R_{ij}}$ are the various reaction enthalpies, θ_0 is the temperature of the inlet stream. k_W represents the heat transfer coefficient, A_R is the surface of the cooling jacket and m_k is the mass of the coolant. The rate coefficients k_1, k_2 and k_3 depend on the reaction temperature via Arrhenius' law

$$k_i(\theta) = k_{0i} \cdot \exp\left[\frac{-E_A(i)}{R(\theta + 273.15)}\right]. \tag{9}$$

For the values of the parameters in the non-linear model for the reaction system considered here, the reader is referred to Engell and Klatt (1993). All parameters here are only known with limited accuracy. The manipulated variables are the inverse of the residence time $\dot{V}/V_R$ and the amount of heat removed by the coolant, $\dot{Q}_K$. They are restricted in the ranges:

$$5h^{-1} \le \frac{\dot{V}}{V_R} \le 35h^{-1} \qquad \text{and} \qquad -8500\frac{kJ}{h} \le \dot{Q}_K \le 0\frac{kJ}{h}. \tag{10}$$

The reactant A is fed into the reactor with concentration c_{A0} and temperature θ_0. The variation of the reactant concentration c_{A0} is considered as the main unmeasurable disturbance of the system. It varies in the range,

$$4.5\frac{mol}{h} \le c_{A0} \le 5.7\frac{mol}{h}. \tag{11}$$

The goal of the control design is to control the product concentration c_B of the reactor in the range,

$$0.7\frac{mol}{l} \le c_B \le 0.95\frac{mol}{l}. \tag{12}$$

As a test signal, the reference input for the concentration is

$$c_{B,ref}(t) = 0.9 - 0.2u(t-10) + 0.25u(t-60) \quad \text{[mol/l]}, \tag{13}$$

while the reactor temperature θ should be unchanged.

5.2 Nominal plant model and uncertainty description

Considering the product concentration c_B and the reactor temperature as the output variables, linearization at the main operating point,

$$c_A = 1.078\frac{mol}{l},\ c_B = 0.825\frac{mol}{l},\ \theta = 135.0^\circ C,\ \theta_K = 130.9^\circ C,\ \frac{\dot{V}}{V_R} = 16.3h^{-1},\ \dot{Q}_K = -3555\frac{kJ}{h},$$

which corresponds to the educt concentration c_{A0} = 5.1 mol/l, yields the nominal design model {**A**, **B**, **C**, **D**}(all time constants in minutes) where

$$\mathbf{A} = \begin{bmatrix} -1.412 & 0 & -0.0630 & 0 \\ 0.8873 & -1.1588 & 0.0132 & 0 \\ 2.4417 & 3.4708 & -0.5970 & 0.5138 \\ 0 & 0 & 1.4450 & -1.4450 \end{bmatrix} \qquad \mathbf{B} = \begin{bmatrix} 0.0670 & 0 \\ -0.0138 & 0 \\ -0.0833 & 0 \\ 0 & 0.0017 \end{bmatrix} \tag{14}$$

$$\mathbf{C} = \begin{bmatrix} 0 & 1 & 0 & 0 \\ 0 & 0 & 1 & 0 \end{bmatrix} \qquad \mathbf{D} = \begin{bmatrix} 0 & 0 \\ 0 & 0 \end{bmatrix}. \tag{15}$$

The corresponding plant transfer matrix $\mathbf{G}_n(s) = \mathbf{C}(sI - \mathbf{A})^{-1}\mathbf{B} + \mathbf{D}$ has a transmission zero at 2.89 in the right-half-plane. We will use a robust linear controller designed for the above linear nominal model to control the

original non-linear system. The uncertainty in the robust design of the linear controller therefore consists of two major parts due to the non-linearity and due to uncertain physical/chemical parameters (e.g., rate coefficients, activation energies, and reaction enthalpies). Letting **G**(s) be the linear transfer function of the system at a stationary point in the operation range, we write

$$\mathbf{G}(s) = \mathbf{G}_n(s) + \Delta(s)\,. \tag{16}$$

The uncertainty Δ(s) from the non-linearity can be represented by uncertainty bands obtained by linearizing the model for extreme values of c_B (Müller and Trierweiler, 1995):

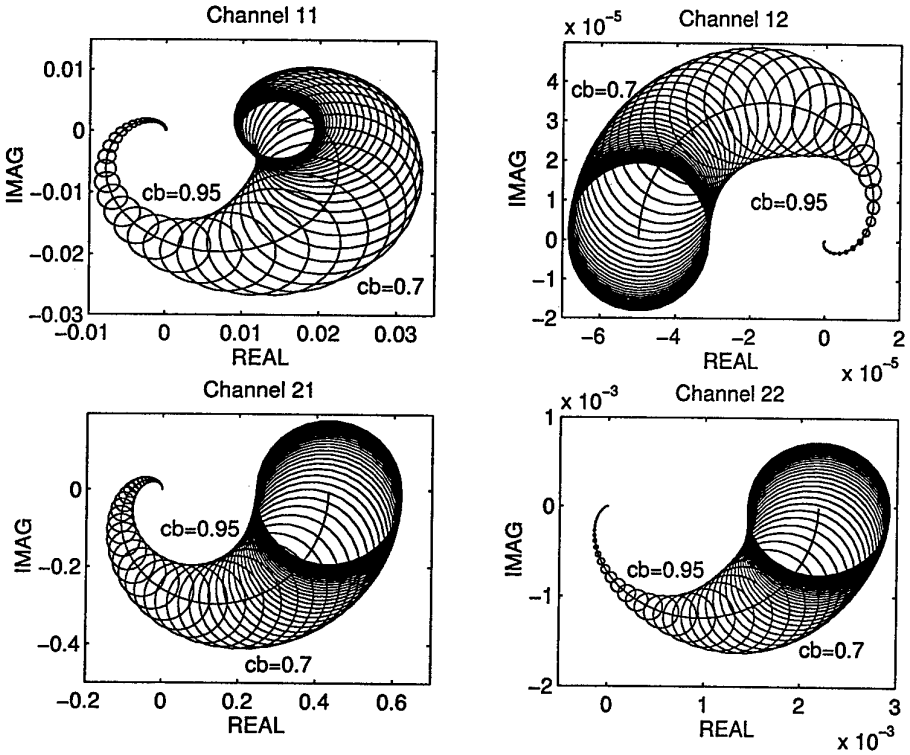

Figure 3 Nyquist diagram of each channel with uncertainty bounds

$$|\Delta_{11}(s)| \le \frac{0.004805(0.001001s+1)(0.009398s+1)(0.3586s+1)}{(0.001001s^2+0.03855s+1)(0.158s+1)} \tag{17}$$

$$|\Delta_{12}(s)| \le \frac{-0.00001877(0.0003883s+1)(0.00361s+1)(0.04372s+1)}{(0.004281s^2+0.0547s+1)(0.1484s+1)} \tag{18}$$

$$|\Delta_{21}(s)| \le \frac{0.1887(1.0e-6s^2+0.001471s+1)(0.8382s+1)}{(0.01169s+1)(0.1176s+1)(0.8222s+1)} \tag{19}$$

$$|\Delta_{22}(s)| \le \frac{7.439e-4(1..888e-6s^2+0.001023s+1)(0.2156s+1)}{(0.008591s^2+0.1264s+1)(0.2895s+1)} \tag{20}$$

The Nyquist diagram of each channel with nonlinearity uncertainty bounds is shown in Figure 3. These bounds illustrate that our nominal plant is reasonable if we consider the nonlinearity of the system as uncertainty of the

linear plant used in the linear controller design. As a representative of the uncertainty of the parameters, we assume that the activation energy of the reaction corresponding to k_1 and k_2, $E_A(1)$ and $E_A(2)$ in equation (9) increases by 2% corresponding to a variation of the reaction rates by 40%.

5.3 Design of the robust decentralized controller

In this section the design strategy described in section 4 will be used to design a robust decentralized controller for the CSTR. The desired closed-loop is chosen to have 3 minutes rise time in the concentration channel and 1 minute rise time in the temperature channel; both channels should have 10% overshoot for step inputs. This leads to the desired closed-loop transfer matrix

$$\mathbf{T}_0(s) = \{\frac{1}{2.2s^2 + 1.754s + 1}, \quad \frac{1}{0.2444s^2 + 0.5846s + 1}\}. \tag{21}$$

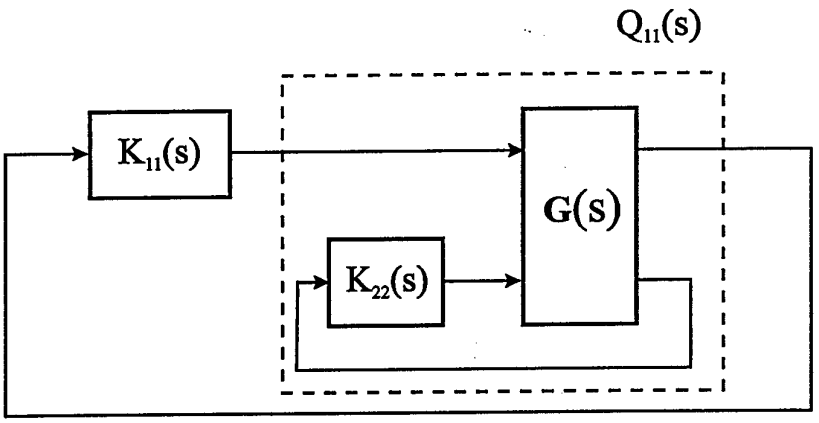

Figure 4 Control structure for the sequential design

In our design method the restrictions on the manipulated variables $\dot{V}/V_R$ and $\dot{Q}_k$ are considered by choosing a reasonable rise time in each channel. This can be done by estimating the smallest duplication time[1] in each channel under the restrictions on the manipulated variables. The minimum duplication time for the reference step 0.2u(t) is 1.8 minutes for the concentration channel and 0.4 minutes for the temperature channel (Müller, 1996). The rise times of our desired closed-loop system are consistent with these duplication times.

Since the temperature channel is the fast channel, the design begins with the second loop. For the minimum phase element $g_{22}(s)$, a weighting function $C_2(s)$ was optimized:

$$C_2(s) = \frac{3.6643s + 0.7440}{s} \times 10^3 \tag{22}$$

with the design parameter ρ_2 = 100 and γ_{min2} = 1.7687. The H_∞-controller $\{\mathbf{A}_{k2}, \mathbf{B}_{k2}, \mathbf{C}_{k2}, \mathbf{D}_{k2}\}$ was computed for $g_{22}(s)\cdot C_2(s)$ by standard algorithms. The order of the overall controller

$$K_{22}(s) = (\mathbf{C}_{k2}(sI - \mathbf{A}_{k2})^{-1}\mathbf{B}_{k2} + \mathbf{D}_{k2}) \cdot C_2(s) \tag{23}$$

in the second channel is 6. After order reduction we obtained the following PI-controller:

[1] The duplication time is the minimum time at which the output response crosses the final value.

$$K_{22}^{r}(s)=\frac{2512s+464.93}{s}. \tag{24}$$

With the controller $K_{22}^{r}(s)$ we closed the second loop, the transfer function $Q_{11}(s)$ was calculated, which is non-minimum-phase and has a zero at 2.89 in RHP. In order to avoid the approximation of an unstable ideal controller, the transfer function of the desired closed-loop system was multiplied by (1+ s/2.89) for the approximation of the controller (Engell, 1988). With $\rho_1 = 160$ we obtained the following weighting function:

$$C_1(s)=\frac{16.318s+27.26}{s} \tag{25}$$

leading to a maximum stability margin γ_{min1} ($1/\varepsilon_{min1}$) = 1.8406. For this weighting function, an H_∞-controller $\{\mathbf{A}_{k1}, \mathbf{B}_{k1}, \mathbf{C}_{k1}, \mathbf{D}_{k1}\}$ was computed. The controller for the first channel is

$$K_{11}(s)=(\mathbf{C}_{k1}(sI-\mathbf{A}_{k1})^{-1}\mathbf{B}_{k1}+\mathbf{D}_{k1})\cdot C_1(s). \tag{26}$$

This controller can also be reduced to a PI-controller:

$$K_{11}^{r}(s)=\frac{17.444s+17.872}{s}. \tag{27}$$

The final robust decentralized controller thus is

$$\mathbf{K}(s)=\begin{bmatrix} K_{11}^{r}(s) & 0 \\ 0 & K_{22}^{r}(s) \end{bmatrix}=\frac{1}{s}\begin{bmatrix} 17.444s+17.872 & 0 \\ 0 & 2512s+464.93 \end{bmatrix}. \tag{28}$$

The simulation of the above controller is shown in Figure 5. Because the design specification is satisfied, no iteration was necessary.

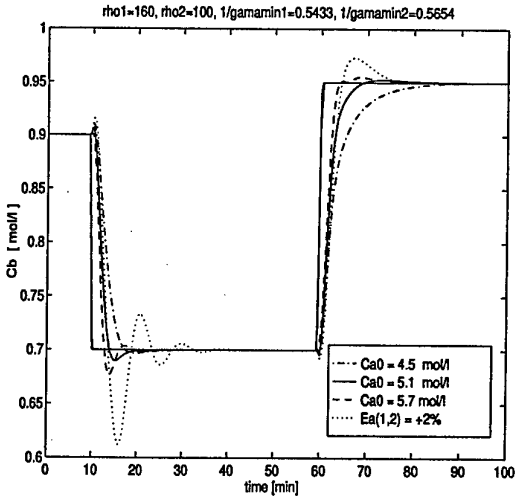

Figure 5 Simulation of CSTR with the PI-Controller (28)

For $\rho_1 = 85$, the corresponding robust decentralized controller is

$$\mathbf{K}_1(s) = \begin{bmatrix} \dfrac{21.9536s + 15.76}{s} & 0 \\ 0 & \dfrac{2512s + 464.93}{s} \end{bmatrix}. \tag{29}$$

The simulation of this controller is shown in Figure 6.

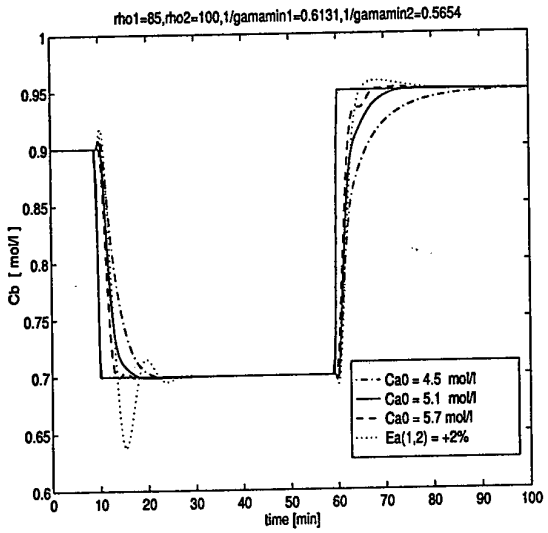

Figure 6 Simulation of the CSTR with the PI-Controller (29)

Comparing Figure 6 and Figure 7 the robustness of the closed-loop is increased by changing the design parameter ρ_1 at the expense of a slightly slower response.

6 Conclusion

A new sequential design procedure for robust decentralized controllers is proposed. In each step of the design a new robust design procedure is used to design an individual controller. To reduce the complexity of the controller and also of the plant transfer function in the following steps, the order of the computed SISO controller in each loop is reduced by the FRA method and then the corresponding loop is closed with the low order controller. The design procedure is demonstrated for a CSTR with complex reaction scheme, the simulation results show that the design is successful.

References

Amann, N. and Allgöwer, F. (1994). μ-Suboptimal design of a robustly performing controller for a chemical reactor. *Int. J. Control*, Vol. 59, No.3, 665-687

Chiu, M.-S.and Y. Arkun (1992). A methodology for sequential design of robust decentralized control systems. *Automatica*, **28**(5), 997-1001.

Davison, E. J. and I. J. Ferguson (1981). The design of controllers for the multivariable robust servomechanism problem using parameter optimization methods. *IEEE Trans. Autom. Control*, AC-26, 93-110.

Engell, S.(1988). Compensator design by frequency-weighted approximation. *Proceedings of the IEE International Conference on Control, Control 88*, pp.253-258. (London: The Institution of Electrical Engineers, Publication No. 285).

Engell, S. and Klatt, K.-U. (1993). Nonlinear Control of a Non-Minimum-Phase CSTR. *Proceedings of the 1993 American Control Conference*, pp.2041-2045.

Engell, S. and Müller, R.(1993). Multivariable controller design by frequency response approximation. *Proceedings of 2nd European Control Conference*, pp.1715-1720.

Kantor, J. C. (1986). Stability of State Feedback Transformation for Nonlinear Systems — Some Practical Considerations. *Proceedings of American Control Conference*, Seattle, Washington, U. S. A., 1014-1016.

Mayne, D. Q. (1973). The design of linear multivariable systems. *Automatica*, vol. **9**, 201-207.

McFarlane, D. C. and Glover K.(1990). *Robust controller design using normalized coprime factor plant descriptions*. Berlin: Springer-Verlag.

Müller, R. and Trierweiler, J. O. (1995). Robust Dencentrlized Control of a CSTR with Complex Reaction Scheme, DYCORD+'95 (IFAC Symposium), pp.69-74.

Sandell, N. R., P. Varaiya, M. Athans and M. G. Safonow (1978). Survey of decentralized control methods for large scale systems. *IEEE Transaction on Automatic Control*, AC-23, 108-128.

Skogestad, S. and M. Morari (1989). Robust performance of decentralized control systems by independent design. *Automatic*, **25**(1), 119-125.

Wang, W., Engell, S. and Müller, R.(1996). Robust Controller Design by a Combination of Loop Shaping and Frequency Response Approximation. *Proceedings of the 13th IFAC World Congress*, Volume H, pp.339-344.

Wang, W., Trierweiler, J. O. and Engell, S.(1997). Robust Controller Design for a Heating System, *Proceedings of Symposium on Quantitative Feedback Theory and Other Frequency Domain Methods and Applications*, University of Strathclyde, Glasgow, pp.143-149.

1999 International Symposium on
Quantitative Feedback Theory and Robust Frequency Domain Methods

A Modified QFT Design Method for a Cascaded Multiple Loops System and Its Application in Idle Speed Control

Sy-Kang Shen†;Bor-Chyun Wang†; Ching-Yin Lee‡; Tsung-Chih Lin*

† *Chung Shan Institute of Science and Technology, P.O. Box 90008-16-29, Lung-Tan, Taoyuan 325, Taiwan, R.O.C.; Tel:886-2-26739638 ext.355681;Fax:886-3-4711277;e-mail:ew0451@ms19.hinet.net*

‡ *Department of Electrical Engineering, National Taipei University of Technology, Taipei, Taiwan, R.O.C.;*

* *Department of Electronics Engineering, Feng-Chia University, Taichung, Taiwan, R.O.C.*

Abstract

In this paper, a frequency domain design methodology for Equivalent Disturbance Rejection (EDR) in a multiple-input-single-output (MISO) plant which has a special cascaded multiple loops structure is addressed. First, EDR method transfers not only the maximum variation of the plant uncertainty to the values of equivalent external disturbance at the plant output with a fixed nominal plant, but also the maximum variation of the desired output tolerance to the fixed values at some specified frequencies. Therefore, the uncertain plant design problem will become an EDR problem. Similarly, once the control input constraints expressed in the time domain with bandwidth limitation are mapped into a set of target transfer functions, they can also be treated as an equivalent external disturbance upon being transferred to the output. Thus, the control design problem coping with the control inputs and output constraints under a persistent bounded disturbance will also become an EDR problem. Design procedures of the single-input single-output uncertain plant tracking problem and the cascaded multiple loops idle speed control of a V-6 fuel injection engine are provided, respectively, as illustrative examples.

Keywords: Cascaded multiple loops systems, disturbance rejection, Quantitative Feedback Theory(QFT), robust control systems, uncertain plant.

1. Introduction

Quantitative feedback theory (QFT) design method developed by [1] requires templates (value sets) of the uncertain plant on the Nichols chart in addition to matching the system's specifications in order to obtain the bounds at some given frequencies. Once those bounds are determined, a systematic approach can be applied to design a compensator and a prefilter so that the two-degree-of-freedom (2DOF) system satisfies the specifications and performance.

An alternative concept provided by [2] which was not used in the synthesis of uncertain feedback control system can transfer the plant uncertainty to an equivalent external disturbance with fixed nominal plant. Although [3] used this concept on plant uncertainty and developed an Equivalent Disturbance Attenuation Method (EDAM) to solve this problems, it still needs to calculate the bounds by figuring out the mid-points of the uncertain plant and system's specification, which will be neither efficient nor accurate.

Equivalent Disturbance Rejection (EDR) method uses the maximum variations of the system tolerance as well as the maximum variations of the uncertain plant which can be transferred to the plant output as an equivalent external disturbance to calculate the values of bounds at some specified frequencies through an algebraic equation. In this case, the uncertain plant design problem will become an EDR problem. This alternative concept for plant uncertainty is being extended to solve various control design problems resulting from output and control constraints under a persistent bounded disturbance [4,5,6,7] of a special cascaded multiple-loop (CML) structure. Those constraints and bounded disturbance will be represented as the time domain limitation and step input response respectively. [5] proposed a frequency domain design methodology for disturbance rejection in multiple-input single-output (MISO) plant which has a special parallel structure. To make the loop transmission function maintained within the bounds obtained from the prespecified constraints,

it used two different inequality equations at any arbitrary phase angle, $-2\pi \leq \phi \leq 0$, to obtain the three dimensional tube-type bound [6]. This makes the design procedures a little touchy although it works well to solve the problems of output and control constraints under a persistent bounded disturbance.

For a general MISO parallel plant structure as shown in Figure 1, where u_i(s), i=1,...,n, and y(s) denote control inputs and system output constraints respectively, and ω(s) denotes persistent bounded disturbance. The corresponding cascaded multiple-loop system which closes each loop with a controller is shown in Figure 2. Consequently, the objective is to synthesize the controllers one at a time so that the prespecified time domain constraints and bandwidth limitations are satisfied when a step disturbance is applied. Each of the time domain constraints will be transferred to an equivalent target transfer function which coincides with the amplitude and bandwidth limitations. The target transfer functions will map to the plant output as an equivalent external disturbance. The equivalent external disturbance will be treated just like that in the alternative concept of plant uncertainty.

This paper is organized as follows. In Section 2, an alternative concept of plant uncertainty for a QFT-type design methodology is presented. The CML system design procedures are developed in Section 3. In Section 4, two examples are provided to demonstrate the results of single-input-single-output (SISO) uncertain plant tracking problem and the CML structure idle speed control problem of a V-6 fuel injection engine. Conclusions are included in Section 5.

2. Uncertain plant tracking problem

In this section, we develop a different concept for the plant uncertainty which will be transferred to an equivalent external disturbance. Then the nominal plant without any uncertainty will be adopted to design the 2DOF system to satisfy the system's specifications and performance. The concept will be extended to solve the problems of system output and control input constraints under a persistent bounded disturbance of a CML structure as shown in the next Section.

2.1. Problem statement

Consider a linear time-invariant (LTI) single-input-single-output (SISO) 2DOF feedback system as shown in Figure 3a, where $\wp$ set is the set of the plant transfer function P(s). P_o(s) is the nominal plant transfer function of P(s). The compensator G_c(s) and prefilter F(s) are realizable transfer functions. u(s) and y(s) are input and output transfer functions respectively. u''(s) is the equivalent external disturbance. T(s) and T_o(s) are the perturbed and nominal system response transfer functions from u(s) to y(s) respectively. $L_o(s) = P_o(s)G_c(s)$, is the nominal loop transmission function.

The design objective in this problem is to synthesize a controller G_c(s) and a prefilter F(s) to satisfy

$$\gamma_1(t) \leq |y(t) - y_o(t)| \leq \gamma_2(t),$$

subject to the constraints

$$P(s) \in [\wp \; set],$$

where y(t) and y_o(t) are the perturbed and nominal system responses from u(t) to y(t) respectively. And γ_1(t) and γ_2(t) are the allowable upper and lower time domain bounds of $|y(t) - y_o(t)|$.

2.2. Design procedures

2.2.1. Transfer the time domain bounds γ_1(t) and γ_2(t) into the frequency domain bounds B_l(s) and B_u(s) respectively.

Although so far there is no known way to transfer the rigorous time domain bounds into the frequency domain bounds, by using a simple first or second order transfer function coupled with computer simulation facilities the corresponding frequency domain bounds can be obtained, and the prespecified time domain bounds can also be satisfied.

2.2.2. Derive the bounds through an algebraic equation

Following lemmas are introduced to obtain the equivalent external disturbance at plant output due to plant uncertainty and the bounds from some algebraic equations.

Lemma 1 :
Consider a linear SISO, 2DOF system as shown in Figure 3a, the overall transfer function from u''(s) to y(s) can be expressed as follows:

$$\frac{1 - T_o(s)/T(s)}{1 - P_o(s)/P(s)} = \frac{1}{1 + L_o(s)}, \text{ or}$$

$$\frac{T_o(s)/T(s)}{P_o(s)/P(s) + L_o(s)} = \frac{1}{1 + L_o(s)},$$

proof : From Figure 3a, the overall nominal transfer function T_o(s) from u(s) to y(s) with nominal plant transfer function P_o(s) is

$$T_o(s) = F(s)\frac{L_o(s)}{1 + L_o(s)}.$$

Multiplying both sides by $(1 + L_o(s))$, we get

$$(1 + L_o(s))T_o(s) = F(s)L_o(s). \tag{1}$$

The output y(s) with plant transfer function, P(s), equals

$$y(s) = F(s)\frac{P(s)G_c(s)}{1 + P(s)G_c(s)}u(s),$$

or equivalently,

$$(1 + P(s)G_c(s))y(s) = F(s)P(s)G_c(s)u(s).$$

After some simple manipulations, it yields

$$(\frac{1}{P(s)} + G_c(s))T(s) = F(s)G_c(s),$$

and multiplying both side by P_o(s), we obtain

$$(\frac{P_o(s)}{P(s)} + P_o(s)G_c(s))T(s) = P_o(s)F(s)G_c(s),$$

or,

$$(\frac{P_o(s)}{P(s)} + L_o(s))T(s) = L_o(s)F(s). \tag{2}$$

Substituting equation (1) into equation (2) yields

$$(\frac{P_o(s)}{P(s)} + L_o(s))T(s) = (1 + L_o(s))T_o(s). \tag{3}$$

Equation (3) can be rewritten as

$$(1 + L_o(s))(T(s) - T_o(s)) = (1 - \frac{P_o(s)}{P(s)})T(s). \tag{4}$$

Simple manipulation yields

$$\frac{1 - T_o(s)/T(s)}{1 - P_o(s)/P(s)} = \frac{1}{1 + L_o(s)}. \tag{5}$$

Similarly, from (3), we may obtain

$$\frac{T_o(s)/T(s)}{P_o(s)/P(s) + L_o(s)} = \frac{1}{1 + L_o(s)}. \tag{6}$$

Q.E.D.

Thus, $1 - P_o(s)/P(s)$ or $P_o(s)/P(s) + L_o(s)$ can be treated as an input at u''(s) and $1 - T_o(s)/T(s)$ or $T_o(s)/T(s)$ as an output at y(s). The overall closed loop transfer function from $u''(s)$ to y(s) can be expressed as $1/(1 + L_o(s))$. As a result, the block diagram in Figure 3a can also be redrawn as shown in Figure 3b.

Note that equation (5) can also be expressed as

$$|\frac{1}{1+L_o(s)}|_{dB} = |\frac{\Delta T(s)}{T(s)}|_{dB} - |\frac{\Delta P(s)}{P(s)}|_{dB},$$

where $\Delta T(s) = T(s) - T_o(s)$, $\Delta P(s) = P(s) - P_o(s)$. Hence $L_o(s)$ should be designed to satisfy

$$|\frac{1}{1+L_o(s)}|_{dB} \leq |\frac{\Delta T(s)}{T(s)}|_{dB} - |\frac{\Delta P(s)}{P(s)}|_{dB}. \tag{7}$$

Lemma 2 :
Consider a equivalent external disturbance system as shown in Figure 3a, the overall transfer function from u''(s) to y(s) can be expressed as shown in (5) or (6), then the bounds of nominal loop transfer function L_o(s) at any given frequencies can be expressed as follows:

$$L_o(s) = \frac{T_o(s)/T(s) - P_o(s)/P(s)}{1 - T_o(s)/T(s)} \tag{8}$$

where T_o(s)/T(s) and P_o(s)/P(s) are the maximum variations of system response tolerance and uncertain plant, respectively.

proof: The proof follows directly from equations (5) and (6) and therefore, is omitted. *Q.E.D.*

Let $L_o(s) = 1/$Q(s), then equation (7) becomes

$$|\frac{Q(s)}{1+Q(s)}|_{dB} \leq |\frac{\Delta T(s)}{T(s)}|_{dB} - |\frac{\Delta P(s)}{P(s)}|_{dB}. \tag{9}$$

It should be noticed that the relation between Q(s) and Q(s)/(1+Q(s)) is exactly the open loop and closed loop relation used in the Nichols chart and likewise, the relation between L_o(s) and $1/(1+L_o(s))$ is the open and closed loop relation used in the inverse Nichols chart.

Also note that the upper bounds of the loop transmission function L_o(s) obtained by $|1/(1 + L_o(s))|_{dB}$ are a set of the closed-loop contours in the inverse Nichols chart.

2.2.3. Determine the Compensator G_c(s) and the prefilter F(s)

Once those bounds are determined, the shaping of the nominal loop transmission function L_o(s) can be obtained to satisfy the system response tolerance. The compensator G_c(s) is determined by using the relation G_c(s) = L_o(s)/P_o(s). Then, the prefilter F(s) is designed to make the system response satisfy the system performance.

Two choices for the nominal plant, the extreme value of the uncertain plant, will be selected as the nominal plant and the design procedures will be shown in the next Section.

3 CML structure with control inputs and output constraints under persistent bounded disturbances.

3.1. Problem statement

Consider the CML structure as shown in Figure 2., the control objective is to design a set of controllers G_{c1}(s), ..., G_{cn}(s) to satisfy

$$|y(t) - y_o(t)| \leq \gamma \tag{10}$$

subject to the constraints

$$|u_i(t) - u_{oi}(t)| \leq \beta_i, \; i = 1, 2, \ldots, n \tag{11}$$

on the control inputs for all time $t \in [0, \infty)$ due to a unit step disturbance, where γ and β_i, $i=1,\ldots,n$, represent scalar bounded constraints. And $y_o(t)$, $u_{oi}(t)$, $i=1,\ldots,n$, are the nominal values of control inputs and output constraints corresponding to the disturbance $\omega(s) = 0$. It is also desirable to reduce the cost of feedback as reflected by the bandwidth of each compensator. In other words, in order to reduce any noise amplification that tends to saturate the actuators, the bandwidth of each controller should be minimized.

The design procedures will be systematically presented as follows.

3.2. Design procedures

3.2.1. Target transfer function

The target transfer functions are chosen so that the unit step disturbance signal can be injected to verify that this target transfer function satisfies the time domain and bandwidth (rise time) constraints of the control inputs and system output. Let

$$T_y(s) \triangleq \frac{y(s)}{\omega(s)},$$

and

$$T_{ui}(s) \triangleq \frac{u_i(s)}{\omega(s)}, \; i = 1, \ldots, n,$$

denote those target transfer functions. Once the target transfer functions are determined, the equivalent external disturbances at the plant output will be obtained. Then, Lemma 2 will be applied to get the bounds. Without losing generality, it is assumed that the controller synthesis begins by opening all the inner loops except the outer most loop. Once the outer most loop controller is designed, the outer most inner loop is synthesized with the outer most loop controller in place. The design procedure is repeated until all the inner loops are closed.

3.2.2. Loop 1 closure:

Considered in this situation is that all the inputs $u_2(s)$ through $u_n(s)$ have been opened. The target transfer function $T_{u1}(s)$ from $\omega(s)$ to $u_1(s)$ is transferred to be an equivalent disturbance $T'_{u1}(s)$ from $\omega(s)$ to $u'_1(s)$ at plant output as shown in Figure 4. Then $T'_{u1}(s)$ can be treated as an input at $u''_1(s)$ denoted as an equivalent external disturbance $T''_{u1}(s)$ from $\omega(s)$ to $u''_1(s)$. The transfer function from $u''_1(s)$ to y(s) is

$$\frac{y(s)/\omega(s)}{u''_1(s)/\omega(s)} = \frac{T_y(s)}{T''_{u1}(s)} = \frac{1}{1 + L_1(s)},$$

where $L_1(s) = G_{c1}(s)G_1(s)P_1(s)$, and $T_y(s)$ and $T''_{u1}(s)$ are the maximum output variation and maximum equivalent disturbance variation respectively.

The values of bound for $L_1(s)$ will be obtained from Lemma 2. The loop transmission function $L_{1o}(s)$ and the compensator $G_{c1}(s)$ can be obtained from the conventional QFT method.

3.2.3. Loop 2 closure:

From Figure 2 where all the inputs $u_3(s)$ through $u_n(s)$ have been opened. The block diagram representation of this situation is shown in Figure 5. The two-loop closed loop transfer function from equivalent external disturbance $u''_2(s)$ and $u'_2(s)$ to output y(s) are

$$\frac{y(s)/\omega(s)}{u''_2(s)/\omega(s)} = \frac{T_y(s)}{T''_{u_2(s)}} = \frac{1}{1 + L_{12}(s)}, \tag{12}$$

and

$$\frac{y(s)/\omega(s)}{u'_2(s)/\omega(s)} = \frac{T_y(s)}{T'_{u_2}(s)} = \frac{1}{1 + L_1(s)} \frac{1}{1 + L_{12}(s)}, \tag{13}$$

where $L_1(s) = G_{c1}(s)G_1(s)P_1(s)$, $L_2(s) = G_{c2}(s)P_2(s)$, $L_{12}(s) = \frac{L_2(s)}{1+L_1(s)}$. Since

$$T''_{u_2}(s) = T'_{u_2}(s) \frac{1}{1 + L_1(s)} \tag{14}$$

and L_1(s) is obtained in loop 1 closure, L_{12}(s) will be determined from (13). L_2(s) can also be derived by

$$L_2(s) = L_{12}(s)(1 + L_1(s)). \tag{15}$$

Then the upper bounds of the loop transmission function L_2(s), which can be obtained by $|\frac{1}{1+L_2(s)}|_{db}$, is a set of closed-loop contours in the inverse Nichols chart. Once bounds on L_2(s) are obtained at each frequency, loop shaping L_2(s) and the compensator G_{c2}(s) can be determined.

3.2.4. Loop j closure:

After j-1 loops have been closed, i.e., G_{c1}(s), G_{c2}(s), ..., $G_{c(j-1)}$(s) have been determined accordingly. Next is to synthesize G_{cj}(s). Consider the block diagram shown in Figure 6 where u_{j+1}(s) through u_n(s) have been opened. Following the procedure outlined from the Loop 2 closure, the j-loop closed loop transfer function from equivalent external disturbance u_j''(s) and u_j'(s) to output y(s) are

$$\frac{y(s)/\omega(s)}{u_j''(s)/\omega(s)} = \frac{T_y(s)}{T_{u_j}''(s)} = \frac{1}{1 + L_{1j}(s)}, \tag{16}$$

and

$$\begin{aligned} \frac{y(s)/\omega(s)}{u_j'(s)/\omega(s)} = \frac{T_y(s)}{T_{u_j}'(s)} &= \frac{1}{1 + L_1(s) + L_2(s) + \ldots + L_{j-1}(s)} \frac{1}{1 + L_{1j}(s)} \\ &= \frac{1}{1 + L_1(s)} \frac{1}{1 + L_{12}(s)} \cdots \frac{1}{1 + L_{1(j-1)}(s)} \frac{1}{1 + L_{1j}(s)}, \end{aligned} \tag{17}$$

where $L_j(s) = G_{cj}(s)P_j(s)$, $L_{1j}(s) = \frac{L_j(s)}{1+L_1(s)+L_2(s)+\ldots+L_{j-1}(s)}$, and

$$\begin{aligned} T_{u_j}''(s) &= T_{u_j}'(s) \frac{1}{1 + L_1(s) + L_2(s) + \ldots + L_{j-1}(s)} \\ &= T_{u_j}'(s) \frac{1}{1 + L_1(s)} \frac{1}{1 + L_{12}(s)} \cdots \frac{1}{1 + L_{1(j-1)}(s)}. \end{aligned} \tag{18}$$

L_{1j}(s) can be derived from (17), (19) as well as the values obtained from previous loop closure procedures, i.e., L_1(s), L_{1i}(s), *i=2,...,j-1*. Then L_j(s) and G_{cj} will be obtained accordingly.

3.2.5. Outline of CML design procedures

(1) Obtain the target transfer functions T_y(s) and T_{ui}(s), *i=1,...,n*.

(2) Loop 1 closure: Transfer the target transfer function T_{u1}(s) to be the equivalent external disturbance T_{u1}''(s) at output. Using T_{u1}''(s), T_y(s), and Lemma 2, determine the bounds of L_1(s). Then, loop transmission function L_{1o}(s) and compensator G_{c1}(s) will be obtained through the conventional QFT method.

(3) Loop 2 closure: Transfer the target transfer function T_{u2}(s) to be the equivalent external disturbance T_{u2}''(s) at output. Using T_{u2}''(s), T_y(s), and Lemma 2, derive the bounds of L_{12}(s). Then, the bouds of L_2(s) will be obtained from equation (15). Once the bounds of L_2(s) is determined, loop transmission function L_{2o}(s) and compensator G_{c2}(s) will be obtained through the conventional QFT methods.

(4) As G_{c1}(s), G_{c2}(s), ..., G_{cn}(s) have been detemined, the design procedures is finished.

Presented in the next section as an example for the purpose of illustrating the proposed design technique is an Idle speed control of the V-6 fuel injection engine [4,5] which has a cascaded multiple-loop structure.

4. Illustrative examples

Example 1: (SISO uncertain plant tracking problem) Consider a system as shown in Figure 3a, where the plant is $P(s)=\frac{K}{s(s+a)}$, K $\in$ [1, 10], $a \in [0.2, 5]$, $|L/(1+L)| \leq 3$ db and the system response tolerance of time and frequency domains are shown in Figures 8 and 9 respectively.

Solution :

(a) Choose $P_o(s)$ as the maximum values of the uncertain plant, i.e., $P_o(s) = \frac{10}{s(s+0.2)}$, and $|T_o|_{db}$ as the maximum value of the system response tolerance. By using (8), the bounds and shape of the $L_o(s)$ will be obtained through the conventional QFT method as shown in Figure 7. The procedures of obtaining the values of bound are shown in Table 1.

Where the nominal loop transmission function $L_o(s)$ is

$$L_o(s) = \frac{576}{s} \frac{(\frac{s}{3}+1)(\frac{s}{20}+1)((\frac{s}{40}+1)}{(\frac{s}{0.2}+1)(\frac{s}{15}+1)(\frac{s}{32}+1)(\frac{s^2}{70^2}+\frac{1.1s}{70}s+1)},$$

and the prefilter F(s) is

$$F(s) = \frac{(\frac{s}{4}+1)(\frac{s}{65}+1)(\frac{s}{100}+1)(\frac{s}{150}+1)}{(\frac{s}{1.8}+1)(\frac{s}{10}+1)(\frac{s}{20}s+1)(\frac{s}{3450}+1)}.$$

Figure 8 shows that, as far as the four extremes of the uncertain plant are concerned, the frequency responses all fall inside of the system bounds. Similarly, the unit step responses also fall inside of the bounds as shown in Figure 9.

(b) Choose $P_o(s)$ as the minimum values of the uncertain plant, i.e., $P_o(s) = \frac{1}{s(s+5)}$, and $|T_o|_{db}$ as the minimum value of the system response tolerance. By using (8), the bounds can be obtained and the $L_o(s)$ can be shaped through the conventional QFT method as shown in Figure 10. The procedures of obtaining the values of bound are shown in Table 2. The nominal loop transmission function $L_o(s)$ is

$$L_o(s) = \frac{17.5}{5.5s} \frac{(\frac{s}{27}+1)(\frac{s}{50}+1)}{(\frac{s}{35}+1)(\frac{s}{70}+1)(\frac{s^2}{120^2}+\frac{2.2s}{120}+1)},$$

and the prefilter F(s) is

$$F(s) = \frac{(\frac{s}{6}+1)(\frac{s}{25}+1)}{(\frac{s}{2.5}+1)(\frac{s}{4.5}+1)(\frac{s}{40}s+1)}.$$

For the four extremes of the uncertain plant, the frequency responses all fall inside of the system bounds as shown in Figure 11, and the unit step responses also fall inside of the bounds as shown in Figure 12.

Discussion: The cost of feedback (COF) for a feedback system evaluated by the plant input with a sensor noise is defined as follows [1]

$$COF = \frac{L_o(s)}{P_o(s)}.$$

The COFs of these two nominal plants are demonstrated in the Bode plot as shown in Figure 13. It also includes for comparison the results of the method in [3] and conventional QFT method [3]. Results show that the proposed method which chooses P_o as the maximum value of the uncertain plant achieves the minimum COF, i.e., the minimum noise amplification.

Example 2: (CML idle speed control) The engine model linearized at an idle (steady-state) operating speed of 800 rpm has a parallel structure as shown in Figure 14 [4,5]. For a single scalar disturbance input ω, the control objective is to maintain the engine idle speed within a prespecified tolerance by using the ignition timing u_1 and idle valve setting u_2 as control inputs. The cascaded multiple loops structure corresponding to Figure 14 is shown in Figure 15. The transfer functions for each block shown in Figure 15 are

$$P_1(s) = \frac{s+3}{s^2+2.2s+5.62},$$

$$P_2(s) = \frac{1}{s^2 + 2.4s + 4.6},$$

$$G_1(s) = 15.9e^{-0.04s},$$

$$G_2(s) = 9.62e^{-0.16s},$$

and G_{c1}(s) and G_{c2}(s) are the controllers to be designed. At the steady-state operating condition, the maximum available control efforts and allowable engine speed variation are

$$\textit{Ignition timing} : \pm 20^o,$$

$$\textit{Idle air valve setting} : \pm 80 \textit{ counts},$$

$$\textit{Engine speed variation} : \pm 20 \textit{ rpm}$$

Moreover the bandwidth constraints of the ignition timing and idle valve are

$$\textit{Ignition timing} : \omega_S \geq 20 \textit{ rad./sec.},$$

$$\textit{Idle air valve setting} : \omega_I \geq 1 \textit{ rad./sec.}$$

where those lower bounds on the bandwidth assure a minimum rise time for the actuator. The G_{c1}(s) and G_{c2}(s) will be so designed that the prespecified constraints given above are satisfied when the engine is subject to a step torque disturbance of 15 Nm which represents the demands from an automotive air conditioner. It is also required that there should be no steady-state error in engine speed and ignition timing.

Solution: Since the idle valve and ignition timing control loops have delays of 0.16 second and 0.04 second respectively. [8] shows that for a first order model with time delay, its integral squared error of first order padé approximation for a unit step input will be about less than 1.57×10^{-5} when the delay time is less than 0.1. Thus, the first order padé approximation adopted for time delay terms is pertinent but it will cause a right half plane zero to the plant. Then, G_1(s) and G_2(s) can be expressed as follows:

$$G_1(s) = 15.9\frac{\frac{-s}{50} + 1}{\frac{s}{50} + 1},$$

$$G_2(s) = 9.62\frac{\frac{-s}{12.5} + 1}{\frac{s}{12.5} + 1}.$$

[9] shows that the maximum achievable bandwidth for each loop with non-minimum phase system is limited. The maximum cross over frequency of the idle air valve loop with a 0.16 second time delay should be limited to about $\omega_I \leq 0.5 \times \frac{1}{0.16/2} = 6.25$ rad./sec. for phase margin 36.8^o. Similarly, for a 36.8^o phase margin on the ignition timing loop, the cross over frequency can be limited to about $\omega_s \leq 0.5 \times \frac{1}{0.04/2} = 25$ rad./sec.. Thus, the bandwidth constraints of those two loops are

$$\textit{Ignition timing} : 25 \geq \omega_S \geq 20 \textit{ rad./sec.},$$

$$\textit{Idle air valve setting} : 6.25 \geq \omega_I \geq 1 \textit{ rad./sec.}$$

Based on the maximum available control efforts, allowable engine speed variation and bandwidth limitations, the design procedures will be presented as follows.

(1) The target transfer functions chosen to satisfy the maximum available control efforts and allowable engine speed variation are

$$\frac{u_1(s)}{\omega(s)} = T_{u1}(s) = \frac{20}{\frac{s}{10} + 1},$$

$$\frac{u_2(s)}{\omega(s)} = T_{u2}(s) = \frac{80}{\frac{s}{5} + 1},$$

$$\frac{y(s)}{\omega(s)} = T_y(s) = \frac{20}{\frac{s}{10} + 1}(1 - \frac{1}{(\frac{3s}{4} + 1)^4})$$

(2) Loop 1 (ignition loop) closure: From Figure 16, the equivalent external disturbance derived from the target transfer function is

$$T'_{u1}(s) = T''_{u1}(s) = T_{u1}(s)P_1(s) = \frac{20}{\frac{s}{10}+1}\frac{s+3}{s^2+2.2s+5.62}$$

The transfer function from u''_1(s) to y(s) is

$$\frac{y(s)/\omega(s)}{u''_1(s)/\omega(s)} = \frac{T_y(s)}{T''_{u1}(s)} = \frac{1}{1+L_1(s)}$$

The values of bound at some specified frequencies will be obtained from Lemma 2. The procedures of obtaining the values of bound and phase shift due to right half plane zero are shown in Table .3. Since $G_1(s)P_1(s)$ is a non-minimum phase plant, the method of [10] is adopted. The nominal minimum phase plant P_{1o}(s) and N_{1o}(s) are

$$P_{1o}(s) = \frac{s+3}{s^2+2.2s+5.62}\frac{15.9}{\frac{s}{50}+1},$$

$$N_{1o}(s) = \frac{s}{50}+1.$$

From Table 3, the minimum phase bounds B_{1mo} and non-minimum phase bounds B_{1no} are shown in Figure 17 respectively. According to B_{1no} and bandwidth limitation, the loop transmission function L_{1mo}(s) is

$$L_{1mo}(s) = \frac{9.15}{\frac{s}{1000}+1}\frac{\frac{s}{3}+1}{\frac{s^2}{5.62}+\frac{2.2s}{5.62}+1}.$$

Then compensator G_{c1}(s) is

$$G_{c1}(s) = \frac{L_{1mo}(s)}{P_{1o}(s)N_{1o}(s)} = \frac{1.078}{\frac{s}{1000}+1}.$$

(3) Loop 2 (idle air valve loop) closure: From Figure 18, the equivalent external disturbance obtained from target transfer function are

$$T'_{u2}(s) = T_{u2}(s)P_2(s) = \frac{80}{\frac{s}{5}+1}\frac{1}{s^2+2.4s+4.6},$$

and

$$T''_{u2}(s) = T'_{u2}(s)\frac{1}{1+L_1(s)}.$$

The transfer function from u''_2(s) to y(s) is

$$\frac{y(s)/\omega(s)}{u''_2(s)/\omega(s)} = \frac{T_y(s)}{T''_{u2}(s)} = \frac{1}{1+L_{12}(s)}$$

where $L_{12}(s) = \frac{L_2(s)}{1+L_1(s)}$, $L_1(s) = G_{c1}(s)G_1(s)P_1(s)$, $L_2(s) = G_{c2}(s)G_2(s)P_2(s)$. Since $L_2(s) = L_{12}(s)(1+L_1(s))$, the values of bound for $L_{12}(s)$ and $L_2(s)$ at some specified frequencies will be determined. The procedures of obtaining the values of bound and phase shift due to right half plane zero are shown in Table 4. Since $G_2(s)P_2(s)$ is a non-minimum phase plant, the nominal minimum phase plant $P_{2o}(s)$ and $N_{2o}(s)$ are

$$P_{2o}(s) = \frac{1}{s^2+2.4s+4.6}\frac{9.62}{\frac{s}{12.5}+1},$$

$$N_{2o}(s) = (\frac{s}{12.5}+1).$$

From Table 4, the minimum phase bounds B_{2mo} and non-minimum phase bounds B_{2no} are shown in Figure 19 respectively. According to B_{1no} and bandwidth limitation, the loop transmission function L_{2mo}(s) is

$$L_{2mo}(s) = \frac{7.1}{s} \frac{1}{\frac{s^2}{4.6} + \frac{2.4s}{4.6} + 1}$$

Then compensator G_{c2}(s) is

$$G_{c2}(s) = \frac{L_{2mo}(s)}{P_{2o}(s)N_{2o}(s)} = \frac{3.395}{s}$$

(4) Discussion: As G_{c1}(s) and G_{c2}(s) have been obtained, the time domain responses of the cascaded two loops idle speed control system are shown in Figure 20 for a 15 Nm disturbance torque. The results show that the two inputs and the engine speed remain within the prespecified time domain tolerance. The transient and steady-state responses are fairly good when compared with the QFT-type design methods [5] as shown in Figure 20. Although the H_∞ controllers were not given by [5], its results was not provided in Figure 20. However, judging from the disturbance responses shown in Figure 20 and that in [4], the transient responses are also extremely good when compared with the H_∞ design method [4]. Furthermore, in [4] and [5], they all have two three-state compensators, while the controllers obtained via the proposed approach consist of just two one-state compensators. Apparently it paves a better way for hardware implementation and experimental evaluation.

5. Concluding remarks

In the alternative concept of plant uncertainty, no matter which nominal plant of the uncertain plant is chosen, very similar results will be obtained. Therefore, through the concept of equivalent external disturbance, the EDR method can also be extended to solve the cascaded multiple loops system with control inputs and output constraints under a persistent bounded disturbance. The result shows EDR is an effective and easy frequency domain design methodology for the idle speed control of a V-6 fuel injection engine. Even though the plant uncertainty is not considered in this example, the equivalent external disturbance which implicitly includes the plant uncertainty demonstrates the robustness inherent in the system.

Reference

[1] Horowitz, I., and Sidi, M., Synthesis of feedback systems with large plant ignorance for prescribed time-domain tolerances. Int. J. Control, vol.16, No.2, pp.287-309, 1972.

[2] Horowitz, I. M., Quantitative synthesis of uncertain multiple input-output feedback system. Int. J. Control, Vol.30, No.1, pp.81–106, 1979.

[3] Chien,C.M. and Wang,B.C., An SISO Uncertain System Designed by An Equivalent Disturbance Attenuation Method. Control Theory and Advanced Technology, 6, pp.257-271, 1990, Japan.

[4] Williams, S. J.,Hrovat, D., Davey, C., Maclay, D., Crevel, J. W. v., Chen, L. F., Idle speed control design using an H-infinity approach. proceedings of the ACC, pp.1950-1956, Pittsburgh, Pennsylvania,1989, U.S.A.

[5] Jayasuriya, S., Franchek, M, A., A QFT-type design methodology for a parallel plant structure and its application in idle speed control. Int. J. Control, vol.60, No.5, pp.653-570, 1994.

[6] Jayasuriya, S., Franchek, M, A., Frequency domain design for a maximum rejection of persistent bounded disturbance. Journal of Dynamics Systems, Measurement and Control, 113, pp.195-205, 1991.

[7] Sobhani, M., Jayasuriya, S., Control design for the size of a step disturbance in non-minumim phase, unstable uncertain systems. Int. J. Control, vol.59, No.2, pp.561-581, 1994.

[8] Xue, D., Atherton, D. P., A suboptimal reduction algorithm for linear systems with a time delay. Int. J. Control, vol.60, No.2, pp.181-196, 1994.

[9] Horowitz, I., Liao, Y. K., Limitations of non-minimum-phase feedback systems. Int. J. Control, vol.40, No.5, pp.1003-1013, 1984.

[10] Horowitz, I., Sidi, M., Optimum synthesis of non-minimum phase feedback systems with plant uncertainty. Int. J. Control, vol.27, No.3, pp.361-386, 1978.

Table 1. Values of bound

ω	$\lvert T_o\rvert_{db}$	$\lvert T_{min}\rvert_{db}$	$v_t = \frac{T_o}{T}$	$v_p = \frac{P_o}{P}$	L_o (8)	$\lvert\frac{1}{(1+L_o)}\rvert_{db}$
1	0.5	-2.5	1.4125	50	117.7771	-41.4947
2	0.7	-6.25	2.2259	26.7922	20.0399	-26.4609
5	-1.78	-15	4.5814	14.1308	2.6664	-11.2847
10	-7.1	-25	7.8524	11.1781	0.4853	-3.4365
20	-13.4	-39.3	19.7242	10.3072	-0.5029	6.0717

Table 2. Values of bound

ω	$\lvert T_o\rvert_{db}$	$\lvert T_{max}\rvert_{db}$	$v_t = \frac{T_o}{T}$	$v_p = \frac{P_o}{P}$	L_o (8)	$\lvert\frac{1}{(1+L_o)}\rvert_{db}$
1	-2.5	0.5	0.7079	0.02	2.3555	-10.5153
2	-6.25	0.7	0.4493	0.0373	0.7480	-4.8507
5	-15	-1.78	0.2183	0.0708	0.1887	-1.5014
10	-25	-7.1	0.1274	0.0895	0.0434	-0.3692
20	-39.3	-13.4	0.0507	0.0970	-0.0488	0.4345

Table 3. Values of bound

ω	T_y	T''_{u1}	L_1 (8)	$\lvert\frac{1}{(1+L_1)}\rvert_{db}$	phase shift (°)
0.05	2.9933	10.6802	3.8563	-13.7260	-0.1146
0.1	5.9468	10.6924	0.9593	-5.8421	-0.2292
0.2	11.5755	10.7411	-0.0789	0.7142	-0.4584
2	20.9533	15.0809	-0.2943	3.0277	-4.5812
5	17.8495	4.6808	-0.7815	13.2129	-11.4212

Table 4. Values of bound

ω	T_y	T''_{u2}	L_{12} (8)	L_2(15)	$\lvert\frac{1}{(1+L_2)}\rvert_{db}$	phase shift (°)
0.05	2.9933	3.5817	0.2952	1.4335	-7.7245	-0.4584
0.2	11.5759	18.9269	0.6951	0.6402	-4.2981	-1.8333
0.5	23.8216	39.9833	0.7082	0.3124	-2.3616	-4.5812
2	20.9533	21.7587	0.0404	0.0258	-0.2440	-18.1806
3	19.2320	14.8816	-0.2386	-0.1304	1.2132	-26.9915
5	17.8495	10.9387	-0.4101	-0.0896	0.8155	-43.6028

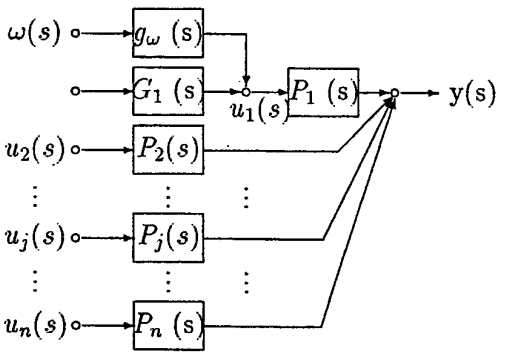

Figure 1. General multiple-input-single-output (MISO) parallel structure system

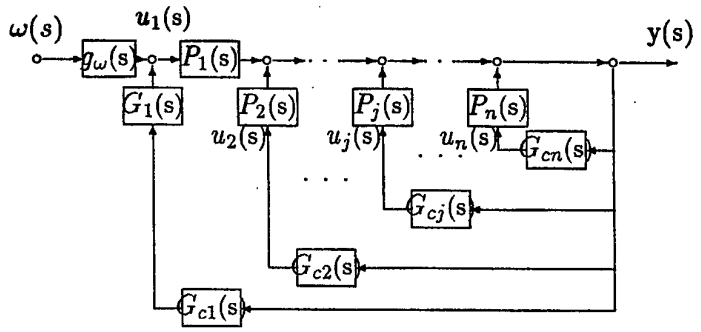

Figure 2. General cascaded multiple-loop (CML) system

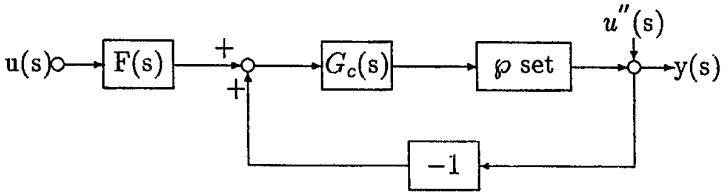

Figure 3a. 2DOF feedback system

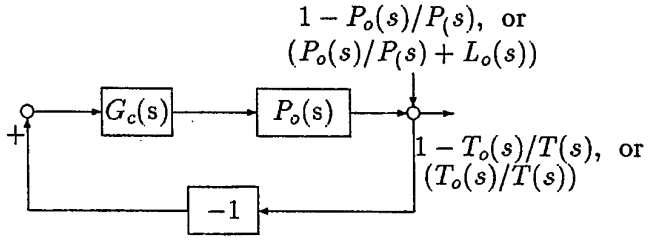

Figure 3b. A EDR system

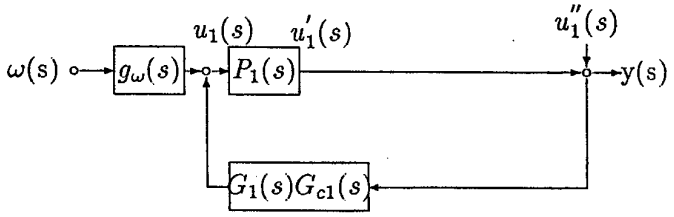

Figure 4. Loop 1 closure

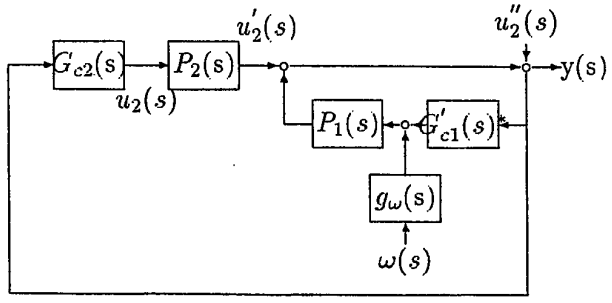

*$G'_{c1}(s) = G_1(s)G_{c1}(s)$

Figure 5. Loop 2 closure

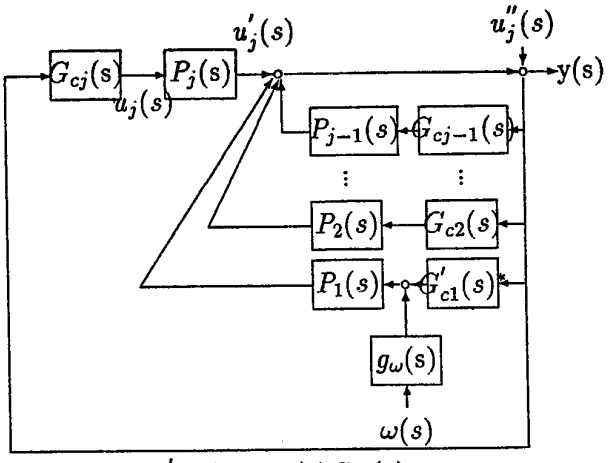

$^*G'_{c1}(s) = G_1(s)G_{c1}(s)$

Figure 6. Loop j closure

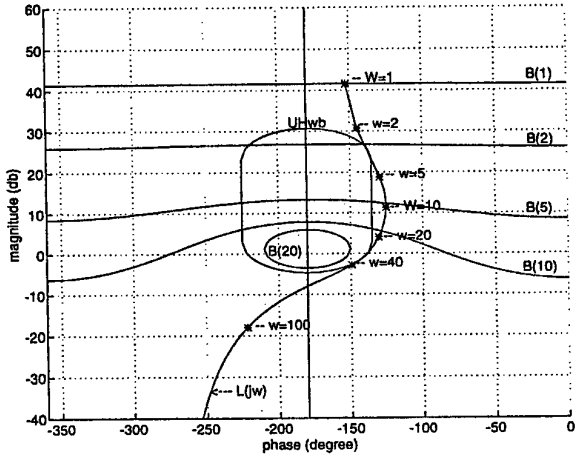

Fig. 7. Bounds on the inverse Nichols chart and L_o - example 1(a)

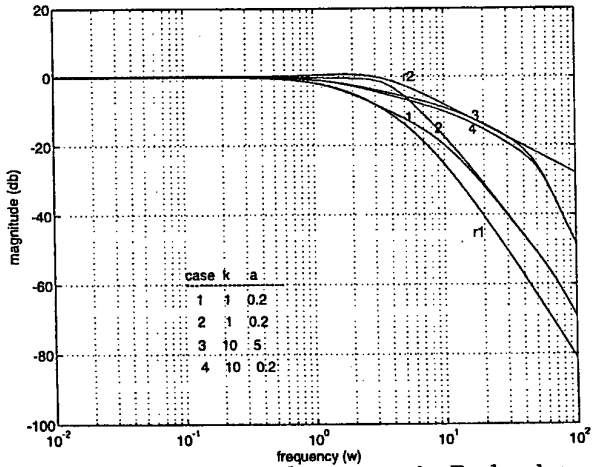

Fig. 8. Freq. domain spec. and response in Bode plot - example 1 (a)

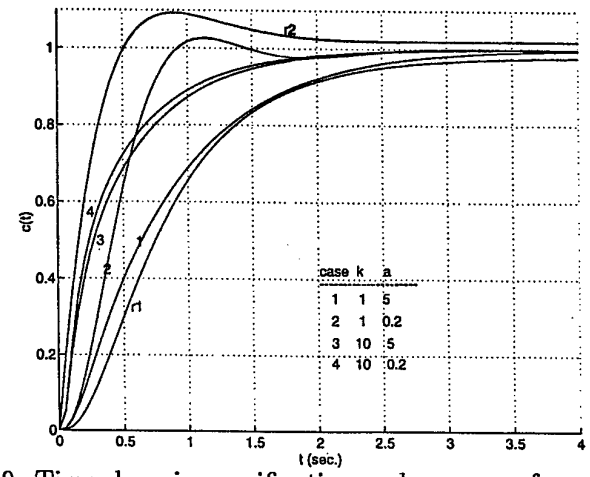

Fig. 9. Time domain specification and response for example 1 (a)

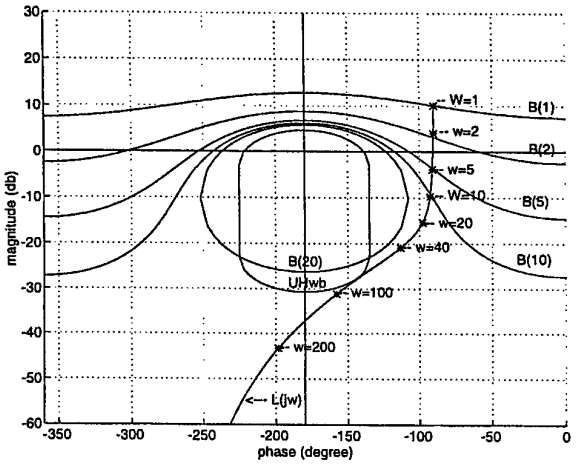

Fig. 10. Bounds on the inverse Nichols chart and L_o for example 1 (b)

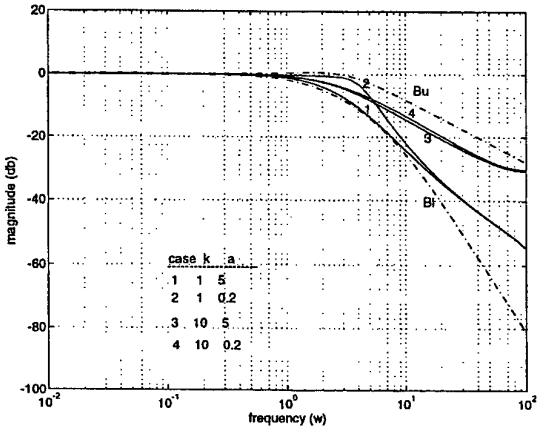

Fig. 11. Freq. domain spec. and response in Bode plot - example 1 (b)

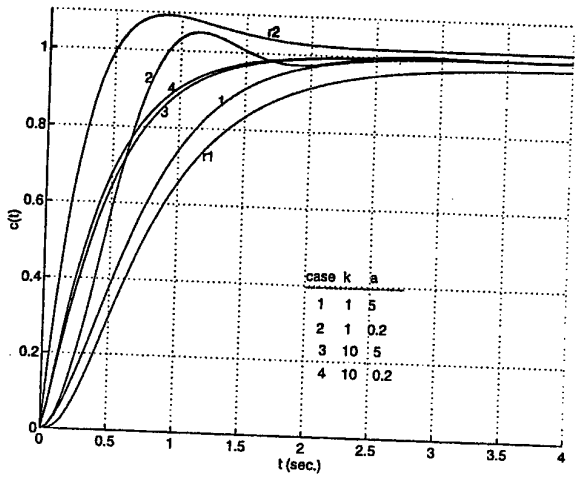

Figure 12. Time domain specification and response for example 1 (b)

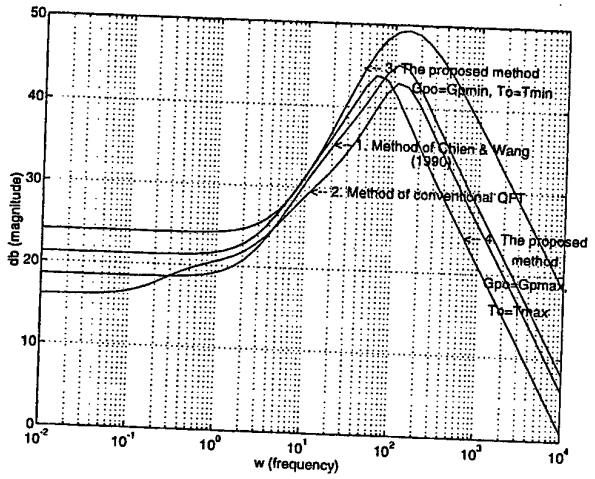

Figure 13. Bode plot of cost of feedback

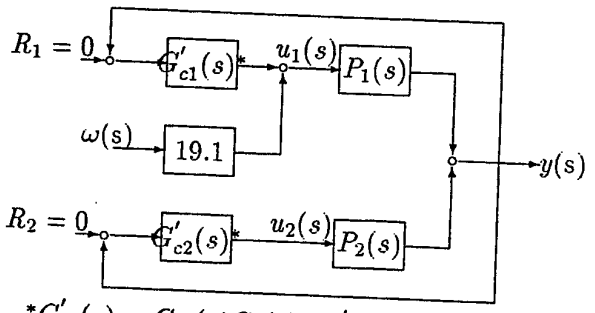

$^*G'_{c1}(s) = G_{c1}(s)G_1(s),\ G'_{c2}(s) = G_{c2}(s)G_2(s)$

Figure 14. Parallel structure of V-6 fuel engine model

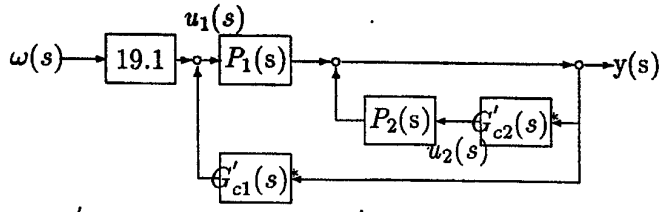

$^*G'_{c1}(s) = G_1(s)G_{c1}(s),\ G'_{c2}(s) = G_2(s)G_{c2}(s)$

Figure 15. Cascaded multiple-loop structure of V-6 fuel engine model

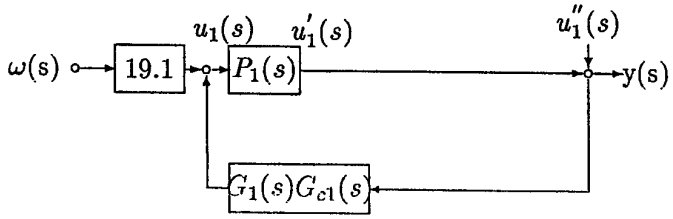

Figure 16. Loop 1 (Ignition timing) closure

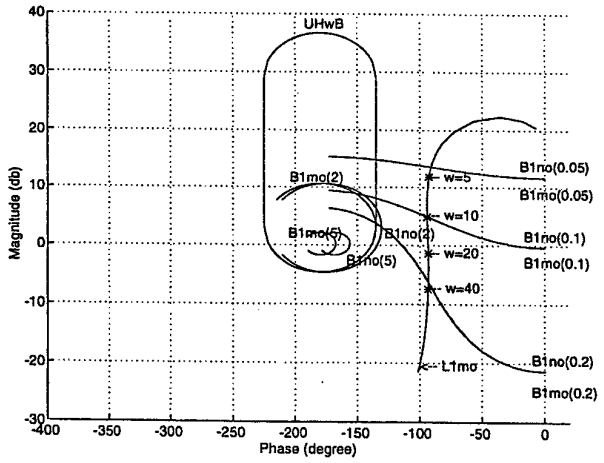

Figure 17. Bounds on inverse Nichols chart and $L_{1mo}(s)$

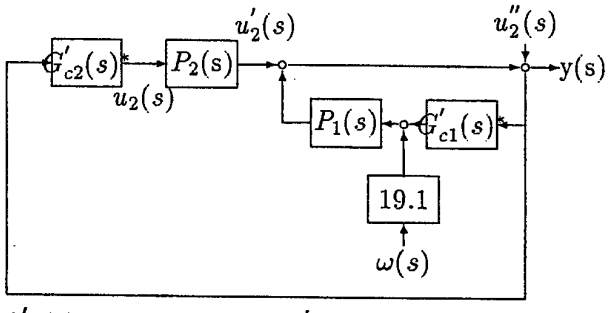

$^*G'_{c1}(s) = G_1(s)G_{c1}(s),\ G'_{c2}(s) = G_{c2}(s)G_2(s)$

Figure 18. Loop 2 (Idle air valve) closure

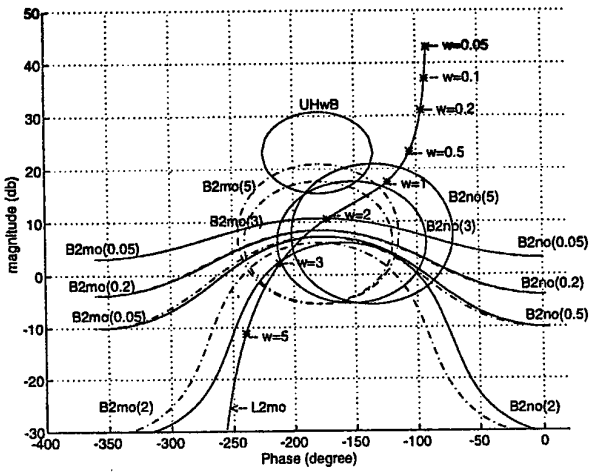

Figure 19. Bounds on inverse Nichols chart and $L_{2mo}(s)$

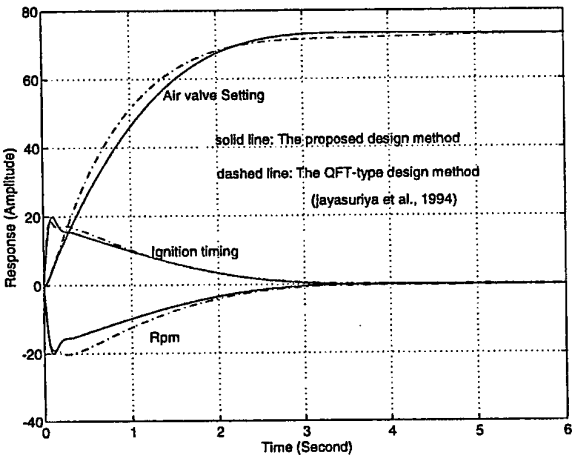

Fig. 20. 15 Nm step torque disturbance responses of a V-6 injection engine

1999 International Symposium on
Quantitative Feedback Theory and Robust Frequency Domain Methods

ROBUST CONTROL OF A TRIPLE-EFFECT EVAPORATOR
A desktop case study

Pierre Greeff and Phillip L. de Vaal
Department of Chemical Engineering, University of Pretoria, Pretoria, 0002

ABSTRACT
Multiple-effect evaporators are integrated by their nature and as such provide a good candidate process for evaluating multivariable control schemes. The aim of this work was to test the applicability and utility of linear robust analysis tools when applied to a typical chemical engineering operation. A linear nominal plant with bounded perturbations describing the entire range of plant operating conditions was found. Useful information could be obtained from robust analysis.

1. INTRODUCTION

The need for feedback control originates from uncertainty; either model uncertainty or uncertain disturbances. Model uncertainty has several sources (Skogestad & Morari, 1987; Morari & Zaffiriou, 1989): processes that are not fully understood, the application of linearised models to inherently non-linear processes, the variation of process parameters over time and with operating point, neglected dynamics, etc.

Tools for analysing the robustness of linear systems have been developed by several workers (Doyle, 1982; Postlethwaite, Edmunds & MacFarlane, 1982; Kouvaritakis & Latchman, 1985a,b; Skogestad & Morari, 1987; etc.). Firstly, the family of all possible plants is described by perturbing a linear, nominal plant model with a bounded uncertainty matrix. As the perturbation varies over the allowed bounds, a set of plants encompassing the family of possible plants is generated. Following this, the stability and performance of the entire set of plants can now be evaluated in a second step. This is discussed further in section 2.

In this study the applicability and utility of linear multivariable robustness techniques to a typical chemical engineering system was investigated. In particular the difficulties associated with obtaining an uncertainty description was considered. It appears as if the second step in the discussion above has received far more attention than the first. Of course even the most elegant mathematical tools used in the second step, have their usefulness determined by the accuracy and ease with which the first step can be completed.

In order to facilitate investigation of the relevant phenomena in a fast, efficient and safe manner, it was decided to create a rigorous computer model of a typical chemical engineering process. A triple-effect evaporator was chosen for this purpose. Multiple-effect evaporators are integrated by their nature and as such provide a good candidate process for evaluating multivariable control schemes. After implementation the computer model was regarded as a "black box" in subsequent work. The plant is described further in section 3.

Following this an identification procedure was used to find a nominal, linear model with bounded perturbation describing the entire operating range of the plant. The identification procedure used directly resulted in a frequency domain plant description. Multivariable controllers were designed for the nominal model. This is discussed in sections 4 and 5 respectively. Hereafter robust analysis was applied to the resulting closed loop system. This is discussed in section 6.

2. LINEAR ROBUST ANALYSIS AND THE MΔ-STRUCTURE

2.1 EVALUATING NOMINAL PERFORMANCE

Consider the nominal feedback loop shown in figure 1.

It follows that the error, e(s), is given by

$$e(s) = S(s)r(s) - S(s)G_d(s)d(s) \qquad (1)$$

with the sensitivity, S, given by

$$S(s) = [I + G(s)K(s)]^{-1} \tag{2}$$

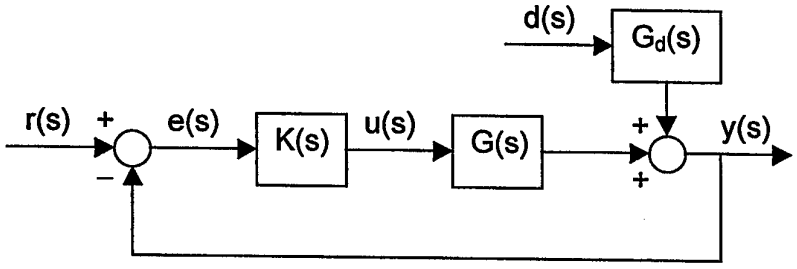

Figure 1: *Nominal feedback loop*

With reference to (1), it follows that the performance of the feedback loop can be evaluated by considering its sensitivity function. A typical performance specification is given by the weighted sensitivity (Skogestad & Postlethwaite, 1996):

$$\|W_P(s)S(s)\|_\infty < 1 \tag{3}$$

with a typical weighting function given by

$$W_P(s) = diag\left\{\frac{s/M_1 + \omega_{B,1}}{s + \omega_{B,1}A_1}, \ldots, \frac{s/M_j + \omega_{B,j}}{s + \omega_{B,j}A_j}, \ldots\right\} \tag{4}$$

where M_j = peak height of S (typically a value of 2 is used)
ω_{BJ} = bandwidth (related to the speed of response)
A_J = value of S at low frequencies (steady state error)

2.2 THE MΔ-STRUCTURE

The family of all possible plants is described by perturbing a linear, perfectly known, nominal plant model with bounded sources of uncertainty, δ's (Skogestad & Morari, 1987). Three commonly used perturbations are: additive, input- and output multiplicative (Maciejowski, 1989). As the δ's vary over the allowed bounds, a set of plants encompassing the family of possible plants is generated.

The only bounds considered restrict the spectral nom of the δ's, $\sigma^*(\delta) \leq a$, disregarding any phase information. In what follows δ refers to the smallest uncertainty element with a bound imposed on it.

It is always possible to isolate all sources of uncertainty, all δ's, into a single block-diagonal matrix, Δ

$$\Delta = diag\{\delta_1, \delta_2, \ldots, \delta_m\} \tag{5}$$

Of course each of the blocks has a specific size. The only allowed Δ-matrices are the ones with the required block-diagonal structure that satisfy the constraints on the individual blocks. Let the set of block-diagonal matrices with the required structure be denoted by BD_∞. This is commonly represented using the so-called MΔ-structure shown in figure 2.

M is partitioned so that $\begin{pmatrix} y \\ x \end{pmatrix} = \begin{pmatrix} M_{11} & M_{12} \\ M_{21} & M_{22} \end{pmatrix} \begin{pmatrix} v \\ z \end{pmatrix}$ (6)

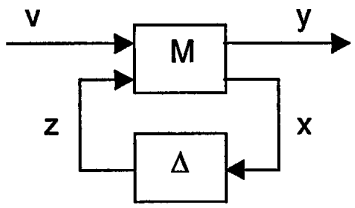

Figure 2: *MΔ-structure*

It is customary to include scaling matrices in M so that the uncertainty bounds are all reduced to

$$\sigma^*(\delta_i) \leq 1 \quad , \quad \forall \omega, \forall i \tag{7}$$

2.3 ROBUST STABILITY

It can be shown (Doyle ,1982) that for the class of perturbations considered here, robust stability is achieved if and only if

$$\mu(M_{22}(j\omega)) < 1, \quad \forall \omega \tag{8}$$

given that scaling as described above has been performed and nominal stability achieved. Analysing robust stability is hereby reduced to evaluating an upper bound on a scalar function of frequency, namely μ or the structured singular value (SSV). Although the SSV itself can not be calculated, fairly accurate upper bounds can be established (Maciejowski, 1989).

2.4 ROBUST PERFORMANCE

It can be shown that robust performance can be evaluated using only the theory developed thus far. A fictitious, full-block inverse output multiplicative uncertainty, Δ_P, is added to the plant. Using the main loop theorem from Packard & Doyle (1993), it can be shown that robust performance is equivalent to robust stability with respect to the appended uncertainty, diag{Δ_P,Δ}.

3. PLANT DESCRIPTION

The plant considered is a triple-effect, falling film evaporator used for concentrating a solution of water and a non-volatile solute. Steam generated in one effect is used as heating medium in the next effect. (Effects are numbered in the direction of steam flow). Process flow is from the 3rd effect to the 1st, and from there to the 2nd. The controlled variables are the final product composition ($X_{p,2}$, the process fluid leaving the second effect), and the heights in all the sumps (h_1, h_2 and h_3). The manipulated variables are the flow rate of fresh steam, V_{st}, and the process flows from all the effects ($F_{p,1}$, $F_{p,2}$ and $F_{p,3}$). The most important disturbances acting on the process are the feed flow rate (F_{feed}) and composition (X_{feed}).

The range of operating conditions of these variables is shown in table 1.

Table 1: *Range of operating conditions*

VARIABLE	UNITS	MINIMUM	MAXIMUM
F_{feed}	kg/s	2,3777	4,4157
X_{feed}	Mass/mass	0,075	0,1
V_{st}	kg/s	0,1983	0,7583
$F_{p,1}$	kg/s	0,2001	2,2001
$F_{p,2}$	kg/s	0,1184	1,1184
$F_{p,3}$	kg/s	0,8942	4,8942
$X_{p,2}$	Mass/mass	0,392	0,557
h_1	M	0,2	0,5
h_2	M	0,24	0,54
h_3	M	0,24	0,54

4. DETERMINATION OF NOMINAL MODEL AND UNCERTAINTY

There are a number of templates that can be used for describing parametric SISO uncertainty; gain uncertainty, pole uncertainty, zero uncertainty etc. (Skogestad & Postlethwaite, 1996). It is also stated that very often a lumped description yields good results, especially where neglected dynamics or a number of parametric uncertainties need to be considered. For the MIMO case such standard templates are not so abundant. When uncertainty can be attributed to measurement or manipulated variable uncertainty, use of respectively diagonal output and -input perturbations, is justified (Skogestad & Postlethwaite, 1996). For general cases no clear guidelines exist. The problem of course being that all multiplicative perturbations affect either entire rows or columns.

When approaching the uncertainty description for this plant, there were really two questions to be answered. First of all the choice of nominal plant model, secondly the choice of uncertainty description and uncertainty bounds. It was decided to make use of independent , additive uncertainty in the transfer function matrix elements. This can be written as:

$$\begin{pmatrix} X_{p,2} \\ h_1 \\ h_2 \\ h_3 \end{pmatrix} = G \begin{pmatrix} V_{st} \\ F_{p,1} \\ F_{p,2} \\ F_{p,3} \end{pmatrix} + \Delta \begin{pmatrix} V_{st} \\ F_{p,1} \\ F_{p,2} \\ F_{p,3} \end{pmatrix} \tag{9}$$

where G is the nominal plant and each element of Δ satisfies:

$$\sigma^*(\delta_{i,j}) \leq a_{i,j} \tag{10}$$

This type of uncertainty description is potentially very conservative, since it does not allow for coupling between elements, but allows them to vary independently (Morari & Zafiriou, 1989). Also, such descriptions may prove to be quite useless for plants with large RGA elements (Skogestad & Postlethwaite, 1996). This was not the case here.

This type of uncertainty description however has the advantage that it reduces the choice of nominal plant model and perturbation norm to a number of SISO problems. It is now simple to find a useful nominal plant model. Similar to Skogestad & Postelthwaite (1996), it was decided to use the central plant (corresponding to the smallest norm bound on the uncertainty). Since the uncertainty is norm-bounded and phase information disregarded, the resulting uncertainty regions are disk-shaped. The smallest uncertainty bound therefore corresponds to the smallest disk.

The identification problem can now be formulated as: for each transfer function matrix element, find the nominal plant, $g_{i,j}$, so that the smallest possible bound on the uncertainty, $\sigma^*(\delta_{i,j})<a_{i,j}$, describes the entire range of possible plants.

The following procedure yielded a nominal model with uncertainty description describing the entire range of plant operation in table 1, directly in the frequency domain. The results were calculated over a discrete grid of frequency values.

- Pulse tests were performed at a large number of possible operating points and the results Fourier transformed. This resulted in a number of points in the complex plane for each input output pair, at each frequency.
- The smallest circle including this set of points for each input output pair at each frequency was now determined. This was done using the novel algorithm below.
- The nominal plant, $g_{i,j}$, was defined as the centre of the circle.
- The additive uncertainty norm bound, $a_{j,j}$, was defined as the radius of the circle.

The smallest circle through any 2 points is the circle with the 2 points on a diameter. Further, a circle in the plane is uniquely determined by any 3 points on it's boundary, except where two points corresponding to a diameter is given. This leads to the following algorithm for finding the smallest circle enclosing a number of points in the complex plane:

- All possible combinations of two points from the set of possible plants were selected and the two points yielding the largest distance retained.
- If all points are included in the circle constructed using the two retained points as the end-point of a diameter, stop. This is the desired circle.
- Else
  - Select all possible combinations of three points
  - Construct a circle through the three points. This can be conveniently done using a result concerning central lead lines from geometry (Baker & Bourne, 1920).
  - The smallest circle including all points is the desired circle.
  - Stop

Typical results are shown in figures 3 and 4.

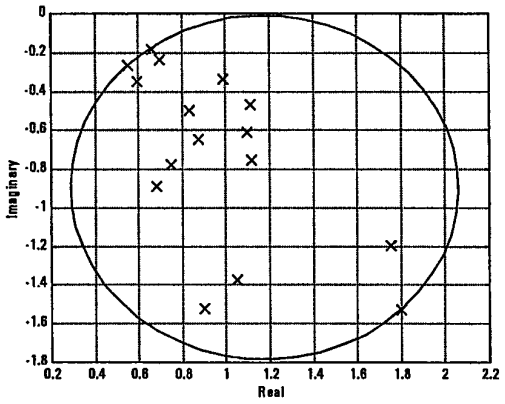

Figure 3: *Family of possible plants and least conservative norm-bound for* $g_{1,1}(\omega=6,707\times10\text{-}4)$

It was found that 11 of the 16 transfer function matrix elements had significant size, indicating a multivariable problem, namely entries $g_{1,1}$, $g_{2,1}$, $g_{3,1}$, $g_{4,1}$, $g_{1,2}$, $g_{2,2}$, $g_{3,2}$, $g_{3,3}$, $g_{1,4}$, $g_{2,4}$ and $g_{4,4}$. Furthermore, sizeable uncertainty (more than 10 % of the nominal plant magnitudes) was present in 7 of these elements, namely entries $g_{1,1}$, $g_{1,2}$, $g_{1,4}$, $g_{2,1}$, $g_{3,1}$, $g_{4,1}$ and $g_{3,2}$.

A full-block output multiplicative uncertainty could also have been used in this case. It is however not a simple matter to find the nominal plant model for this type of description. Picking the centre of the operating range as the nominal model does not necessarily result in the smallest uncertainty bound. In fact the nominal model corresponding to the centre of the operating range resulted in a useless uncertainty description when tried for the additive case. The region of possible plants was not symmetric around this operating point. However the point furthest away determines the size of the uncertainty bound. The resulting disk covered the origin, implying a sign change of the model. The family of plants allowed by such a description can never be integral controllable (Skogestad & Morari, 1987).

Three serious limitations of the proposed methodology should however be stated. Performing a sufficient number of identification runs on real equipment may prove to be prohibitive. This procedure could however be applied to a rigorous model, as was done here. Independent uncertainty in the transfer function matrix elements may be very conservative, since coupling between elements is not taken into account. A simple way of circumventing this difficulty is however not apparent. Lastly, a lot of the uncertainty considered here, is in fact well known non-linearity. An approach allowing for this will surely prove superior.

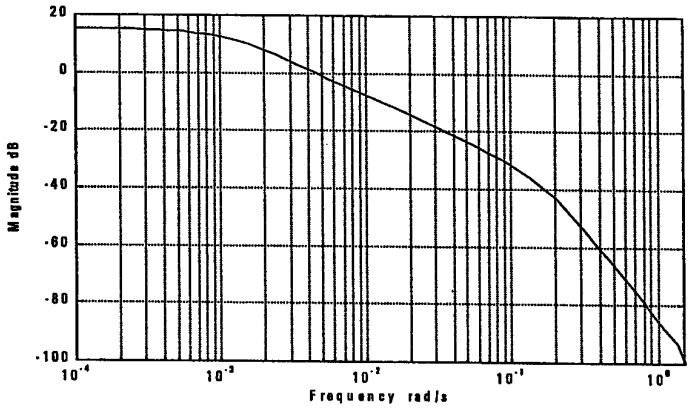

Figure 4a: $g_{1,1}$ - *amplitude ratio*

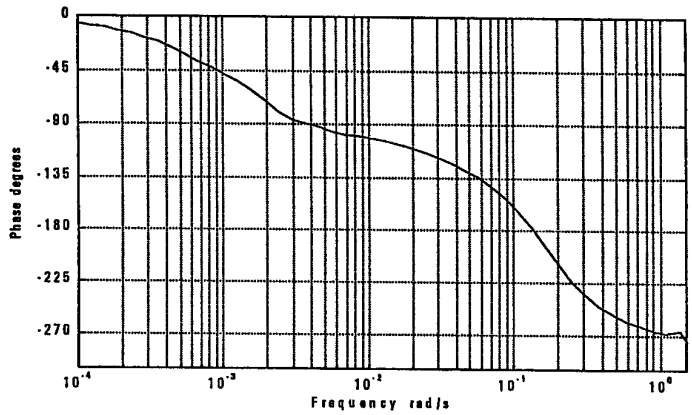

Figure 4b: $g_{1,1}$ - *phase angle*

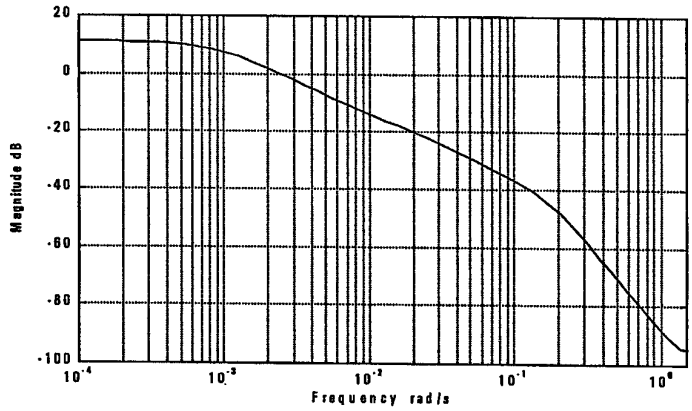

Figure 4c: $a_{1,1}$ - *magnitude*

5. CONTROLLER DESIGN

Given that the frequency response of the nominal plant was determined directly during the identification, it was decided to perform controller design using an algorithm requiring only the frequency response of the nominal plant. Use was made of the characteristic locus method (MafFarlane & Belletruti, 1973; MacFarlane & Kouvaritakis, 1977). The aim of this design method is to directly shape the plant's characteristic loci, using approximately commutative controllers at high, medium and low frequency.

The designed controller was subsequently used for robust analysis.

6. ROBUST ANALYSIS

In order to perform robust analysis as discussed in section 2, all that is required is frequency responses. These are available over a discrete grid for the nominal plant and uncertainty bounds, and can be quite easily calculated for the controller over the same grid, by simply applying the substitution rule.

In Agamennoni et al (1989) a controller is designed and then detuned trhough multiplication with a scalar constant, q. This is done in order to try and better meet robustness requirements. Here nominal stability, robust stability, nominal perfromance and robust performance were investigated over a range of q values, namely q = 0,1; 0,25; 0,5; 0,75; 1 and 1,25.

6.1 NOMINAL STABILITY

Applying the standard Nyquist test it was found that the closed loop system was stable over the entire range of controller detunings, values of q, investigated. It is imperative that nominal stability be ensured prior to investigating robust stability and performance using the techniques outlined in section 2.

6.2 ROBUST STABILITY

As indicated in section 4, 7 of the 16 elements showed significant uncertainty. Two of these, namely $g_{3,1}$ and $g_{3,2}$, however have h_2 as output. Since the manipulated variable associated with h_2, $F_{p,2}$, does not affect any other output variable, this uncertainty can not lead to instability. Attempts to include these 2 elements result in singular matrices, since no mechanism exists whereby uncertainty in these two elements can be fed back into the system.

The approach to casting the robust stability problem with independent uncertainty in the transfer function matrix elements into the standard block-diagonal form used by the MΔ-structure used here and subsequently, follows Morari & Zafiriou (1989). The MΔ-structure for this problem is shown in figure 5.

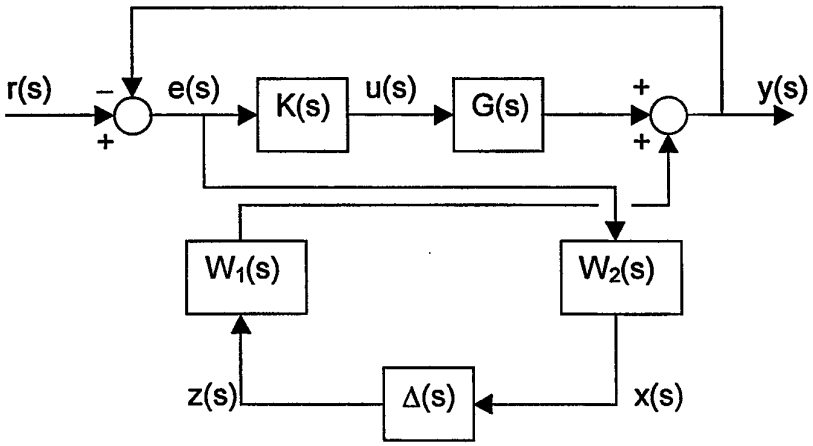

Figure 5: *MΔ-structure for additive uncertainty*

W_1 and W_2 are scaling matrices making Δ(s) a block diagonal matrix with unit norm-bounds on the individual blocks. All blocks are 1×1. Δ, W_1 and W_2 are given by:

$$\Delta(s) = diag\{\delta_1(s), \delta_2(s), \ldots, \delta_5(s)\}, \quad |\delta_i| \le 1 \tag{11}$$

$$W_1 = \begin{pmatrix} 1 & 0 & 0 & 1 & 1 \\ 0 & 1 & 0 & 0 & 0 \\ 0 & 0 & 0 & 0 & 0 \\ 0 & 0 & 1 & 0 & 0 \end{pmatrix} \qquad W_2(s) = \begin{pmatrix} a_{1,1}(s) & 0 & 0 & 0 \\ a_{2,1}(s) & 0 & 0 & 0 \\ a_{4,1}(s) & 0 & 0 & 0 \\ 0 & a_{1,2}(s) & 0 & 0 \\ 0 & 0 & 0 & a_{1,4}(s) \end{pmatrix} \tag{12, 13}$$

A simple calculation shows that the transfer function matrix of which the SSV needs to be calculated with respect to Δ in (11), is given by:

$$M_{22}(s) = -W_2(I + KG)^{-1}KW_1 \qquad (14)$$

The calculated bounds on the SSV for robust stability is shown in figure 6.

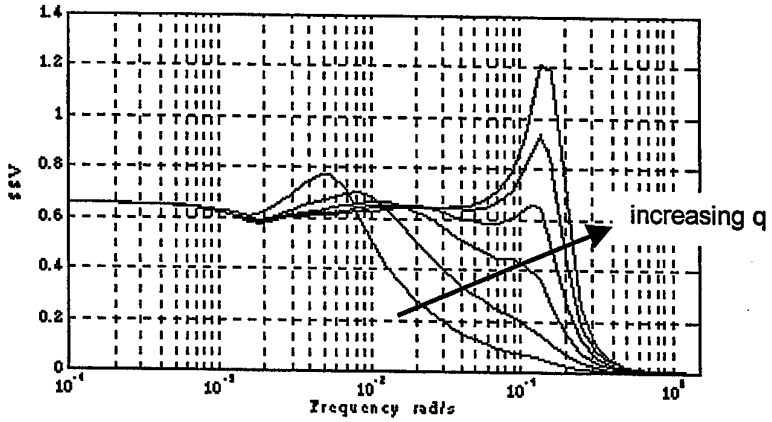

Figure 6: *SSV for robust stability (q=0,1; 0,25; 0,5; 0,75; 1 and 1,25)*

It follows from figure 6 that the feedback connection is robustly stable for all detunings except 1,25. It also appears that q = 0,5 gives the largest safety margin over the entire frequency range. The fact that the SSV for all detunings is the same at low frequencies can be explained by noting that GK>>I at low frequencies. Therefore (14) simplifies to:

$$\begin{aligned} M_{22}(s) &= -W_2(I + KG)^{-1}KW_1 \\ &\approx -W_2(KG)^{-1}KW_1 = -W_2G^{-1}W_1 \end{aligned} \qquad (15)$$

This is independent of K.

6.2 PERFORMANCE

Based on an analysis of the expected disturbances, it was decided that the bandwidth requirements were as follows:

output 1: 0,005 rad/s
output 2: 0,001 rad/s
output 3: 0,005 rad/s
output 4: 0,03 rad/s

6.2.1 Nominal performance

Nominal performance can be evaluated more simply than using the SSV. For the purpose of comparison the SSV was used here. The MΔ-structure shown in figure 7 is used.

Δ_P is a single 4×4 block uncertainty with $\sigma^*(\Delta_P) \leq 1$. Robust stability of this structure is equivalent to nominal performance, where W_P is the sensitivity weighting in (3). With reference to (4) and the bandwidth requirements stated above, W_P was chosen as:

$$W_P(s) = diag\left\{\frac{s/2 + 0{,}005}{s + 0{,}005 \times 0{,}03}; \frac{s/2 + 0{,}001}{s + 0{,}001 \times 0{,}03}; \frac{s/2 + 0{,}001}{s + 0{,}001 \times 0{,}03}; \frac{s/2 + 0{,}03}{s + 0{,}03 \times 0{,}03}\right\} \qquad (16)$$

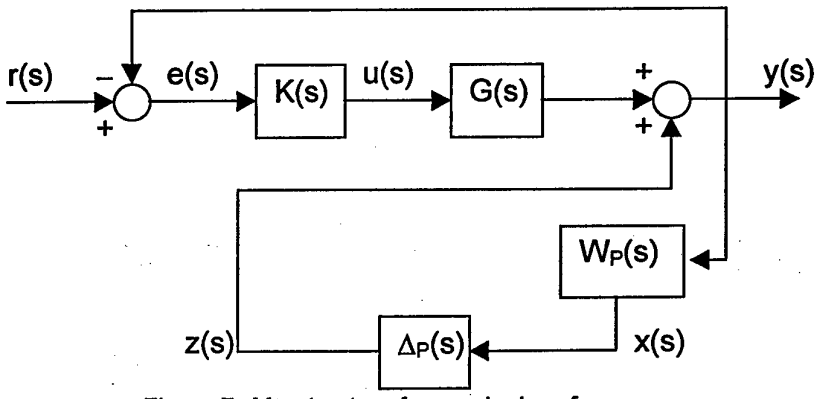

Figure 7: *MΔ-structure for nominal performance*

A simple calculation shows that the transfer function matrix of which the SSV needs to be calculated with respect to Δ_P is given by:

$$M_{22}(s) = W_P(I + GK)^{-1} \qquad (17)$$

The calculated upper bound on the SSV is shown in figure 8.

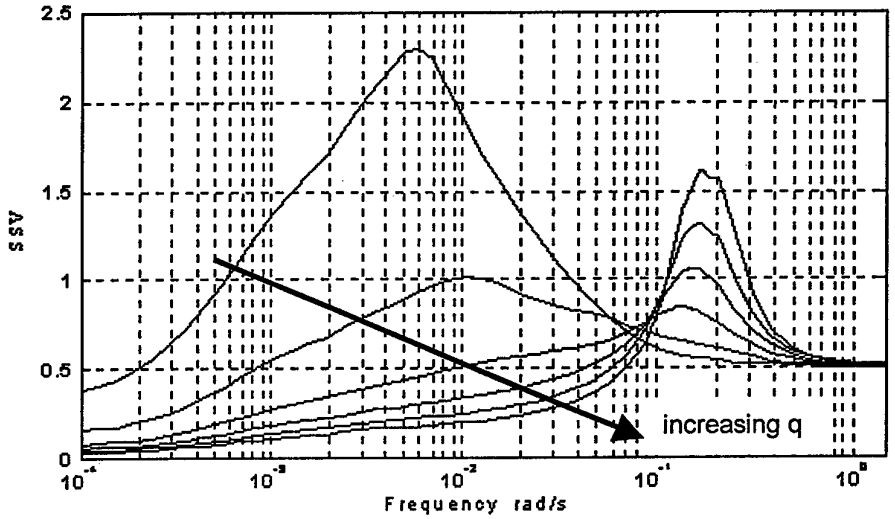

Figure 8: *SSV for nominal performance (q= 0,1; 0,25; 0,5; 0,75; 1 and 1,25)*

It can be concluded that nominal performance is only achieved for q = 0,25 and 0,5, with 0,75 just failing. Low frequency violations (smaller q values) are a result of bandwidth requirements, while high frequency violations (bigger q values) are a result of sensitivity peak height.

6.2.2 Robust performance

When evaluating robust performance all 7 significant additive uncertainties discussed in section 4 had to be included. The MΔ-structure shown in figure 9 was used.

Δ_P is a single 4×4 block with $\sigma^*(\Delta_P) \leq 1$. Δ is a diagonal matrix with seven 1×1 blocks, each with unit bound, on its diagonal. W_P is diagonal matrix similar to (16), except that the peak magnitude in S (see (4)) had been increased to 5. This was done to obtain meaningful graphs, but in practice corresponds to very oscillatory behaviour. W_1 and W_2 is given by

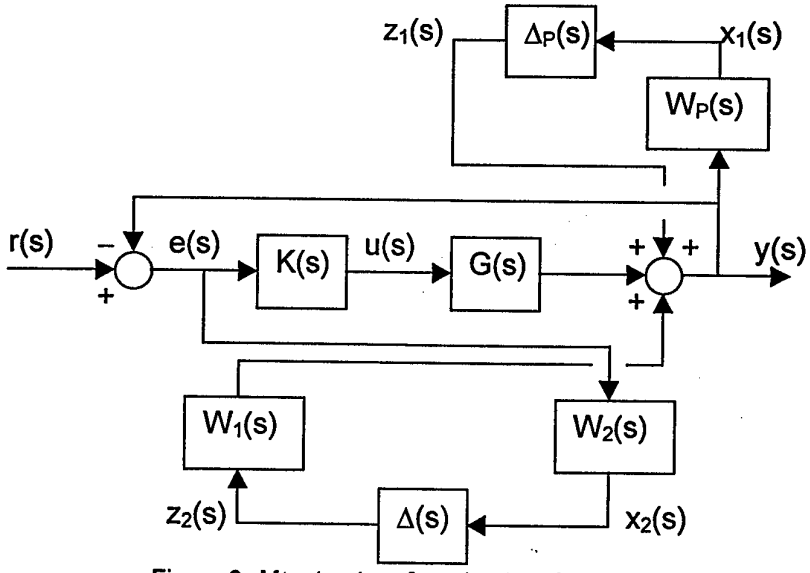

Figure 9: *MΔ-structure for robust performance*

$$W_1 = \begin{pmatrix} 1 & 0 & 0 & 0 & 1 & 0 & 1 \\ 0 & 1 & 0 & 0 & 0 & 0 & 0 \\ 0 & 0 & 1 & 0 & 0 & 1 & 0 \\ 0 & 0 & 0 & 1 & 0 & 0 & 0 \end{pmatrix} \quad W_2(s) = \begin{pmatrix} a_{1,1}(s) & 0 & 0 & 0 \\ a_{2,1}(s) & 0 & 0 & 0 \\ a_{3,1}(s) & 0 & 0 & 0 \\ a_{4,1}(s) & 0 & 0 & 0 \\ 0 & a_{1,2}(s) & 0 & 0 \\ 0 & a_{3,2}(s) & 0 & 0 \\ 0 & 0 & 0 & a_{1,4}(s) \end{pmatrix} \qquad (18,19)$$

A simple calculation shows that the transfer function matrix for which the SSV must be calculated with respect to the appended structure diag{Δ_P. Δ}, is given by:

$$M = \begin{pmatrix} W_P(I+GK)^{-1} & W_P(I+GK)^{-1}W_1 \\ -W_2(I+KG)^{-1}K & -W_2(I+KG)^{-1}KW_1 \end{pmatrix} \qquad (20)$$

The bound on the SSV shown in figure 10 was calculated.

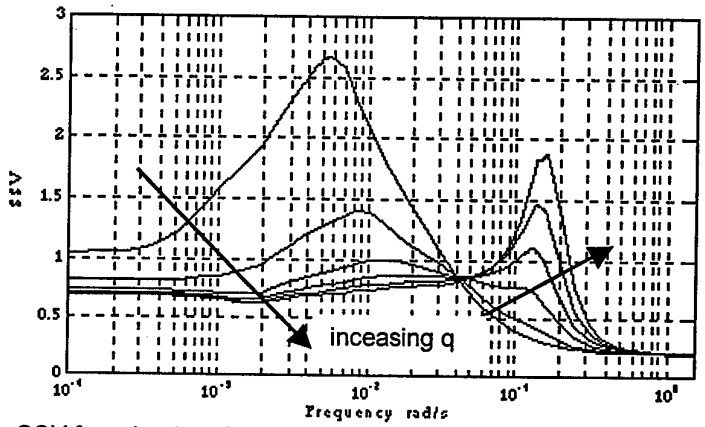

Figure 10: *SSV for robust performance (q = 0,1; 0,25; 0,5; 0,75; 1 and 1,25)*

Robust performance is only achieved for q=0,5, despite the increase in sensitivity peak to 5. This deterioration from the nominal case is to be expected, since the worst possible performance of all plants allowed by the uncertainty description is determined.

7. CONCLUSIONS

It is possible to derive a linear plant model with norm-bounded perturbation describing the entire operating range of the triple-effect evaporator. The uncertainty description used (independent uncertainty in the transfer function matrix elements) is convenient, since it reduces the identification problem to a number of SISO problems. Determining the nominal model and uncertainty bound is now simple. It however does not allow for possible coupling between elements and may be very conservative.

Robust analysis is a useful aid during controller design. The detuning of controllers used here, is just a simple application of this. More powerful techniques, directly shaping closed loop transfer functions should be ideal for this (e.g. H_∞ mixed sensitivity or μ-synthesis (Balas et al, 1995)).

Finally it is felt that a lot of what is treated as uncertainty in this approach is in fact well known non-linearity. An approach directly treating non-linearities, should prove to be superior. The validity of all results obtained is heavily dependent on the tightness of the uncertainty description.

REFERENCES

Agamennoni, O., Rotstein, H., Desages, A., and Romagnoli, J. A. (1989). "Robust controller design methodology for multivariable chemical processes: structured perturbations." *Chemical engineering science*, 44(11), 2597-2605.

Balas, G.J., Doyle, J.C., Glover, K., Packard, A. and Smith, R. (1995). *μ-Analysis and synthesis toolbox for use with MATLAB.* The Math Works, Inc.

Baker, W.M., and Bourne, A.A. (1920). *Elementary geometry*, G. Bell and Sons, London.

Doyle, J. (1982). "Analysis of feedback systems with structured uncertainties." *Proceedings of the IEE Part D*, 129(6), 242-250.

Kouvaritakis, B., and Latchman, H. (1985a). "Singular-value and eigenvalue techniques in the analysis of systems with structured perturbations." *International journal of control*, 41(6), 1381-1412.

Kouvaritakis, B., and Latchman, H. (1985b). "Necessary and sufficient stability criterion for systems with structured uncertainties: the major principal direction alignment principle." *International journal of control*, 42(3), 575-598.

MacFarlane, A. G. J., and Belletrutti, J. J. (1973). "The characteristic locus design method." *Automatica*, 9, 575-588.

MacFarlane, A. G. J., and Kouvaritakis, B. (1977). "A design technique for linear multivariable feedback systems." *International Journal of Control*, 25(6), 837-874.

Maciejowski. (1989). *Multivariable feedback design*, Addison-Wesley Publishing Company.

Morari, M., and Zafiriou, E. (1989). *Robust process control*, Prentice Hall, Englewood Cliffs.

Packard, A., and Doyle, J. (1993). "The complex structured singular value." *Automatica*, 29(1), 71-109.

Postlethwaite, I., Edmunds, J. M., and MacFarlane, A. G. J. (1981). "Principal gains and principal phases in the analysis of linear multivariable feedback systems." *IEEE transactions on automatic control*, AC-26(1), 32-46.

Skogestad, S., and Morari, M. (1987). "Design of resilient processing plants-IX. Effect of model uncertainty on dynamic resilience." *Chemical engineering science*, 42(7), 1765-1780.

Skogestad, S., and Postlethwaite, I. (1996). *Multivariable feedback control, analysis and design*, John Wiley&Sons.

1999 International Symposium on
Quantitative Feedback Theory and Robust Frequency Domain Methods

Multivariable Control System Design for the MEC Benchmark Challenge on Gasifier Control

E. Kontogiannis and N. Munro
Control Systems Centre, UMIST
Sackville Str., Manchester
M60 1QD, UK

Abstract

In this paper two different multivariable control systems designs are presented for the MEC Benchmark Challenge on gasifier control. The design methods employed were: a Sequential Loop Closing (SLC), and an H_∞ optimal control design method. Both methods satisfied the design specifications, as shown in the simulation results. A comparison between the methods is given and the importance of specific steps taken in each of the design methods is discussed to provide a better insight into the problem.

Keywords: Multivariable Control; Sequential Loop Closing (SLC); H_∞ Optimal Control.

1 Introduction

The gasifier (Fig.1) is a real industrial nonlinear, multivariable system, having five controllable inputs: *coal extraction flow (WCOL), limestone mass flow (WLS), air mass flow (WAIR) and char extraction flow (WCHR)*; and four outputs: *fuel gas pressure (PGAS), fuel gas temperature (TGAS), bed mass (MASS) and fuel gas calorific value (CVGAS)* with a high degree of coupling between them. The sixth input shown in Fig.1 is a *sink pressure (PSINK)* disturbance input, representing pressure disturbances as the downstream gas turbine fuel inlet valve is opened and closed. Because limstone absorbs sulphur in the coal, the limestone mass flow is set to a 1:10 fixed ratio of coal flow. This effectively reduces the controllable inputs to 4. The aim of the benchmark challenge [1] was the design of a controller, based on the linearised model of the gasifier at the 100% load operating point, which satisfies the design specifications on the system outputs, inputs and input rate of change shown in Table 1, when a step pressure disturbance is applied to the system. Additionally, the robustness of the controller is to be tested by evaluating its performance when applied to the linearized gasifier models at the 50% and 0% load operating points. Finally, the performance of the controller is also to be tested when a sine wave pressure disturbance input is applied to the system at the 0%, 50% and 100% load operating points.

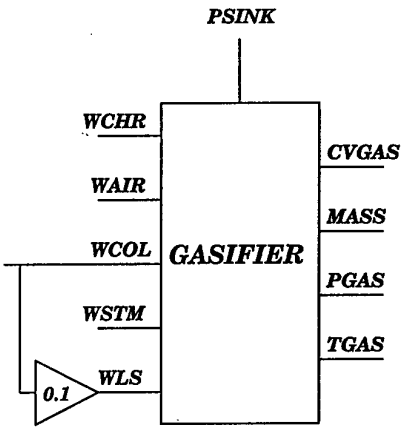

Figure 1: The gasifier

INPUTS	RANGE	RATE
WCOL(kg/s)	[0, 10]	0.2
WAIR (kg/s)	[0, 20]	1.0
WSTM (kg/s)	[0, 6]	1.0
WCHR (kg/s)	[0, 3.5]	0.2
OUTPUTS	**RANGE**	
CVGAS (J/kg)	±10000	
MASS (kg)	±500	
PGAS (N/m^2)	±10000	
TGAS (C)	±1	

Table 1: Design Specifications

The gasifier data were provided by GEC Alsthom in the form of the 25^{th} order state space

models.

2 The Sequential Loop Closing (SLC) Approach

The 100% load linearized model is stable but very ill-conditioned, as indicated by the wide spread of the singular values shown in Fig.2. The units of the outputs were very different,

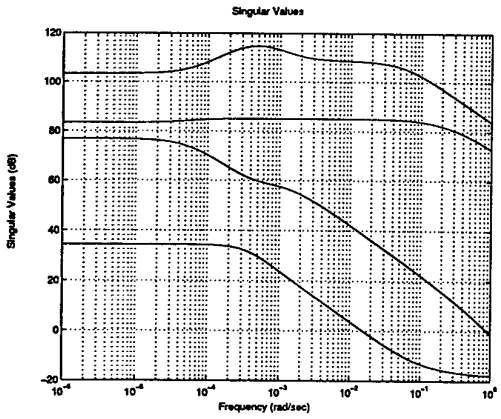

Figure 2: Singular Value Plot of the 100% load state space linear model of the gasifier

and thus an initial output scaling was considered necessary before any interaction analysis was carried out. The post-multiplying scaling matrix, $\mathbf{K_{post}}$, applied to the system outputs was

$$\mathbf{K_{post}} = diag\{10^{-5}, 10^{-3}, 10^{-3}, 10^{-1}\} \quad (1)$$

An interaction analysis on the scaled system, $\mathbf{K_{post}G_{gas}}(s)$, revealed its high interacting behaviour. Table 2 shows Rosenbrock's column diagonal dominance as well as the fundamental dominance measure, a less conservative dominance criterion, at various frequencies within the bandwidth [2]. In an attempt to improve this, the Relative Gain Array (RGA) was employed as a guide to finding the best input/output pairs. This is a basic step in the well known control structure design, and should be the initial and very important step in every multivariable control systems design [4]. The steady-state Relative Gain Array ($\Lambda(0) = [\lambda_{ij}]$) of the gasifier suggested that the first input; namely, the char offtake; should control the second output; namely, the bed mass; as shown in Eq.(2)[1] The

[1]Note that the same pairing was used in the validation procedure of the linearised models for reasons explained in the problem documentation.

Column Dominance	Fundamental Dominance	Frequency (rad/sec)
1.87e+001	6.80e+000	1.00e-005
1.50e+001	5.60e+000	2.63e-005
1.23e+001	4.60e+000	4.28e-005
1.07e+001	3.68e+000	6.95e-005
1.14e+001	3.31e+000	1.12e-004
1.67e+001	3.16e+000	2.97e-004
3.37e+001	3.83e+000	7.84e-004
4.97e+001	4.41e+000	1.27e-003
7.54e+001	5.04e+000	2.06e-003
1.73e+002	6.71e+000	5.45e-003
2.62e+002	8.66e+000	8.85e-003
6.25e+002	1.32e+001	1.43e-002
4.00e+003	2.89e+001	2.33e-002
1.23e+003	1.46e+001	3.79e-002
1.54e+003	1.03e+001	6.15e-002
2.43e+003	7.91e+000	1.00e-001

Table 2: Diagonal Dominance of the scaled system

element λ_{21} of the RGA is closer to 1, which indicates that the aforementioned pairing is the most favorable.

$$\Lambda(0) = \begin{bmatrix} 0.4133 & -0.0724 & 0.4187 & 0.2404 \\ 0.5781 & -0.0302 & 0.4246 & 0.0274 \\ 0.0150 & 0.9066 & 0.0519 & 0.0265 \\ -0.0064 & 0.1959 & 0.1048 & 0.7056 \end{bmatrix} \quad (2)$$

Re-ordering the system outputs as suggested by the RGA is equivalent to left-multiplying the transfer function matrix representing the gasifier by the corresponding permutation matrix. Then, a simple input shaping compensator of PI type was applied, and the corresponding loop was closed with unity feedback. Consequently, it was found that the remaining 3×3 system, $\mathbf{G_{3\times3}}(s)$, defined as

$$\mathbf{G_{3\times3}}(s) = \begin{bmatrix} 0 & 1 & 0 & 0 \\ 0 & 0 & 1 & 0 \\ 0 & 0 & 0 & 1 \end{bmatrix} \mathbf{K_{post}G_{gas}}(s) \begin{bmatrix} 0 & 0 & 0 \\ 1 & 0 & 0 \\ 0 & 1 & 0 \\ 0 & 0 & 1 \end{bmatrix} \quad (3)$$

could be made diagonal dominant by simple scaling for all frequencies up to 0.01 rad/sec, which was far greater than the desired closed-loop bandwidth.

The rest of the control loops were closed in a sequential fashion. The SLC design method is an iterative procedure based on the successive closing of the loops, ensuring at each step that

the previously closed loops continue to meet the design specifications. In each step, the best input/output scaling-permutation matrices were found using a normalisation procedure [3], and the remaining interaction was removed using the Align algorithm [3]. More specifically, the normalisation algorithm calculates input and output constant scaling-permutation matrices, such that the resulting system is as diagonal dominant as possible. The Align algorithm on the other hand, attempts to calculate a real approximation of the inverse of a complex matrix. The resulting constant decoupling, or near decoupling, compensator, is then connected in cascade with a PI controller designed to shape the input of the corresponding loop. It is important to note that the faster loops are closed first, and any nasty behaving elements, such as non-minimum phase for instance, are usually the last to be closed. This is why gas temperature, which had non-minimum phase characteristics, was the last loop to be closed. Also, the frequency at which the scaling and the align algorithm were applied, was found to be very critical. The fact that the system numerics were so ill-conditioned made the selection of the right frequency even more important. However, in general this is an ad-hoc procedure.

Following this procedure, the resulting 4×4 input shaping compensator ($\mathbf{K_{pre}}(s)$) is defined as the product of a full constant decoupling compensator ($\mathbf{K}_d$) times a dynamic diagonal compensator formed by appending for each iteration (loop) on the diagonal the PI controller designed for the corresponding loop [5].

$$\mathbf{K_{pre}}(s) = \mathbf{K_d} \cdot diag\left\{ \left[\begin{array}{c} \frac{100s+0.01}{s} \\ \frac{s+0.01}{s+0.02} \\ \frac{s}{0.0015s+0.00000075} \\ \frac{s(s+0.001)}{s} \end{array} \right]^T \right\} \quad (4)$$

The resulting closed-loop input and output responses, as well as the input rates of change, to a sink-pressure step disturbance of magnitude $-20000N/m^2$ at time t=30s are shown in Appendix A.

Comparing the results in these figures with the design specifications given in Table 1, it is clear that all specification are met for the 100% load case apart from the coal flow rate, which is exceeded when the step disturbance is applied. This controller was then applied to the linear models corresponding to the 0% and 50% operating points to test the robustness of the design. As expected there were violations of the performance specifications in both cases, as can be seen in the figures given in the Appendix.

The SLC based controller designed is very simple, of very low order, and hence, easily maintainable. However, it is not robust, which suggests that different controllers should be designed for the various opearating points, and then a scheduling should be performed across the gasifier's operating envelope.

3 The H_∞ Design Approach

A mixed sensitivity H_∞ design approach [4] will now be presented in this section. First, the desired disturbance specifications are directly translated into weights on the the sensistivity and the complementary sensitivity functions, which are then used to define the H_∞ optimisation problem in hand. The solution to this problem sub-optimally determines a controller which satisfies the design specifications, as will be shown in the sequel. The weight selection and the results obtained will be further analysed below.

3.1 H_∞ Scheme

The one degree of freedom H_∞ control scheme shown in Fig.3 was adopted. The same configuration but in the usual generalised plant form is given in Fig.4.

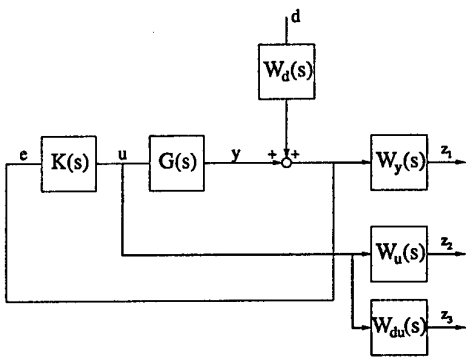

Figure 3: H_∞ control scheme

The resulting exogenous outputs $\mathbf{z}_i(s)$; i =

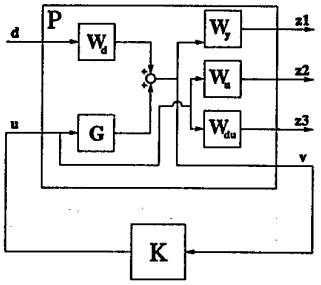

Figure 4: Closed-loop representation using the Generalised Plant

1, 2, 3; given by:

$$\mathbf{z}_1 = \mathbf{W}_y\,[y_1, y_2, y_3, y_4]^T + \mathbf{W}_d\,d \quad (5)$$

$$\mathbf{z}_2 = \mathbf{W}_u\,[u_1, u_2, u_3, u_4]^T \quad (6)$$

$$\mathbf{z}_3 = \mathbf{W}_{du}\,[u_1, u_2, u_3, u_4]^T \quad (7)$$

can be expressed in terms of the disturbance input d as:

$$\begin{bmatrix}\mathbf{z}_1\\ \mathbf{z}_2\\ \mathbf{z}_3\end{bmatrix} = \begin{bmatrix}\mathbf{W}_y\mathbf{S}\mathbf{W}_d\\ \mathbf{W}_u\mathbf{K}\mathbf{S}\mathbf{W}_d\\ \mathbf{W}_{du}\mathbf{K}\mathbf{S}\mathbf{W}_d\end{bmatrix} d \quad (8)$$

where $\mathbf{S} = (\mathbf{I} + \mathbf{GK})^{-1}$ is the sensitivity function, and $\mathbf{W}_d, \mathbf{W}_y, \mathbf{W}_u, \mathbf{W}_{du}$ are the weights to be chosen. Note that the variable s in all transfer functions has been dropped for notation simplicity.

Let $\mathbf{T}_{z,d}(s)$ denote the closed-loop transfer function relating the exogenous outputs to the disturbance input (eq.8). The objective hence becomes the minimisation of the infinity norm of this closed-loop transfer function, i.e.,

$$\|\mathbf{T}_{z,d}(s)\|_\infty \quad (9)$$

3.2 Weights Selection

The selection of the weights to be used is discussed in this section. The intial selection of the weights was based on the SLC design and the contraints on the input signals. Specifically, the initial choice of $\mathbf{W}_d(s)$, which is related to the disturbance attenuation properties of the design, was based on the closed-loop bandwidth achieved by the SLC design. The weights $\mathbf{W}_u$ and $\mathbf{W}_{du}$ were actually the given bounds of the input and input rate of change, respectively. All the weights were then tuned iteratively, until an adequate response for the nominal case of 100% load was found. Then, the weights were further tuned to achieve robustness across the full operating range.

Selection of $\mathbf{W}_d(s)$

This is the performance related weight matrix, where performance in this problem corresponds to the closed-loop disturbance rejection properties of the system. Assuming $\mathbf{W}_y(s) = I_4$, eq.(8) shows that closed-loop noise amplification will appear at the frequencies where $|\mathbf{S}(j\omega)\mathbf{W}_d(j\omega)| > 1$. In fact our design has to ensure that $|\mathbf{S}(j\omega)\mathbf{W}_d(j\omega)| < 1$, $\forall\omega$, which alternatively can be written as $|\mathbf{S}(j\omega)| < (|\mathbf{W}_d(j\omega)|)^{-1}$, $\forall\omega$.

Since the disturbances are assumed to be acting directly on the outputs, $\mathbf{W}_d(s)$ should be considered as a model of the disturbance *psink* acting upon the different channels. A typical form of this weight for each channel is a low pass filter of the form [4]:

$$\mathbf{W}_d(s) = k\,\frac{s/M + \omega_B}{s + \omega_B A} \quad (10)$$

where k is a constant gain, ω_B is the required bandwidth, $A \leq 1$ and $M \geq 1$.

Choosing a diagonal weight matrix $\mathbf{W}_{dd}(s)$ [2] to be

$$\mathbf{W}_{dd}(s) = diag\left\{\begin{bmatrix}\frac{s/2+0.15}{s+0.15\ 0.05}\\ \frac{s/2+0.01}{s+0.01\ 0.05}\\ \frac{s/2+0.2}{s+0.1\ 0.05}\\ \frac{s/2+0.1}{s+0.1\ 0.05}\end{bmatrix}^T\right\} \quad (11)$$

the closed-loop system is required to reject disturbances at low frequencies by a factor of 200 to 1 (see Fig.5), thus producing a good steady-state disturbance rejection. A gain matrix which is equal to the steady-state gain of the given disturbance response $\mathbf{G}_d(s)$ is then multiplied, such that the direction of the model disturbance is the same as that of the actual disturbance *psink*, resulting in

$$\mathbf{W}_d(s) = |\mathbf{G}_d(0)|\ \mathbf{W}_{dd}(s) \quad (12)$$

Selection of $\mathbf{W}_y(s)$

This weight is used for fine tuning of the design, and was chosen to be the constant diagonal weighting matrix given below:

$$\mathbf{W}_y = diag\{1, 0.1, 1, 100\} \quad (13)$$

[2] The subscripts "dd" correspond to directionless disturbance

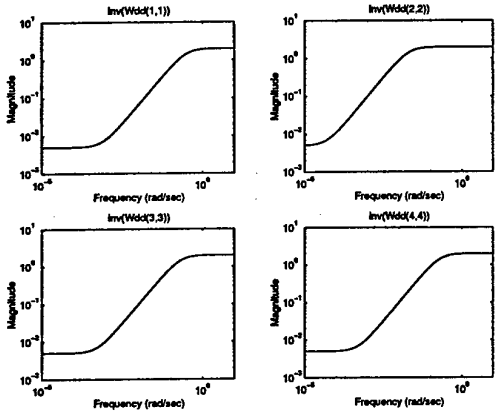

Figure 5: The inverse of the weight $\mathbf{W}_{dd}(s)$

Selection of $\mathbf{W}_u(s)$
This weight is used to penalise the control effort, ensuring that the input constraints in the design specifications are met. $\mathbf{W}_u$ was chosen to be the diagonal constant matrix given below:

$$\mathbf{W}_u = diag\{1, 10, 70, 10\} \qquad (14)$$

Selection of $\mathbf{W}_{du}(s)$
This weight is used to penalise the control input rates of change, ensuring that the input rate constraints in the design specifications are met. $\mathbf{W}_{du}$ was chosen to be the diagonal matrix given below:

$$\mathbf{W}_{du}(s) = diag\{1000, 500, 5000, 100\}\, w_{dif}(s) \qquad (15)$$

where $w_{dif}(s) = \frac{s + 0.00001}{0.00001\ s + 1}$ behaves like a differentiator across the wide frequency range $[10^{-5}, 10^{5}]$ rad/sec.

3.3 Application of the $H\infty$ optimisation

For the set of weights given in the previous section, the best $H\infty$ norm was found to be 0.8533. The resulting augmented plant is of 33^{rd} order and thus so is the resulting compensator. The order of the controller could be decreased by applying model-order reduction techniques to the plant and the resulting controller. However, since this is an academic exercise and since any reduction in the order of the controller would result in a decrease in the controller's performace, it was ommitted.

The time responses of the closed-loop system at the 100% load case to a *sink pressure step disturbance of* $-20000N/m^2$ and to a *sine wave disturbance of amplitude* $20000N/m^2$ *and of frequency 0.04 Hz* are given in the Appendix. The responses show that the design specifications were all met.

To check the robustness of the controller the same time responses for the 50% and 0% load cases are also included. For the case of 50% load, no violations of the performance specifications occur when the step disturbance input is applied. When the sine wave disturbance input is applied, the fuel gas pressure output ($PGAS$) is violated by $2000N/m^2$.

For the case of 0% load, there was a violation of the design specifications when the step disturbance input was applied. The fuel gas pressure output ($PGAS$) is violated by $3250N/m^2$. Controllers, which met the design specifications for the fuel gas pressure, violated the control rate constraints, and vice versa. This indicates that either the $PGAS$ or the input rate constraints may have to be relaxed. Also, when the sine wave disturbance input is applied there are two violations. The fuel gas pressure disturbance is violated by $6200N/m^2$, and the fuel gas calorific value is violated by $5000J/Kg$.

4 Conclusions

The SLC based controller is very simple and of very low order, and easy to implement. However, it is not robust, and hence different controllers should be designed for the various system opearating conditions and then a scheduling should be performed across the full operating envelope. On the other hand, the H_∞ controller is robust but of very high order and mainly very complicated. The weights considered were selected, after a lot of trial designs, in order to satisfy the design specifications across the operating envelope as much as possible. Due to the large uncertainty in the system description, however, the use of a single controller for the whole operating envelope is not possible. Some of the specifications were also found to be in conflict, and maybe some design specifications may have to be relaxed.

5 References

[1] R.Dixon, A.W. Pike and M.S. Donne, "Overview: The MEC Benchmark Challenge On Gasifier Control", Proc. of the Seminar on

MEC Benchmark Challenge On Gasifier Control, Coventry University, June 1998.

[2] E. Kontogiannis and N. Munro, "Robust Stability Conditions for MIMO Systems with Parametric Uncertainty", in N. Munro (Ed.), "The Use of Symbolic Algebra in Control Systems Analysis and Design", IEE Press, 1998.

[3] E. Kontogiannis, N. Munro and S.T. Impram, "Frequency Domain Control Structure Design Tools", EURISCON '98, Athens, July 1998.

[4] S. Skogestad and I. Postlethwaite, "Multivariable Feedback Control: Analysis and Design", Wiley, 1996.

[5] N. Munro, J.M. Edmunds, E. Kontogiannis and S.T. Impram, "A Sequential Loop Closing Approach to the Gasifier Problem", Proc. of the Seminar on MEC Benchmark Challenge On Gasifier Control, Coventry University, June 1998.

Appendix

The time responses of the closed-loop system at the 100%, and 0% load designed using the SLC (Fig.6-17) and the H_∞ method (Fig.18-29) are given below.

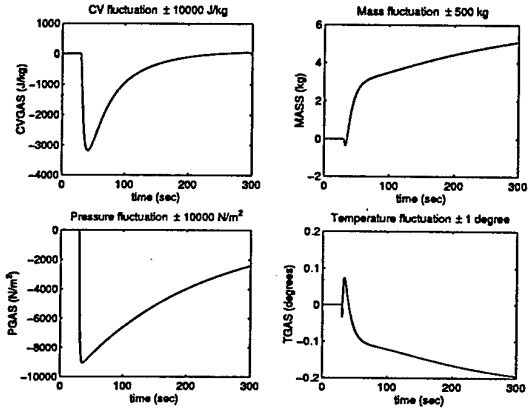

Figure 6: Closed-loop time responses to a step disturbance input of the outputs for the 100% load case

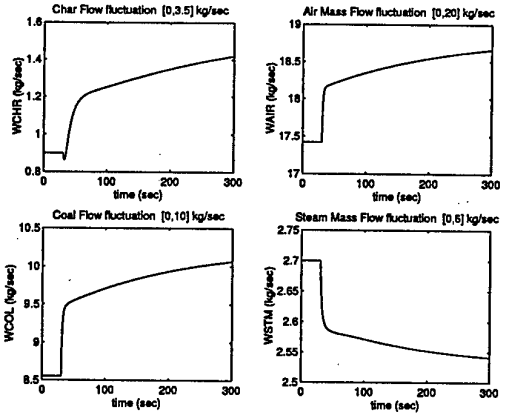

Figure 7: Closed-loop time responses to a step disturbance input of the inputs for the 100% load case

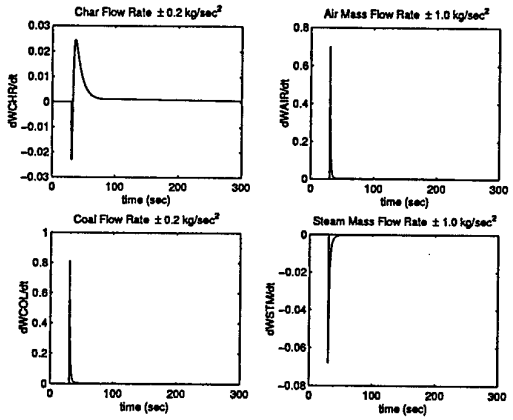

Figure 8: Closed-loop time responses to a step disturbance input of the input rate of change for the 100% load case

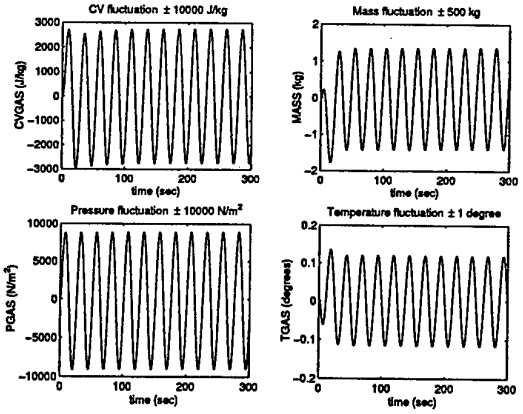

Figure 9: Closed-loop time responses to a sine wave disturbance input of the outputs for the 100% load case

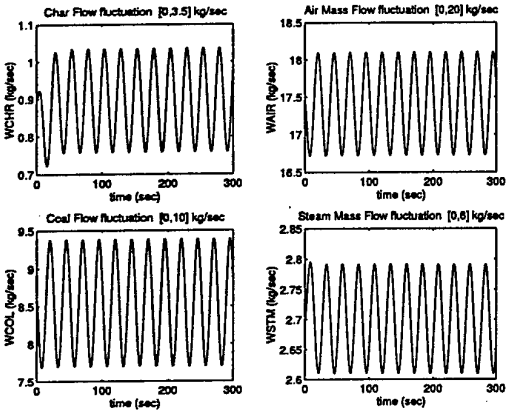

Figure 10: Closed-loop time responses to a sine wave disturbance input of the inputs for the 100% load case

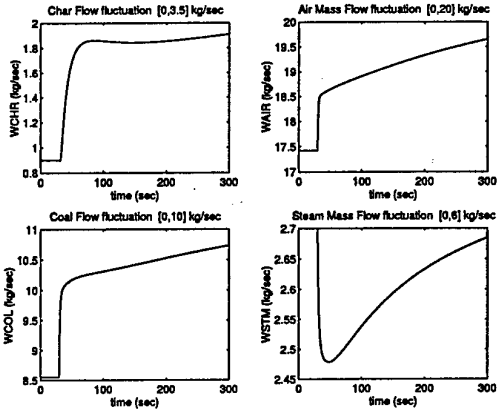

Figure 13: Closed-loop time responses to a step disturbance input of the inputs for the 0% load case

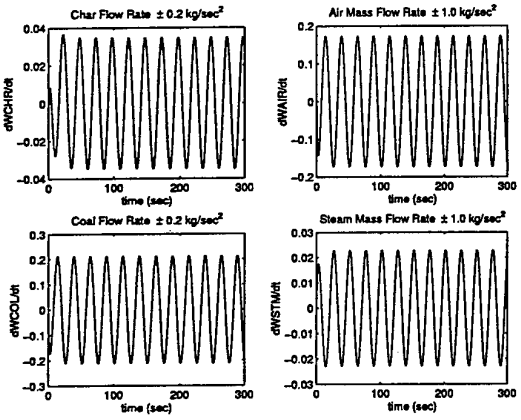

Figure 11: Closed-loop time responses to a sine wave disturbance input of the input rate of change for the 100% load case

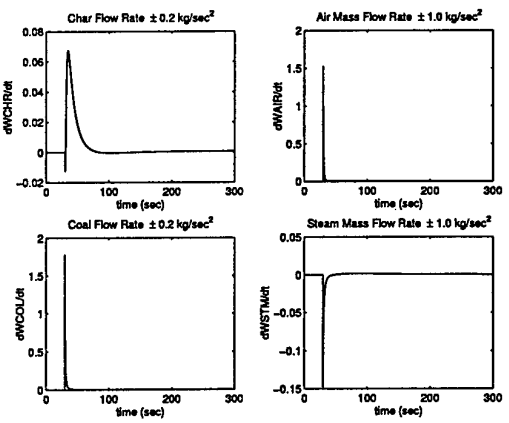

Figure 14: Closed-loop time responses to a step disturbance input of the input rate of change for the 0% load case

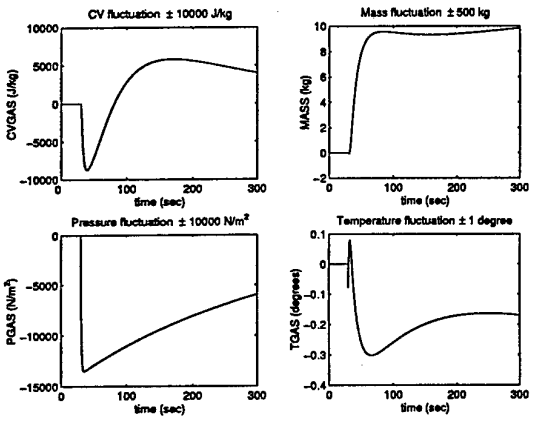

Figure 12: Closed-loop time responses to a step disturbance input of the outputs for the 0% load case

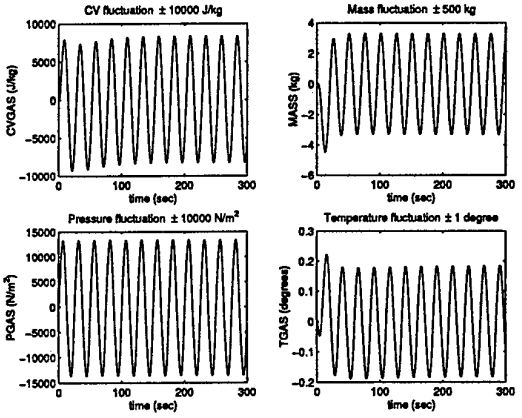

Figure 15: Closed-loop time responses to a sine wave disturbance input of the outputs for the 0% load case

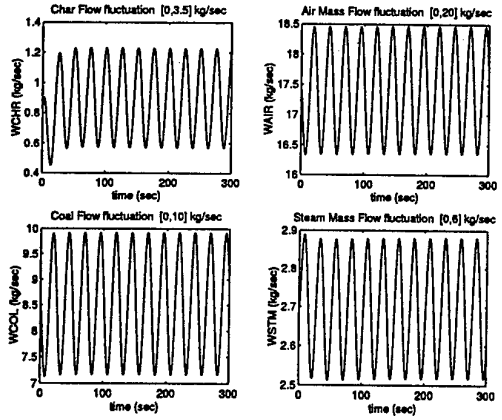

Figure 16: Closed-loop time responses to a sine wave disturbance input of the inputs for the 0% load case

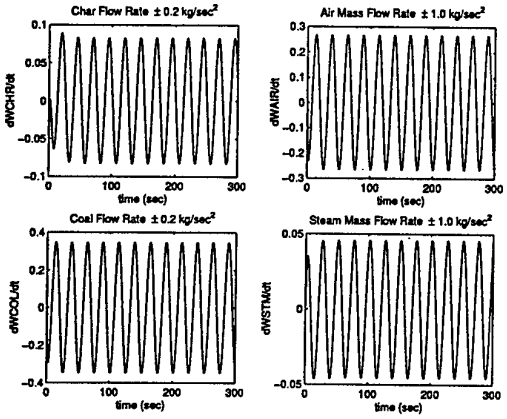

Figure 17: Closed-loop time responses to a sine wave disturbance input of the input rate of change for the 0% load case

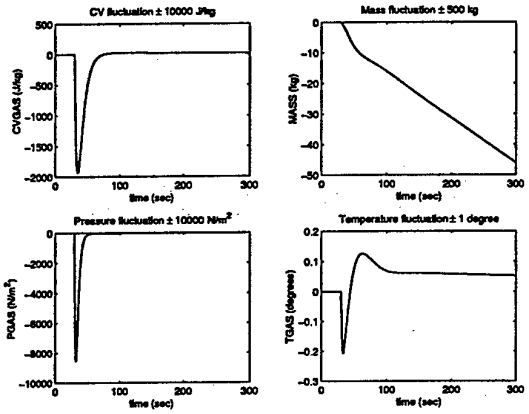

Figure 18: Closed-loop time responses to a step disturbance input of the outputs for the 100% load case

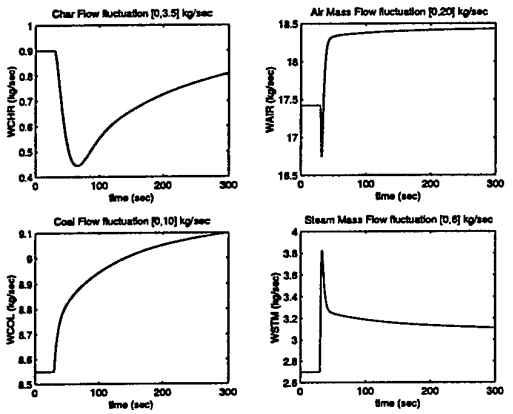

Figure 19: Closed-loop time responses to a step disturbance input of the inputs for the 100% load case

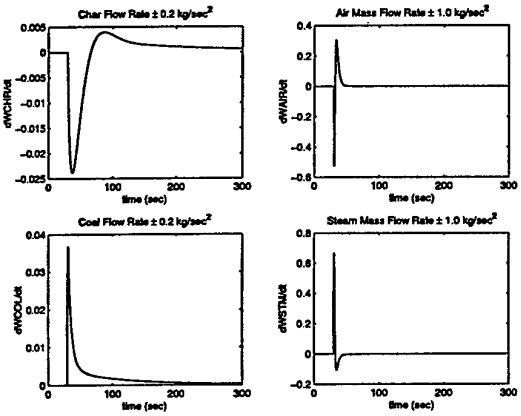

Figure 20: Closed-loop time responses to a step disturbance input of the input rate of change for the 100% load case

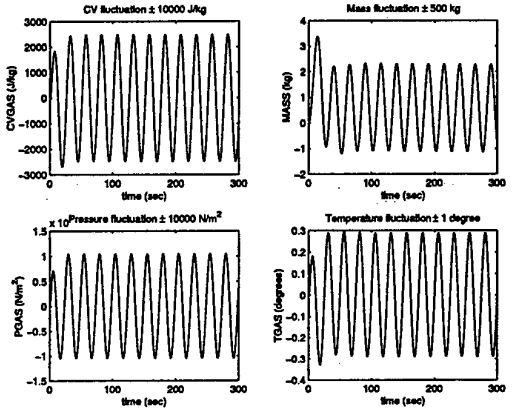

Figure 21: Closed-loop time responses to a sine wave disturbance input of the outputs for the 100% load case

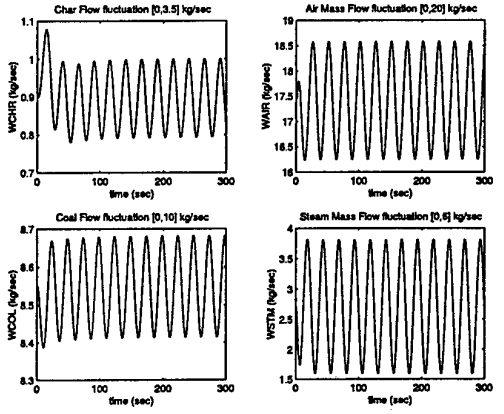

Figure 22: Closed-loop time responses to a sine wave disturbance input of the inputs for the 100% load case

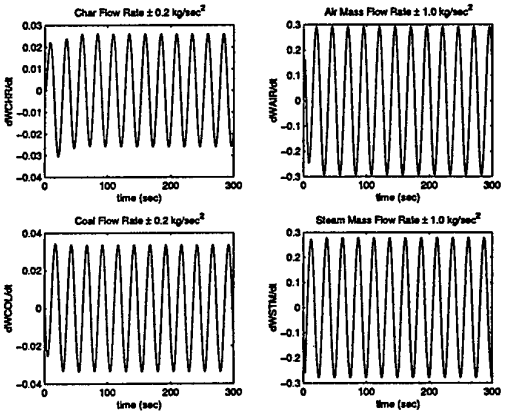

Figure 23: Closed-loop time responses to a sine wave disturbance input of the input rate of change for the 100% load case

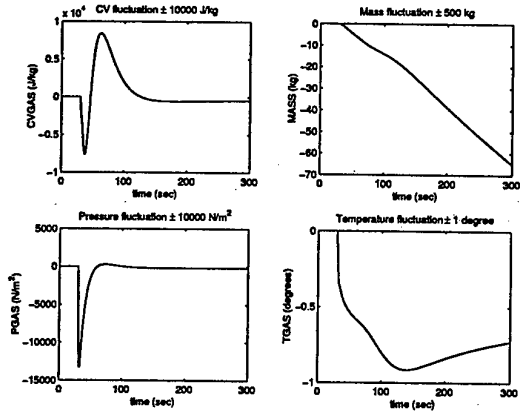

Figure 24: Closed-loop time responses to a step disturbance input of the outputs for the 0% load case

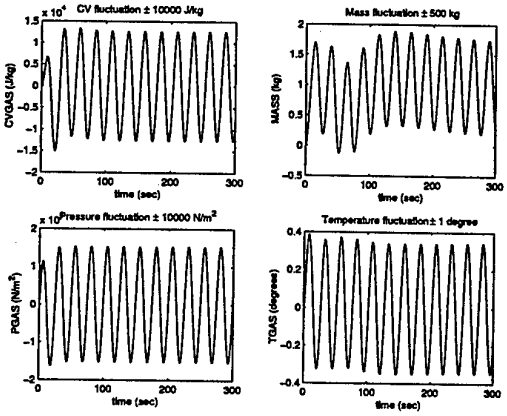

Figure 27: Closed-loop time responses to a sine wave disturbance input of the outputs for the 0% load case

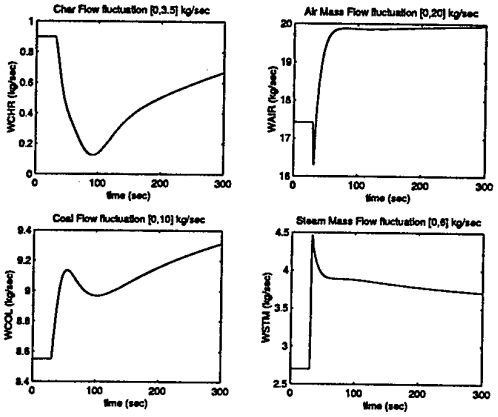

Figure 25: Closed-loop time responses to a step disturbance input of the inputs for the 0% load case

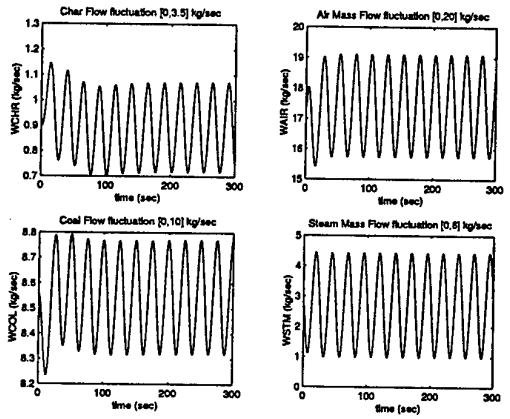

Figure 28: Closed-loop time responses to a sine wave disturbance input of the inputs for the 0% load case

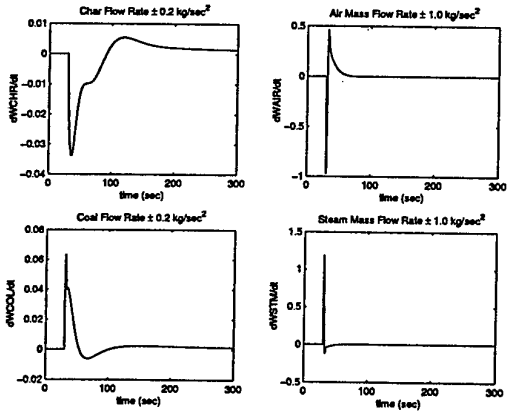

Figure 26: Closed-loop time responses to a step disturbance input of the input rate of change for the 0% load case

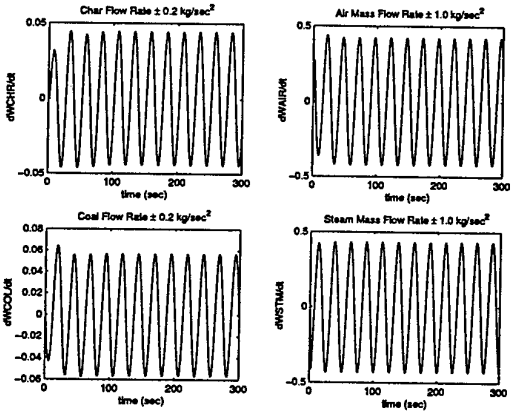

Figure 29: Closed-loop time responses to a sine wave disturbance input of the input rate of change for the 0% load case

1999 International Symposium on
Quantitative Feedback Theory and Robust Frequency Domain Methods

μ-Synthesis of a 3 DOF Robot Manipulator

L. González, L. Aguilar and S. Andrade

Centro de Investigación y Desarrollo de Tecnología Digital
Ave. del parque #1310, Mesa de Otay, C.P. 22510, Tijuana, B.C., México
Instituto Tecnológico de La Laguna, Coah., México

Abstract. This paper deals with the design of a stabilizing controller using the μ-synthesis approach for a 3 DOF arm manipulator affected by non-modeling dynamics, non-linearities, actuator dynamics and sensor noise. The performance specifications were expressed as weighting transfer functions that express the magnitude and frequency content of load disturbance, sensor noise, error signal that guarantee an exact tracking and also the weighting function that normalize the H∞ norm of the uncertainty. A controller was computed by solving the corresponding H∞ optimization problem. The results showed robust stability and nominal performance, but not robust performance. Then, tuning the performance weighting function and using the D-K iteration approach a design that achieve robust stability, nominal performance and robust performance specification was obtained.

1. Introduction

Many robot manipulators show undesirable dynamics present on their performance. A small didactic five DOF robot manipulator has this problem. This robot has already feedback P control on every servo imposing a degree of linearity to the robots. Due to the mechanical design, non-linearities are still present on the system that affect the performance of the robot as bad repeatability, steady state errors to step inputs and poor regulation on every configuration. Here, the robot was taken as a stable but unknown system. An important research topic in robotics is the development of more arm manipulator to carry on dangerous tasks or work in environment that may affect the operation of the robot. Robustness of a robot can be enhanced by designing mechanical sturdy components or by using modern control methodologies to design robust controlled systems. Among the methodologies developed for the purpose of enhancement of robustness of a system, we can name H∞ optimal technique and μ-synthesis. Adaptive design technique is also a very valuable and important tool for this purpose (Kelly, 1989). Here μ-synthesis approach has been chosen to design a robust control for an arm manipulator. Application of μ-synthesis to robotics (Pannu, 1996), aviation (Lind, 1997), industrial (Buso, 1999) have shown the applicability of the technique. Analysis of the behavior of the uncontrolled robot (González, 1999), produce non-parametric frequency dependent multivariable nominal model and additive uncertainty upper bounds. A weighting function that cover the upper bound of the additive uncertainty was chosen and used along the design procedure, weighting functions are chosen as the main variable parameters to tune the controlled system. Many works have been dedicated to find a general method to choose the weighting function, (Postlethwaite, 1989), (Ali, 1997) (Lundström, 1991), but mostly they are, application dependent. The weighting functions were chosen as diagonal matrices to model the reference commands, disturbances and noise from sensors. The third joint shown to respond to a higher frequencies spectrum than the other two joints. So, frequency band of the corresponding weighting functions were chosen wider and in some cases of second-order. A sequence of two H_∞ design with tuning on the weighting function ended with a robust stable and with nominal performance controlled system. Then a *D-K* iteration was applied to reduce the margin of robustness $\mu(M)$ with fine results. The design obtained proved to achieved performance objectives and show improved closed-loop time dynamics.

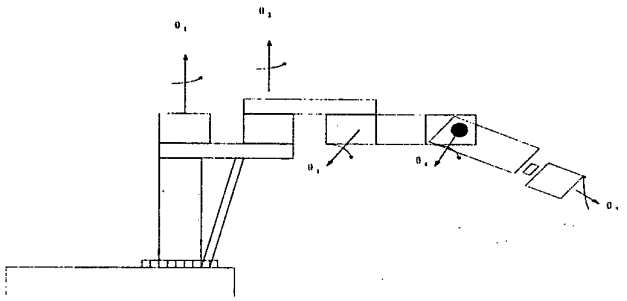

Figure 1: Experimental Setup

2. Non-Parametric Models

For this experiment two of the links, the wrist and the end-effector were not taken into design process. Therefore we take the robot as a three degrees of freedom robot. Under this assumption the robot was viewed as a three control inputs, three measured outputs linear stable, time invariant multivariable system. We found out that the robot responses to control input were different at different configuration, therefore a set of frequency analysis experiments were carried out in order to derive a set of non-parametric models corresponding to a set of different configurations of the robot.The experiment gave as result 27 non-parametric models corresponding to 27 different configurations respectively. Figure 2 shows the results of nine of the experiments.

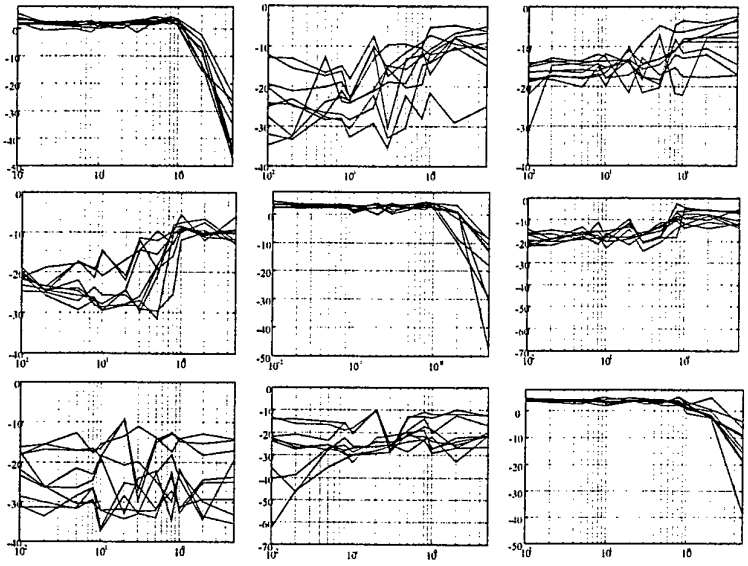

Figure 2: Family of models from the experiments

2.1 Nominal Model

Since what we are looking for was a decoupled robust multivariable control it was proposed a diagonal nominal model of the form:

$$G_n(s) = \begin{bmatrix} G_{n1}(s) & 0 & 0 \\ 0 & G_{n2}(s) & 0 \\ 0 & 0 & G_{n3}(s) \end{bmatrix} \quad (1)$$

where

$$G_{n1}(s)=\frac{5.64s^2+5.56s+4.2}{s^4+5.46s^3+10s^2+8.06s+3.9}$$
$$G_{n2}(s)=\frac{5.89s^2+5.2s+0.706}{s^4+5.13s^3+8.65s^2+5.08s+0.606} \quad (2)$$
$$G_{n3}(s)=\frac{11.96s^2-2.41s+41.74}{s^4+6.4s^3+14.33s^2+23.86s+34.45}$$

2.2 Additive Unstructured Uncertainty

Due to the structure of the nominal model proposed the following additive unstructured uncertainty was considered:

$$\Delta_a(j\omega)=\begin{bmatrix}\Delta_1(j\omega) & G_{12}(j\omega) & G_{13}(j\omega)\\ G_{21}(j\omega) & \Delta_2(j\omega) & G_{23}(j\omega)\\ G_{31}(j\omega) & G_{32}(j\omega) & \Delta_3(j\omega)\end{bmatrix} \quad (3)$$

where $G_{ij}(j\omega)$ are the family of curves off the main diagonal of the experimental matrix and $\Delta_i(j\omega)$ i=1,2,3 are the additive uncertainty of the diagonal elements respectively. So the set of plant models in which the real plant resides in:

$$G := \{G_n + \Delta_a W_a : \|\Delta_a W_a\| \le 1\} \quad (4)$$

where W_a is a weighting function matrix.

An approximate of the upper bound frequency response for the additive uncertainty of the main diagonal $\Delta_i(j\omega)$ i=1,2,3 was derived. For more details on the derivation of the nominal plant and bounds for the additive uncertainty see (González, 1999)

3. Control Objectives

We looked for design a robust stable system to additive uncertainties present on the model. Also, we want robust performance of the controlled system as to regulate the system for load disturbances, mainly on the joint three, output attenuation of high frequency noise present in the sensors and good tracking of reference signals. The interconnection structure used in the design procedure is shown in Figure 3.

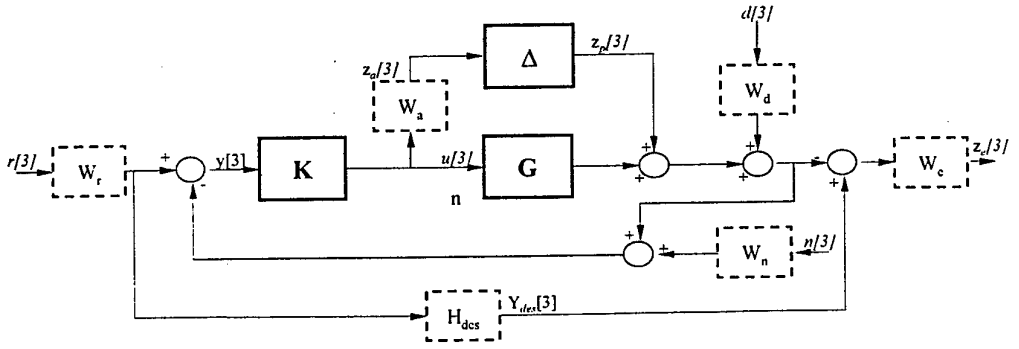

Figure 3: Controlled system

G_n represents the multivariable linear nominal model of the system represented by Equation 2. W_a is a stable weighting transfer function which together with Δ_a are used to model plant uncertainty. It is assumed that Δ_a is unknown but norm bounded such that $\|W_a\Delta_a\| \le 1$. The frequency dependent weighting functions W_d, W_n, W_r and W_e are used to define performance objectives. K was derived from the set of real rational transfer function matrix, which internally stabilize the close loop system. The design objective is to find a stabilizing controller K such that for stable perturbation Δ_a with $\|W_a\Delta_a\| < 1$ the perturbed close loop system remains stable and satisfies:

$$\|F_u(F_l(G,K),\Delta_a)\|_\infty \le 1 \tag{5}$$

where G is the open loop matrix function and $F_l(G,K)$ is the close loop matrix transfer function from the external inputs $w=[r^T \quad d^T \quad n^T]^T$ to objective output z_e. In this problem the unstructured additive uncertainty covers the inertia variations and uncertainty in the linear and angular accelerations produced by the generated torque. The uncertainty weight W_a is a 3×3 diagonal transfer function matrix that was taken to model the additive uncertainty of the unknown dynamics of the mechanical structure. The maximum singular values frequency response of W_a covers the upper bound of the additive uncertainty as shown in Figure 5. The W_a used in this paper was $W_a = diag(\frac{1.73(s+.3)}{s+1}, \frac{1.73(s+.3)}{s+1}, \frac{1.73(s^2+0.806s+0.15)}{s^2+1.2s+0.75})$

The block W_e is used to normalize specifications, in this case to set the performance objective $\|W_eS\|_\infty < 1$. The block H_{des} is an ideal model that we want the closed loop system to match. The input angular deviation command signals are normalized with respect to maximum expected command signals by means of the weighting function W_r. The block named W_d is used to characterize the low frequency load disturbance affecting the system. Finally, the block designated as W_n is used to model the corruption by sensor noise of each actual angular position measurement.

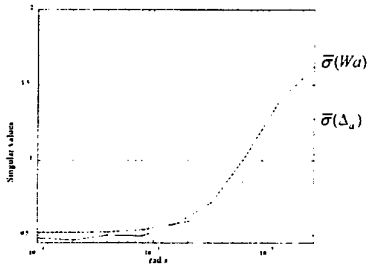

Figure 4: Maximum singular value of Δ_a

Before, we try μ-synthesis, it was worth to start with the design of an H∞ optimal controller by using W_a as uncertainty weighting function and low order performance weighting functions to keep the order of the controller low and chosen as to reflect engineering specifications as close loop stability, tracking error, disturbance rejection, and/or noise attenuation. Then, carry out a μ-analysis of the controlled system to see if robust stability and nominal performance are satisfied. Usually, the H∞ optimal controller achieved one or two of these specifications. If not, refine the H∞ design by adjusting the performance weighting functions to achieve robust stability and nominal performance without spoiling the engineering specifications. Once an H∞ optimal or suboptimal controller is derived synthesize a robust controller for the μ problem. Finally, verify if the controlled system satisfies the engineering specifications for the original set of plants.

A former H∞ optimal control design was derived for a set of weighting functions chosen based on desired performance. W_d was chosen as a 3x3 diagonal transfer function matrix that model the low frequency load disturbances with a 50 DC gain. The cut-off design frequencies for links 1, 2, and 3 were 0.012, 0.056, and 0.12

rad/s respectively. W_e was also chosen as a 3x3 diagonal transfer function matrix, such that at low frequency we have 1.5 % errors in tracking the reference signals, and a shift of 0.3° from reference for disturbance inputs in every angular position. The crossover frequencies for each link were 0.1. 0.4, and 1.5 rad/s respectively. W_r was chosen as a 3x3 diagonal transfer function matrix with low gain to attenuate the maximum command signals at low frequencies and with a first order roll-off at frequencies larger than 2 rad/s. Finally, W_n was chosen as a 3x3 diagonal transfer function matrix with high pass filters on every element with a crossover frequency of 21.3 rad/s in order to model the noise introduced to the system by the position sensors of the servos. In this first design H_{des} was not used. With this weighting functions an augmented plant was formed and it was used on the H∞ design and a 29 order controller $K_1(s)$ with $\gamma = 0.0066$ was obtained. Then, we start with the μ-analysis of the performance of the closed loop system with respect to robust stability and nominal performance, The closed loop transfer function $F_l(G,K)$ for this problem is:

$$F_l(G,K) = \left[\begin{array}{c|cc} W_a KS & W_a KSW_r & -W_a KSW_d \quad -W_a KSW_n \\ \hline -W_e S & W_e(H-T)W_r & -W_e SW_d \quad W_e TW_n \end{array}\right] = \left[\begin{array}{c|c} M_{11} & M_{12} \\ \hline M_{21} & M_{22} \end{array}\right] \tag{6}$$

where $S = (I+GK)^{-1}$ is the output sensitivity matrix and $T = I - S$ is the complementary sensitivity matrix. Robust stability is achieved when:

$$\left\| W_a KS \right\|_\infty < 1 \tag{7}$$

The closed loop system achieves nominal performance if the performance objective is satisfied for the nominal plant model G_n. In this problem, that is equivalent to:

$$\left\| W_e(H_{des} - T)W_r \quad -W_e SW_d \quad W_e TW_n \right\|_\infty < 1 \tag{8}$$

The closed loop system achieves robust performance if the closed loop system is internally stable for all $G \in \{G_n + W_a \Delta_a\}$ and

$$\left\| F_l(G,K) \right\|_\infty < 1 \tag{9}$$

is satisfied for every $G \in \{G_n + W_a \Delta_a\}$.

The controlled system under $K_1(s)$ only satisfied the robust stability performance as can be seen in Figure 5.

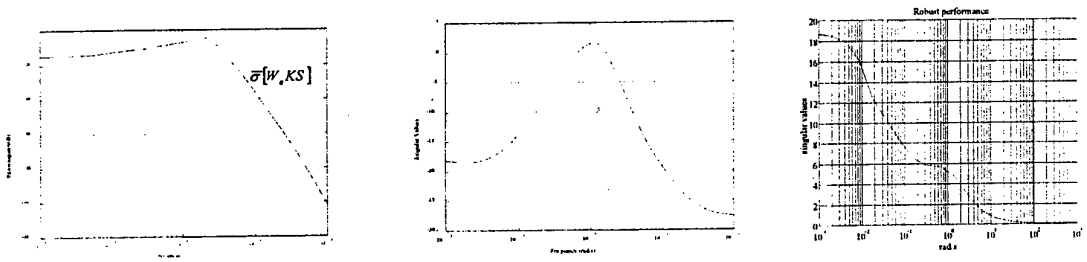

Figure 5: Robust stability, Nominal performance and robust performance for $K_1(s)$

Since our final goal is to minimize μ approximated by the scaled singular value $\bar{\sigma}(DMD^{-1})$ the diagonal blocks of $F_l(G,K)$ are not affected by the D-scales, so these blocks were worked out by means of the weighting functions as our design parameters in order to achieved an H∞ optimal control design that satisfy Equation 7 and Equation 8. As in our first design we work only out 3×3 diagonal weighting functions matrices with first order transfer function in order not to provoke untractable controllers *K(s)*. In this second design, H_{des} was proposed

as a diagonal matrix with first order transfer functions with a bandwidth of 1.4 rad/s. So from Equation 8 to achieve tracking objective we need $\|W_e(H_{des}-T)W_r\|_\infty < 1$. At low frequencies $\|H_{des}\|_\infty \approx 1$ and $\|W_e(I-T)W_r\|_\infty \approx \|W_eSW_r\|_\infty < 1$. W_eS is the (2,1) submatrix of $F_l(G,K)$ and here is used as to characterize also good performance by making $\|W_eS\|_\infty < 1$. In this design W_e was chosen as a 3x3 diagonal matrix with a 15 low frequency gain and a 0.3 rad/s crossover frequency to achieved $\|W_eS\|_\infty < 1$. W_r was chosen with maximum singular value plot below the plot of $\|W_eS\|_\infty^{-1}$. At high frequencies ($\omega > 1.8$ rad/s), the $\|S\|_\infty \approx 1$ and W_e and W_r roll-off as first-order systems. Disturbance attenuation objective is reached if $\|W_eSW_d\|_\infty < 1$. For effective disturbance rejection at low frequencies we setup $\|W_d\| > \|W_eS\|_\infty^{-1} > 1$. A first order diagonal W_d with 0.8 rad/s general crossover frequency was used. Finally, noise attenuation at the output is achieved if $\|W_eTW_n\|_\infty < 1$. At low frequencies $T \approx 1$ and $\|W_eW_n\|_\infty < 1$ so $\|W_n\| < \|W_e\|^{-1}$. and at high frequencies $T \approx GK$ so $\|W_eGKW_n\|_\infty < 1$, since ||GK|| and ||We|| rolls-off as a second and first-order system, respectively, then ||Wn||>1. Therefore, W_n was chosen as a high pass filter with first-order transfer functions with 80 rad/s as crossover frequency The weighting function modified under the above criteria's were

$$W_e(s) = diag\left\{\frac{15(.04s+1)}{100s+1}, \frac{15(.04s+1)}{100s+1}, \frac{15(.003s+1)}{1/.015s+1}\right\} \tag{10}$$

$$W_d(s) = \left\{\frac{10(2s+3)}{1/.008s+1} * I_3\right\} \tag{11}$$

$$W_r(s) = diag\left\{\frac{0.5(1/66s+1)}{s+1}, \frac{0.5(1/66s+1)}{s+1}, \frac{0.5(1/66.7s+1)}{0.5s+1},\right\} \tag{12}$$

$$W_n(s) = \left\{\frac{0.035(s+5.556)}{0.1s+85} * I_3\right\} \tag{13}$$

and the ideal model was

$$H_{des}(s) = \left\{\frac{0.1s+1}{s+1} * I_3\right\} \tag{14}$$

For this case the H_∞ optimal control design resulted in a 31-order $K_2(s)$ controller with $\gamma \approx 0.0688$. Clearly, nominal performance and robust stability but not robust performance was achieved by the controlled system as can be seen in Figure 6.

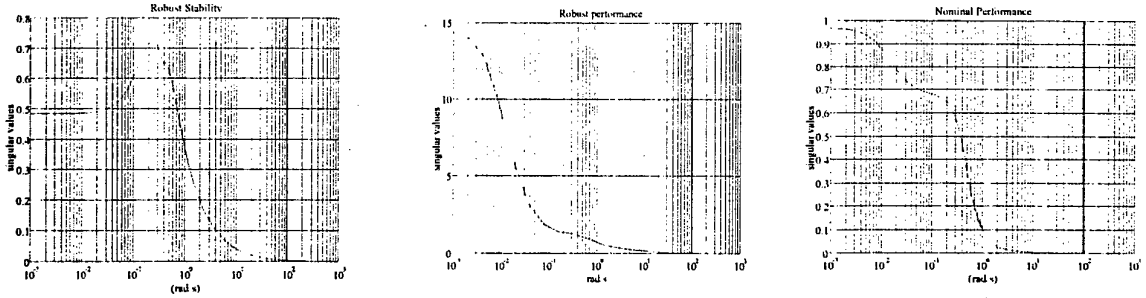

Figure 6: Robust stability, Nominal performance and robust performance for $K_2(s)$

This improvement in performance with respect to the first design was not without penalties since, the crossover frequencies for disturbance rejection and noise attenuation were smaller and larger than the previous design respectively.

4. μ-Synthesis

In terms of the Linear Fractional Transformation $F_\ell(G,K) = M(G,K)$ the perturbed transfer function $(w \to z_e)$ can be drawn as shown in Figure 7.

Figure 7: Linear Fractional Transformation

Partition of the transfer function matrix M as shown in Equation 6 with

$$\begin{aligned} M_{11} &= W_a KS \qquad M_{12} = [W_a KSW_r \quad -W_a KSW_d \quad -W_a KSW_n] \\ M_{21} &= -W_e S \qquad M_{22} = [W_e(H_{des} - T)W_r \quad -W_e SW_d \quad W_e TW_n] \end{aligned} \tag{15}$$

The left block diagram in Figure 7, shows the feedback arrangement for which system analysis of robust stability and nominal performance is based for a perturbation matrix Δ_a representing the uncertainty. Under the condition the system M(G,K) is nominally stable by K the following results apply,

- Stability is robust if and only if
$$\bar{\sigma}(M_{11}(j\omega)) < 1 \quad \forall\, \omega \tag{16}$$

- Nominal performance is satisfied if and only if
$$\bar{\sigma} = (M_{22}(j\omega)) < 1 \quad \forall\, \omega \tag{17}$$

The right block diagram in Figure 7 is used for robustness performance, Δ_f $(\|\Delta_f\|_\infty \le 1)$ is a fictitious "performance perturbation" connecting z_e to w. Provided that the closed-loop is nominally stable the non-conservative necessary and sufficient condition for robust performance is

$$\sup_w \mu_\Delta(M(j\omega)) < 1 \tag{18}$$

where $\Delta = diag\{\Delta_a, \Delta_f\}$

Briefly, the structured singular value μ of a complex matrix M is defined as

$$\mu_\Delta(M) := \frac{1}{\min\{\bar{\sigma}(\Delta):\ \det(I - M\Delta) = 0\}} \tag{19}$$

where $\Delta = diag\{\Delta_1, \Delta_2, \ldots, \Delta_p\}$ with $\|\Delta\|_\infty < 1$ and Δ_i are real or complex perturbations. Unless no Δ makes I-MΔ singular, in which case $\mu_\Delta(M) := 0$. Exact computation of the structured singular value is not possible though computable upper and lower bounds for μ have been developed. For a general Δ with real and complex

blocks $\mu_\Delta(M) \le \bar{\sigma}(M)$. The bound is refined with transformation on M that do not affect $\mu_\Delta(M)$, but do affect $\bar{\sigma}(M)$. The transformation is a block real-complex diagonal matrix $D \in \mathbf{D} = \{diag[d_1 I_1, d_2 I_2, ..., d_p I_p, I] : d_i > 0\}$ and $D\Delta = \Delta D$. A very important results is: $\mu_\Delta(M) = \mu_\Delta(DMD^{-1})$. Here we only consider the upper bound so replace the $\mu_\Delta(M)$ by the upper bound of $\mu, \bar{\sigma}(DMD^{-1})$. The goal of the μ-synthesis is to minimize over all stabilizing controllers K, the peak value of $\mu_\Delta(F_\ell(G,K))$ *or* $\bar{\sigma}(DF_\ell(\overline{G},K)(j\omega)D^{-1})$ at every frequency ω. That is

$$\min_K \min_{D_w \in \boldsymbol{D}} \bar{\sigma}[DF_\ell(G,K)(j\omega)D^{-1}] \tag{20}$$

where D_w is chosen to belong to $\boldsymbol{D}$ at every ω.
In this paper only complex perturbation Δ_a is considered and the set $\boldsymbol{D}$ is of the form $\boldsymbol{D} = \mathbf{D} = \{diag[d_1 I_1, I] : d_1 > 0\}$ where the scaling d_1 is a real rational, stable, minimum-phase transfer function. The optimization is for this problem

$$\min_K \min_{\hat{D}(s) \in \mathbf{D}} \left\| \hat{D} F_\ell(P,K) \hat{D}^{-1} \right\|_\infty \tag{21}$$

In this way the optimization problem of minimizing the worst case performance has been fit into the H_∞ synthesis framework. Optimizing over K and D simultaneously is in general not convex. An indirect scheme called the D-K iteration is used. D-K iteration optimizes over the stabilizing K(s) while holding $\hat{D}$(s) fixed and then optimizes over stable, minimum phase D(s) keeping K(s) fixed. For more details on the practicalities of this procedure can be found in (Balas, 1994) (Zhou. 1994).

5. Experimental Results.

The open-loop transfer function matrix of the 15 inputs and 9 outputs interconnection shown in Figure 3 is of the form:

$$G = \begin{bmatrix} 0 & 0 & 0 & 0 & W_a \\ -W_e & W_e H_{des} W_r & -W_e W_d & 0 & -W_e G_n \\ I & W_r & -W_d & -W_n & -G_n \end{bmatrix} \tag{22}$$

The block structure of the uncertainty for the robust performance objective was defined of the form $\Delta = diag\{\Delta_a, \Delta_f\}$. The appropriate D-scaling set is

$$\mathbf{D} := \left\{ D_i = \begin{bmatrix} dI_3 & 0 \\ 0 & I_3 \end{bmatrix}, D_d^{-1} = \begin{bmatrix} \frac{1}{d} I_3 & 0 \\ 0 & I_9 \end{bmatrix} : d > 0 \right\} \tag{23}$$

Robust performance analysis for the last H_∞ optimization design gave as results the plots shown in Figure 7. The μ-plot shows that robust performance is not achieved, since a peak-value of 14.5 at ω = 0.001 rad/s was obtained. That means that a perturbation matrix Δ_a with $\|\Delta_a\|_\infty = \frac{1}{14.5}$ make $\|W_e S\|_\infty > 1$. In this μ-synthesis, two iterations of the D-K iteration procedure were performed. For the first iteration we pick a second-order *d(s)*. Plots of robust stability, nominal and robust performance for the first iteration are shown in Figure 9. Clearly, robust stability, and nominal performance are achieved. Figure 9(c) shows the $\bar{\sigma}(\bullet)$ and $\mu_{\Delta_a}(\bullet)$. Clearly, the structured singular value analysis shows that the μ-synthesis yields an upper bound $\bar{\sigma}$=1.2, but the mu-bounds

still not achieved $\mu_{\Delta}(M)$ be less than one. A second iteration was carried out with a second –order *d(s)*. This new iteration brought a modest reduction of $\overline{\sigma}(\bullet)$ and the mu-bounds

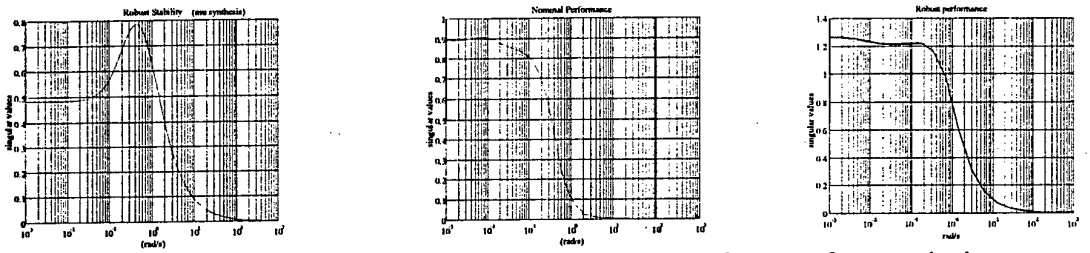

Figure 8: Robust stability, Nominal performance and robust performance for μ-synthesis

remained to be larger than one. Therefore, we kept the first iteration 42-order controller in order not to end with a too complex controller. To illustrate the robustness of close loop system in time domain the perturbed step responses for a 20° step reference on the third joint for the nominal and worst configuration of the controlled and uncontrolled system are shown in Figure 9. The controlled system tracks the reference signals without significant error for both configurations. Similar results were derived for the others joints.

(a) (b)

Figure 9: 20° step responses for two configurations (a) controlled system and (b) uncontrolled system

Figure 10 shows the effect of the load disturbance on third joint with and without controller for the nominal configuration. The mu-synthesis produced satisfactory regulation against load disturbances.

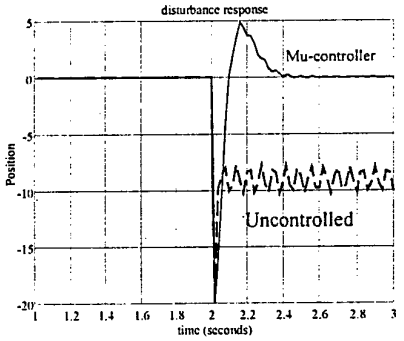

Figure 10: Load disturbance response on third joint

6. Conclusion

In this paper we applied an approach to robust controller synthesis, the μ-synthesis, to a 3-DOF arm manipulator. The robot already has a feedback linearization on each link, but due to mechanical design non-linearities are still

present that translate into bad performances and a system prone to instability. The design procedure applied started with an H∞ design based on a choice of weighting functions relying on engineering specifications. μ - analysis of this former controlled system shows a robust stable system that met the specifications but not achieved nominal performance neither robust performance. A second H∞ design with weighting functions chosen as to satisfy nominal performance was derived. A μ-analysis shows that the controlled system achieved robust stability and nominal performance. Finally, a μ-synthesis by use of D-K iteration with the last choice of weighting functions achieved robust stability, nominal performance and $\mu(M)$=1.2.

7. References

1. Ali, A. Edmunds J., 1997 "Choice of H∞ weighting functions to mould signal responses" Control system centre report No. 809, UMIST U.K.
2. Balas G., Doyle J., Glover K., Packard A. and Smith R., 1994 "Mu analysis and synthesis toolbox" Mathworks Inc.
3. Buso S., 1999 "Design of a robust voltage controller for a buck-boost converter using μ-synthesis", IEEE Trans. Aut. Cont. Vol.7 No. 2 222-229
4. González L. and Aguilar L. 1998 "H∞ robust control system design for a 3 DOF robot manipulator", Progress in system and robot analysis and control design. Ed Springer.
5. Kelly R., Carelli R., Ortega R., 1989 "Adaptive motion control design for robot manipulators" IEEE Trans. On robotics and automation, Vol. 50 No. 6 pp2563-2581.
6. Lind R., Brenner, M., 1997 "Worst case flutter margins from F/A-18 aircraft aeroelastic data" NASA Dryden Flight Research Center.
7. Lundström P, Skogestad S., and Doyle J., 1999 "Two degree of freedom controller design for an Ill-conditioned distillation process using μ-synthesis", IEEE Trans. Aut. Contr. Vol. 7 No.1
8. Lundström P., Skogestad S and Wang Z., 1991 "Uncertainty weight selection for H-infinity and mu-control methods", American Control Conference 1537-1542.
9. Packard A, Doyle J. and Balas G., 1993 "Linear, Multivariable Robust Control with μ Perspective", ASME 426-438.
10. Pannu S., Kazerooni H., Becker G. and Packard A. 1995 "μ-synthesis control for a walking robot" IEEE Control systems 20-25
11. Postlethwaite, I., Lin, J., 1992 "Weighting function selection for H∞ control design", IFAC 7th Congress Tallinin Estonia, USSR.
12. Gunnarsson K., 1997 "A μ-synthesis approach" Internal report of Group for aeronautical research and technology in Europe.
13. Zhou, K and Doyle J, 1998 "Essentials of robust control", Upper Saddle River, N.J., Prentice Hall.

1999 International Symposium on
Quantitative Feedback Theory and Robust Frequency Domain Methods

Robust frequency compensation of a low distortion audio power amplifier based on the listener perception

Wilmar Hernández * Augusto Mayer †

Abstract

In this work a design of an audio power amplifier is proposed where the performance characteristics are based in the listener perception by means of Quality Function Deployment (QFD) and Paired Comparison Analysis (PCA) techniques. An still important problem in audio is the non-linear distortion (magnitude and phase), it is a difficult technical problem to solve. μ-control is applied to design an ultra-linear HI-FI audio power amplifier with total harmonic distortion (THD) below the human perception limits. It is shown that the achievement of an appropriate distortion performance depends tremendously in the right choice of the control scheme, and not only in the components used. The results show a satisfactory relationship between THD and human auditory perception.

keywords: Quality Function Deployment (QFD), Paired Comparison Analysis (PCA), negative feedback (NFB), μ control, total harmonic distortion (THD), intermodulation distortion (IMD).

1 Introduction

The main objective of the present paper is the application of μ-control [1,2] to the compensator design of a class-B HI-FI audio power amplifier.

In audio amplifiers there is an ongoing concern about the benefits of negative feedback (NFB) in abating distortion, and it is evident that some quite conflicting views exist concerning the amount of NFB that shoul be used [3,4].

In an audio application, the power that must be delivered may vary from few watts to several kilowatts, with a flat amplitude frequency response from about 20 Hz to 20 kHz and linear phase. Unlike other power electronic systems, the most critical design consideration is not power efficiency but low distortion [5]. The output of an audio amplifier should

*W.Hernández is with the Electronics Department at Enginyeria La Salle, Universitat Ramon Llull, Paseo Bonanova 8, 08022 Barcelona, Spain. FAX: 3493-2902416. E-mail: cde002@salleURL.edu .

†A. Mayer is Innovation Director at Zanini Auto Grup, S.A., C/ Marineta 2, 08150 Paret del Valles, Barcelona, Spain. FAX: 34.93.5730164. E-mail: am-mjm@mail.cinet.es

be as closely as possible a replica of the input signal with larger amplitude, the transfer function must be linear and the gain must be constant (with linear phase) across the audio-frequency range [6]. The more difficult property to achieve is the linearity, and distortion o deviation from linearity is usually characterised by the total harmonic distortion (THD). The THD is rather a crude measure, and it does not necessarily indicate the perceived quality of the sound, because high-order harmonics are much more noticeable than low-order harmonics [7], but it is a useful indication of performance. An excellent explanation of the distortion mechanisms can be found in [4].

As a design example the amplifier of Fig. 1 designed in accordance with the philosophy of Self in [4] is considered, and both its THD and IMD (intermodulation distortion) are improved applying a robust frequency compensation [1,2].

In Section 2, we shall focus on the statement of the design objectives and their translation into requirements for the controller implementation, we will use quality function deployment (QFD) [8] and paired comparison analysis (PCA) [9] techniques to optimize performance from a users perspective. Section 3 is devoted to show the *blameless amplifier* proposed by Self in [4] and Section 4 shows the application of μ control. Finally, in Section 5, a comparison between both amplifiers is made and it is shown that the achievement of an appropriate distortion performance depends strongly in the right choice of the control scheme.

2 Translation of the design objectives

By *loop shaping* we mean a design method that involves explicitly shaping the magnitude of the loop transfer function, $|L(s)|$, [1,2]. Here $L(s) = G(s)K(s)$ where $K(s)$ is the feedback controller to be designed and $G(s)$ is the product of all other transfer functions around the loop, including the plant, the actuator and the measurement device. However, we must bridge the gap between this pure control theory approach and the final user quality criteria perspective. We need to establish clearly the attributes that our amplifier must have.

The QFD method [8] analyses the relation between the "**WHATs**" and the "**HOWs**". The **what** attributes have been obtained analyzing audio articles from specialized magazines in "high end" audio amplification and reproduction such as *Hi-Fi world, Revue du Son, Stereo Review*, etc. Table 1 shows the parameters of the QFD and , in Table 2, the user requirements are shown in the first column and their translation to electronic design are shown in the first row; here, symbol $\bullet\bullet$ represents a very high ($score = 10$), $\bullet$ high ($score = 8$), $\circ$ medium ($score = 6$), $\ominus$ low ($score = 2$), and N represents *no relationship.*

To focus on the **how** evaluation it is important to grade the relative importance of the amplifier attributes. For this purpose the PCA methodology [9] was used over the following target group: 5 seller specialists, 10 "high end" audio customers and 5 audio specialists. Fig. 2 shows the summary of the application of the PCA to the target group.

Table 3 shows the relation of **HOW's** vs. **WHATs** between the electronic engineer and the control engineer, where the **HOW's** of Table 2 have become the **WHAT's**. Table 3 shows the trade-offs in the controller implementation, where symbol $\overline{\sigma}(\star)$ represent larger singular value of "$\star$", $\underline{\sigma}(\star)$ represent smallest singular value of "$\star$", $\bullet$ repre-

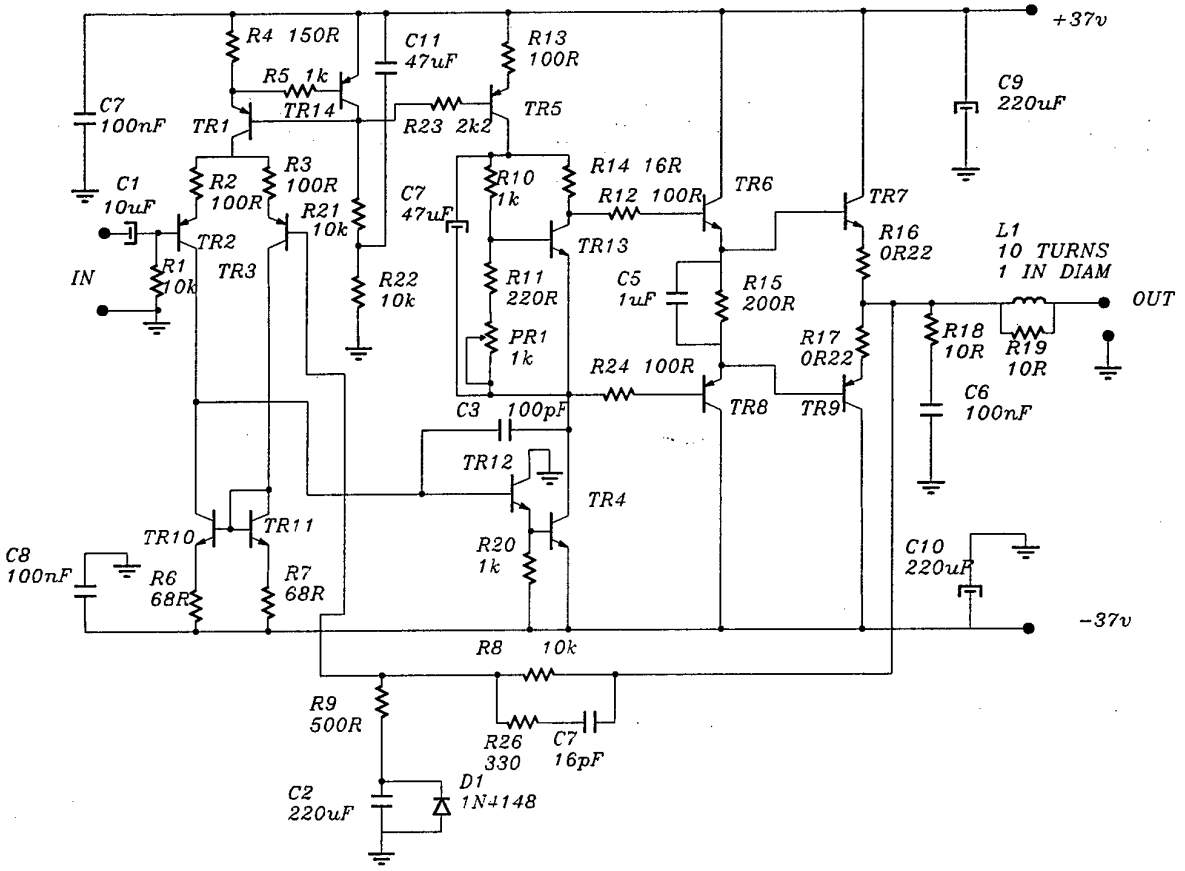

Figure 1: $50W$ class-B audio power amplifier.

sents strong positive relationship ($score = 10$), $\circ$ represent medium positive relationship ($score = 5$), $\times$ represent medium negative relationship ($score = -5$), and $\bigtriangledown$ strong negative relationship ($score = -10$).

As we can see in Table 3, the conflicting design objectives mentioned are generally in different frequency ranges, and we meet most of the objectives by using a large loop gain ($|L| > 1$) at low frequencies below crossover, a small gain ($|L| < 1$) at high frequencies above crossover, making the slope of $|GK|$ to be about -1 in the crossover region, and a roll-off of 2 or larger at higher frequencies (beyond the bandwidth).

Before finishing this section, it is important to say that Tables 2 and 3 show the basic requirements that are in conflict with the electronic design. However there are other requirements that are common for all audio amplifiers, and must be taken into consideration before building any audio amplifier. These are low noise transistors, low THD, an excellent power supply, and high quality loudspeakers, among others (see [12]).

	W_1	W_2	W_3	W_4	W_5	W_6	W_7	W_8	SIZE OF THE EQUIPMENT	SCORE	IMPORTANCE
W_1		W_1-1	0	W_1-2	W_5-1	W_1-1	W_1-3	0	W_1-3	10	15.38 %
W_2			W_3-1	W_2-1	W_5-1	0	W_2-3	W_8-1	W_2-3	7	10.77 %
W_3				W_3-2	W_5-1	W_3-1	W_3-3	0	W_3-3	10	15.38 %
W_4					W_5-2	W_6-1	W_4-2	W_8-2	W_4-3	5	07.69 %
W_5						W_5-1	W_5-3	W_5-1	W_5-3	13	20.00 %
W_6							W_6-3	W_8-1	W_6-3	7	10.77 %
W_7								W_8-3	W_7-3	3	04.62 %
W_8									W_8-3	10	15.38 %
SIZE OF THE EQUIPMENT										0	00.00 %
									TOTAL SCORE	65	

PREFERENCE WEIGHTINGS
0 - No difference in importance
1 - Slighly more important
2 - Reasonably more important
3 - Much more important

Figure 2: Paired Comparison Analysis

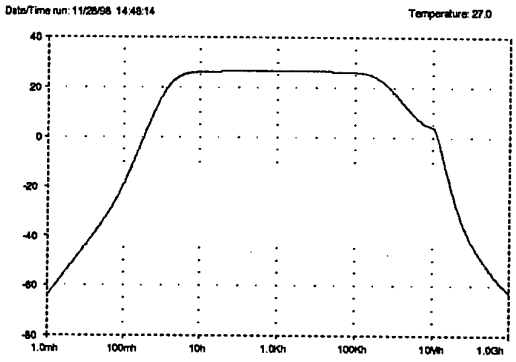

Figure 3: Magnitude plot of the closed-loop system: magnitude (dB) vs frequency (Hz), fequency is in *log scale*

3 Analysis of the class-B HI-FI audio power amplifier

The class-B audio power amplifier (the *blameless amplifier* [4]) is shown in Fig. 1, it is intended for domestic audio and, with the values shown, it delivers $50W/8\Omega$ from $1V_{rms}$ input. A detailed analysis of their performance is well discussed in [4].

3.1 Frequency compensation

According to Self [4], the NFB factor was chosen as 26.4 dB at 20 kHz which should give generous stability margin. Input resistor R_1 and feedback R_8 are made equal and kept as low as possible consistent with a rasonably high input impedance. The value of C_2 shown with R_9 give a low frequency roll-of that is -3 dB at 1.4 Hz, to prevent low frequency distortion rise due to capacitor non-linerity. C_7 provides some stabilising phase advance and limits the closed loop bandwidth; R_{26} prevents it upsetting Tr_3. Fig. 3 shows the PSpice magnitude plot (*PSpice 8.0*) of the closed-loop gain (from IN to OUT). PSpice Fourier analysis shows that the THD is about $2.43 \cdot 10^{-2}\%$ at 1 kHz (see Table 4).

	Definitons
W1	Denotes that the electronic equipment has to respond to rapid changes in intensity of various instrumens ($score = 10$)
W2	Ability to reproduce sudden strokes ($score = 7$)
W3	Ability to locate the sound sources in a precise point in the sound scene ($score = 10$)
W4	Amplification free of noise ($score = 5$)
W5	Pitch perception ($score = 13$)
W6	Timbre perception ($score = 7$)
W7	Low consumption ($score = 3$)
W8	No degradation of performance ($score = 10$)
H1	Bandwidth $\geq$ 80 kHz
H2	Slew-rate $\geq 40V/\mu sec$
H3	Phase linearity (error $\leq 5°$)
H4	Cut-off of the audio band with Gaussian shape
H5	High efficiency (class-B output stage)
H6	Noise attenuation
H7	Disturbance rejection
H8	Robust stability

Table 1: Parameters of the QFD

3.2 Comments

Fig. 3 shows that the compensated class-B HI-FI audio power amplifier has big amplification when signals at frequencies lying outside the audio band are fed into it. This subject has been object of discussions for many years in the audio community; however, a detailed analysis of the phase characteristic showed linear phase (see Fig. 4), which is very important for audio purposes [6]. It is important that the amplifier presents as linear phase as possible for stereophonic audio applications, this avoids a nebulous perception of a point source.

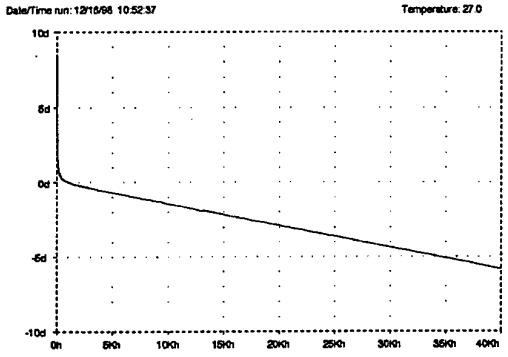

Figure 4: Phase (degrees) vs frequency (Hz), frequency is in *linear scale.*

WHATs vs. HOWs	**H1**	**H2**	**H3**	**H4**	**H5**	**H6**	**H7**	**H8**
W1 (10)	●	●●	*N*	*N*	*N*	*N*	*N*	*N*
W2 (7)	●	●	●	●●	*N*	*N*	*N*	*N*
W3 (10)	●	*N*	●●	*N*	*N*	*N*	*N*	*N*
W4 (5)	⊖	○	*N*	*N*	*N*	●●	●●	*N*
W5 (13)	●	●	●●	*N*	*N*	●	●	*N*
W6 (7)	●●	●	●●	●	*N*	●	●	*N*
W7 (3)	⊖	*N*	*N*	●	●●	○	○	○
W8 (10)	*N*	*N*	*N*	*N*	*N*	●	●●	●●
scoring:	406	346	356	150	30	308	328	118

Table 2: First stage of the QFD that shows the relationship between the need of the users and its translation into technical objectives of the electronic designer

HOWs→ *WHATs↓*	$\underline{\sigma}(GK)$ *large at* low frequencies	$\overline{\sigma}(GK)$ *small at* high frequencies	$\overline{\sigma}(K)$ *small at* high frequencies	*Slope of* $\lvert GK \rvert$ *to be about* -1 in the crossover region, and a roll-off of 2 or larger at higher frequencies (beyond the bandwidth)
H7 (8)	●	○	○	no relationship
H6 (7)	●	●	○	no relationship
H1,H2,H4 (10)	●	×	×	no relationship
H5 (5)	▽	●	●	○
H8 (6)	○	●	●	○
H1,H3,H4 (9)	●	○	×	●
scoring:	350	215	90	145

Table 3: Second stage of the QFD relating the control design to the technical objectives of the electronic designer

4 Robust frequency compensation

In this section, we shall use μ analysis and synthesis [1,2] to achieve robust stability and robust performance. Besides, other robust frequency domain techniques like the QFT (Quantitative Feedback Theory) technique can be used [16-19].

In our design example, stability is not the only property of closed-loop system that must be robust to perturbations; there are disturbances acting on the system (noise from the power supply system, component noise, nonlinearity in the stages of the amplifier, etc.) that result in nonlinear distortions.

4.1 Design and MATLAB simulation

Taking advantages of the design proposed by Self (Fig. 1) we keep the same basic structure, but without the phase advance network (C_7 and R_{26}). Since the amplifier in open loop presents a gain higher than 100 dB, an extraordinary input impedance and very low output impedance, we can consider in practical terms that it behaves as an operational amplifier [10]. Thus, its transfer function is

$$G_p(s) = \frac{sC_2(R_8 + R_9) + 1}{sC_2R_9 + 1} \tag{1}$$

For that reason the feedback network determines the closed loop dynamic response. Eq. 1 shows the plant transfer function.

We considered the case of *multiplicative input uncertainty* with performance defined in terms of weighted sensitivity [1,2]. The specifications $\| w_iT \|_\infty < 1$ and $\| w_pS \|_\infty < 1$ put bounds on the bandwidth and allow us to specify the roll-off of $L(s)$ above the bandwidth. From these bounds the uncertainty and performance weight were chosen as follows

$$w_i(s) = \frac{1.77 \cdot 10^{-7}s + 0.1}{3.54 \cdot 10^{-10}s + 1}$$

$$w_p(s) = \frac{0.625s + 9.42 \cdot 10^5}{s + 94.25}$$

where $w_i(s)$ represents the weight for the *closed loop transfer function* ($T(s)$) and $w_p(s)$ represents the weight for the *sensitivity function* ($S(s)$).

We used *DK-iteration* for obtaining the μ-optimal controller. Here K is the $\mathcal{H}_\infty$ controller and D is a scaling matrix that rescales the inputs and outputs to the trasnfer function to the input of the perturbations [1,2]. This method combines $\mathcal{H}_\infty$-synthesis and μ-analysis. The idea is to find a controller that minimizes the peak value over frequency, minimizing with respect to either K or D (while holding the other fixed).

Using the functions *hinfsyn*, *mu* and *musynflp*, among others, of the μ-Analysis and Synthesis Toolbox of Matlab [13], the $\mathcal{H}_\infty$ software gave a 7 state controller with an infinite-norm of the closed-loop system of 0.9132. This controller gave a peak value of μ of 0.9132 and Fig. 5 shows the μ-plot with μ-optimal controller (*Matlab 5.2*).

The controller equation is eq. 2, but it is too large. The control law is too complex with regard to practical implementation. So, we will reduce the controller's order. That

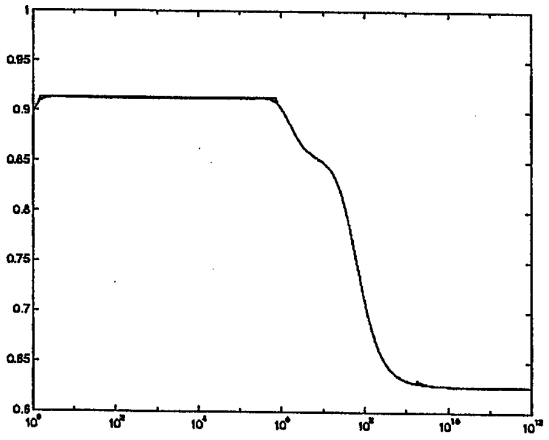

Figure 5: μ-plots with μ-"optimal" controller vs frequency (rad/sec).

is, given a high-order linear time-invariant stable model $K(s)$, we find a low-order approximation $K_a(s)$ such that the infinity ($\mathcal{H}_\infty$ or $\mathcal{L}_\infty$) norm of the difference, $\| K - K_a \|_\infty$, is small [1,2].

$$K(s) = \frac{1 \cdot 10^{-10} s^7 + 5.6 \cdot 10^2 s^6 + 1.8 \cdot 10^{12} s^5 + 6.7 \cdot 10^{20} s^4 + \\ +2.1 \cdot 10^{28} s^3 + 4.1 \cdot 10^{29} s^2 + 2.1 \cdot 10^{30} s + 1.9 \cdot 30}{s^7 + 3.2 \cdot 10^8 s^6 + 2.1 \cdot 10^{16} s^5 + 3.9 \cdot 10^{23} s^4 + \\ +4 \cdot 10^{25} s^3 + 3.8 \cdot 10^{26} s^2 + 4.7 \cdot 10^{26} s + 1 \cdot 10^{26}} \quad (2)$$

We used the "balanced truncation" method [1,2] to reduce the controller's order, obtaining the following Hankel singular values:

$$\Sigma = [8.9 \cdot 10^3, 2.7 \cdot 10^2, 4.9 \cdot 10^1, 8.3 \cdot 10^{-3}, 6.4 \cdot 10^{-4}, 5.9 \cdot 10^{-6}, 1.1 \cdot 10^{-6}]$$

As we known, after a balanced realization [1,2] each state is just as controllable as it is observable, and a measure of state's joint observability and controllability is given by its associated Hankel singular value. Then we can obtain $K_a(s)$ by truncating the balanced realization of $K(s)$ to the first $(r_1 + ... + r_k)$ state. Then

$$\| K(s) - K_a(s) \|_\infty \leq 2(\sigma_{k+1}, \sigma_{k+2}, \cdots, \sigma_N)$$

Taking into consideration the performance requirements, the best choice is the order three reduced controller. Then, the new controller transfer function is

$$K_a(s) = \frac{1 \cdot 10^{-10} s^3 + 5.5 \cdot 10^4 s^2 + 5.6 \cdot 10^5 s + 5.4 \cdot 10^5}{s^3 + 9.6 \cdot 10^1 s^2 + 1.3 \cdot^2 s + 2.9 \cdot 10^1} \quad (3)$$

4.2 Implementation and results

The performance of the closed-loop system with compensator eq. 3 has been examined using PSpice simulations. Fig. 6 shows the configuration of the new class-B HI-FI audio

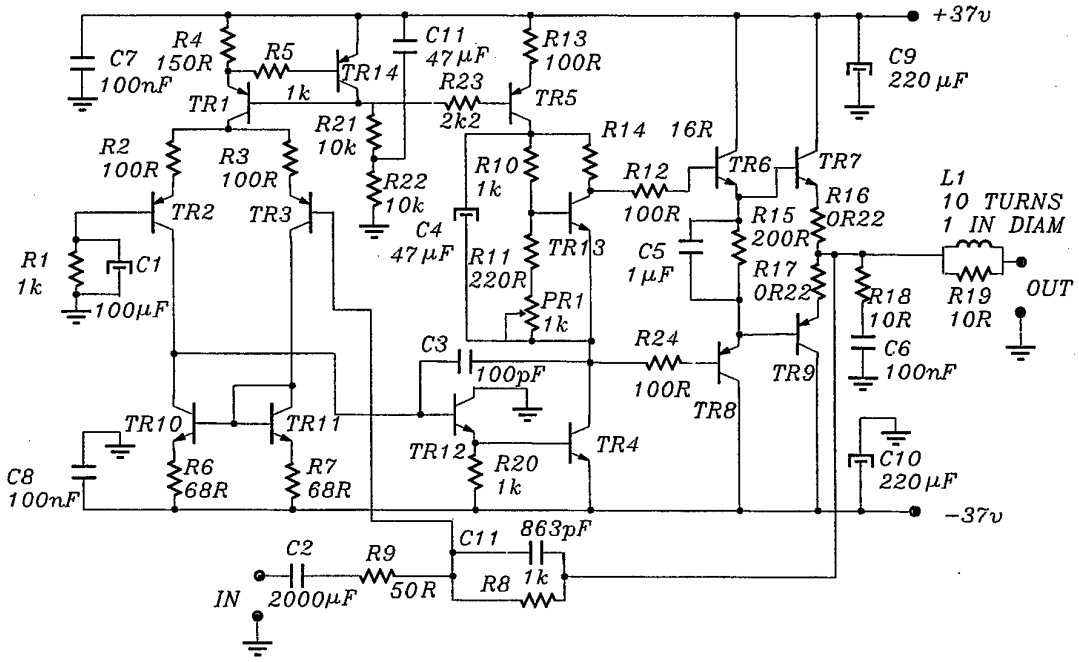

Figure 6: $50W$ class-B audio power amplifier using the robust compensation

power amplifier. It has been implemented taking advantage of the well-known operational properties of the amplifier [10]. That is, we shaped the open-loop transfer function to implement a closed-loop transfer function which will be multiplied by a gain factor, so that the desired frequency response is achieved.

The THD for the amplifier shown in Fig. 6 is about $8.149 \cdot 10^{-3}\%$ (see Table 4) which is approximately 3 times better than the one obtained before (Self's amplifier). Besides, its frequency response (see Fig. 7) is in total accordance with the audio-frequency range. This way, we fit the closed-loop bandwidth by using an electronics structure obtained from the implementation of the robust closed-loop transfer function.

5 Comparison and discussion of the results

According to Tuinenga [11], among others [3,4,12], signal distortions can be of many kinds (most of them undesirable) and are usually the result of nonlinearity in the gain or in the phase, of a circuit. *Harmonic distortion* comes from nonlinear gain. The output of the circuit contains harmonics of the input frequencies. *Phase ditortion* comes from nonlinear phase versus frequency response. This gives rise to "echoes" in the output that precede and follow the main response, resulting in a distortion of the output signal when the input signal is not a pure sinusoid. And *Intermodulation distortion* comes from mixing signals at different frequencies. The output of the circuit contains signals at multiples of the sum

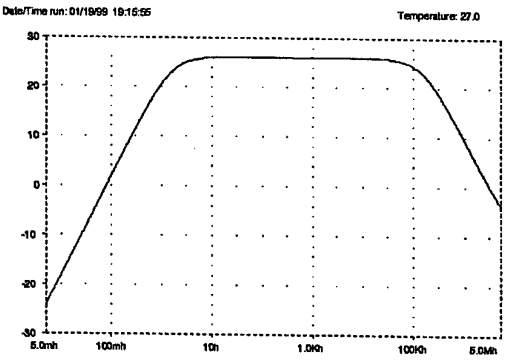

Figure 7: Magnitude plot of the robust design: magnitude (dB) vs frequency (Hz), frequency is in *log scale*

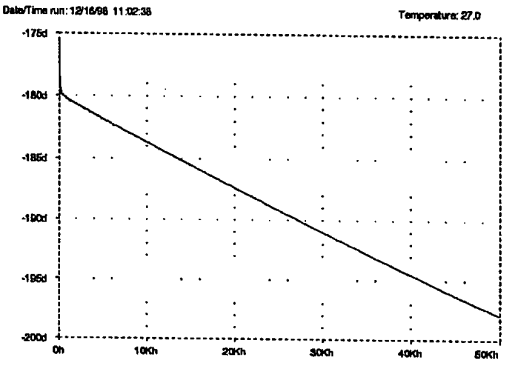

Figure 8: Phase (degrees) versus linear frequency (Hz) for the robust design

and difference of the original frequencies.

5.1 Analysis of the THD and the phase distortion

For both power amplifier designs the phase characteristic was satisfactory (see Fig. 4 and Fig. 8). Table 4 shows the Fourier components of the two designs. Note the benefits of using the μ controller: THD for the robust design is better than for the classical one.

The THD obtained in this work is reported for a single input frequency at 1 kHz, which is one of the performance characteristics typically used by the HI-FI audio amplifier manufacturers (see the "Fletcher-Munson curves" [14,15,6] and [7]).

With the phase characteristics shown in Fig. 4 and Fig. 8 we assure that the phase distortions of both audio power amplifers are not affecting the localization of the apparent direction of the sound source. Some experiments [6] have shown that the average localization errors for sounds straight ahead are of the order of 5° while errors for sounds off to the side are of the order of 10° or 15°. Note that both amplifers shown in this work have ultra-linear phase characteristics.

Frequency (Hz)	**Fourier component Fig. 1**	**Fourier component Fig. 6**
$1.000 \cdot 10^3$	$1.890 \cdot 10^1$	$1.800 \cdot 10^1$
$2.000 \cdot 10^3$	$3.237 \cdot 10^{-3}$	$1.019 \cdot 10^{-3}$
$3.000 \cdot 10^3$	$2.029 \cdot 10^{-3}$	$6.300 \cdot 10^{-4}$
$4.000 \cdot 10^3$	$1.465 \cdot 10^{-3}$	$4.234 \cdot 10^{-4}$
$5.000 \cdot 10^3$	$1.192 \cdot 10^{-3}$	$4.144 \cdot 10^{-4}$
$6.000 \cdot 10^3$	$9.471 \cdot 10^{-4}$	$2.781 \cdot 10^{-4}$
$7.000 \cdot 10^3$	$8.790 \cdot 10^{-4}$	$3.486 \cdot 10^{-4}$
$8.000 \cdot 10^3$	$7.065 \cdot 10^{-4}$	$2.253 \cdot 10^{-4}$
$9.000 \cdot 10^3$	$7.017 \cdot 10^{-4}$	$2.827 \cdot 10^{-4}$
$1.000 \cdot 10^4$	$5.141 \cdot 10^{-4}$	$1.898 \cdot 10^{-4}$
THD (%)	$2.430 \cdot 10^{-2}$	$8.149 \cdot 10^{-3}$

Table 4: Fourier components of the transient responses for both amplifiers

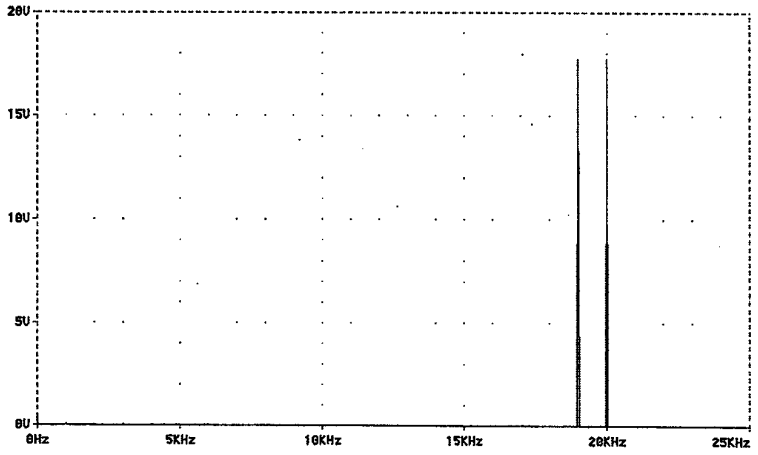

Figure 9: The IMD characteristic for the amplifier of Fig. 6

5.2 Analysis of the IMD

Finally, figures 9 and 10 show the intermodulation distortion (IMD) characteristics for both amplifers. Amplitudes of 19 kHz and 20 kHz input signals can be seen on the graphs. Any intermodulation created by these two signals would appear as peaks at 1 kHz intervals, the frequency difference between the two signals, across the frequency bandwidth. From Fig. 9 can be seen that IMD the is less than -50 dB for the amplifier of Fig. 6, whereas the IMD is very poor for the amplifier of Fig. 1. Another form of IMD would appear at 39 kHz, the sum of the two input signals frequencies. Such a distortion, even if it existed, would be irrelevant because it is far beyond the audible range.

Besides, Fig. 10 shows a bad amplification of signals around 20 kHz by the first amplifier (Fig. 1), because of the sudden changes in the magnitude plot of the Self's amplifier around 20 Hz, 20 kHz and 10 MHz (see Fig. 3); although the last frequency is not important for this application. This shows a nonlinear gain distortion. However, the frequency

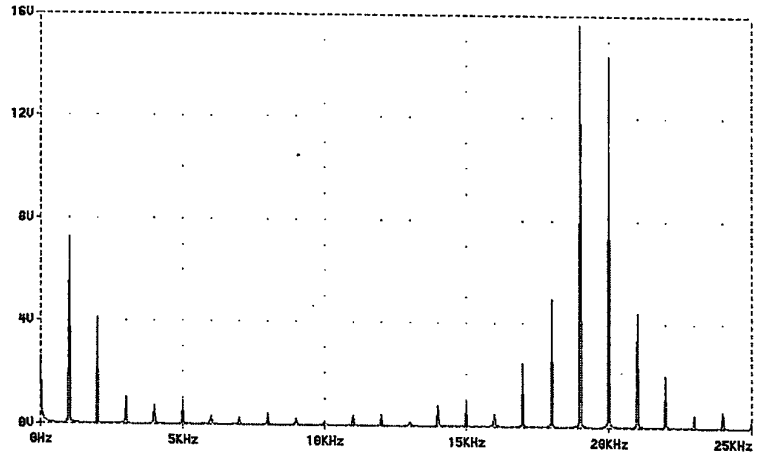

Figure 10: The IMD characteristic for the amplifier of Fig. 1

response of the robust amplifier (see Fig. 7) is ultra-linear in all the frequency range of analysis. All these results justify the application of high performance optimization techniques for designing HI-FI audio amplifiers.

Conclusions

In the first sections we focused on the difficulties and translation of the design objectives into the requirements of the loop transfer function. In order to resolve better the trade-offs on $L(s)$ for a clear understanding of the design process we used QFD and PCA techniques. As a result a robust linear controller was designed and compared with the results obtained using classical electronic techniques. The results helped us to understand that the robust approach is really necessary when a system is subjected to real operating conditions. The use of robust frequency domain tehcniques let us to optimize the feedback network of the amplifier, by using a minimal number of components.

Acknowledgement

We want to thanks Professors Dr. Josep Martì Roca and Robert Bartí, Enginyeria La Salle (Barcelona, Spain), for many helpful discussions on HI-FI audio reproduction; and Professor Dr. Ricard Villà, Universitat Politènica de Catalunya, Barcelona, for his valuable cooperation in the draft of this paper. Also, the first author wants to thank Professors Dr. Isaac Horwitz (Professor Emeritus, Weizmann Institute of Science, and Professor Emeritus, University of California), Dr. Oded Yaniv (Tel Aviv University), Dr. Yossi Chait (University of Massachusetts, Amherst), and Dr. Constantine Houpis (Professor Emeritus Electrical Engineering, Air Force Institute of Technology) for their kind cooperation in his introduction to QFT techniques. This work has been supported by Enginyeria La Salle, Universitat Ramon Llull, Barcelona, Spain.

References

[1] Zhou, K., Doyle, J. C. and Glover, K., *Robust and Optimal Control.* Prentice-Hall, 1996.

[2] Skogestad, S. and Postlethwaite, I., *Multivariable Feedback Control.* John Wiley & Sons, 1996.

[3] Baxandall, P. J., "Audio power amplifier design", *Electronics World and Wireless World,* January 1978 to February 1979.

[4] Self, D., "Distortion in power amplifiers", *Electronics World and Wireless World,* August 1993 to March 1994.

[5] Ross, J. N., *The Essence of Power Electronics.* Prentice-Hall, 1997.

[6] Dowling, W. J. and Harwood, D. L., *Music Cognition.* Academic Press, 1986.

[7] Yue Lin, H., "Measurement of Auditory Distortion with Relation Between Harmonic Distortion and Human Auditory Sensation", *IEEE Transactions on Instrumentation and Measurement,* Vol. IM-35, No.2, June 1986.

[8] Clausing, D., "The House of Quality", *Harvard Business Review,* May-June, 1988.

[9] Basadur, M., *The Power of Innovation.* Pitman Publishing, London, 1995.

[10] Gray, P. R. and Meyer, R. G., *Analysis and Design of Analog Integrated Circuits.* John Wiley & Sons, 1977.

[11] Tuinenga, P. W., *SPICE: A Guide to Circuit Simulation And Analysis Using PSpice.* Prentice-Hall, 1998.

[12] Paradiso, J. A., "Electronic music: new ways to play", *IEEE Spectrum,* pages 18-30, December 1997.

[13] Balas, G. J., Doyle, J. C., Glover, K., Packard, A. and Smith, R., *μ-Analysis and Synthesis Toolbox User's Guide.* MUSYNC Inc. and The MathWorks, Inc., 1995.

[14] Fletcher, H. and Munson, W. A., "Loudness, its definition, measurement, and calculation", *Journal of the Acoustical Society of America,* Vol. 5, pages 82-105, 1933.

[15] Hassall, J. R. and Zaveri, K., *Acoustic Noise Measurements.* Brüel & Kjaer, 1979.

[16] Horowitz, I. M., *Synthesis of Feedback Systems.* Academic-Press, New York, 1963.

[17] Horowitz, I. M., "Survey of quantitative feedback theory", *Int. J. Control,* 53 (2), pages 255-291, 1991.

[18] Houpis, C. H., Sating, R., Rasmussen, S. and Sheldon, S., "Quantitative feedback theory technique and applications", *Int. J. Control,* 59 (1), pages 39-70, 1994.

[19] Borghesani, C., Chait, Y. and Yaniv, O., *Quantitative Feedback Theory Toolbox.* The MathWorks, Inc., 1994.

1999 International Symposium on
Quantitative Feedback Theory and Robust Frequency Domain Methods

$\mathcal{H}_\infty$ Loop Shaping for Systems with Hard Bounds

Wolfgang Reinelt

Division of Automatic Control, Dept of Electrical Engineering,
Linköping University, 581 83 Linköping, Sweden,
email: wolle@isy.liu.se, http://www.control.isy.liu.se/~wolle/

Abstract

We study multivariable control systems with hard bounded control signals. The reference signals are hard-bounded in their amplitude and speed, which appears in many applications. This description leads therefore to a non-conservative controller design. The design procedure itself is based on $\mathcal{H}_\infty$ Loop Shaping; the problem of systematic adaption on the weights when receiving a too large control signal after a loop shaping step is discussed. Finally, design examples are given.

Keywords: Robust Control, $\mathcal{H}_\infty$ Loop Shaping, Multivariable Systems, Hard Bounds, Saturations.

1 Introduction and Motivation

Most practical control problems are dominated by *hard bounds*. Valves can only be operated between fully open and fully closed, pumps and compressors have a finite throughput capacity and tanks can only hold a certain volume. These input- or actuator-bounds convert the linear model into a nonlinear one. Exceeding these prescribed bounds causes unexpected behaviour of the system – large overshoots, low performance or (in the worst case) instability. Furthermore, process models are always inaccurate – even extremely detailed models may contain unknown or slowly changing physical parameters; so the controller has to manage the difference between the model (used for design) and the real plant. Bridging the gap between model and real plant is the field of *robust controller design*.

$\mathcal{H}_\infty$ Loop Shaping is a popular design method to form the open loop (i.e. its singular values in the frequency range of interest) by introduction of weights, in order to fulfill certain aims as disturbance rejection etc. We shortly state this method in section 2.

We discuss an extension of this procedure in order to meet a prescribed hard bound for the control signal. In the case of more control signals, we are able to handle a hard bound for each of them. The first step is to calculate the maximum of the control signal(s) for a given set of reference signals: the reference signal and its first derivative are bounded. This appears in many systems, for example in a tank, not only the liquid-level is bounded (by the tank's height), additionally the liquid cannot change its level arbitrarily fast. All in all, the componentwise handling of the control signal bounds and the described class of reference signals produce a non-conservative controller. We discuss this in section 3.

One main point is the systematic adjustment of the design weights during the loop shaping procedure in the case that the bounds are not met. We derive an explicit relation between maximum control variable and the singular values of the corresponding transfer function, visible during the loop shaping procedure. The procedure works for LTI multivariable plants and is presented in section 4. The handling of the problem in the discrete time case is briefly outlined in section 5.

Two detailed examples are given in section 6. The first example – the control of the vertical dynamics of an aircraft – demonstrates the usage of the procedure in the multivariable and continuous time case. As a second example, we discuss the two-mass-spring benchmark problem (as posed on the 1992 ACC) in the discrete time domain. We discuss the controller design and analyse robust stability and performance with regard to parameter changes.

2 $\mathcal{H}_\infty$ Loop Shaping Design Procedure – basic facts

As we adapt the $\mathcal{H}_\infty$ Loop Shaping Design Procedure (LSDP) in some way, we present its basic facts first. All results including the proofs and more details can be found in [4]. We use the notation from standard robust control theory textbooks [3].
A continuous time state-space system

$$\begin{aligned} \dot{x}(t) &= Ax(t) + Bu(t) \\ y(t) &= Cx(t) + Du(t) \end{aligned}$$

will be denoted (A, B, C, D) or $\left[\begin{array}{c|c} A & B \\ \hline C & D \end{array}\right]$. The corresponding transfer-function is given by $G(s) = C(sI-A)^{-1}B + D$ and will be abbreviated as $G(s) \stackrel{s}{=} (A, B, C, D)$ or $G(s) \stackrel{s}{=} \left[\begin{array}{c|c} A & B \\ \hline C & D \end{array}\right]$. As "degree" of a transfer-function we will understand the McMillan degree. The ∞-norm of a transfer-function matrix G is defined by $\|G\|_\infty := \sup_\omega \overline{\sigma}(G(i\omega))$ where $\overline{\sigma}(\cdot)$ denotes the maximum singular value. $\mathcal{H}_\infty$ denotes the space of all real rational transfer-function matrices with finite ∞-norm and no poles in $Re(s) > 0$. Let P and Q the controllability resp. observability gramian of G. The Hankel singular values of G are given by $\sigma_j := \lambda_j^{1/2}(PQ), j = 1, \ldots, n$, where n is the degree of G and λ_j denotes the eigenvalue. The Hankel singular values are ordered by convention: $\sigma_1 \geq \sigma_2 \geq \cdots \geq \sigma_n \geq 0$. The Hankel Norm of G ist given by $\|G\|_H := \sigma_1(G)$. Due to Nehari's Theorem, $\|G\|_H \leq \|G\|_\infty$ holds.

Let $G = M^{-1}N$ be the plant to be controlled, represented in the normalized left coprime factorization (NLCF) and G_Δ be a perturbation of this nominal plant. The uncertainty is straightforward modelled as an error of the coprime factors (N, M):

$$G_\Delta = (M + \Delta_M)^{-1}(N + \Delta_N). \tag{1}$$

For $\epsilon > 0$ a perturbation $\Delta = [\Delta_N, \Delta_M]$ of a transfer function as described in eqn.(1) is called (ϵ-) admissible, when $\|\Delta\|_\infty < \epsilon$ holds. The set of all (ϵ-)admissible perturbations is denoted by $\mathcal{D}_\epsilon$:

$$\mathcal{D}_\epsilon := \{\Delta : \Delta \in \mathcal{H}_\infty; \|\Delta\|_\infty < \epsilon\} \tag{2}$$

This approach has several advantages: the error bounds of the coprime factors can be choosen smaller than those of e.g. a multiplicative error and all participated "components" – numerator, denominator and their errors – are stable even if the plant itself is unstable. Additional advantages become clear when discussing robust stabilization within this framework:

2.1 Robust Stabilization Theorem The controller K stabilizes the uncertain plant $G_\Delta = (M+\Delta_M)^{-1}(N+\Delta_N)$ for all $\Delta = [\Delta_N, \Delta_M] \in \mathcal{D}_\epsilon$ iff it stabilizes the nominal plant G and the following equation holds:

$$\left\| \begin{bmatrix} K(I-GK)^{-1}M^{-1} \\ (I-GK)^{-1}M^{-1} \end{bmatrix} \right\|_\infty \leq 1/\epsilon. \tag{3}$$

Moreover, the theorem comes with a calculation of the controller K for a given ϵ, details are given in [4]. It it clear from the Robust Stabilization Theorem 2.1, that we are in principle looking the largest positive number $\epsilon (= \epsilon_{max})$, which fulfils equation (3). In this case, we will have "maximal robustness". Because of the NLCF representation, this *maximum stability margin* can be obtained in a surprisingly explicit manner by:

$$\epsilon_{max} = \left(\inf_{\text{stab K}} \left\| \begin{bmatrix} K \\ I \end{bmatrix} (I-GK)^{-1}M^{-1} \right\|_\infty \right)^{-1} = \sqrt{1 - \|[N, M]\|_H^2} \tag{4}$$

We refer to the controller, ensuring the maximum stability margin ϵ_{max}, as the *optimal* controller. All other controllers producing an $\epsilon < \epsilon_{max}$ are called *suboptimal* controllers. For the suboptimal controllers we define the *performance factor* f by $f := \epsilon_{max}/\epsilon \quad (> 1)$. In practice, this performance factor

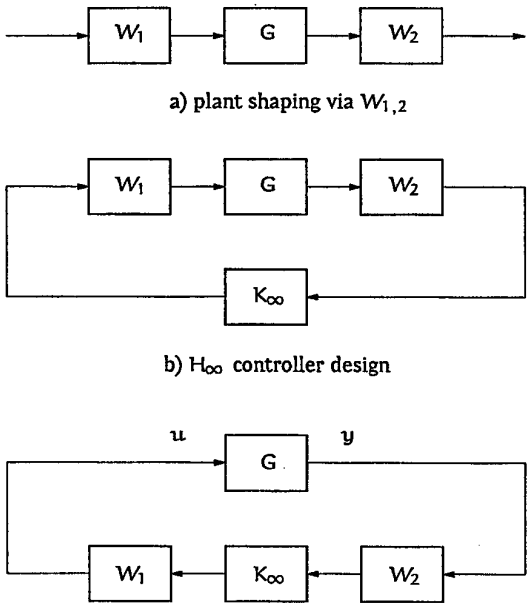

Figure 1: Loop shaping and controller design in three steps.

is the design-parameter for the computation of the controller. Because the maximum stability margin ϵ_{max} is not known a-priori, the designer decides via performance factor f, whether an optimal or a suboptimal controller is wanted. To avoid numerical problems, it is common to design a suboptimal controller with performance factor as $f = 1.1$.

The results until now enable us to robustly stabilize uncertain plants. Performance features as disturbance rejection etc. are encorporated by open loop shaping. The open loop is shaped using input- and output-weights, until a desired shape is reached. A major drawback is inherent in all open loop shaping methods: one can only shape the plant instead of the open loop (consisting of plant *and* controller) and the shape of the open loop has to be checked after the controller design. Within this technique, this problem is solved elegantly: a large stability margin, resulting from the controller design, ensures a similar shape of shaped plant and final open loop. Clear from eqn.(4), that the stability margin ranges in $(0, 1)$. In practice, a stability margin of about $\epsilon \geq 0.3$ is large enough.

All in all, the complete $\mathcal{H}_\infty$ Loop Shaping Design Procedure consists of the following steps (see figure 1):

1. Choose a performance factor f and weights W_1 and W_2 to shape the plant.
2. Controller-design ($\mathcal{K}_\infty$) for the shaped plant and calculation of the stability margin ϵ.
3. Calculation of the final controller (including the weights).
4. Decide whether the design-objectives are fulfilled or not:
   - Is the stability margin ϵ large enough?
   - Are the performance-objectives fulfilled?

   If not, choose other weights W_1, W_2 (and/or another performance factor f) and go back to the first step.

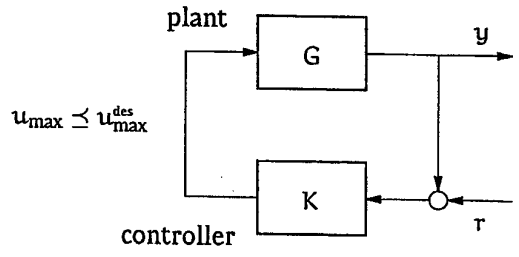

Figure 2: Control loop with constraint control variable u.

3 Maximum Control Signal in a Control System

As motivated in the introduction, we study control systems with reference signals, bounded in amplitude and speed. Aim of the controller design is to handle hard bounds of the control signal. The signals are depicted in the standard control loop in figure 2. We start with the following definitions, which are extensions of those given by Reichel [6] to the multivariable case, as outlined in [7]:

3.1 Definition (Admissible Reference Signal) Given $0 \preceq R, \dot{R} \in \mathbb{R}^n$. Then a vector-valued reference signal r is called $(R, \dot{R})$-admissible, when the following properties hold:

1. $r(t) = 0$ for all $t \leq 0$,
2. $|r(t)| \preceq R$ for all $t > 0$ and
3. $|\dot{r}(t)| \preceq \dot{R}$ for all $t > 0$,

whereas $\preceq$ denotes componentwise $\leq$ and $|\cdot|$ has to be evaluated componentwisely in this context. The set of all $(R, \dot{R})$-admissible reference signals is denoted by $\mathcal{A}(R, \dot{R})$.

3.2 Definition (Maximum Control Signal) Given the internally stable standard control loop as in figure 2. We call

$$u_{max} := \begin{pmatrix} \sup\{\|u_1\|_\infty;\ \forall r \in \mathcal{A}(R, \dot{R})\} \\ \vdots \\ \sup\{\|u_n\|_\infty;\ \forall r \in \mathcal{A}(R, \dot{R})\} \end{pmatrix} \tag{5}$$

the Maximum Control Signal.

The definition of the admissible reference signal is quite straightforward from the motivation. The componentwise definition of the maximum control signal enables us to handle hard bounds for each of the control signals, which is a clear advantage compared to the ∞-*norm* of a vector-values signal, for example. Additionally, we state the following system-theoretic result given by Reichel [6]:

3.3 Theorem and Algorithm (Reichel, 1984) Given a linear and time invariant SISO system with input $x(t)$ and output $y(t)$. Let the input be $(X, \dot{X})$-admissible.

(a) There exists an algorithm that determines the maximum output of this system: $y_{max} = \sup_{t>0} |y(t)|$ for all admissible reference signals.

(b) An $(X, \dot{X})$-admissible input exists, so that y_{max} is achieved.

The algorithm outlined in the original work [6] constructs a worst case input x. This solution is also discussed in [9]. An alternative numerical solution of the problem, based on nonlinear optimization, has been shown in [7]. Independent of the numerical solution, Theorem 3.3 can be used in the SISO case to determine the maximum control signal u_{max}, when the reference signal $r(t)$ is $(R, \dot{R})$-admissible (with the obvious replacement r instead of x and u instead of y).

In the following we will see, that it is also usefull in the multivariable case. Let us first look onto a system with one output y and k inputs $x = (x_1, \ldots, x_k)^T \in \mathcal{A}(X, \dot{X})$. Then $y(s)$ is given by

$$y(s) = H_1(s) \cdot x_1(s) + \cdots + H_k(s) \cdot x_k(s) \tag{6}$$

We abbreviate $\tilde{y}_i(s) = H_i(s) \cdot x_i(s)$. Now we are looking for the maximum output amplitude y_{max}. Using eqn. (6), the maximum output amplitude is given by

$$y_{max} = \sum_{i=1}^{k} \tilde{y}_{i,max}. \tag{7}$$

It follows directly, that y_{max} is achieved for a certain *vector* $x = (x_1, \ldots, x_k)^T \in \mathcal{A}(X, \dot{X})$.

In the multivariable case with n outputs, we simply apply the first step: according to the definition, the components $y_{max,j}$ of y_{max} can be computed as in equation (7).

The method presented in this section enables us to calculate the maximum output of a system with certain input restrictions; in particular, it enables us to calculate the maximum control signal of a control system, when the external signal, i.e. the reference signal fulfills these constraints. We will exploit this in the next section.

4 $\mathcal{H}_\infty$ Loop Shaping for Systems with Constraints

Given a (multivariable) plant G, restrictions $R, \dot{R} \succeq 0$ for the reference signal and a desired maximum control signal $u_{max}^{des} \succ 0$ we extend the Loop Shaping Procedure (see sec. 2, figure 1) in the following way:

1. Choose a performance factor f and weights W_1 and W_2 to shape the plant.
2. Controller-design for the shaped plant and calculation of the stability margin ϵ.
3. Calculation of the final controller (including the weights).
4. Decide whether the design-objectives are fulfilled or not:
   - Is the stability margin ϵ large enough?
   - Are the performance-objectives fulfilled?
   - Does $u_{max} \preceq u_{max}^{des}$ hold?

   If not, choose other weights W_1, W_2 (and/or another performance factor f) and go back to the first step.

Theorem 3.3 enables us to determine the maximum control signal u_{max} within the control loop, which allows the check for the desired bound on the control signal in step 4. This additional check is the only difference to the classical LSDP. We refer to this procedure in the following with Extended Loop Shaping Design Procedure (ELSDP).

Finally, we discuss a question we dropped when repeating the classical LSDP: after a first choice of weights, our design objectives are usually *not* fulfilled – the weights have to be adjusted. In the case of a too small stability margin ϵ the strategy is clear from the classical LSDP: because there is no explicit relation known between achieved stability margin and weights, we have to examine the singular values of the shaped plant and the achieved open loop. In the frequency range with a significant difference, our weights are incompatibel with the plant and have to be adjusted.In the following we discuss the remaining open question: Is there a strategy for correct and systematic adjustment of the weights, when the control signal bound fails after a loop shaping step?

Within loop shaping, we work on the singular values of different interesting transfer functions. Thus we are searching for a relation between the singular values of the transfer function and the maximum control signal u_{max}. The relation between reference signal and control signal is given by

$$\begin{aligned} u(s) &= H(s) \cdot r(s) \quad \text{resp.} \\ u(t) &= h(t) \star r(t) \end{aligned}$$

where "$\star$" denotes the convolution. Because of the componentwise definition of the maximum control sariable, we restrict our following examinations to the case of a single control variable. The generalization follows immediately as in the previous section (by componentwise usage).

Well known from linear system theory is the following inequality

$$\|u\|_\infty \leq \|h\|_1 \|r\|_\infty, \tag{8}$$

where $\|h\|_1$ denotes the 1-norm of the impulse response $\|h\|_1 := \int_0^\infty |h(t)|dt$. To get the link from the (time domain) impulse response to the (frequency domain) transfer function, we state a result from model reduction [2]:

4.1 Lemma (Glover, Curtain and Partington, 1985) Let H be a asymptotically stable and strictly proper transfer function, then

$$2 \cdot \|H\|_N \geq \|h\|_1 \geq \|H\|_\infty \tag{9}$$

holds whereas $\|\cdot\|_N$ denotes the nuclear norm $\|H\|_N := \sum_{j=1}^{n} \sigma_j(H)$ and $\sigma_1 \geq \sigma_2 \geq \cdots \geq \sigma_n > 0$ are the Hankel singular values in descending order.

Combining equation (8) and (9) we have the following situation:

$$\|u\|_\infty \leq \|h\|_1 \cdot \|r\|_\infty \leq 2 \cdot \|H\|_N \cdot \|r\|_\infty. \tag{10}$$

Exploiting $\sigma_1(H) = \|H\|_H \leq \|H\|_\infty$, the previous equation (10) degenerates to

$$\|u\|_\infty \leq 2n \cdot \|H\|_\infty \cdot \|r\|_\infty \tag{11}$$

where n denotes the McMillan degree of H.

We now turn back to our final aim: the relation between the singular values of H and $\|u\|_\infty$. As the control loop is internally stable, the transfer function H is stable. Following equation (11), we see that decreasing the ∞-norm of $H(s)$ decreases an upper bound for the maximum control signal.

Suppose, the maximum control signal is too high after a loop shaping step. We then have to decrease the maximum singular value of H in the frequency range where the ∞-norm appears. In the case of a too low maximum control signal, we have to increase the maximum singular value in that frequency range. We point out, that this affects only an *upper bound* for the maximum control signal. This practical value of this guideline is shown in the examples.

The last question to answer is, if a relation between the singular values of the weights and those of the transfer function H exists. Using the relations $H(s) = (I - G(s)K(s))^{-1}K(s)$ and $K(s) = W_1(s)K_\infty(s)W_2(s)$, from the loop shaping procedure, we get

$$\begin{aligned} \overline{\sigma}(H) = \overline{\sigma}((I-GK)^{-1}K) &\leq 1/\underline{\sigma}(I-GK)\ \overline{\sigma}(K) \\ &\approx \overline{\sigma}(K) \quad (\text{at freq. with } \overline{\sigma}(GK) \ll 1) \qquad (12) \\ &= \overline{\sigma}(W_1 K_\infty W_2) \\ &\leq \overline{\sigma}(W_1)\ \overline{\sigma}(K_\infty)\ \overline{\sigma}(W_2). \qquad (13) \end{aligned}$$

Obvious from the last inequality (13), decreasing the weights decreases the transfer function H. As the ∞-norm of H appears at high frequencies (where the open loop gain is low), the restriction on certain frequencies (used in step 12) causes no trouble.

We solved the problem of correct weight-adjustment in the face of a too high maximum control signal. An initial choice of the weights should attack the general shape of the open loop and is discussed in context with original Loop Shaping Design Procedure by McFarlane & Glover [4] and textbooks on robust control, e.g. [3].

5 Discrete Time Case

In order to handle discrete time problems in the same framework, we map the z transfer function to the so-called q-domain by the transformation [1]:

$$G^{\#}(q) := G^{*}(z)\Big|_{z=\frac{1+q\frac{T}{2}}{1-q\frac{T}{2}}} \tag{14}$$

(where T is the sampling time). The q transfer functions has the same properties concerning stability as the s transfer function in the continuous time domain, so we are able to apply the LSDP directly in the q-domain. An equivalent result to Reichel's Theorem 3.3 in the z-domain was derived by Peng [5]: for discrete time SISO system with input r fulfilling $r(k) = 0$ $(k < 0)$, $|r(k)| \leq r_{max}$ and $|r(k) - r(k+1)| \leq \Delta r_{max}$ $(k \geq 0)$ the output maximum $u_{max} := \sup_{k\geq 0} |u(k)|$ can be calculated.

Thus the ELSDP, formulated in section 4, can be applied in the q-domain, with a check for the maximum control signal in the z-domain.

6 Illustrative Examples

6.1 Vertical Plane Dynamics Control of an Aircraft

We study a multivariable, continuous time plant, an aircraft model, which also examined by McFarlane & Glover [4] and others. The model has three inputs and five states. The first three of them are the plant outputs. Its state space model is given by

$$G(s) \triangleq \left[\begin{array}{ccccc|ccc} 0 & 0 & 1.1320 & 0 & -1 & 0 & 0 & 0 \\ 0 & -0.0538 & -0.1712 & 0 & 0.0705 & -0.1200 & 1 & 0 \\ 0 & 0 & 0 & 1 & 0 & 0 & 0 & 0 \\ 0 & 0.0485 & 0 & -0.8556 & -1.0130 & 4.4190 & 0 & -1.6650 \\ 0 & -0.2909 & 0 & 1.0532 & -0.6859 & 1.5750 & 0 & -0.0732 \\ \hline 1 & 0 & 0 & 0 & 0 & 0 & 0 & 0 \\ 0 & 1 & 0 & 0 & 0 & 0 & 0 & 0 \\ 0 & 0 & 1 & 0 & 0 & 0 & 0 & 0 \end{array}\right] \tag{15}$$

Throughout the example, we determine suboptimal controllers ($f = 1.1$). McFarlane & Glover state the usual performance and stability objectives and the following limits on the control signal $u(t)$:

$$|u_1(t)| < 40, \quad |u_2(t)| < 10, \quad |u_3(t)| < 40. \tag{16}$$

To solve this problem with the ELSDP, we restrict the reference signal by the following values:

$$R = [1,1,1]^T, \quad \dot{R} = [5,11,3]^T. \tag{17}$$

Analysis of the McFarlane & Glover design

One of the McFarlane & Glover designs [4, section 7.4, design (2)] works with the following diagonal weight $W(s)$:

$$\begin{aligned} w_c(s) &= \frac{s+0.4}{s} \\ w_1(s) = w_3(s) &= 24 \cdot w_c \\ w_2(s) &= 12 \cdot w_c \\ W(s) &= \mathrm{diag}\{w_1(s), w_2(s), w_3(s)\}. \end{aligned}$$

The usage of *one diagonal weight* ensures a better oversight during the LSDP. Therefore, we restrict ourselves to this class of weights. The gain increases the open loop and thus increases the 0dB

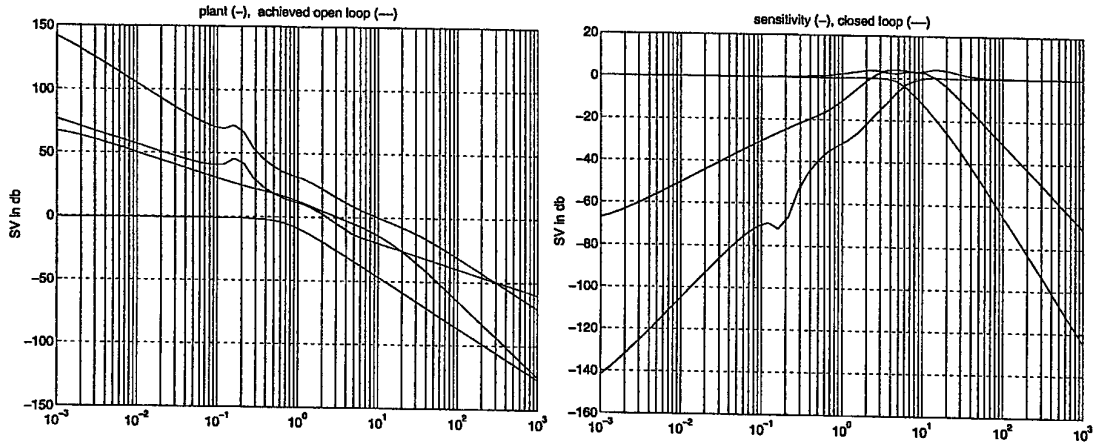

Figure 3: McFarlane & Glover design: singular values of plant and achieved open loop (left) and of sensitivity and closed loop (right).

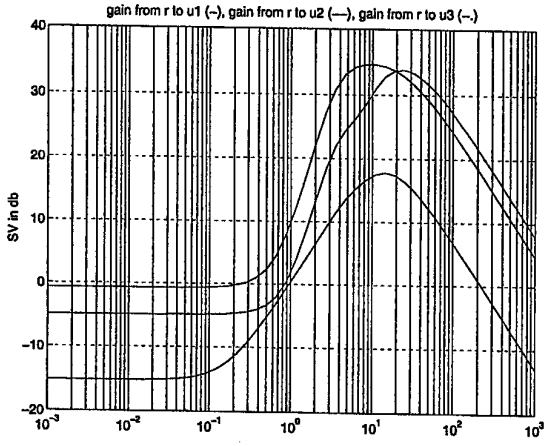

Figure 4: McFarlane & Glover design: singular values for the components of the control variable.

crossover frequency. The integral action will improve the low frequency performance. Looking at the singular values of the unshaped plant (see figure 3–left), the zeros at -0.4 limit the integrator to the low frequency range, so that a too high roll-off rate near the crossover frequency is prevented. This would cause poor robustness properties (i.e. a small stability margin) or even instability (known from Bode's Gain-Phase relations). Starting with this McFarlane & Glover weight for a first study we get the following result for the maximum control signal:

$$u_{max} = [32.1605, 10.9964, 59.6279]^T$$

and achieve a stability margin of $\epsilon = 0.3444$. Figures 3 and 4 show the singular values[1]. Our aim $|u_3(t)| < 40$, failed clearly, the value for $u_{2,max}$ too large, as well.

Adjustment of the weights

We adjust the weight from the step above in order to achieve the desired maximum control variable. According to the results derived in section 4, we are looking at the singular values of H in figure 4. We see, that they are too high for the frequencies [1.5, 100]. Therefore, we decrease the weights w_2

[1]Throughout this example, we only show the maximum and the minimum singular values due to a better overview.

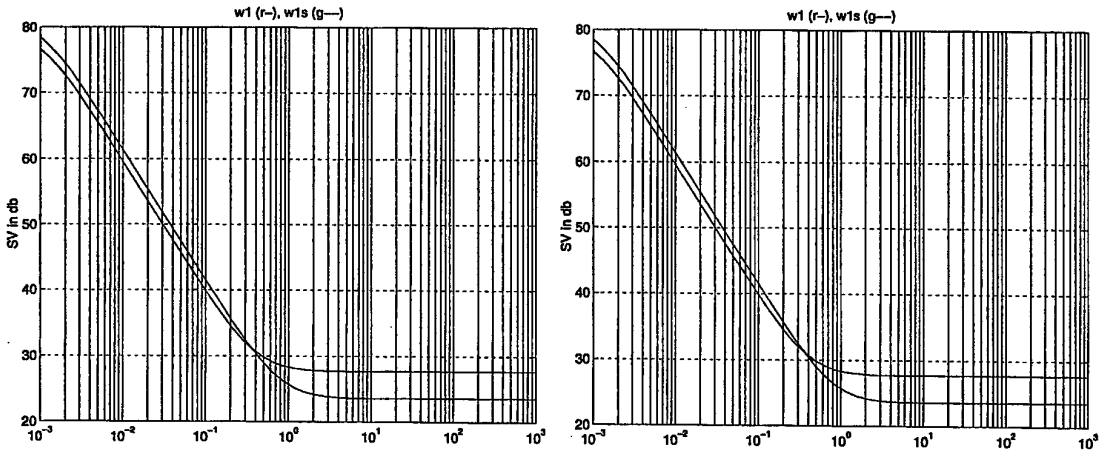

Figure 5: Adjustment of the weights: singular values of the diagonal entries w_1 and w_2.

and w_3 in this frequency range and work with the following weight W_s, see figure 5:

$$\begin{aligned} w_{1s} &= \frac{15.13s + 11.79}{s + 0.001} \\ w_{2s} &= \frac{6.44s + 4.661}{s + 0.001} \\ w_{3s} &= \frac{14.63s + 11.39}{s + 0.001} \\ W_s &= \mathrm{diag}\{w_{1s}, w_{2s}, w_{3s}\} \end{aligned}$$

Using this new weight, we get the following result on the maximum control signal:

$$u_{\max} = [35.2007, 8.5889, 31.4148]^T$$

and achieve a stability margin of $\epsilon = 0.3205$.

Our design objectives regarding the constraint control variable are fulfilled, figures 6 shows the singular values for the final controller design. The singular values of the transfer functions to the single components of the control signal, depicted in figure 7, have been decreased in the interesting frequency range.

During these designs, the following effect has been observed: comparing two controllers K_i with different performance factors f_i (but produced by the same weights), the resulting maximum control signals fulfilled $u_{2,\max} < u_{1,\max}$ (for $f_1 < f_2$). In general, this would be a usefull feature within the procedure. When a large stability margin was achieved, but the meeting of the bounds fails "slightly". Increasing the performance factor would decrease the maximum control signal (and of course decrease the stability margin slightly, too) and the problem is solved without new adjustment of the weights.

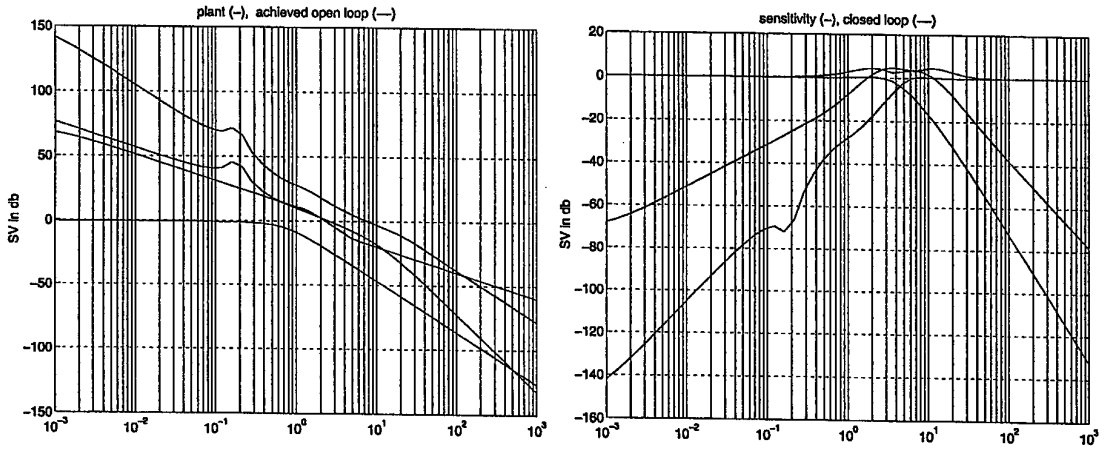

Figure 6: Design with adjusted weights: singular values of plant, achieved open loop, sensitivity and closed loop.

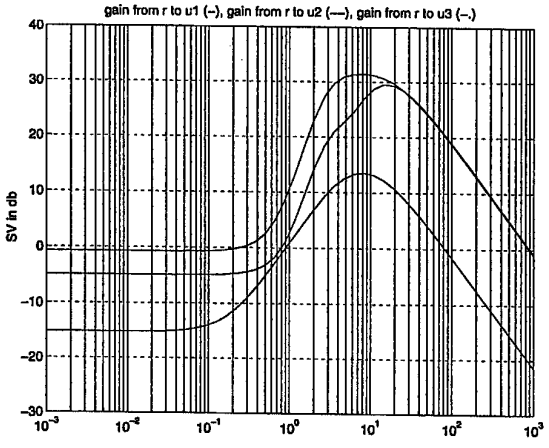

Figure 7: Design with adjusted weights: singular values for the transfer functions to the components of the control variable.

6.2 Two Mass Spring Benchmark Problem

The following problem is a popular problem for robust controller design, discussed for example on the 1992 ACC and described in [10]. The designs presented here are due to [11].

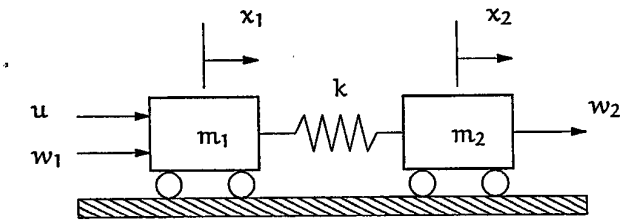

Figure 8: Two mass spring system with uncertain parameters.

Consider the two mass spring system shown in figure 8. It is assumed that for the nominal system $m_1 = m_2 = 1$ and $k = 1$ hold. The control force u acts on body 1, while the position of body 2 is measured. The system can be represented in the state-space form:

$$\begin{bmatrix} \dot{x}_1 \\ \dot{x}_2 \\ \dot{x}_3 \\ \dot{x}_4 \end{bmatrix} = \begin{bmatrix} 0 & 0 & 1 & 0 \\ 0 & 0 & 0 & 1 \\ -k/m_1 & k/m_1 & 0 & 0 \\ k/m_2 & -k/m_2 & 0 & 0 \end{bmatrix} \begin{bmatrix} x_1 \\ x_2 \\ x_3 \\ x_4 \end{bmatrix} + \begin{bmatrix} 0 \\ 0 \\ 1/m_1 \\ 0 \end{bmatrix} (u + w_1) + \begin{bmatrix} 0 \\ 0 \\ 0 \\ 1/m_2 \end{bmatrix} w_2 \tag{18}$$

$$y = x_2 \tag{19}$$

or as transfer-function:

$$G(s) = \frac{k}{m_1 m_2 s^4 + k(m_1 + m_2)s^2} = \frac{y(s)}{u(s)} \tag{20}$$

The aim of one of the problems posed in the benchmark collection [10, problem # 4], is to design a linear feedback-controller with constant gain, with the following properties of the control system:

- **A1** control signal for unit step output command tracking is limited to $|u| \leq 1$
- **A2** performance: settling time and overshoot are both to be minimized
- **A3** robustness: performance and stability with respect to the three uncertain parameters are both to be maximized

The problem is discussed in the discrete time domain. Using a sample time of $T = 0.1s$, the transfer function in the q-domain using transformation (14) is

$$G^{\#}(q) = \frac{0.0001q^3 - 0.0017q^2 - 0.0502q + 1.0033}{q^4 + 2.0067q^2}.$$

To solve the problem with the ELSDP, we replace property A1 by

A1' control signal must be $|u(k)| < 1$ for all $k \geq 0$ for any reference signal with

$$|r(k)| \leq 1 \text{ for all } k \geq 0 \text{ and } |r(k) - r(k-1)| \leq 1 \text{ for all } k \geq 1 \tag{21}$$

In contrast to the first example, we have a *parametric* or *structured* uncertainty. Therefore, we analyse our results looking at variations of the three uncertain parameters k, m_1 and m_2. One popular method doing this is μ analysis. Indeed, we studied this problem in the continuous time domain using this method [8]. In the q-domain, the structure of the plant is more complicated due to the two transformations, therefore we examine stability and maximum control signal by variation of the

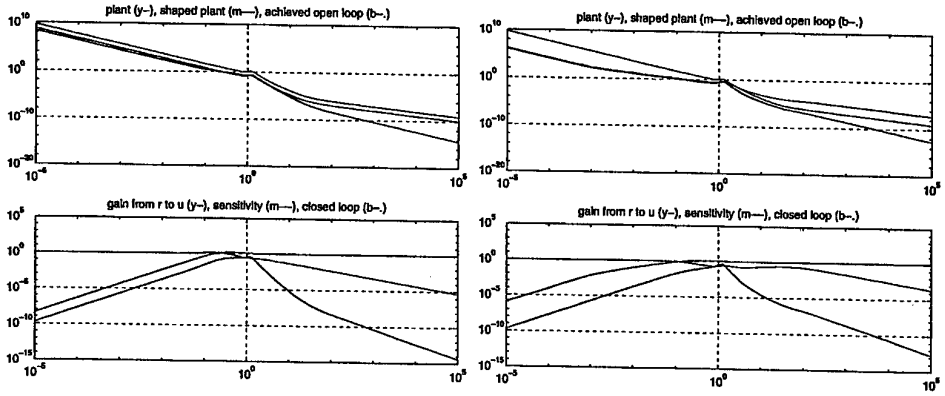

Figure 9: Bode plots for designs #0 and #2.

parameters. The result of this analysis is therefore a "stability"-interval" and a "control signal sufficiently small"-interval" for the examined parameter.

Controller Design

As in the first example, we choose the Performance Factor $f = 1.1$. We start with a constant weight $w = 0.1775$ and receive a stability margin of $\epsilon = 0.3619$ and a maximum control signal $u_{max} = 0.9973$. This result fulfils property A1' for the nominal case, but analysis of the control system shows, that slight changes of the parameters k, m_1 and m_2 will lead to control signals > 1. Assume $m_1 = m_2 = 1$ then the system is stable for $k \in [0.5414, 1.0229]$, but A1' is fulfilled in the unsatisfactory small interval $k \in [0.9985, 1.0229]$. Therefore, we decrease the weight to $w_{const} = 0.125$ receiving

ϵ	u_{max}	controller K(z)
0.3684	0.6347	$\frac{-0.0233z^4+0.0460z^3+0.0002z^2-0.0460z+0.0231}{z^4-3.7707z^3+5.3486z^2-3.3804z+0.8027}$

This design will be quoted as design #0. Bode plots are shown in fig 9 (left). Using this weight as an initial weight for higher order designs, we increase the gain it in the frequency range [1, 100] (in order to achieve a higher maximum control signal and a higher stability margin) using a second order weight. The Bode plots for design #2 are shown in fig 9 (right):

ϵ	u_{max}	weight $w_2(z)$
0.6290	0.9885	$\frac{9.5037z^2-15.6981z+6.1947}{z^2+0.3110z-0.2130}$

Simulation results

In the following, we are going to simulate the two systems with regard to parameter changes. Remarkable, that (in contrast to a series of other works) we have no problems with a too large control signal when changing the parameters. The price we pay for this feature is of course a slower control system. First, we simulate the step responses of the nominal systems, depicted in fig. 10. The two controllers produce a quite different behaviour, design #2 is successful in minimizing the overshoot because it damps the resonance, inherent in the system.

Variation of spring constant k

Table 1 below shows the allowed intervals for k, when $m_1 = m_2 = 1$ are assumed to keep their nominal values. We expect in some meaning from the different stability margins, that the stability interval for design #2 is larger than for design #0, which is not falsified in this experiment. In the case of design #0, the range of a sufficiently small control signal is smaller than the stability interval. Fig. 11 shows the step response for $k = 1.15$, which is out of the stability range for design design #0. Obviously, a step input is sufficient for a unbounded output in this control system.

$m_1 = m_2 = 1$		stability for $k_{min} \leq k \leq k_{max}$		$\|u\| \leq 1$ for $k_{min} \leq k \leq k_{max}$	
weight	ϵ	k_{min}	k_{max}	k_{min}	k_{max}
w_{const}	0.3684	0.4289	1.0176	*0.4825*	1.0176
w_2	0.6290	0.3734	1.5853	0.3734	1.5853

Table 1: Variation of spring constant k.

Variation of masses m_1 and m_2
Variation of the parameters m_1 and m_2 assuming constant $k = 1$ is depicted in table below. Fig. 12 shows selected simulations for $k = 1$ and $m_1 = m_2 = 2$. In tendency the same results appear in the case $k = 1$ and $m_1 + m_2 = 2$. Again,, in both cases the interval of stability is larger than the interval of a sufficiently small control signal.

$k = 1$ $m_1 = m_2$		stability for $m_{1,min} \leq m_1 \leq m_{1,max}$		$\|u\| \leq 1$ for $m_{1,min} \leq m_1 \leq m_{1,max}$	
weight	ϵ	$m_{1,min}$	$m_{1,max}$	$m_{1,min}$	$m_{1,max}$
w_{const}	0.3684	0.9828	2.5864	0.9828	2.5864
w_2	0.6290	0.6449	2.9027	*0.9510*	2.9027
$m_2 = 2 - m_1$					
w_{const}	0.3684	0.8685	1.1315	0.8685	1.1315
w_2	0.6290	0.3924	1.6076	*0.4924*	1.6076

Table 2: Variation of the masses $m_1 = m_2$ resp. $m_1 = 2 - m_2$.

The study of the two mass spring problem shows the usage of the ELSDP in the discrete time domain. We analysed robustness due to parameter changes. However, the treatment of multivariable problems turns out to be difficult in this framework, because due to the transformations from q-domain to z-domain and back, numerical difficulties appear. Sometimes, slightly damped system poles are mapped to unstable ones in the z-domain. Therefore, future directions tend to apply the loop shaping directly in the z-domain (instead of the q-domain).

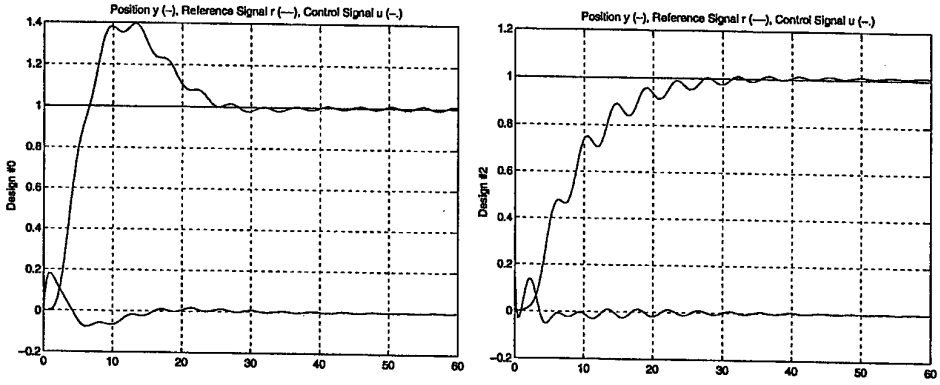

Figure 10: Step responses for $k = m_1 = m_2 = 1$.

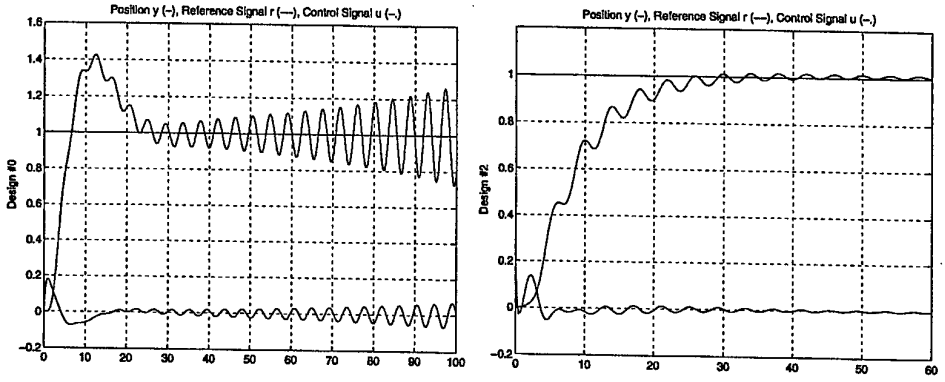

Figure 11: Step responses for $k = 1.15$, $m_1 = m_2 = 1$.

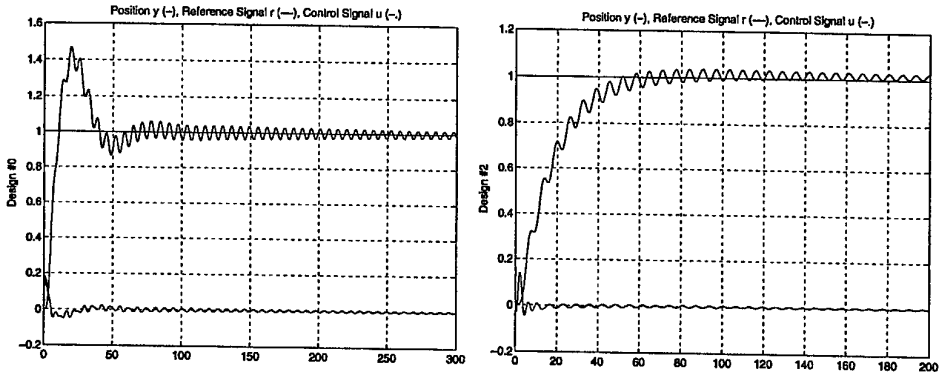

Figure 12: Step responses for $k = 1$, $m_1 = m_2 = 2$.

7 Conclusions

We studied the control of multivariable control systems with hard bounded control signals. One main point within the extension of the $\mathcal{H}_\infty$ Loops Shaping was the calculation of the maximum control signal for the set of admissible reference signals. The other main point was the systematic adaption on the weights with respect to the control signal. Examples were given for the continuous and discrete time case. Numerical problem appear in the discrete time and multivariable case. Therefore, future reasearch directions will study the loop shaping directly in the z-domain instead of the q-domain. Moreover, the following problems will be studies in future: constraints for other signals than the control signal, speed constraints for the control signal (important for flight control applications for example) and applications with mixed hard and soft bounds.

Acknowledgement

The preparation of the two mass spring benchmark example by Irina Zacharias is gratefully acknowledged.

References

[1] F. Gausch, A. Hofer, and K. Schlacher. *Digitale Regelkreise*. Oldenbourg Verlag, München, Germany, 1993.

[2] K. Glover. Model reduction: A tutorial on hankel-norm methods and lower bounds on L^2 errors. In *Proc. of the 10th IFAC World Congress*, München, Germany, 1987.

[3] M. Green and D. J. N. Limebeer. *Linear Robust Control*. Prentice Hall, 1995.

[4] D. C. McFarlane and K. Glover. *Robust Controller Design Using Normalized Coprime Factor Plant Description*. Number 138 in Lecture Notes in Control and Information Science. Springer Verlag, 1989.

[5] X. Peng. *Rechnerunterstützte Synthese von Abtastregelkreisen mit Beschränkungen*. PhD thesis, Dept of EE, University of Paderborn, 33095 Paderborn, Germany, 1992.

[6] R. W. Reichel. *Synthese von Regelsystemen mit Beschränkungen bei stochastischen Eingangsgrössen*. PhD thesis, Dept of EE, University of Paderborn, 33095 Paderborn, Germany, 1984.

[7] W. Reinelt. *Robust Control of Systems subject to Hard Constraints*. PhD thesis, Dept of EE, Univ of Paderborn, 33095 Paderborn, Germany, Apr. 1998.

[8] W. Reinelt. The two-mass-spring benchmark problem: An unstructured uncertainty approach for the constrained control problem. Technical report, Dept of EE, Univ of Paderborn, 33095 Paderborn, Germany, Oct. 1998.

[9] W. Reinelt. Maximum output amplitude of linear systems for certain input constraints. Technical Report LiTH-ISY-R-2165, Dept of EE, Linköping University, Linköping, Sweden, June 1999.

[10] B. Wie and D. S. Bernstein. Benchmark problems for robust control design. *Journal of Guidance, Control and Dynamics*, 1(5):1057–1059, Sep/Oct 1992.

[11] I. Zacharias. Robuste Regelung von Abtastsystemen unter Berücksichtigung von Stellgrössenbeschränkungen. Master's thesis, Dept of Math, University of Paderborn, 33095 Paderborn, Germany, Feb. 1999.

1999 International Symposium on
Quantitative Feedback Theory and Robust Frequency Domain Methods

Frequency Response Identification of the Fast Control Coil system of a Tokamak

D.J.N. Limebeer, A.S. Sharma and J.P. Wainwright,
Centre for Process Systems Eng. and Dept. of Electrical Eng.,
Imperial College, London SW7 2BY, United Kingdom.
Email: j.wainwright@ic.ac.uk, d.limebeer@ic.ac.uk and a.s.sharma@ic.ac.uk

A. Favre, J.B. Lister and P. Vyas
Centre de Recherches en Physique de Plasmas,
École Polytechnique Fédérale de Lausanne, 1015 Lausanne, Switzerland.
Email: Alain.Favre@epfl.ch Jo.Lister@epfl.ch and Parag.Vyas@epfl.ch

Abstract

In this paper we describe a frequency response identification of the fast voltage coils mounted inside the vacuum vessel of the Tokamak à Configuration Variable (TCV). These coils are used for the control of highly unstable plasmas where the response of the coils external to the vacuum vessel is found to be too slow. The aim of this current work was two-fold; firstly it is a crucial step en-route to the system identification of a Tokamak operating with a highly unstable plasma and secondly it was used to test an a-priori Tokamak model. The test signal was designed to be suitable for $\mathcal{H}^\infty$ system identification. The results obtained suggested that the a-priori model was based on incorrect data and the best values for these data were obtained using two methods. A frequency based minimisation of several cost functions was performed and a least-squares fit to the temporal data. Both methods showed good agreement and the database of experimental values has been adjusted accordingly.

1 Introduction

The limited supply of fossil fuels and the environmental risks associated with fission reactors are driving research into alternative sources of electrical power production. One of the most interesting is the possibility of power generation using the same power source as the sun, thermonuclear fusion. The easiest terrestrially achievable fusion reaction uses the Hydrogen isotopes Deuterium and Tritium, where Deuterium occurs plentifully in sea water and Tritium may be extracted from Lithium. The reaction occurs at temperatures of the order of $10^8\,^oC$ and release more energy per gramme than any other realistic fuel. The difficulties associated with handling the extremely hot fuel (which is in the plasma state) are compensated for by the facts that there are no greenhouse gases, long-lived radioactive waste or possibility of uncontrolled runaway reactions.

A Tokamak is a doughnut shaped, plasma confinement device which uses magnetic fields to restrict the motion of the plasma (a plasma in an ionised gas and therefore consists of charged

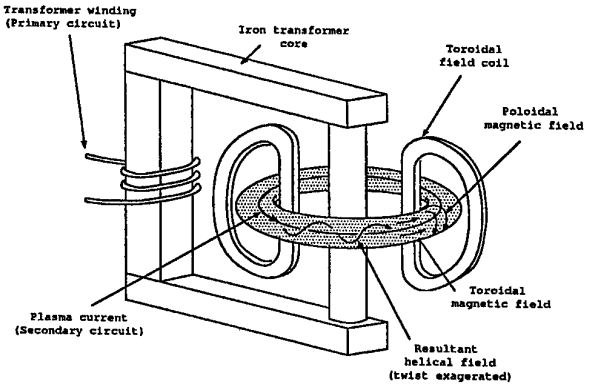

Figure 1: A generalised Tokamak.

particles). The basic principles of this device are illustrated in Figure 1. Essentially a doughnut shaped magnetic field is created from two separate magnetic field sources, a field which passes the long way around the torus (toroidal) and a field which passes the short way around the torus (poloidal). The toroidal field is generated by external field coils while the poloidal field is generated by an inductively driven plasma current. Not shown in this figure are a set of toroidally wound coils which are used to position the plasma and stop it interacting with the containment vessel. These coils generate a poloidal magnetic field and are called the poloidal field coils (PF coils). They may be seen in Figure 2, which shows the poloidal cross section of the Tokamak à Configuration Variable (TCV), a medium sized Tokamak based in Lausanne. All plasma control is via the PF coils and we shall refer to those PF coils located outside the vacuum vessel as external and those within as internal.

It is found to be beneficial to operate a Tokamak at its highest possible plasma current. This is because we create plasmas with higher densities and temperatures, both of which are necessary to the achieving of sustainable fusion conditions. For a fixed toroidal field coil set, it is found that we can sustain a higher plasma current in a plasma which has a elongated cross section. However the process by which we shape the plasma introduces an instability in the vertical plasma position and active control is usually necessary.

Last year we successfully applied an $\mathcal{H}^\infty$ system identification technique to create a linear model of the response of a Tokamak plasma to voltages applied to the external poloidal field coils [1, 2]. The plasma-coil system was and is MIMO, continuous time and unstable. In this previous study the plasma was unstable but not so unstable that control was impossible with the external coil set. (Typically a highly unstable plasma has a growth rate of a few thousand rad/s while the previous experiments operated with a plasma instability of a few hundred rad/s). The results gave great confidence to the Tokamak models which were being examined, in particular one of the simplest, RZIP [1], was found to be low order and accurate. It is this model which would be used in the current campaign of experiments. In order to investigate highly elongated (and therefore highly unstable) Tokamak plasmas another set of coils must be used to stabilize the plasma. These are the G coils, situated inside the vacuum vessel and therefore able to act directly on the plasma, without the screening effect of the metal vessel. In this paper we will discuss the experiments which were performed in order to confirm our model of the G coil set in the absence of a plasma.

In Section 2 we describe the system to be identified and discuss how practical constraints affected the design of the identification input signal. In Section 3 we show results from a series of experiments performed on TCV and show how they were consistent with an error in the

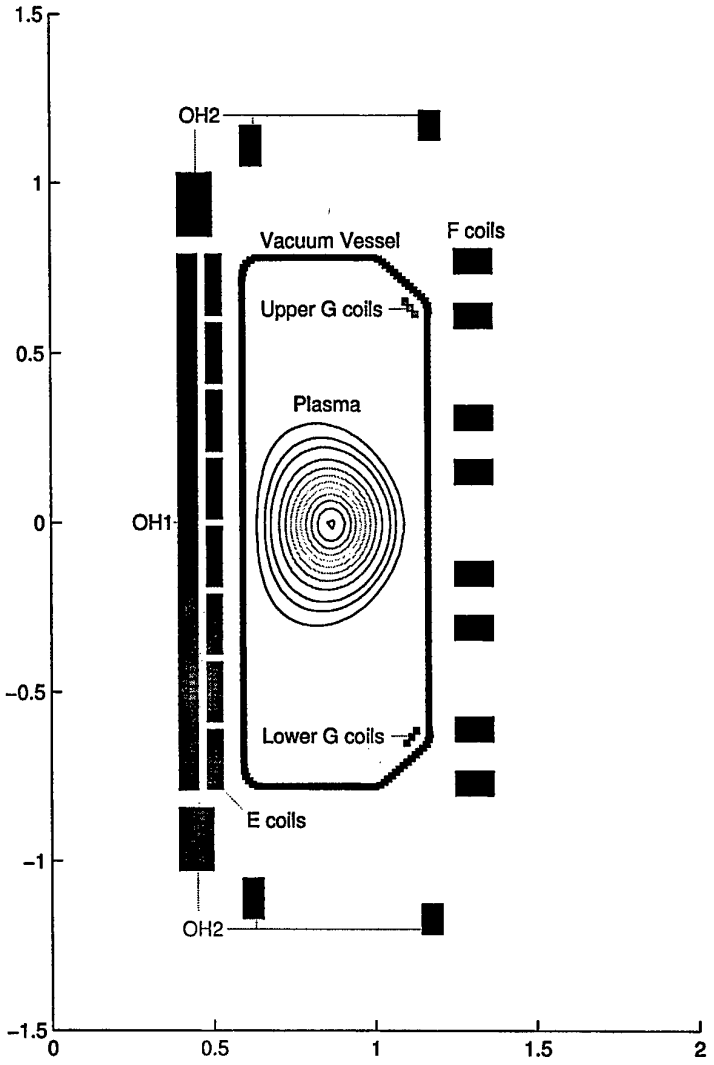

Figure 2: TCV cross-section showing the position of the poloidal field (E, F, G and OH) coils. The contour shows a typical plasma cross-section.

Tokamak model. The resolution of this inaccuracy is detailed in Section 4 and the current conclusions are presented in Section 5.

2 The TCV G-coil system and experiment design.

TCV is a Tokamak which is ideally suited to a plasma control and modelling study as it possesses a relatively large number of independently driven poloidal field coils (Figure 2). This leads to an flexibility not available in other machines. These coils comprise an inner set(E, 8 coils), an outer set(F, 8 coils), a single large ohmic coil (OH1), a set of smaller ohmic coils (OH2, 6 coils) and the G coil set, 6 coils situated inside the vacuum vessel. The ohmic coils are ideally positioned for driving the inductive plasma current while the E and F coils are ideally suited to plasma shaping and positioning. The G coil set is used for the control of plasmas which are vertically unstable with a high growth rate. They are operated in an up-down asymmetric manner which means that the same voltage signal is applied to the upper and lower coil groups, but negatively to the upper set and positively to the lower set. This is the optimum arrangement as it will lead to a purely radial magnetic field at the machine mid-plane. A purely radial magnetic field is ideal for moving a plasma vertically and not radially and the instability is in the vertical position.

The G coils are driven using a fast-power supply which operates in one of two modes, current- or voltage-driven. In voltage-driven mode the power supply tracks the input voltage, while in current-driven mode the power supply switches between three voltage levels (0, +/- 200 V) in order to produce the reference current.

Following our earlier work [2] we designed a multi-sinusoid input to span the necessary bandwidth and suitable for use in a robust identification. The frequency range of interest was estimated from the bode plot of the RZIP model of the plasma-less TCV system (illstrated in the next Section). In the absence of a plasma the RZIP model is essentially a set of circuit equations for the active voltage coils coupled to a discritised filament description of the surrounding continuous metallic structures [1]. The values for the self and mutual inductances for TCV are read from a machine database. RZIP predicted the relevant frequency range as 10-4000 Hz but this does not take account of two experimental considerations, the duration of an experiment and the sampling time of the diagnostics.

A typical plasma shot will last about 0.3 seconds which implies that the lowest frequency of interest is really about 3 Hz or about 19 rad/s, this implies a practical lower limit on the analysis. The TCV data acquisition system operates at 10 KHz and this puts a limit on the highest frequency we can apply. We choose to ensure that there are at least 10 data points in the highest applied signal frequency, in order that it may be clearly identified. However this implies that the highest frequency of note that we could apply was about 6000 Hz. The experimental conditions did not therefore appear to pose any serious constraints.

A signal with 23 frequencies was designed with the following form:

$$\begin{aligned} S(t) &= \sum_{i=1}^{23} a_i \sin(\omega_i t + \Phi_i), \\ \omega_i &= 65 \times 2\pi \tan(\pi i/48), \end{aligned} \tag{1}$$

where a represents a frequency dependent scaling factor used to compensate for the expected attenuation at high frequency and the phases Φ are randomly chosen to minimise the overall amplitude of the signal.

In practice the signal generator which was available to produce this signal could only store 16,000 points. This did impose a constraint on the experiments, as we could not simultaneously use all of the frequencies defined by our signal at our required resolution. We therefore decided to perform a high frequency experiment and a low frequency experiment, with some overlap to ensure continuity. We also decided to omit some frequencies as we expected a smooth transfer function. After consideration of all of the constraints, we constructed experiments of the following form.

Low frequency

$$\begin{aligned} \omega &= 65 \times 2\pi \tan(\pi[1\ 3\ 5\ 7\ 9\ 11\ 13\ 15\ 17]/48) \\ a &= [1\ 1\ 1\ 1\ 1\ 1\ 1\ 1\ 1] \\ \text{Duration} &= 1.5s \\ \text{Sample time} &= 10^{-4}s \end{aligned}$$

High frequency

$$\begin{aligned} \omega &= 65 \times 2\pi \tan(\pi[13\ 14\ 15\ 16\ 17\ 18\ 19\ 20\ 21\ 22\ 23]/48) \\ a &= [.2\ .5\ 1\ 1\ 2\ 2\ 2\ 4\ 4\ 8\ 16] \\ \text{Duration} &= 0.15s \\ \text{Sample time} &= 10^{-5}s \end{aligned}$$

In all we planned 5 experiments. Four of these comprised the low and high frequency experiments for voltage- and current-driven modes. A further voltage shot was performed with the input signal doubled in order to check system linearity.

3 Results from the identification experiments.

We assumed that the plant was essentially linear under teh conditions imposed by the identification experiment and therefore we could expect the simple preservation of frequency throughout the experiment. The experimentally acquired signals were decomposed into the input frequencies by a least-squares fit and the remaining signal was assumed to be noise. In practice this turned out to be a good assumption. The frequency response estimates of various plant relationships could then be constructed by simple division, as this was a single input plant.

Typical input and output traces are illustrated in Figures 3 and 4 respectively. They are taken from the low frequency, voltage-driven experiment (TCV shot number 15053). Figure 3 shows the voltage applied to the G-coils while Figure 4 shows the current in the G-coils. Each graph shows the raw data, the best least-squares fit to the data and the error between these signals. It can be seen that in this voltage-driven experiment the input (voltage) signal decomposes almost exactly, and the output (current) signal shows a reasonable noise level.

We constructed many transfer funstions bt here we will concentrate on the transfer function from the G coil current to the G coil voltage in both current- and voltage-driven modes. The results for the voltage-driven experiments are shown in Figures 5 and an obvious mismatch between the model prediction and the experimental data is apparent. In the next section we outline our approach to investigating this discrepancy.

4 Correcting the Tokamak model.

Due to the simplicity of the RZIP model and its successful operation in the previous experimental campaign, it seemed reasonable to assume that the discrepancy with the data was related to

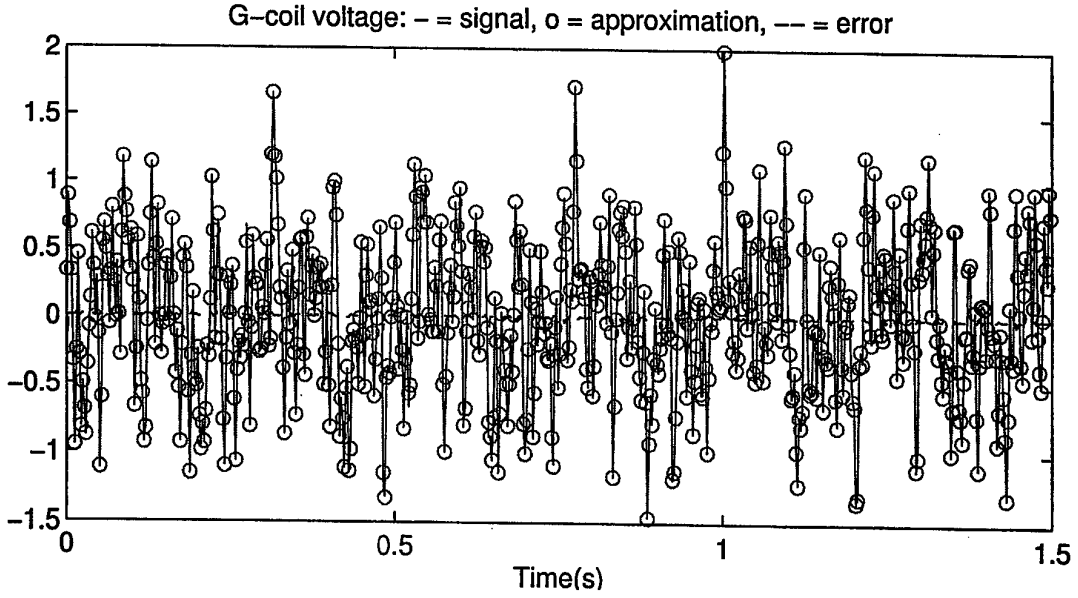

Figure 3: G-coil voltage for the voltage-driven, low frequency experiment. The solid line shows the raw signal, the circles are the best fit to this signal and the dashed line is the difference.

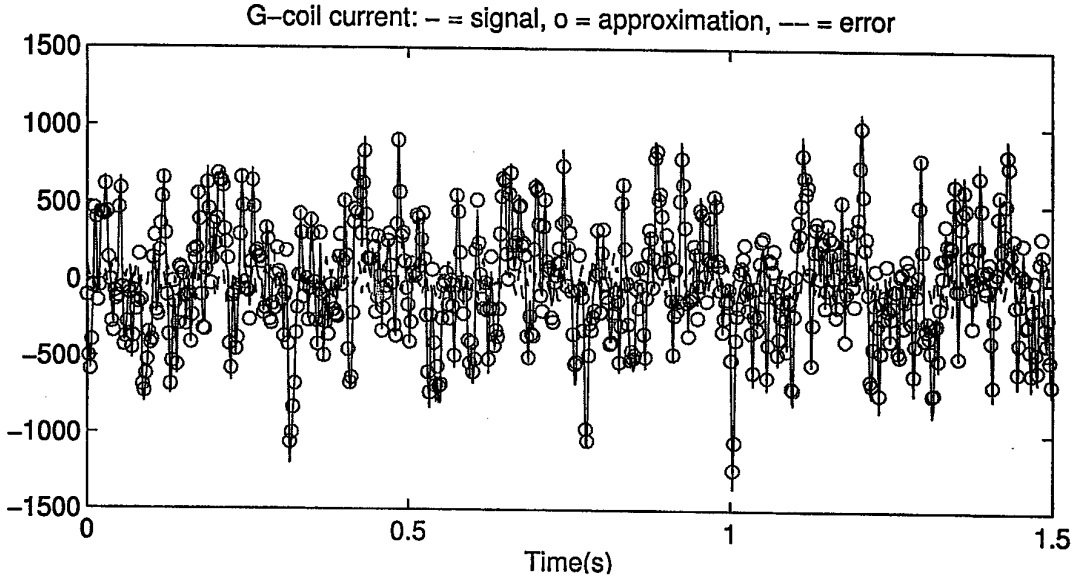

Figure 4: G-coil current for the voltage-driven, low frequency experiment. The solid line shows the raw signal, the circles are the best fit to this signal and the dashed line is the difference.

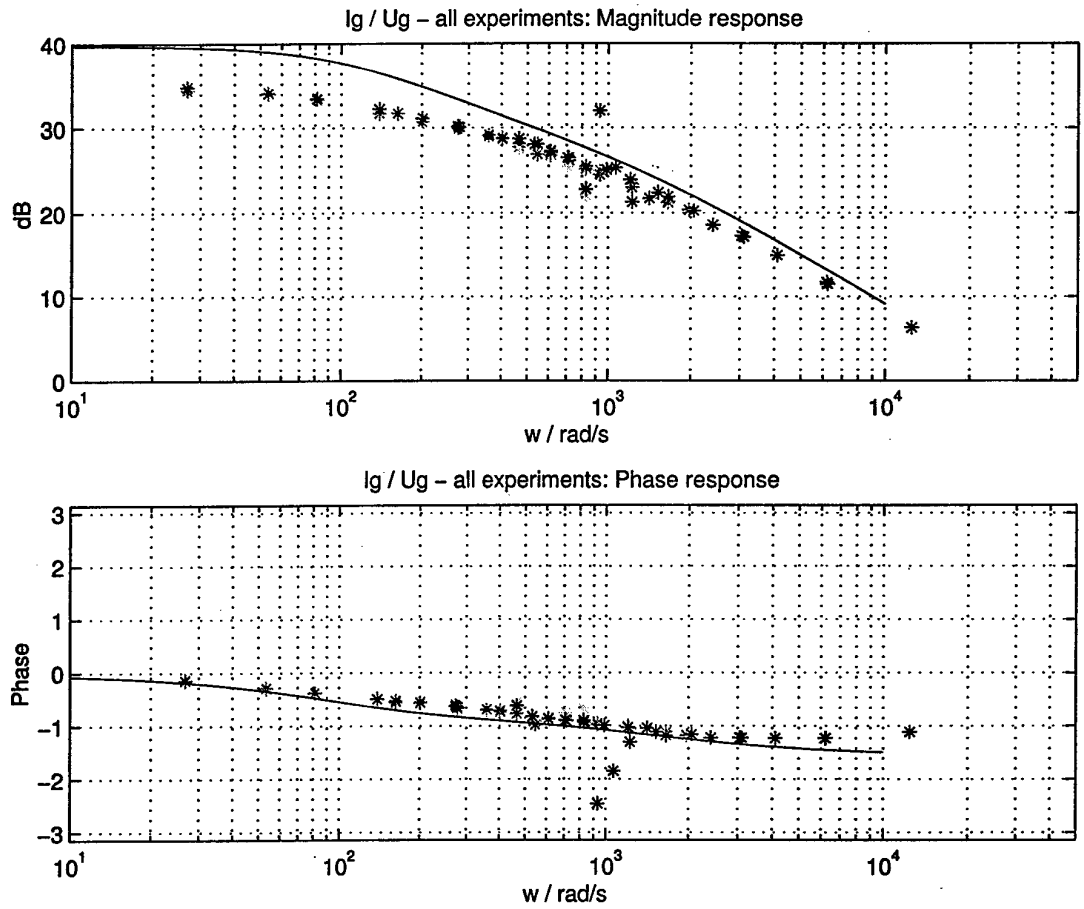

Figure 5: Predicted frequency response from G-coil current (Ig) to G-coil voltage (Ug), voltage-driven mode. All experiments are shown; red - 15048, green - 15049, blue - 15050, cyan - 15052, magenta - 15053, yellow - 15054, black - 15055. The predicted RZIP response is shown as a solid line.

the inclusion of the G-coils. The mutual inductances from the G-coils to the rest of the machine are dominated by their relative positions and are unlikely to be very inaccurate, and we therefore assumed that the G-coil resistance (R_g) and self inductance (L_g) were the only sources of error. We approached the problem of finding the best values for the G-coil self inductance and resistance in two ways, a frequency-domain based approach and one based on the temporal data.

Frequency Domain

In the frequency-space based approach, Four cost functions were defined, based on the difference between the experimental data G_{SI} and model prediction at the experiment frequencies G_{RZIP}. A cost function was chosen to minimise the infinity norm of difference between the measured and predicted (complex) transfer functions:

$$cost1_{\max(\delta G)} = \min_{L_g,R_g} \left(\left\| G_{SI}(\omega_i) - G_{RZIP}(\omega_i, L_g, R_g) \right\|_\infty \right).$$

The values of L_g and R_g that minimised the cost function were taken to be the true values of the fast coil self inductance and resistance.

For comparison we define an alternative cost function based on a normalised version of the above:

$$cost2_{\max(\delta G/G)} = \min_{L_g,R_g} \left(\left\| \frac{G_{SI}(\omega_i) - G_{RZIP}(\omega_i, L_g, R_g)}{|G_{RZIP}(\omega_i, L_g, R_g)|} \right\|_\infty \right).$$

This effectively weights the frequencies by the inverse of the transfer function.

It is possible to define a cost function that minimises the maximum error on a Bode plot, however although the fit appears better, it is only an artifice of the log in the cost function.

$$cost3_{\max(\delta log(G))} = \min_{L_g,R_g} \left(\left\| \log\left(G_{SI}(\omega_i)\right) - \log\left(G_{RZIP}(\omega_i, L_g, R_g)\right) \right\|_\infty \right).$$

Also we use a least squares fit:

$$cost4_{Least\ Squares} = \min_{L_g,R_g} \left((G_{SI}(\omega_i) - G_{RZIP}(\omega_i))(G^*_{SI}(\omega_i) - G^*_{RZIP}(\omega_i)) \right).$$

The results from this analysis were as follows.

Cost function	mode	cost	$L_g(H\ 10^{-4})$	$R_g(\Omega)$
-	TCV database	-	0.96119	0.0102
$\max(\delta G)$	Voltage driven	3.25	1.14	0.018
$\max(\delta G/G)$	Voltage driven	0.21	1.05	0.022
$\max(\delta log(G))$	Voltage driven	0.21	1.04	0.021
Least Squares fit	Voltage driven	58.03	1.09	0.019

The conclusion from these results is that the TCV data-base values of the G-coils are incorrect. For the G-coil resistance, extremely so.

Time Domain

In the time domain based approach, we assumed that the RZIP model was accurate for all but the two parameters L_g and R_g. This assumption allowed us to reconstruct an estimate to the induced currents in the conducting metallic structure, via a least-squares fit to the diagnostic signals. This gave us an estimate for the entire model state for the duration of the experiment. We could then simply find the best L_g and R_g by comparison to the temporal data.

Certain limitations are apparent with this technique. The low frequency response of the G-coil plant is dominated by the resistance of the G-coil; conversely if we wish to get a reasonable model of the plant's DC behaviour, we must consider a long duration of data. In the current analysis this is demonstrated by the poor value of resistance obtained by examination of the high frequency experiments.

The basic results are as follows:

Current Driven

TCV shot	Frequency set	Without eddy current estimate		With eddy current estimate	
		L_g	R_g	L_g	R_g
15049	Low	4.22×10^{-5}	2.83×10^{-2}	1.08×10^{-4}	1.64×10^{-2}
15050	High	3.34×10^{-5}	3.81×10^{-2}	1.25×10^{-4}	-0.2!

Voltage Driven

TCV shot	Frequency	Without eddy current estimate		With eddy current estimate	
		L_g	R_g	L_g	R_g
15053	Low	5.71×10^{-5}	2.29×10^{-2}	1.09×10^{-4}	1.71×10^{-2}
15054	High	4.16×10^{-5}	3.65×10^{-2}	1.09×10^{-4}	-1.76×10^{-2}!

The importance of including the structural eddy currents is obvious. These results compare favourably with those of the frequency based work. In principle there is a possibility to perform a form of on-line identification, however in order to model the resistive parts of the plant realistically the experiment must be of an appropriate duration. This fact is illustrated in Figure 6, which shows the convergence of results depending on the length of time data used. The agreement of the two approaches is not surprising, they both use the same data, and although it is much easier to work with the temporal data, its application must be handled with care. The final improvement in the fit to the raw data is illustrated in Figure 7, which shows the RZIP model predictions for the transfer function from the G-coil current to the G-coil voltage, based on the previous calculations.

Physically we interpreted the difference between the TCV database values and the experimental values, as being due to the cables connecting the coils with the power supply. In the previous work this was a negligible effect but in this case the G-coils have a low resistance and the resistance of the cables connecting the power supplies to the coils is non-negligible.

5 Conclusions

We have successfully identified the action of the fast-power supply and internal coils on a medium sized Tokamak. The discrepancy between the experimental data and a physics based model was interpreted as an inaccuracy in the values of the resistance and self-inductance of the internal coils. The best values of these parameters were evaluated using two different methods, but produced the same result. The discrepancy was interpreted as being due to the non-negligible values of resistance of the connecting cables between the power supplies and the coils.

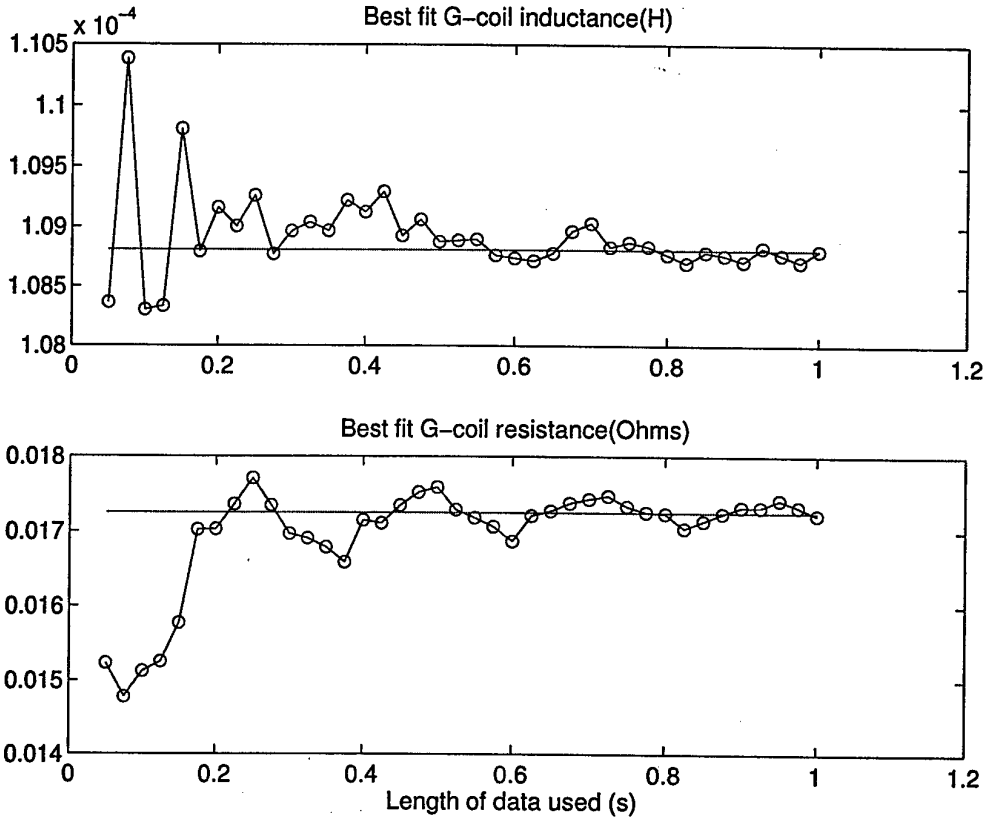

Figure 6: The convergence of L_g and R_g with the length of time analysed. (Taken from shot 15053).

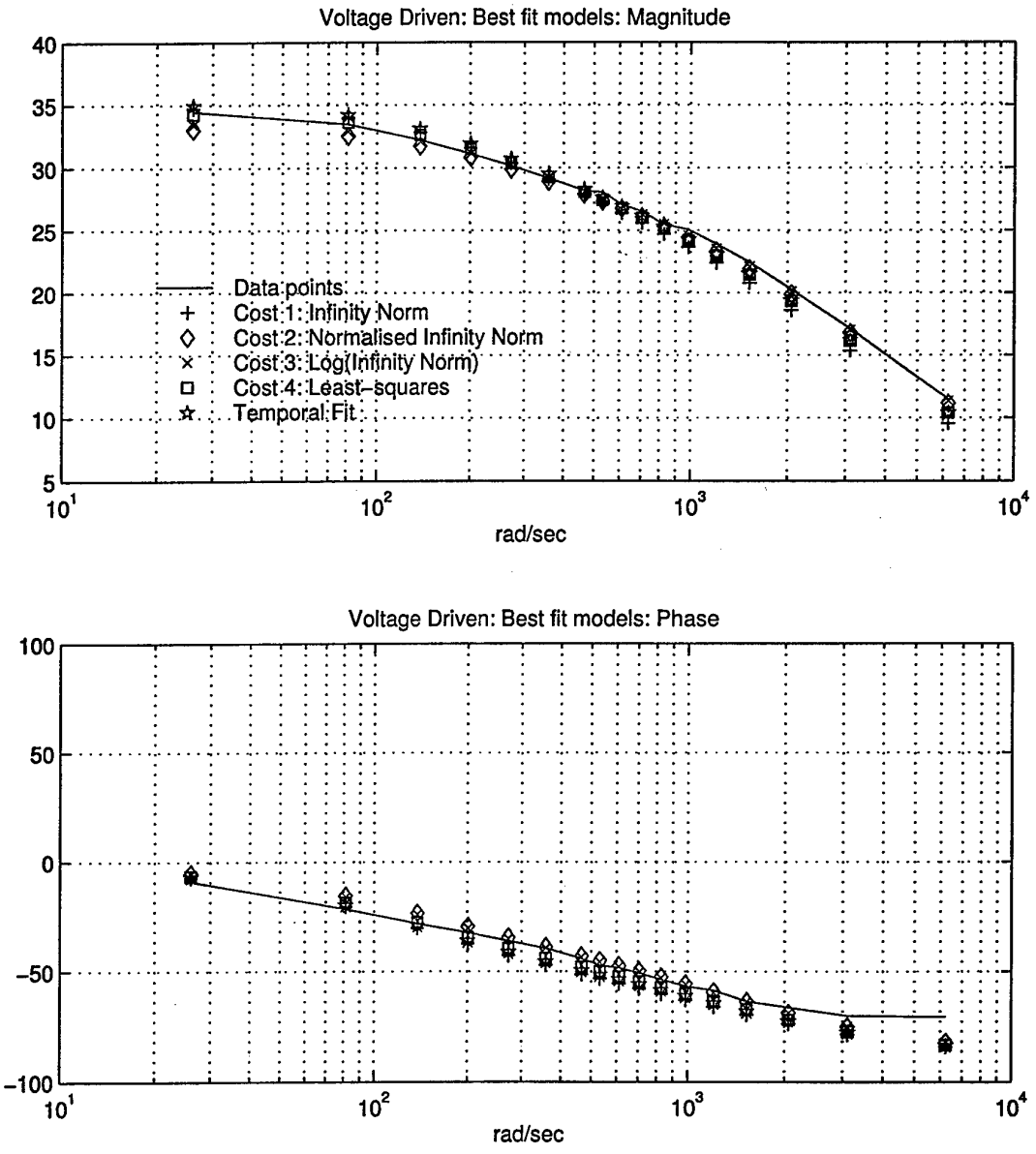

Figure 7: The RZIP predictions based on the values of L_g and R_g found by the various methods.

References

[1] A. C. I. Bandyopadhyay, J. B. Lister, P. Vyas, R. Albanese, D. J. N. Limebeer, F. Villone, and J. P. Wainwright, "Measurement of the open-loop plasma equilibrium response in TCV," *Nuclear Fusion*, vol. 39, no. 5, pp. 663–685, 1999.

[2] A. Coutlis, I. Bandyopapadhyay, J. B. Lister, P. Vyas, R. Albanese, D. J. N. Limebeer, F. Villone, and J. P. Wainwright, "Frequency response identification of the dynamics of a tokamak plasma," Tech. Rep. C98.7, Centre for Process Systems Engineering, Imperial College, 1999. (Accepted for publication in to IEEE Transactions on control systems technology).

1999 International Symposium on
Quantitative Feedback Theory and Robust Frequency Domain Methods

Efficient Computation of the Frequency Representation of Uncertain Systems

M.García-Sanz, P. Vital

Depart. Automática y Computación, Universidad Pública de Navarra, Campus de Arrosadía, 31006 Pamplona, Spain. Tel: +34 948 169387. Fax: +34 948 169281. Email: mgsanz@upna.es

Abstract

One of the main tasks when designing *QFT*-robust controllers is the definition of the process frequency response -*templates*- taking into account the complete *n*-dimensional space of model uncertainty. This paper analyses the high computational burden required for that when the number of uncertain parameters increases, and introduces a two-stages methodology to reduce the amount of operations needed. The major target of the procedure is to find the simplest set of plants that defines the whole *n*-dimensional space of uncertain models of the process -*templates contour*-. The first stage is based on a combination of symbolic computation of a Jacobian-like technique and of a graphical CAD tool to check visually the projections of the *n*-dimensional problem onto the Nichols Chat. The second stage includes a contour-searching algorithm to find the *template contour*. The procedure can deal, in a practical way, with a general problem of any dimension. It has been implemented in a collection of new MATLAB files with the aim of complementing the current *QFT* toolbox.

1. Introduction

Analysis of frequency performance of real processes with parameter uncertainty may become a serious problem due to the high computational burden involved. In that cases the design of a robust controller could be very difficult and time consuming.

Let us consider an uncertain process *P*,

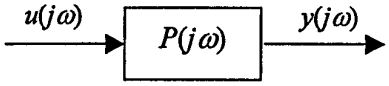

Fig. 1 Process

such that,

$$\boldsymbol{P}_i = \left\{ \begin{array}{l} P(j\omega_i, a_0, \ldots a_l, b_0, \ldots b_m),\ a_0 \in [a_{0\_min}, a_{0\_max}],\ \ldots\ b_m \in [b_{m\_min}, b_{m\_max}]; \\ a_i, b_i \in \Re,\ \ \omega_i \in \Re^+,\ \ i,l,m \in N \end{array} \right\} \qquad (1)$$

is the associated template for $\omega = \omega_i$.

This plant template $\boldsymbol{P}_i$ is a set of complex numbers representing the frequency response of an uncertain plant at a fixed frequency ω_i, that is to say, a projection of the *n*-dimensional parameter space onto $\Re^2$, according to the plant transfer function *P* for a given frequency –Fig. 2–.

The amount of operations that we need to accomplish this calculus (1) depends on the number of uncertain parameters $\Omega_n = (a_0, \ldots a_l, b_0, \ldots b_m)$ and on the desired subdivision factor for each parameter interval. So, if we suppose n uncertain parameters and a subdivision factor of r data for each parameter, the number of operations to build the n-dimensional space, using a brute force approach, will be r^n.

In the last few years some sophisticated template generation algorithms have been developed to reduce such a computational burden (Bailey *et al.* 1988, Bailey and Hui 1989, Barttlet 1993, Barttlet *et al.* 1993, Sardar and Nataraj 1997, Ballance and Chen 1998).

This paper introduces a new methodology to decrease the amount of operations required in the templates generation. So, a theoretical justification and an iterative procedure are developed to find the minimum value k, $1 \le k \le n$, so that the projection of the k-dimensional set Ω_k onto $\Re^2$ delimits the projection of the whole n-dimensional set Ω_n onto $\Re^2$.

In addition, we introduce a CAD tool based on MATLAB for automatic template generation. The new software is also directly connected to the QFT Toolbox developed by Borghesani *et al.* (1995).

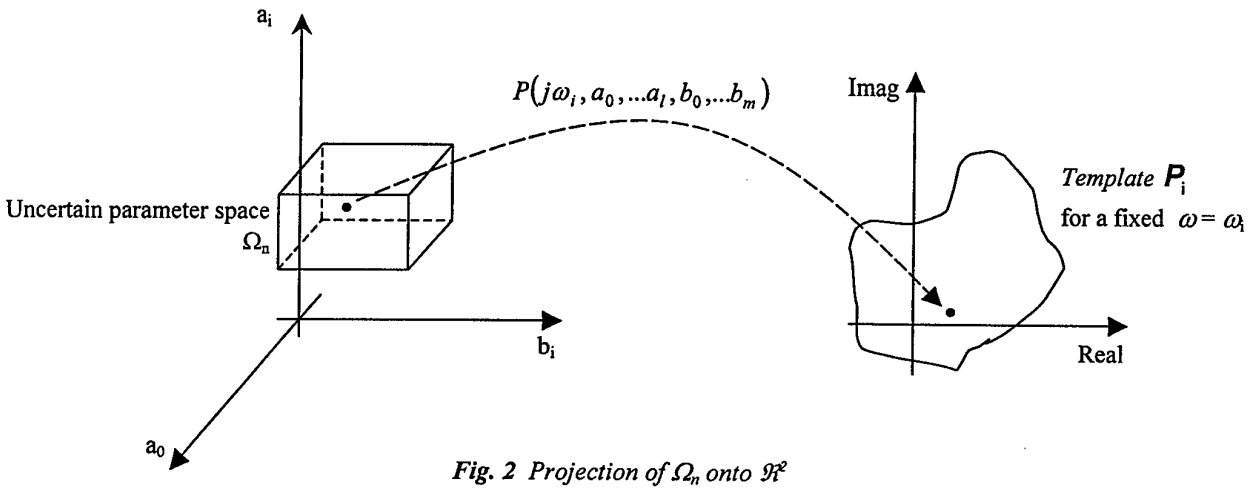

Fig. 2 Projection of Ω_n onto $\Re^2$

2. Theoretical development

In most of practical cases, applying the Maximum Principle (Munkres, 1975), the requested modelling information to carry the design of a robust controller out is reduced to the geometric boundary of the template $\boldsymbol{P}_i$. In this manner, we should find the points of the parameter space $\Omega_n = (a_0, \ldots, a_l, b_0, \ldots, b_m)$ whose projections define the template boundary in the complex plane. In other words, we have to remove the points of the parameter space Ω_n whose projections are interior to the image template.

Generally speaking, a point is interior to a set if it can be completely encircled by a ball of points that also belong to such a set. Now, the projection of this ball will be analysed to find out the demanded conditions to the function P that defines such a projection. These conditions will be such that the projection of the ball encircling the initial interior point contains a two-dimensional ball centred in the projection of the initial point. To satisfy these issues the function P has to perform continuity and derivability and to define a two-dimensional image space.
The first and the second ones are not very restrictive. The third one implies that the rank of the Jacobian matrix of the process has to be two, as it will be shown. With this preliminaries we can state the following theorem.

THEOREM 1

Let us consider **F**: $\Re^n \rightarrow \mathbf{C}$ (or $\Re^n \rightarrow \Re^2$) a continuous and derivable (at least twice) function. Let Λ be a compact set defined on $\Re^n$ and $\mathbf{p}_i \in \Lambda$ an interior point to this compact set. If the rank of the Jacobian matrix $\nabla \mathbf{F}(\mathbf{p}_i)$ is 2, $\forall$ $\mathbf{p}_i$, then all the interior points of the compact set Λ have their equivalent interior points on **C** by the mapping **F**.

The proof of the theorem is attached in Appendix 1.

3. Iterative procedure.

3.1 First stage

The main idea states that if the rank of the Jacobian matrix M (2) of the projection of the uncertain parameter space onto the complex map $\Re^2$, according to the plant transfer function P, is two, then inner points of the initial space are also inner points of the projected space -Fig. 2-. To be more precise, research of the minimum dimension k is reduced to the study of the rank of several sub-matrix of M, so that,

$$M = \begin{bmatrix} \dfrac{\partial\, Re\left[P\left(j\omega_i, a_0, \ldots a_l, b_0, \ldots b_m\right)\right]}{\partial\, a_0} & \cdots & \dfrac{\partial\, Re\left[P\left(j\omega_i, a_0, \ldots a_l, b_0, \ldots b_m\right)\right]}{\partial\, b_m} \\ \dfrac{\partial\, \mathrm{Im}\left[P\left(j\omega_i, a_0, \ldots a_l, b_0, \ldots b_m\right)\right]}{\partial\, a_0} & \cdots & \dfrac{\partial\, \mathrm{Im}\left[P\left(j\omega_i, a_0, \ldots a_l, b_0, \ldots b_m\right)\right]}{\partial\, b_m} \end{bmatrix}_{2\,x\,n} \qquad (2)$$

where $n = l + m + 2$.

To find such a minimum dimension k, we introduce an iterative procedure from $k = n\text{-}1$ to $k = 1$, involving symbolic calculus. For each step it is checked whether the rank of the $\binom{n}{k+1}$ possible sub-matrices of k+1 columns of M is two, for every combination of the k+1 uncertain parameters that correspond with those k+1 columns of each sub-matrix.

Such a checking must be satisfied for the whole 2^{n-k-1} possible combinations of both minimum and maximum of the n-k-1 non-considered parameters in each sub-matrix.

Being the above condition fulfilled, then the projection onto $\Re^2$ of the inner points of the $\binom{n}{k+1} 2^{n-k-1}$ sets Ω_{k+1} will be inner in the template. Hence the $\binom{n}{k} 2^{n-k}$ sets Ω_k will be enough to define the template contour.

The number of points that we could remove from the template is $\sum_{i=k+1}^{n} \left\{ \binom{n}{i} 2^{n-i} (r-2)^i \right\}$, where i corresponds to an iteration that fulfils the rank condition, and where k goes from n-1 to 1.

3.2 Second stage

Once we have reduced by symbolic computation the number of points that define the template, we introduce a second stage, based on a contour-searching algorithm, in order to produce a new points reduction that obtains the pure contour of the template.

The proposed contour-searching algorithm finds the extremun points in the north-south and east-west directions of the template, producing the final contour template that we shall have to use in the QFT robust control design. Fig. 3 shows the contour-computing window.

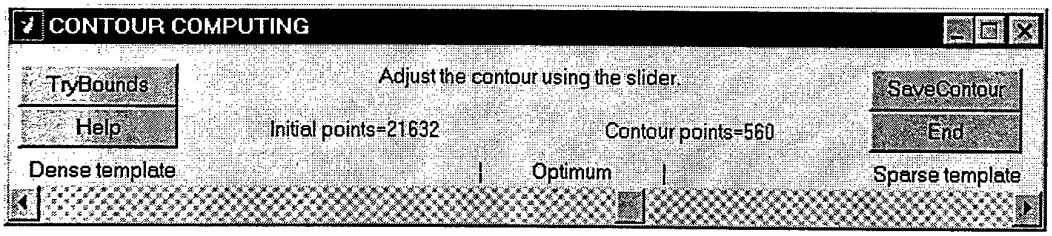

Fig. 3 Contour-searching window

To summarise the two stages up, Fig. 4 shows the projection onto $\Re^2$ of the whole 4-dimensional parameter space, the template reduction until the edges projection case using the symbolic computation, and the final template after applying the contour-searching algorithm, all for $\omega_1 = 5$ rad/s.

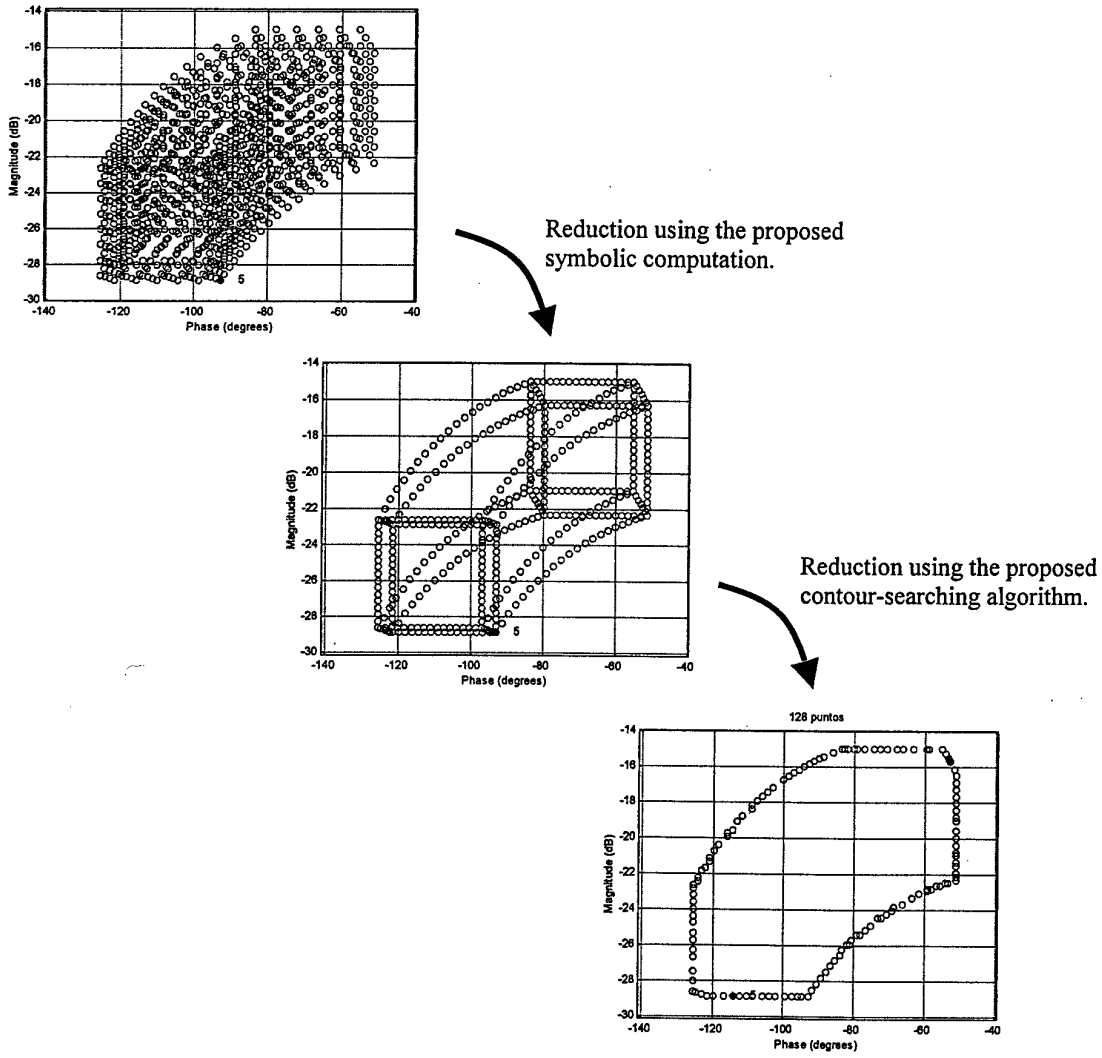

Fig. 4 Templates of the n-dimensional case, of the edges and of the final contour

The presented software offers some additional helpful features. It makes possible a quick introduction and easy management of data -Fig. 9-. It also recognises uncertain parameters with symbolic format, detecting its simultaneous presence in different coefficients of both numerator and denominator. In addition it allows to introduce different subdivision factors -grids- for each uncertain parameter. Finally, it makes easy to find the contour template and to detect quickly and visually the presence of singular points.

4. Examples

The following three examples are included in order to illustrate the difficulty of using symbolic calculus applying the theory proposed here and advanced by Ballance and Chen (1998). In Cases 1 and 2 -low-dimensional systems- symbolic calculus can detect singular points. The difference between both of them is that such points belong to the template contour only in Case 1, but not in Case 2. Case 3 shows a high-dimensional system. This comes in useful to explain the methodology for a general case.

4.1. Case 1

First of all we introduce an example where the symbolic procedure –first stage– cannot reduce the number of points of the template, due to the violation of the rank condition. This case corresponds to the following second order system with time delay,

$$\frac{1}{s^2 + 2\xi\omega_n s + \omega_n^2}, \text{ where } \xi = 0.02,\ \omega_n = [0.7,\ 1.2],\ \tau = [0,\ 2].$$

Fig. 5 shows the template that corresponds to the frequency of 1 rad/s. Cross points are the projections of the parameter space edges.

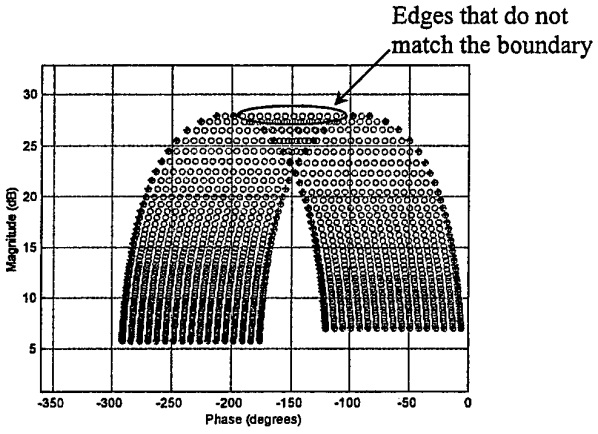

Fig. 5 Projection onto $\Re^2$ of the whole 2-dimensional parameter space, and of the parameter space edges

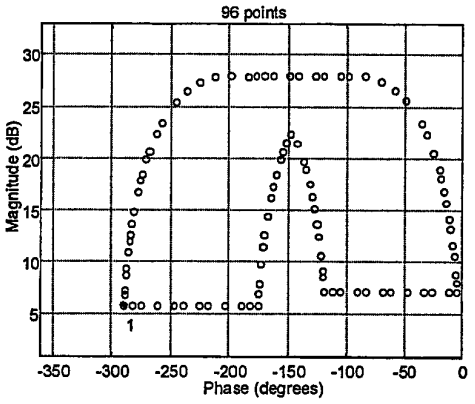

Fig. 6 Template contour

We can observe that the projection of the edges does not match the boundary at the top of the template. Using the symbolic computation -first stage-, we can also detect the problem, so that for the top points of the template we can see that rank(M)<2.Because of this, no reduction is made symbolically, and the result of the first stage is the same set of points that the 2-dimentional initial set. Afterwards, applying the second stage we find the template contour, reducing drastically the necessary number of points in the example from 2074 to 96 –Fig. 6–. Note that here, singular points are necessary to define the whole boundary. However, this is not certain in a general case as following example illustrates.

4.2. Case 2

In order to compare our methodology with the proposed by Ballance and Chen (1998), we introduce the same first example that they suggested in their paper. It corresponds to a vehicle start-up, where the transfer function yields,

$$G(s) = \frac{65.6\,k_c(j_v s^2 + 377\,s + k_s)}{3.07\,s(65.6\,j_v s^2 + 377(65.6 + j_v)s + k_s(65.6 + j_v))}$$

where the uncertain parameters are $k_c = [100\ 800]$, $j_v = [1400\ 11000]$ and $k_s = [58000\ 115000]$.

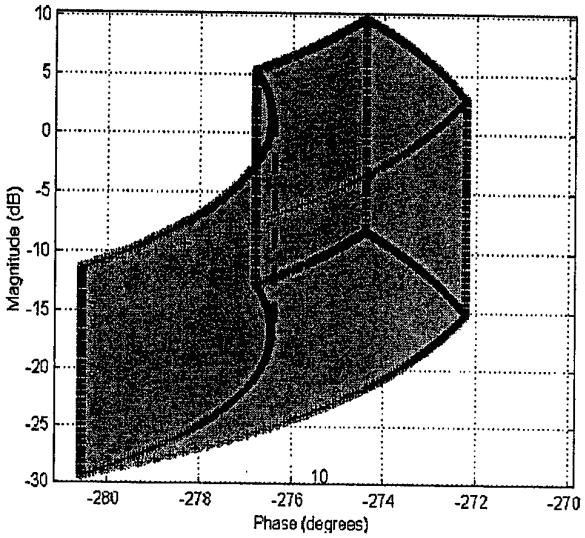

Fig. 7 Projection onto $\Re^2$ of the whole 3-dimensional parameter space, and of the parameter space edges

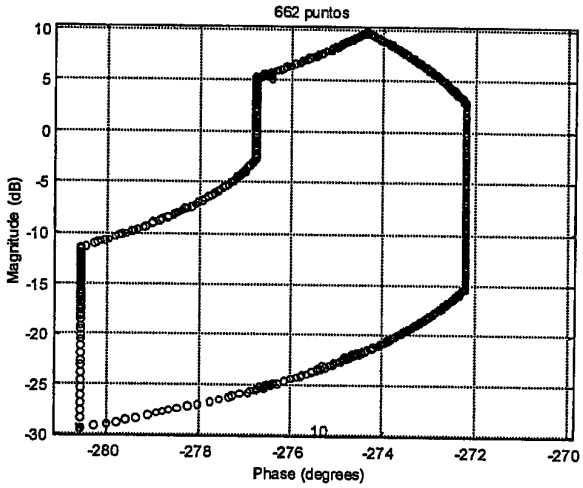

Fig 8 Template contour

Fig. 7 shows the template at $\omega = 10$ rad/s. In this case the proposed symbolic computation -first stage- yields that it is necessary to project the faces of the parameter space –2-dimension–, because the 1-dimension parameter space does not fulfil the rank condition. Simultaneously Ballance and

Chen conclude that it is only necessary to project the edges 1-dimension plus some singular points, denoted by the dashed line.

If we finish the analysis here, in this particular case the Ballance and Chen method would have reduced some more points than the proposed first stage. However, using our graphical CAD software, we can see that these singular points, calculated by Ballance and Chen, are not necessary at all to define the boundary of the template. Moreover, applying the proposed contour-searching algorithm -second stage-, we can reduce the amount of points of the template to the contour –Fig. 8–. Now, the final result obtained by the proposed methodology reduces much more the number of points of the template.

4.3. Case 3

Concerns to symbolic calculus, there is an important limitation in the application of the theory proposed here –first stage– and advanced by Ballance and Chen (1998). It cannot solve cases of high number of uncertain parameters.

However, the new software presented in this paper can deal, in a practical way, with a general problem of any dimension. The only limit is the computing capacity. With such a tool it is possible to test visually whether the projection of edges includes the whole boundary, and it is also possible to project individually vertices, edges, faces or all points in the worst cases. So, we only have to check visually the boundary –new first stage–, and to adjust the number of points of the final contour template –second stage–.

To illustrate this we propose the next eight-dimensional example. Fig. 9 displays the transfer function introduced by the user and the parametric uncertainty window.

$$\frac{b1\,s^3 + b2^2\,s^2 + 12\,s + 12{+}b3{*}5}{12\,s^4 + b4{+}5\,s^3 + b5{*}b1^2\,s^2 + b3{+}8{*}b6\,s + 3{*}b7}\; e^{-\tau s}$$

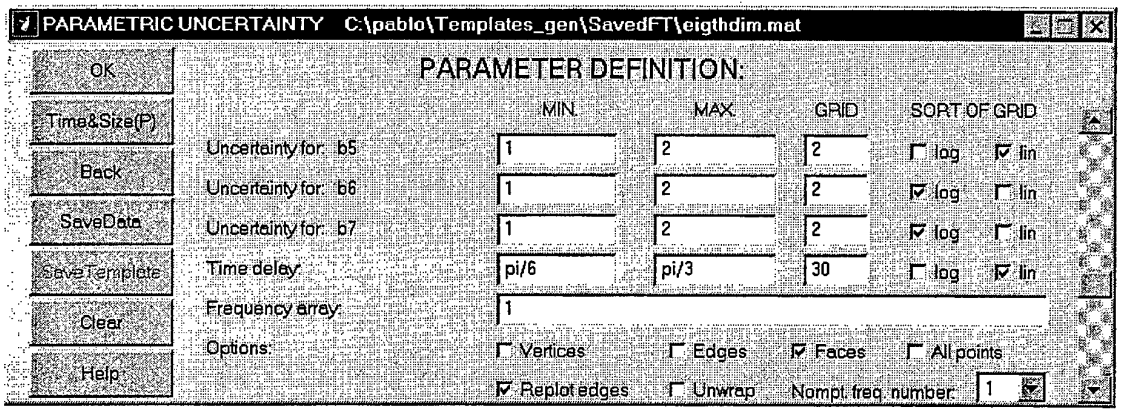

Fig. 9 Some details of the uncertainty introduction window

Using the brute force approach with a subdivision factor -grid- of five data per parameter, a template of $5^8 = 390625$ points will be obtained, making difficult posterior calculus on a reasonable time.

To accomplish efficiently the generation of the contour template, the following practical procedure is proposed. First, we only project vertices -Fig. 10.1-. Then, considering different subdivision factors for each parameter, it is possible to appreciate the sensitivity of the template with respect every parameter. Fig. 10.2 shows a template that regards to the projection of the vertices and the

complete interval of a parameter that is not very relevant. Simultaneously, Fig. 10.3 shows a template with the only two uncertain parameters that are relevant. In that particular case, a great reduction is achieved in the sense that there are six non-relevant parameters. For them, we shall consider a low grid to approach their uncertainties and for the two relevant ones we shall consider a heavier grid. Next step is to guarantee that the projection of the edges includes the template contour. With this aim, we make use of an option that allows us to repaint edges under the rest of the template, checking visually that condition -Fig 10.4-.

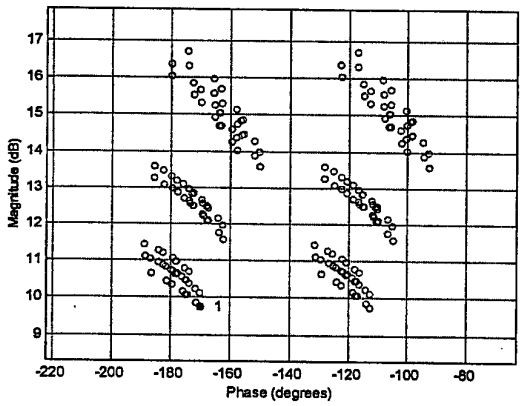

Fig. 10.1 Projection of the vertices

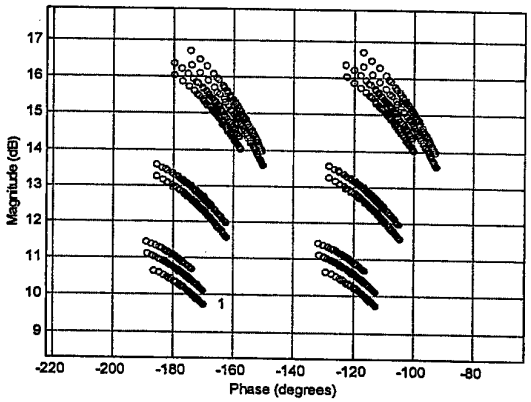

Fig. 10.2 Projection of the vertices plus a non-relevant parameter

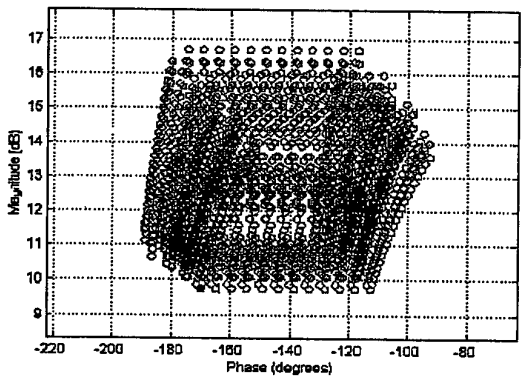

Fig. 10.3 Projection of the vertices plus the two relevant parameters

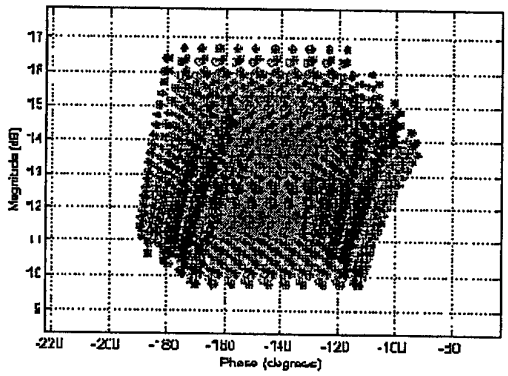

Fig. 10.4 The whole template with repainted edges.

Afterwards, applying the second stage we find the template contour, which has only 83 points –Fig.11–. Now, the subsequent computation in the QFT frame will be very fast.

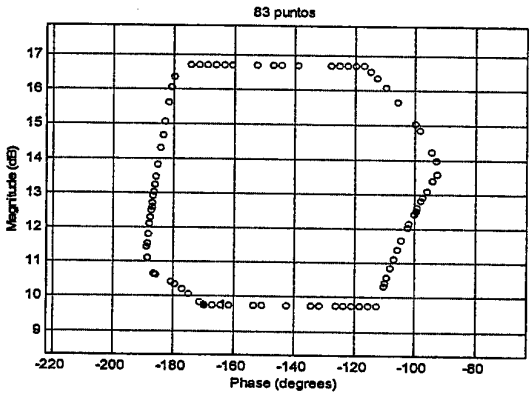

Fig. 11 Template contour

5. Conclusions

In the present paper a theoretical development and a new CAD tool for automatic template generation of processes with parameter uncertainty have been presented.

The new methodology consists of two different stages of calculus. The first one is based on a combination of symbolic computation of a Jacobian-like technique and of a graphical CAD tool to check visually the projections of the *n*-dimensional problem onto the Nichols Chat. The second stage includes a contour-searching algorithm to find the template contour.

The procedure can deal, in a practical way, with a general problem of any dimension. It has been implemented in a collection of new MATLAB files with the aim of complementing the current QFT toolbox.

The new CAD tool makes possible to design QFT robust controllers dealing with high-dimensional uncertain systems.

Appendix 1

PROOF OF THEOREM 1

Let $\mathbf{F}: \Re^n \rightarrow \Re^2$ be a continuous and derivable -at least twice- function. Let Λ be a compact space defined in $\Re^n$ and $\mathbf{p}_i \in \Lambda$ be an interior point to this compact set. To proceed with reductio ad absurdum, let us suppose that the image of $\mathbf{p}_i$ by $\mathbf{F}$ onto $\Re^2$ is a boundary point called $\mathbf{p}_i^* = \mathbf{F}(\mathbf{p}_i)$ –Assumption 1–.

Now, if $\mathbf{p}_i$ is interior to $\Lambda \in \Re^n$, $\exists\ \delta > 0 \mid \mathbf{p}_i+\mathbf{v} \in \Lambda\ \ \forall \mathbf{v} \mid \|\mathbf{v}\| < \delta$. Invoking the Weierstrass theorem (Croom, 1989), as Λ is a compact space, its image by $\mathbf{F}$ is also a compact space. Hence particularly, there exist the images $\mathbf{F}(\alpha)$, $\alpha = \mathbf{p}_i+\mathbf{v}$ of the ball of points in $\Re^2$.

By hypothesis, $\mathbf{F} : \Re^n \rightarrow \Re^2$ is such that the rank of $\nabla\mathbf{F}(\mathbf{p}_i) = 2$. So, the function $\mathbf{T} : \Re^n \rightarrow \Re^2$ that corresponds $\mathbf{v}$ with $\nabla\mathbf{F}(\mathbf{p}_i)*\mathbf{v}$ is lineal and surjective.

Let B_r^d be a *d*-dimensional ball with radius *r*. Since $\mathbf{T}$ is continuous and surjective, the mapping of an open set is open, and an open set includes a ball of differential radius, there exists $\varepsilon > 0$ such that

$$B_{2\varepsilon}^2 \subseteq \mathbf{T}\left(B_1^n\right),$$

where $B_{2\varepsilon}^2 = \{ \mathbf{w} \in \Re^2 \mid \|\mathbf{w}\| < 2\varepsilon \}$ and $B_1^n = \{ \mathbf{v} \in \Re^2 \mid \|\mathbf{v}\| < 1 \}$.

Since $\mathbf{T}$ is lineal, for each $\delta > 0$, $\exists\ \varepsilon > 0$ such that

$$B_{2\varepsilon\delta}^2 \subseteq \mathbf{T}\left(B_\delta^n\right) \tag{3}$$

Now, we calculate the image of the ball $\alpha = \mathbf{p}_i+\mathbf{v}$, $\mathbf{F}(\alpha)$, approaching the function $\mathbf{F}$ by its Taylor polynomial approach centred in $\mathbf{p}_i$ –order 1–. It can be applied because there exist continuous second partial derivatives of $\mathbf{F}$:

$$\mathbf{F}(\mathbf{p}_i+\mathbf{v}) \cong \mathbf{F}(\mathbf{p}_i) + \nabla\mathbf{F}(\mathbf{p}_i)\cdot\mathbf{v} + \|\mathbf{v}\|\cdot\mathbf{H}(\mathbf{v}) \tag{4}$$

where $\|\mathbf{v}\|\cdot\mathbf{H}(\mathbf{v}) = \mathbf{E}(\mathbf{v})$ is the error of order 2.

Taylor theorem states that,

$\lim_{\|v\|\to 0} \|\mathbf{H}(\mathbf{v})\| = 0$. In other words, for $\varepsilon > 0$, from (3), $\exists\, r > 0$ | if $\|v\| < r$, then $\|\mathbf{H}(\mathbf{v})\| < \varepsilon$, and hence $\|\mathbf{E}(\mathbf{v})\| < \varepsilon r$. Now , let $\chi = \min\{\delta, r\}$. If $\|v\| < \chi$, $\mathbf{p}_i + \mathbf{v} \in \Lambda$ and $\|\mathbf{E}(\mathbf{v})\| < \varepsilon\chi \le \varepsilon r$, what is to say, $\mathbf{T}(\mathbf{v}) \supseteq B^2_{2\varepsilon\chi}$, such that $\|v\| < \chi$ and $\mathbf{E}(\mathbf{v}) \subseteq B^2_{\varepsilon\chi}$, such that $\|v\| < \chi$, hence $\{\mathbf{T}(\mathbf{v})+\mathbf{E}(\mathbf{v}) \mid \|v\| < \chi\}$ contains a ball.

Looking at Eq. (4), we find that $\mathbf{F}(\mathbf{p}_i)$ is the projection of the point $\mathbf{p}_i$, the centre of the original n-dimensional ball in $\Re^2$ by $\mathbf{F}$. Hence,

$$\mathbf{F}(\alpha) = \mathbf{F}(\mathbf{p}_i)+\mathbf{T}(\mathbf{v})+\mathbf{E}(\mathbf{v}) = \mathbf{F}(\mathbf{p}_i)+\nabla\mathbf{F}(\mathbf{p}_i)\cdot\mathbf{v}+\|v\|\cdot\mathbf{H}(\mathbf{v}) \tag{5}$$

is a ball of points in $\Re^2$ centred in $\mathbf{F}(\mathbf{p}_i) = \mathbf{p}_i^*$. The term $\nabla\mathbf{F}(\mathbf{p}_i)*(\alpha_k-\mathbf{p}_i)$, for all $\alpha_k \in \alpha$, is the image of a ball centred on the point $\mathbf{0}$, and if we add it to the vector containing the position of $\mathbf{p}_i^*$, it results a ball centred on that point.

So, if the Jacobian matrix $\nabla\mathbf{F}(\mathbf{p}_i)_{2\times n}$ has rank 2, then both rows are linearly independent, and consequently the ball will be 2-dimensional. Since it is centred in $\mathbf{p}_i^*$, this last is encircled completely, and hence it is interior, contradicting the Assumption 1 and completing the proof.

Acknowledgments

The authors gratefully appreciate the support given by the Spanish 'Comisión Interministerial de Ciencia y Tecnología' (CICYT) under grant TAP'97-0471.

References

BAILEY, F. N., and HUI, C. H., 1989, A fast algorithm for computing parametric rational functions. *IEEE Transactions on Automatic Control*, **34**, 1209-1212.

BAILEY, F. N., PANZER, D., and GU, G., 1988, Two algorithms for frquency domain design of robust control systems. *International Journal of Control*, **48**, 1787-1806.

BALLANCE, D.J., AND CHEN, W., 1998, Symbolic computation in value sets of plants with uncertain parameters. *UKACC International conference on control'98*, 1322-1327.

BARTLETT, A. C., 1993, Computation of the frequency response of systems with uncertain parameters: a simplification. *International Journal of Control*, **57**, 1293-1309.

BARTLETT, A. C., TESI, A., and VICINO, A., 1993, frequency response of uncertain systems with interval plants. *IEEE Transactions on Automatic Control*, **38**, 929-933.

BORGHESANI, C., CHAIT, Y., and YANIV, O., *Quantitative Feedback Theory Toolbox – For use with MATLAB*. 1st Edition, The MathWorks Inc., 1995.

CROOM, F. H., 1989. *Principles of Topology*, Ed. The Saunder Series.

D'AZZO, J. J. and C. H. HOUPIS, 1995. Quantitative Feedback Theory (QFT) Technique. In: *Linear Control System Analysis and Design*. 4th Ed. (McGraw Hill, New York), 580-635.

HOROWITZ, I. and M. SIDI, 1972. Synthesis of feedback systems with large plant ignorance for prescribed time-domain tolerances. *International Journal of Control*, **16** (2), 287-309.

HOROWITZ, I., 1991. Survey of quantitative feedback theory. *International Journal of Control*, **53** (2), 255-291.

MEISE, R., and VOGT, D., 1997, *Introduction to Functional Analysis*. Ed. Oxford University Press.

MUNKRES, J. R., 1975 *Topology, a First Course,* Ed. Prentice Hall.

SARDAR, G., and NATARAJ, P.S.V., 1997, A template generation algorithm for non-rational transfer functions in QFT designs. *36th IEEE Decision and control conference*, **3**, 2684-2689.

1999 International Symposium on
Quantitative Feedback Theory and Robust Frequency Domain Methods

QUANTITATIVE FEEDBACK THEORY REVISITED

Osita D. I. Nwokah and Gemunu S. Happawana
Department of Mechanical Engineering
Southern Methodist University
Dallas, Texas 75275-0337

ABSTRACT

This paper reexamines Horowitz's original formulation of the Quantitative Feedback Theory (QFT) problem in the light of recent developments in robust control. A simple proof of optimality of the loop transmission function in the sense of Horowitz is developed. A difficulty with Horowitz's formulation at high frequencies is corrected.

1 INTRODUCTION

Bode's work on feedback amplifier design [1] laid the foundation for accommodating uncertainty in control system design, at least in the high frequency region. Continuing this line of thought, Horowitz [2] raised some fundamental questions in robust control which directly accounted for parametric uncertainty without explicitly dealing with the high frequency uncertainty which Bode had implicitly considered.

The fundamental concept of sensitivity defined by Bode to capture the high frequency uncertainty dilemma was extended by Horowitz to deal with parametric uncertainty as well. Bode's model of the plant was given by: $P_\Delta = P_0(1+\Delta)$, where P_0 is a nominal plant, Δ represents unstructured uncertainty, $\Delta \in RH^\infty$,[+] $|\Delta| < W_2'$, some frequency dependent weighting function while Horowitz's description is: $P_\lambda = P(\lambda, s)$, $\lambda \in \Lambda$, where Λ is a compact and path connected parameter space. If S_B and S_H represent the corresponding sensitivity functions, then they can be expressed as: $S_B = \dfrac{1}{1+P_\Delta C}$ and $S_H = \dfrac{1}{1+CP(\lambda,s)}$ $\forall \lambda \in \Lambda$, where C is the controller designed in Horowitz's case with some nominal P_{λ_0}, $\lambda_0 \in \Lambda$, and in Bode's case with P_0. Both Bode's and Horowitz's models can be combined to give a more comprehensive model:

$$P_{\lambda,\Delta} = P(\lambda,s)[1+\Delta] \ , \ \Delta \in H^\infty,^{++} \lambda_0 \in \Lambda \ , \ |\Delta| < W_2.$$

Here, W_2 is a continuous real function that goes to ∞ no faster than ω^2 and satisfies the Paley-Wiener criterion. It captures the notion that plant uncertainty grows without bound as $\omega \to \infty$.

Then the combined sensitivity function is given by: $S_C = \dfrac{1}{1+CP_{\lambda,\Delta}}$.

Nowadays it is well accepted that most frequency response performance specifications can be written as [8]:

$$W_1(\omega)\left|S_{(.)}\right| \le 1 \ , \ \forall \omega \ge 0 \ , \tag{1.1}$$

where $S_{(.)} \in \{S_B, S_H, S_C\}$, and $W_1(\omega)$ is an L_2 real frequency weighting function satisfying several other technicalities and capturing the frequency domain performance specifications.

Now define $T_0 = \dfrac{L_0}{1+L_0}$, $T_\lambda = \dfrac{L_\lambda}{1+L_\lambda}$.

[+] RH^∞ is the set of all proper, stable and real rational transfer functions.

[++] H^∞ is the set of functions f(s), analytic in the right half complex plane and satisfying $\sup_{s \in \mathbf{C}} |f(s)| < \infty$.

Here, $L_o = CP_o$, $L_\lambda = CP_\lambda$, and $S_\lambda = \dfrac{1}{1+L_\lambda}$.

As shown in section 2, the performance specification for S_C can be reworked into:

$$\eta(\omega,C) = W_1(\omega)\left|S_\lambda\right| + W_2(\omega)\left|T_\lambda\right| \le 1 \ , \ \forall\omega\ge 0 \ , \forall\lambda\in\Lambda \ . \tag{1.2}$$

By putting $W_2 \equiv 0$, Horowitz uses the inequality (1.2) as a starting point in his QFT design technique [3]. The basic idea is to find an internally stabilizing C for which (1.2) is satisfied $\forall\omega\ge 0$, and all $\lambda\in\Lambda$. Horowitz's idea of optimality is the following: from the set of all stabilizing controllers (**C**) satisfying (1.2), choose the one with the minimum gain bandwidth product [4,5] or

$$\min_{C\in\mathbf{C}} \int_0^{\omega_c} \log\left|C\right| d\omega \ , \ \omega_c = \text{bandwidth of } C \ ,$$

subject to:

$$W_1\left|S_{(\lambda)}\right| \le 1 \ , \forall\lambda\in\lambda \ , \forall\omega\ge 0. \tag{1.3}$$

This leads essentially to a constrained Bode optimal cut-off problem [1].

The biggest difficulty with Horowitz's formulation is that **C** is impossible to characterize. Horowitz's optimal solution is obtained by the admissible controller that satisfies the sensitivity constraint with equality in (1.3). By considering the sub-level sets and the corresponding level curves for the sensitivity inequality (1.3) we show herein that a realizable optimal solution does not exist for the Horowitz problem. In fact such an optimal solution cannot exist since the optimal loop transmission function at each frequency, must lie on its corresponding level curve. The high frequency level curve which is a closed curve on the Nichols' chart, then forces the optimal loop transmission function to wrap around it at some particular high frequency, ω_h, implying a sudden increase in loop gain at high frequency. Furthermore, it is not clear how the level curves and sub-level sets can be defined for $\omega > \omega_h$, where ω_h is the high frequency in question. Once the optimal loop function hits the level curve corresponding to ω_h, Horowitz tries to overcome the above dilemma by arbitrarily rolling off L_o as fast as feasible, and without regard to all possible level curves $B(\omega)$ for $\omega > \omega_h$. This of course destroys the original idea of optimality: that L_o lies on $B(\omega)$ for all $\omega \in [0,\infty]$. Horowitz indeed posits that a realizable optimal solution is not feasible, and semi-heuristically looks for the most acceptable or adequate solution one can obtain. This problem arises because of the neglect of W_2. When this is taken into account in the original constraint as in (1.2), in fact it dictates the roll-off rate, and contrary to Horowitz's recommendation to roll-off L_o as fast as possible after ω_h, it turns out we need to roll it off as slowly as possible subject to satisfaction of the constraints in order to approach realistic optimality and insure stability. Indeed the roll-off rate directly influences the order of the rational approximation of L_o : the lower the roll-off rate, the lower the order of the compensator.

This paper is made up of 4 sections of which this is the first one. In section 2, we convert the traditional QFT performance specifications into sensitivity and complementary sensitivity constraints. In section 3 we show that the sensitivity constraint satisfaction with equality is equivalent to optimality in the sense of Horowitz. Finally in section 4, we make some concluding remarks.

2 PERFORMANCE SPECIFICATIONS

In this paper we concentrate on the command response problem of single input, single output QFT, which can be stated as follows: Given a plant family:

$$P_{\Delta,\lambda} := P(\lambda,s)[1+\Delta] \ , \ \Delta\in H^\infty \ , \ |\Delta| < W_2(\omega), \text{ and in general } P(\lambda,s)\in RH^\infty, \forall\lambda\in\Lambda.$$

It is required to find a controller $C\in H^2$, [+++] so that under the standard feedback arrangement, the closed loop operator:

[+++] H^2 is the set of all functions f(s) which are analytic in the right half complex plane **C**, and satisfying $\dfrac{1}{2\pi}\int_{-\infty}^{\infty}\left|f(s)\right|^2 d\omega < \infty$, when $s = i\omega$.

$$T_{\lambda,\Delta}(s) = \frac{CP_{\lambda,\Delta}}{1+CP_{\lambda,\Delta}}(s) \in H^2, \tag{2.1}$$

and satisfies the following inequality (for $s = i\omega$) :

$$\log a(\omega) \le \log\left|T_{\lambda,\Delta}(i\omega)\right| \le \log b(\omega), \tag{2.2}$$

$\forall \lambda \in \Lambda$, $\forall |\Delta| < W_2$ where $a(\omega)$, $b(\omega)$ are L_2 continuous frequency bounding functions which satisfy the Paley-Wiener criterion:

$$\int_{-\infty}^{+\infty} \frac{|\log x(\omega)|}{1+\omega^2} d\omega < \infty \text{ where } x = a \text{ or } b.$$

Furthermore, it is assumed that $a(o) = b(o) = 1$. This last assumption insures time domain zero steady state error. Temporarily suppressing ω, and note that the following computations are valid for each $\omega \in [0,\infty]$:
Write

$$\min_{\substack{\lambda \in \Lambda \\ |\Delta| < W_2}} \left|T_{\lambda,\Delta}\right| = \left|T_{\lambda,\Delta}\right|_{\min} = a. \tag{2.3}$$

Then from (2.2)

$$0 \le \log\left|T_{\lambda,\Delta}\right| - \log\left|T_{\lambda,\Delta}\right|_{\min} \le \log b - \log a. \tag{2.4}$$

or:

$$\frac{\left|T_{\lambda,\Delta}\right|}{\left|T_{\lambda,\Delta}\right|_{\min}} \le \frac{b}{a}. \tag{2.5}$$

Put

$$\frac{\left|T_{\lambda,\Delta}\right|}{\left|T_{\lambda,\Delta}\right|_{\min}} \le \frac{b}{a}, \tag{2.6}$$

so that:

$$\frac{\left|T_{\lambda,\Delta}\right| - \left|T_o\right|}{\left|T_o\right|} \le \frac{b-a}{a}. \tag{2.7}$$

But:

$$\left|T_{\lambda,\Delta} - T_o\right| \ge \left|T_{\lambda,\Delta}\right| - \left|T_o\right|, \tag{2.8}$$

so that:

$$\frac{\left|T_{\lambda,\Delta} - T_o\right|}{\left|T_o\right|} \le \frac{b-a}{a} \Rightarrow \frac{\left|T_{\lambda,\Delta}\right| - \left|T_o\right|}{\left|T_o\right|} \le \frac{b-a}{a}. \tag{2.9}$$

But by the definition of sensitivity function:

$$\frac{\left|T_{\lambda,\Delta} - T_o\right|}{\left|T_o\right|} = \left|\frac{P_{\lambda,\Delta} - P_o}{P_o} \cdot S_{\lambda,\Delta}\right| \le \left|\frac{P_{\lambda,\Delta} - P_o}{P_o}\right| \cdot \left|S_{\lambda,\Delta}\right|. \tag{2.10}$$

where

$$P_o = P(\lambda_o, s),\ \Delta \in H^\infty,\ |\Delta| < W_2(\omega);$$

and

$$S_{\lambda,\Delta} = \frac{1}{1 + CP_{\lambda\Delta}}. \tag{2.11}$$

From (2.9) and (2.10), the specification (2.2) is satisfied if:

$$\frac{a}{b-a}\max_{\lambda\in\Lambda}\left|\frac{P_{\lambda,\Delta}-P_0}{P_0}\right|\cdot\left|S_{\lambda,\Delta}\right|\le 1\ . \tag{2.12}$$

By defining:

$$W_1(\omega)=\frac{a}{b-a}\max_{\lambda\in\Lambda}\left|\frac{P_{\lambda,\Delta}-P_0}{P_0}\right|, \tag{2.13}$$

then (2.12) becomes:

$$W_1(\omega)\left|S_{\lambda,\Delta}\right|\le 1\ . \tag{2.14}$$

This is the sufficient condition for satisfaction of the QFT specification (2.2), which agrees with (1.1). Writing out (2.14) in full gives:

$$\left|\frac{W_1(\omega)}{1+CP_\lambda+GP_\lambda\Delta}\right|\le 1 \tag{2.15}$$

$\Rightarrow$

$$\left|\frac{W_1}{(1+CP_\lambda)\left[1+\frac{CP_\lambda}{1+CP_\lambda}\cdot\Delta\right]}\right|=\left|\frac{W_1S_\lambda}{1+T_\lambda\Delta}\right|\le 1\ , \tag{2.16}$$

where

$$P_\lambda := P(\lambda,s)\ ,\ S_\lambda := \frac{1}{1+CP_\lambda}\ ,\ T_\lambda := \frac{CP_\lambda}{1+CP_\lambda}\ .$$

Simplifying (2.16), and replacing Δ by its upper bounding function W_2 yields:

$$W_1\left|S_\lambda\right|\le 1-W_2\left|T_\lambda\right|\ ,$$

or:

$$\eta(\lambda,\omega,C(i,\omega))=W_1\left|S_\lambda\right|+W_2\left|T_\lambda\right|\le 1 \tag{2.17}$$

as a sufficient condition for satisfaction of the QFT specification (2.2).

Note that in Horowitz's original formulation, $W_2\equiv 0$. The consequences of this omission will be apparent shortly.

To convert (2.17) to bounds on the Nichols' chart as is done in QFT, we proceed as follows:
Define

$$\overline{\eta}(\omega,C(i\omega))=\max_{\lambda\in\Lambda}\eta(\omega,\lambda,C(i\omega))\ . \tag{2.18}$$

The traditional QFT optimization problem is then posed as the following:

Let $\mathbf{C}$ be the set of all stabilizing H^2 controllers for the QFT problem, then the optimization problem is:

$$\min_{C\in\mathbf{C}}\int_0^{\omega_c}\log\left|C(i\omega)\right|d\omega\ , \tag{2.19}$$

subject to:

$$\overline{\eta}(\omega,C(i,\omega))\le 1\ ,\ \forall\,\omega\in[0,\infty]\ . \tag{2.20}$$

While an analytical solution to the above problem does not exist, a quasi heuristic graphical technique which gives acceptable sub-optimal solutions to the problem is available and is the essence of all QFT methodology.

Let $P_0\in\mathbf{P}$ be the nominal plant model and define

$$L_0(i\omega)=P_0C(i\omega) \tag{2.21}$$

for some $C\in\mathbf{C}$. Define a 2-dimensional loop transmission manifold $M\subset C\times R$, and consider the sublevel set [6].

$\Gamma : M \to C$ given by

$$\Gamma(\omega, C(i\omega)) = \{P_o C : \overline{\eta}(\omega, C(i\omega)) \le 1\} \subset C . \tag{2.22}$$

Also consider the map

$f : M \to \Gamma$

which carries M into Γ and the level curve [6]:

$\partial\Gamma : M \to C \setminus \{\infty\}$,

which is given by:

$\partial\Gamma(\omega, C(i\omega)) = \{P_o C : \overline{\eta}(\omega, C(i\omega)) = 1\} : \subset C \setminus \{\infty\}$.

The map

$f : M \to \partial\Gamma \subset C$.

gives bounds on C for which Γ is defined.

It is the function f from which traditional QFT design bounds are developed as follows:

Let

$$P_o = P_{mo} P_{ao} , \tag{2.23}$$

where P_{mo} is minimum phase and P_{ao} is all pass.

Write

$$L_o = L_{mo} \cdot P_{ao} = P_{mo} C \cdot P_{ao} . \tag{2.24}$$

It can be shown [5] that:

$\eta(\omega, \lambda, C(i\omega)) \le 1 \Leftrightarrow$

$$\left| \frac{P_o}{P_\lambda P_{ao}} + L_{mo} \right| - W_2 |L_{mo}| \ge W_1 \left| \frac{P_o}{P_\lambda} \right| \tag{2.25}$$

$$\forall \lambda \in \Lambda , \forall \omega \in [0, \infty] .$$

Define

$$\frac{P_o}{P_\lambda P_{ao}} = p(\lambda, \omega) e^{i\theta(\lambda, \omega)} , \tag{2.26}$$

and

$$L_{mo} = q(\omega) e^{i\phi(\omega)} . \tag{2.27}$$

Substituting (2.26) and (2.27) into (2.25) and simplifying gives:

$\eta(\omega, \lambda, C) \le 1 \Leftrightarrow$

$$f(\omega, \phi, W_1, W_2, q) = \left(1 - W_2^2\right) q^2 + 2p(\lambda)\left[\cos(\theta(\lambda) - \phi) - W_1 W_2\right] q + \left(1 - W_1^2\right) p^2(\lambda) \ge 0 , \tag{2.28}$$

$\forall \lambda \in \Lambda , \forall \omega \in [0, \infty]$.

It is this f which maps M to Γ.

At each ω, one solves (2.28) as a guadratic equation for various $\lambda \in \Lambda$. By examining the solutions over $\phi \in [-2\pi, 0]$ one determines a boundary

$$\partial C_p(\omega, \phi) = \{P_o C : \overline{\eta}(\omega, C(i\omega)) = 1\} \subset C . \tag{2.29}$$

This boundary is precisely $\partial\Gamma$. Let the interior of ∂C_p be $\overset{\circ}{C}_p \subset \mathbf{C}$.

For $W_2 \le 1$ it can be shown that [5]:

$$\Gamma = C \setminus \overset{\circ}{C}_p = \{P_o C : \overline{\eta}(\omega, C(i\omega)) \le 1\} \tag{2.30}$$

while for $W_2 > 1$,

$$\Gamma = \partial C_p \cup \overset{\circ}{C}_p = C_p(\omega, \phi) . \tag{2.31}$$

In this way both $\partial\Gamma$ and Γ can be computed $\forall\,\omega\in[0,\infty]$.

Let N represent the Nichols' plane:

$$N=\{(\phi,r):-2\pi\le\phi\le 0\,,\ -\infty<r<\infty\}\,. \tag{2.32}$$

If $s=qe^{i\phi}$, then the map:

$L_m: s\to N$ sends s to N by the formula:

$$L_m s = r+i\phi = 20\log\left(qe^{i\phi}\right)=20\log q+i\phi\,. \tag{2.33}$$

Hence

$$L_m:\partial\Gamma\to\partial B(\omega,\phi,20\log q), \tag{2.34}$$

converts $\partial\Gamma$ to bounds ∂B on N called design bounds. These bounds are similar to the traditional QFT bounds except that unlike the traditional bounds, $\partial\Gamma$ can be used to generate $\partial B\ \forall\ \omega\in[0,\infty]$, whereas in traditional QFT, ∂B can be generated only up to a certain bound ∂B_h at $\omega=\omega_h<\infty$. This creates difficulties with the statement of the optimization theorem in the traditional QFT framework.

An acceptable $q_o=|L_o|$ must lie on or above $\partial B(\omega)$ at each $\omega\le\omega_h$, for $W_2\le 1$, and for $W_2>1$, and $\omega>\omega_h$, it must lie on or below $\partial B(\omega)$. The least gain admissible $q_o=q_o^*$ lies on $\partial B(\omega)$ for all $\omega\in[0,\infty]$. This is the optimal loop transmission gain.

3 OPTIMIZATION OF LOOP TRANSMISSION FUNCTION L_o

Here we show that any $|L_o|=q$ which lies on ∂B at each $\omega\in[0,\infty]$, must be optimal and that such an $|L_o|$ must also be unique. The following is the main result of this paper and is a more precise statement of Horowitz's original QFT loop transmission function optimization.

Theorem 3.1

Let $P_{\lambda,\Delta}=P(\lambda,s)[1+\Delta]$, $\Delta\in H^\infty$, $P(\lambda,s)\in RH^2$ [++++] $\forall\lambda\in\Lambda$, $|\Delta|<W_2$, be the plant family. A controller $C^*\in\mathbf{C}\subset H^2$ is optimal, that is:

$$I_c\triangleq\min_{C\in\mathbf{C}}\int_0^{\omega_c}\log|C|d\omega=\int_0^{\omega_c^*}\log|C^*|d\omega\,, \tag{3.1}$$

if and only if $\eta\left(\omega,C^*\right)=1\ \forall\,\omega\in[0,\infty]$, where ω_c and ω_c^* are respectively the bandwidth of C and C^*.

The theorem essentially states that the constraint satisfaction with equality everywhere on $\omega\in[0,\infty]$, is equivalent to optimality. Although the original QFT statement assumes that both $P(\lambda,s)$ and C are respectively RH^2 and H^2 functions, the proof of the theorem requires only that $CP(\lambda_o,s)=L_o(s)\in H^2$. Therefore $P(\lambda,s)$ can be in RH^∞ without any difficulties.

Proof

Set $|L_{mo}|=q$.

From the parabolic inequality (2.28), i.e., $$f(\omega,\lambda,W_1,W_2,\phi,q)\ge 0, \tag{3.2}$$

at any given $\omega\in[0,\infty]$, we determine the unique minimum solutions satisfying $q^*\le q$, for which

$$f\left(\omega,\lambda,W_1,W_2,\phi,q^*\right)=0,\ \forall\omega,\ \forall\lambda\in\Lambda\,. \tag{3.3}$$

Corresponding to q^* is a C^* such that

$$\Gamma\left(\omega,C^*\right)=\left\{P_oC^*:\overline{\eta}\left(\omega,C^*\right)=1,\forall\omega\right\}. \tag{3.4}$$

Furthermore

[++++] RH^2 is the set all real rational, stable, and strictly proper transfer functions.

$$\partial\Gamma\left(\omega,C^*\right)=\left\{P_0C^*:\eta\left(\omega,C^*\right)=1,\forall\omega\right\}, \tag{3.5}$$

so that at the minimum solution q^*:

$$\partial\Gamma\left(\omega,C^*\right)=\Gamma\left(\omega,C^*\right). \tag{3.6}$$

But $\partial\Gamma\left(\omega,C^*\right)$ contains only one admissible solution: P_0C^*, and P_0 is fixed. It follows that C^* is unique. But

$$f\left(\omega,\lambda,W_1,W_2,q\right)\geq f\left(\omega,\lambda,W_1,W_2,q^*\right),\ \forall\omega\in[0.\infty] \tag{3.7}$$

implies that

$$q\geq q^*\ ,\ \forall\omega\leq\omega_q\ , \tag{3.8}$$

where ω_q is the bandwidth of q. Or equivalently

$$\int_0^{\omega_c^*}\log q^*\,d\omega\leq\int_0^{\omega_q}\log q\,d\omega\quad\forall\ C\in\mathbf{C}\ . \tag{3.9}$$

Now:

$$\log q^*=\log\left|P_0\right|+\log\left|C^*\right|, \tag{3.10}$$

and

$$\log q=\log\left|P_0\right|+\log\left|C\right|, \tag{3.11}$$

so that

$$\int_0^{\omega_q^*}\log q^*\,d\omega\leq\int_0^{\omega_q}\log q\,d\omega\ ,\quad\forall\ C\in\mathbf{C}\ . \tag{3.12}$$

$\Leftrightarrow$

$$\int_0^{\omega_c^*}\log\left|C^*\right|d\omega\leq\int_0^{\omega_c}\log\left|C\right|d\omega\ ,\quad\forall\ C\in\mathbf{C}\ , \tag{3.13}$$

or:

$$\min_{C\in\mathbf{C}}\int_0^{\omega_c}\log\left|C\right|d\omega=\int_0^{\omega_c^*}\log\left|C^*\right|d\omega\ . \tag{3.14}$$

But when $C=C^*$, $\Gamma\equiv\partial\Gamma$ so that $L_0^*\in\partial\Gamma$, which is the boundary of Γ, $\forall\,\omega\in[0,\infty]$. Hence optimality $\Leftrightarrow$ constraint satisfaction with equality $\Leftrightarrow$ optimal L_0; which is denoted by $L_0^*\in\partial\Gamma$, $\forall\,\omega\in[0,\infty]$.

Since $P_0\in RH^2$, and $W_1\in L_2$, $W_2^{-1}\in L_2$, it is evident that $\left|L_0^*\right|=q^*\in L_2$.

Hence

$$\int_{-\infty}^{+\infty}\frac{\left|\log q^*(\xi)\right|}{1+\xi^2}d\xi<\infty\ .$$

Consequently:

$$\frac{1}{\pi}\int_{-\infty}^{+\infty}\frac{i-i\xi s}{s-i\xi}\cdot\frac{\log q^*(\xi)}{1+\xi^2}d\xi\ .$$

is convergent, and analytic in the right half plane. Therefore, it follows from [7] that:

$$L_0^*(s)=\exp\left[\frac{1}{\pi}\int_{-\infty}^{+\infty}\frac{i-i\xi s}{s-i\xi}\cdot\frac{\log q^*(\xi)}{1+\xi^2}\cdot d\xi\right] \tag{3.15}$$

is analytic and without zeros in the right half plane.

Clearly $L_0^*\in H^2$, and as $P_0\in RH^\infty$ (at worst) it follows that $C^*\in H^2$.

This completes the proof.

Equation (3.15) is all that the QFT loop transmission optimization guarantees. This function is clearly not rational. The practical design aspects of QFT is how to obtain a rational stable $\left(RH^2\right)$ approximation, $\bar{L}_0^*$, to L_0^*. To obtain a rational approximation of (3.15) which would be valid at every $\omega \in [0,\infty]$ clearly needs a rational function of infinite order! That is why the optimal loop transmission function L_0^* is not realizable by a finite order rational function.

Corollary 3.1

Every finite order RH^2 stable, (real rational and strictly proper) approximation of L_0^* which is denoted by $\bar{L}_0^*$ is sub optimal with respect to the constraint (3.1).

Proof: Self evident.

Corollary (3.1) is what gives rise to the traditional QFT controller design methodology of approximating the loop transmission function by a strictly proper rational approximation made up of integrators, first and second order rational factors, and of course some pure gain adjustment when necessary.

4 COMMENTS AND CONCLUSIONS

Given recent developments in robust control and the definition of frequency weighting functions W_1 and W_2 it is possible to convert the original QFT problem formulation into a parameter dependent frequency weighted sensitivity and complementary sensitivity (weighted) function. This should allow some modern synthesis methods for control system design to be partially deployed in the solution of the QFT problem. In particular it was shown that the original QFT optimization problem reduces to constraint satisfaction with equality for a particular frequency weighted sensitivity function, that in turn can be interpreted as a constrained Bode optimal cut-off problem, which was originally treated by Bode in 1945.

Of great interest is the conclusion that a true optimum is not physically realizable, which would appear to agree with everyday engineering design intuition. The quality of the final design in terms of approach to the optimum then rests with the creativity, ingenuity, and experience of a given designer. Thus the QFT design methodology guides design evolution rather than replacing human intervention as would appear to be the case in some control synthesis methodologies. Finally the incorporation of the high frequency weighting function W_2 into the problem formulation, allows us to over come a key difficulty of Horowitz's original formulation at high frequencies.

REFERENCES

[1] Bode, H. W., *Network Analysis and Feedback Amplifier Design*. Van Nostrand, New York, 1945.

[2] Horowitz, I. M., "Fundamental Theory of Linear Feedback Control Systems," *Trans. IRE on Autom. Control*, AC-4, 5-19, 1959.

[3] Horowitz, I. M., "A Survey of Quantitative Feedback Theory," *Int. J. Control*, 53, 255-291, 1991.

[4] Gera, A., and Horowitz, I. M., "Optimization of the Loop Transfer Function, *Int. J. Control*, 31, 289-298-1980.

[5] Horowitz, I. M., "Optimum Loop Transfer Function in Single Loop Minimum Phase Feedback Systems, *Int. J. Control*, 18, 97-113, 1973.

[6] Bailey, F. N., Helton, J. W. and Merino, O., "Generation of Worst Case Performance Functions in Loop Gain-phase Shaping," *Proc. 2nd International QFT Symposium*, Purdue University, West Lafayette, Indiana, 106-113, August 1995.

[7] Robinson, E. A., *Random Wavelets and Cybernetic Systems*, Hoffner, New York, 1962.

[8] Vidyasagar, M., *Control System Synthesis*, MIT Press, Cambridge, MA, 1985.

1999 International Symposium on
Quantitative Feedback Theory and Robust Frequency Domain Methods

An Alternative Design Method for Uncertain Cascaded Multiple-Loop Systems

Bor-Chyun Wang.[†] **Sy-Kang Shen,**[†]
[†] *Chung Shan Institute of Science and Technology, P.O. Box 90008-16-29, Lung-Tan, Taoyuan, Taiwan, R.O.C. Tel:886-2-26739638 ext.355681;Fax:886-3-4711277;e-mail:ew0451@ms19.hinet.net*

Abstract
Horowitz and Sidi (1973) proposed a quantitative synthesis feedback design method for a single-input single-output uncertain cascaded plant with n independent feedback loops system. In essence, bandwidth propagation effect is introduced to design each individual loop controller. The major effort of this paper goes into requiring trade-off between each loop with distinct frequency range to achieve minimum net effect of the n sensor noise sources. Moreover, the bandwidth increase phenomenon from the outer most loop to inner loops exists and can also be limited to minimize the sensor noise effects. Furthermore, an alternative design method for an uncertain cascaded multiple-loop system is presented. It is shown that by the equivalent external disturbance concept, the above trade-off problem modified and the overall design technique is considerably simplified. At the same time, the bandwidth propagation effect can be improved and inner loop transmission functions decrease as quickly as possible.
Keywords: Cascaded multiple-loop systems, equivalent external disturbance, quantitative feedback theory (QFT), uncertain plant.

1. Introduction
It is known that in significant plant uncertainty problem and/or narrow tolerances on the system responses, $|T_1(s)| \leq T(s) \leq |T_2(s)|$, the resulting single loop transmission function $L(j\omega)$ has a large bandwidth far greater than that of $T(s)$. The sensor noise is considerably amplified in this case and tends to saturate the early stages of the plant. To reduce the sensor noise effect, one way is by using multiple-loop structure restricted to the cases where additional plant variables (besides the plant output) are available for feedback purposes. Such a multiple-loop system design technique was first developed in Horowitz and Sidi (1973) for the cascaded structure as shown in Figure 1. For a two-section plant shown in Figure 2 with uncorrelated constraints of P_1 and P_2 parameters, the first step is to wipe out the uncertainty of P_1 so that loop transmission function L_2(s) needs only to cope with the uncertainty on P_2(s). The resulting L_2(s) has therefore less bandwidth than in the single loop system. Once L_2(s) has been designed, it is found that in middle frequency range, it is important to overdesign the outer loop L_2(s) in order to easily find the bounds for P_1(s) uncertainty. The final step is to shape the L_1(s) to stay within the bounds found in the previous step where L_2(s) still satisfies its bounds. Based on this design procedure, the bandwidth increase phenomenon from the outermost loop to inner loops are existent and dependent on trade-off factor as stated in Horowitz and Sidi (1973). Later, Horowitz and Wang (1979, 1988), successfully applied this idea to uncertain cascaded multiple-loop system with plant modification which enabled the designer to overcome the internal signal level increasing problem. For a significant plant ignorance problems, there is a strong tendency to minimize the sensor noise effect which is so highly amplified as to saturate the early plant input. These noise response transfer functions as shown in Figure 2 are

$$\left|\frac{X_1(s)}{N_1(s)}\right| = \frac{G_1(s)}{(1+L_1(s))(1+L_2(s))}, \tag{1}$$

$$\text{where } L_1(s) = G_1(s)P_1(s),\ L_2(s) = G_2(s)P_2(s)P_{1e}(s),\ P_{1e}(s) = \frac{G_1(s)P_1(s)}{1+G_1(s)P_1(s)},$$

$$\left|\frac{X_1(s)}{N_2(s)}\right| = \frac{G_1(s)G_2(s)}{(1+L_1(s))(1+L_2(s))}. \tag{2}$$

The noise components are most important in the high frequency range. Hence equa-

tions (1) and (2) show that it is desirable to decrease loop transmission functions $|L_1|$ and $|L_2|$ vs. ω as fast as possible in the high frequency range. However, the bandwidth increase phenomenon from the outer most loop to inner loops are limited to minimize the sensor noise effects.
An alternative concept for uncertain systems provided by Horowitz (1979) which transfers the plant uncertainty to an equivalent external disturbance can be used to design the fixed nominal plant system as a disturbance rejection problem. The proposed design method shows that this alternative concept can be used for multiple-loop design, in which case the bandwidth propagation effect can be improved and loop transmission functions decrease as quickly as possible. Major results are that the sensor noise effects can be minimized where all the specifications can be satisfied and the overall design technique is considerably simplified.
The remainder of this paper is organized as follows: In Section 2, the equivalent external disturbance concept is described. In Section 3, the problem is described. In Section 4, the proposed design method for uncertain cascaded multiple-loop system is developed. In Section 5, an illustrative example is provided to demonstrate the results of the proposed method. Conclusion is included in Section 5.

2. Equivalent external disturbance concept

Consider a linear time-invariant single-input-single-output (SISO), two-degree-of-freedom (2DOF) system as shown in Figure 3, where P_p set is the set of the plant transfer function P_1(s). The compensator G_1(s) and prefilter F(s) are realizable transfer functions. Input and output transfer functions are u(s) and y(s) respectively. u'(s) is the equivalent external disturbance. T(s) and T_o(s) are the perturbed and nominal system response transfer functions from u(s) to y(s) respectively. P_{1o}(s) is the nominal plant transfer function of P_1(s). $L_{1o}(s) = P_{1o}(s)G_1(s)$ is the nominal loop transmission function.
The design objective is to synthesize a controller G_1(s) and prefilter F(s) to satisfy

$$\gamma_1(t) \leq |y(t) - y_o(t)| \leq \gamma_2(t), \tag{3}$$

subject to the constraints

$$P_1(s) \in P_p \text{ set}, \tag{4}$$

where y(t) and y_o(t) are the perturbed and nominal system responses from u(t) to y(t) in the time domain respectively. And γ_1(t) and γ_2(t) are the allowable upper and lower time domain bounds of $|y(t) - y_o(t)|$.
Although so far there is no known way to transfer the rigorous time domain bounds into the frequency domain bounds, by using a simple first or second order transfer function coupled with computer simulation facilitates, the corresponding frequency domain bounds can be obtained and the prespecified time domain bounds can also be satisfied (Jayasuriya and Franchek, 1991).
Following lemmas are introduced to obtain from some algebraic equations the equivalent external disturbance at plant output due to plant uncertainty and the bounds .
Lemma 1: Consider a linear SISO, 2DOF system as shown in Figure 3, the overall transfer function from u'(s) to y(s) can be expressed as follows:

$$\frac{1 - T_o(s)/T(s)}{1 - P_{1o}(s)/P_1(s)} = \frac{1}{1 + L_{1o}(s)}, \tag{5}$$

proof: From Figure 3, for the nominal plant transfer function P_{1o}(s), the output y_o(s) equals

$$y_o(s) = F(s)\frac{G_1(s)P_{1o}(s)}{1 + G_1(s)P_{1o}(s)}u(s), \tag{6}$$

Multiplying both sides by $(1 + L_{1o}(s))$ and $\frac{1}{u(s)}$, it yields

$$(1 + L_{1o}(s))T_o(s) = F(s)G_1(s)P_{1o}(s). \tag{7}$$

For the perturbed plant transfer function, P_1(s), the output y(s) equals

$$y(s) = F(s)\frac{G_1(s)P_1(s)}{1+G_1(s)P_1(s)}u(s), \tag{8}$$

After some simple manipulations, it yields

$$(\frac{P_{1o}(s)}{P_1(s)} + L_{1o}(s))T(s) = F(s)G_1(s)P_{1o}(s). \tag{9}$$

Substituting Equation (7) into Equation (9) yields

$$(\frac{P_{1o}(s)}{P_1(s)} + L_{1o}(s))T(s) = (1+L_{1o}(s))T_o(s). \tag{10}$$

Equation (10) can be rewritten as

$$(1+L_{1o}(s))(T(s)-T_o(s)) = (1-\frac{P_{1o}(s)}{P_1(s)})T(s). \tag{11}$$

Simple manipulation yields

$$\frac{1-T_o(s)/T(s)}{1-P_{1o}(s)/P_1(s)} = \frac{1}{1+L_{1o}(s)}. \qquad \square \tag{12}$$

Thus, $1-P_{1o}(s)/P_1(s)$ can be treated as an input at u'(s) and $1-T_o(s)/T(s)$ as an output at y(s). The overall closed loop transfer function from $u'(s)$ to y(s) can be expressed as $1/(1+L_{1o}(s))$. As a result, the block diagram in Figure 3 can also be redrawn as shown in Figure 4.

Lemma 2: Consider a equivalent external disturbance system as shown in Figure 4, the overall transfer function from u'(s) to y(s) can be expressed as shown in (5), then the bounds of nominal loop transfer function L_{1o}(s) at any given frequencies can be expressed as follows:

$$L_{1o}(s) = \frac{T_o(s)/T(s) - P_{1o}(s)/P_1(s)}{1-T_o(s)/T(s)} \tag{13}$$

where T_o(s)/T(s) and P_{1o}(s)/P_1(s) are the maximum variations of system response tolerance and uncertain plant, respectively.

proof: Equation (5) can be rewritten as follows

$$(1-\frac{T_o(s)}{T(s)})(1+L_{1o}(s)) = 1-\frac{P_{1o}(s)}{P_1(s)}. \tag{14}$$

After some simple manipulations, it yields

$$(L_{1o}(s)+1) = \frac{1-P_{1o}(s)/P_1(s)}{1-T_o(s)/T(s)}, \tag{15}$$

then

$$L_{1o}(s) = \frac{T_o(s)/T(s) - P_{1o}/P_1(s)}{1-T_o(s)/T(s)}. \qquad \square \tag{16}$$

Note that Equation (5) can also be expressed as

$$|\frac{1}{1+L_{1o}(s)}|_{dB} = |\frac{\Delta T(s)}{T(s)}|_{dB} - |\frac{\Delta P_1(s)}{P_1(s)}|_{dB}, \tag{17}$$

where $\Delta T(s) = T(s) - T_o(s)$, $\Delta P_1(s) = P_1(s) - P_{1o}(s)$. Hence $L_{1o}(s)$ should be designed to satisfy

$$|\frac{1}{1+L_{1o}(s)}|_{dB} \leq |\frac{\Delta T(s)}{T(s)}|_{dB} - |\frac{\Delta P_1(s)}{P_1(s)}|_{dB}. \tag{18}$$

Let $L_{1o}(s) = 1/\mathrm{Q(s)}$, then equation (18) becomes

$$|\frac{Q(s)}{1+Q(s)}|_{dB} \leq |\frac{\Delta T(s)}{T(s)}|_{dB} - |\frac{\Delta P_1(s)}{P_1(s)}|_{dB}. \tag{19}$$

It should be noticed that the relation between Q(s) and Q(s)/(1+Q(s)) is exactly the open loop and closed loop relation used in the Nichols Chart and, likewise, the relation between L_{1o}(s) and $1/(1+L_{1o}(\mathrm{s}))$ is the open and closed loop relation used in the inverse Nichols Chart.
Also note that the lower bounds of the loop transmission function L_{1o}(s) obtained by $|1/(1+L_{1o}(s))|_{db}$ are a set of the closed-loop contours in the inverse Nichols Chart. The values of L_{1o}(s) are obtained from the Lemma 2. Once those bounds are determined, the shaping of the nominal loop transmission function L_{1o}(s) can be obtained to satisfy the system response tolerance through the conventional QFT method (Horowitz and Sidi, 1972). The compensator G_1(s) is determined by using the relation $G_1(\mathrm{s}) = L_{1o}(\mathrm{s})/P_{1o}(\mathrm{s})$. Then, the prefilter F(s) is designed to make the system response satisfy the system performance.

3. Problem statement

Consider a linear time-invariant SISO uncertain multiple-loop system with n cascaded plant P_i, $i = 1, \ldots, n$, as shown in Figure 1, the control objective is to design prefilter F(s) and a set of controller G_i(s), $i = 1, \ldots, n$, to satisfy

$$T_2(s) \leq \quad |T(s)| \quad \leq T_1(s), \tag{20}$$

where T_1(s) and T_2(s) are the upper and lower bounds of the system response tolerances respectively. They are subject to the uncertain plant $P_i(s,q)$ described as follows

$$\begin{aligned} P_i(s;q) &= \frac{b_i(s;q)}{a_i(s;q)} \\ &= \frac{\sum_{l=1}^{m1} b_{il}(q)s^l}{\sum_{l=1}^{m2} a_{il}(q)s^l}, \; i = 1, \ldots, n, \end{aligned} \tag{21}$$

where the coefficients $a_{il}(q)$ and $b_{il}(q)$ are affine functions of the form

$$\begin{aligned} a_{il}(q) &= a_{ilo} + \sum_{m=1}^{n_q} a_{ilm} q_m \\ b_{il}(q) &= b_{ilo} + \sum_{m=1}^{n_q} b_{ilm} q_m \end{aligned} \tag{22}$$

q=[q_1,q_2, ...,q_{n_q}] is the perturbation parameter vector and they are elements of the hyper-rectangle Q defined as

$$Q \quad = \quad \{q_m | \underline{q}_m \leq q_m \leq \overline{q}_m, \; for \; m = 1, 2, \ldots, n_q\}, \tag{23}$$

where $\overline{q}_m$ and $\underline{q}_m$ are the upper and lower bounds of the parametric uncertainties. The compensators G_i(s), $i = 1, \ldots, n$, and prefilter F(s) are realizable transfer functions. Input and output transfer functions are u(s) and y(s) respectively. T(s) and T_o(s) are the perturbed and nominal system response transfer functions from u(s) to y(s) respectively. P_{io}(s) is the nominal plant transfer function of P_i(s). $L_{io}(s) = P_{io}(s)G(s)$

is the nominal loop transmission function.
It is also desirable to reduce the cost of feedback as reflected by the bandwidth of loop transmission function. In other words, in order to reduce any noise amplification that tends to saturate the early stages of the plant, the bandwidth of each loop transmission function should be minimized.

4. Main results

Without losing generality, it is assumed that the controller synthesis begins by opening all the outer loops except the inner most loop as shown in Figure 5. Once the inner most loop controller is designed, the outer inner most loop is synthesized with the inner most loop controller in place as shown in Figure 6. The design procedures are repeated until all the loops are closed.

4.1 Loop 1 closure: Considered in this situation is that all the loops P_2 through P_n have been opened as shown in Figure 5.

Lemma 3: The overall transfer function from u'(s) to y(s) as shown in Figure 5 can be expressed as follows:

$$\frac{1 - T_o(s)/T(s)}{1 - P_{1o}(s)/P_1(s)} = \frac{1}{1 + L_{1o}(s)}, \tag{24}$$

proof : The overall nominal transfer function $T_o(s)$ from u(s) to y(s) with nominal plant transfer function P_{1o} is

$$T_o(s) = P^1(s)\frac{L_{1o}(s)}{1 + L_{1o}(s)}G^1(s)F(s), \tag{25}$$

where $P^1(s) = P_n(s)\ldots P_2(s)$, $L_{1o} = P_{1o}(s)G_1(s)$ and $G^1(s) = G_2(s)\ldots G_n(s)$. Multiplying both sides by $(1 + L_{1o}(s))$, it yields

$$(1 + L_{1o}(s))T_o(s) = P^1(s)L_{1o}(s)G^1(s)F(s). \tag{26}$$

The output y(s) with uncertain plant P_1(s) is

$$y(s) = P^1(s)\frac{G_1P_1(s)}{1 + G_1(s)P_1(s)}G^1(s)F(s)u(s), \tag{27}$$

After some simple manipulations, it yields

$$(\frac{1}{P_1(s)} + G_1(s))T(s) = P^1(s)G_1(s)G^1(s)F(s), \tag{28}$$

and multiplying both side by P_{1o}(s), we obtain

$$(\frac{P_{1o}(s)}{P_1(s)} + L_{1o}(s))T(s) = P^1(s)L_{1o}(s)G^1(s)F(s), \tag{29}$$

Substituting Equation (26) into Equation (29) yields

$$(\frac{P_{1o}(s)}{P_1(s)} + L_{1o}(s))T(s) = (1 + L_{1o}(s))T_o(s). \tag{30}$$

Equation (30) can be rewritten as

$$(1 + L_{1o}(s))(T(s) - T_o(s)) = (1 - \frac{P_{1o}(s)}{P_1(s)})T(s). \tag{31}$$

Simple manipulation yields

$$\frac{1 - T_o(s)/T(s)}{1 - P_{1o}(s)/P_1(s)} = \frac{1}{1 + L_{1o}(s)}. \tag{32}$$

□

Thus, the block diagram in Figure 5 can also be redrawn as shown in Figure 4. The bounds of nominal loop transfer function L_{1o}(s) at any given frequencies can also be obtained by Lemma 2. Also note that the lower bounds, $B(\omega)$, of the loop transmission function L_{1o}(s) obtained by $|1/(1+L_{1o}(s))|_{dB}$ are a set of closed-loop contours in the inverse Nichols Chart. Once these bounds are determined, the shaping of the nominal loop transmission function L_{1o}(s) can be obtained to satisfy the system response tolerance. The compensator G_1(s) is determined by using the relation G_1(s) = L_{1o}(s)/P_{1o}(s).

4.2 Loop 2 closure: In Figure 1, all the plants P_3 through P_n have been opened. The block diagram representation of this situation is shown in Figure 6.

Lemma 4: The overall transfer function from u'(s) to y(s) as shown in Figure 6 can be expressed as follows:

$$\frac{1-T_o(s)/T(s)}{1-P_{2o}(s)P_{1eo}(s)/P_2(s)P_{1e}(s)} = \frac{1}{1+L_{2o}(s)}, \tag{33}$$

where $P_{1eo}(s) = \frac{P_{1o}(s)G_1(s)}{1+P_{1o}(s)G_1(s)}$ and $P_{1e}(s) = \frac{P_1(s)G_1(s)}{1+P_1(s)G_1(s)}$.

proof: Similarly, from Section 4.1, it yields

$$(1+L_{2o}(s))T_o(s) = P^2(s)L_{2o}(s)G^2(s)F(s), \tag{34}$$

where $G^2(s) = G_3(s)\ldots G_n(s)$, $P^2(s) = P_n(s)\ldots P_3(s)$, $L_{2o}(s) = P_{2o}(s)P_{1eo}(s)G_2(s)$ and

$$(\frac{P_{2o}(s)P_{1eo}(s)}{P_2(s)P_{1e}(s)} + L_{2o}(s))T(s) = P^2(s)L_{2o}(s)G^2(s)F(s), \tag{35}$$

Substituting Equation (34) into Equation (35) yields

$$(\frac{P_{2o}(s)P_{1eo}(s)}{P_2(s)P_{1e}(s)} + L_{2o}(s))T(s) = (1+L_{2o}(s))T_o(s). \tag{36}$$

Equation (36) can be rewritten as

$$\frac{1-T_o(s)/T(s)}{1-P_{2o}(s)P_{1eo}(s)/P_2(s)P_{1e}(s)} = \frac{1}{1+L_{2o}(s)}, \qquad \square \tag{37}$$

Thus, $1-P_{2o}(s)P_{1eo}(s)/P_2(s)P_{1e}(s)$ can be treated as an input at u'(s) and $1-T_o(s)/T(s)$ as an output at y(s). The overall closed loop transfer function from $u'(s)$ to y(s) can be expressed as $1/(1+L_{2o}(s))$. As a result, the block diagram in Figure 6 can also be redrawn as shown in Figure 7.

Similarly, from (33) the lower bounds of nominal loop transfer function L_{2o}(s) at any given frequencies can be obtained as follows:

$$L_{2o}(s) = \frac{T_o(s)/T(s) - P_{2o}(s)P_{1eo}(s)/P_2(s)P_{1e}(s)}{1-T_o(s)/T(s)} \tag{38}$$

After loop shaping, the compensator G_2(s) is determined by using the relation G_2(s) = L_{2o}(s)/P_{2o}(s)P_{1eo}(s).

Remark 1: If the maximum magnitudes of P_1(s) are chosen as the nominal plant, then for the area at the bottom of universal high frequency bound (UHωB) (see Horowitz and Sidi, 1972), the variation of P_1(s) uncertainties are downward vertical lines. The stability of L_{20}(s) at this area will not be affected by P_1(s) uncertainty. And the lower bounds of L_{20}(s) at low and middle frequencies can be derived as (38). The height of UHωB (B_h) can be determined to handle P_2(s) uncertainty only and the trade-off factor (Horowitz and Sidi, 1973) improved. It can be expressed as follows:

$$B_h = 20 * log_{10}\frac{P_{20}(\omega)}{P_2(\omega)}\Big|_{\omega\to\infty} \qquad \square \tag{39}$$

Remark 2: If the minimum magnitudes of $P_1(s)$ are selected as the nominal plant, then the variation of $P_1(s)$ uncertainties at low frequency range are upward. The bounds of $L_{20}(s)$ at this area will not be affected by $P_1(s)$ uncertainty. The lower bounds of $L_{20}(s)$ can be expressed as follows:

$$L_{2o}(s) = \frac{T_o(s)/T(s) - P_{2o}(s)/P_2(s)}{1 - T_o(s)/T(s)} \tag{40}$$

And the height of UHωB (B_h) which is still less than single loop system can be obtained as follows:

$$B_h = (20 * log_{10} \frac{P_{2o}(\omega)}{P_2(\omega)}\Big|_{\omega=\infty}) \text{ and } (20 * log_{10} \frac{P_{1eo}(\omega)}{P_{1e}(\omega)}\Big|_{\omega=\infty}). \quad \square \tag{41}$$

4.3 Loop j closure: After $j-1$ loops have been closed, i.e., $G_1(s)$, $G_2(s)$, ..., $G_{j-1}(s)$ will be determined accordingly. Next is to synthesize $G_j(s)$. Consider the block diagram as shown in Figure 1 where $P_{j+1}(s)$ through $P_n(s)$ have been opened. The block diagram representation of this situation is shown in Figure 8.

Lemma 5: The overall transfer function from $u'(s)$ to $y(s)$ as shown in Figure 8 can be expressed as follows:

$$\frac{1 - T_o(s)/T(s)}{1 - P_{jo}(s)P_{(j-1)eo}(s)/P_j(s)P_{(j-1)e}(s)} = \frac{1}{1 + L_{jo}(s)}, \tag{42}$$

where

$$P_{(j-1)eo}(s) = \frac{G_{(j-1)}(s)P_{(j-1)o}(s)P_{(j-2)eo}(s)}{1 + G_{(j-1)}(s)P_{(j-1)o}(s)P_{(j-2)eo}(s)} \tag{43}$$

$$P_{(j-1)e}(s) = \frac{G_{(j-1)}(s)P_{(j-1)}(s)P_{(j-2)e}(s)}{1 + G_{(j-1)}(s)P_{(j-1)}(s)P_{(j-2)e}(s)} \tag{44}$$

proof : Following the proof of Lemma 4, the similar result can be derived as follows: For the nominal and uncertain plant transfer functions, $P_{jo}(s)$ and $P_j(s)$, it yields

$$(1 + L_{jo}(s))T_o(s) = P^j(s)L_{jo}(s)G^j(s)F(s), \tag{45}$$

$$(\frac{P_{jo}(s)P_{(j-1)eo}(s)}{P_j(s)P_{(j-1)e}(s)} + L_{jo}(s))T(s) = P^j(s)L_{jo}(s)G^j(s)F(s), \tag{46}$$

where $L_{jo}(s) = G_j(s)P_{jo}(s)P_{(j-1)eo}(s)$. Substituting (45) into (46) and after some manipulations, Equation (42) is obtained. $\square$

Therefore, the block diagram in Figure 8 can also be redrawn as shown in Figure 9. The lower bounds of nominal loop transmission function $L_{jo}(s)$ at any given frequencies can also be derived as follows:

$$L_{jo}(s) = \frac{T_o(s)/T(s) - P_{jo}(s)P_{(j-1)eo}(s)/P_j(s)P_{(j-1)e}(s)}{1 - T_o(s)/T(s)} \tag{47}$$

And the height of UHωB (B_h) can be obtained as follows:

$$B_h = (20 * log_{10} \frac{P_{jo}(\omega)}{P_j(\omega)}\Big|_{\omega=\infty}) \text{ and } (20 * log_{10} \frac{P_{(j-1)eo}(\omega)}{P_{(j-1)e}(\omega)}\Big|_{\omega=\infty}). \tag{48}$$

Remark 3: If any of maximum magnitude of stages P_i, i=1,...,j-1, is chosen as the nominal plant, $P_{io} = P_i$ is substituted into Equation (48) but Equation (47) will remain

unchanged. □

Remark 4: If any of minimum magnitude of stages P_i, i=1,...,j-1, is chosen as the nominal plant, $P_{io} = P_i$ is substituted into Equation (47) but Equation (48) will remain unchanged as well. □

As the controllers, $G_1(s)$,$G_2(s)$, ..., $G_n(s)$, have been determined and the prefilter, F(s), is designed to make the system response satisfy the system performance, the design procedures are finished.

5. Illustrative example

Example: Consider a system as shown in Figure 2, where the plant is P= P_1P_2, $P_i = \frac{K_i}{s}$, $i = 1, 2$, $K_1 \in [1.71, 30.14]$, $K_2 \in [1.71, 13.58]$ with independent uncertainties. The design specifications shown as frequency domain in Figure 10 and as time domain in Figure 11 can be expressed as

$$T_1 = \frac{(\frac{s}{0.65}+1)(\frac{s}{13}+1)^2}{(s+1)(\frac{s}{3}+1)^2(\frac{s}{8}+1)}$$
$$T_2 = \frac{1}{(\frac{s}{2}+1)(\frac{s}{3}+1)^2(\frac{s}{7}+1)^2(\frac{s}{16}+1)} \quad (49)$$

The disturbance response requirement is 2 dB.

Solution:

(1) Loop 1 closure:

(1a) Choose nominal plant P_{1o}(s) as the maximum values of the uncertain plant, i.e., $P_{1o}(s) = \frac{30.14}{s}$, and nominal system response $|T_o|_{dB}$ as the maximum values of the system response tolerance, $|T_o|_{dB} = |T_1|_{dB}$. $P_1(s) = \frac{1.71}{s}$ and $|T|_{dB} = |T_2|_{dB}$ are selected to achieve the maximum variations of uncertain plant as well as system response tolerance. The procedures of obtaining the values of bound by using (13) are shown in Table 1. The shape of the L_{1o}(s) will be obtained through the conventional QFT method (Horowitz and Sidi, 1972) as shown in Figure 12. Note that vertical height of the universal high frequency bound (UHωB) for the nominal plant chosen as the maximum values of the uncertain plant is

$$B_h = 20 * log_{10}\frac{30.14}{1.71} = (25\ dB)_{upward}. \quad (50)$$

The UHωB is also shown in Figure 12.

The nominal loop transmission function L_{1o}(s) is

$$L_{1o}(s) = \frac{35}{s}\frac{1}{\frac{s^2}{44100}+\frac{s}{210}+1}, \quad (51)$$

and the compensator G_1(s) is

$$G_1(s) = \frac{35}{30.14}\frac{1}{\frac{s^2}{44100}+\frac{s}{210}+1}. \quad (52)$$

(1b) Choose nominal plant P_{1o}(s) as the minimum values of the uncertain plant, i.e., $P_{1o}(s) = \frac{1.71}{s}$, and nominal system response $|T_o|_{dB}$ as the minimum values of the system response tolerance, $|T_o|_{dB} = |T_2|_{dB}$. $P_1(s) = \frac{30.14}{s}$ and $|T|_{dB} = |T_1|_{dB}$ are selected to achieve the maximum variations of uncertain plant as well as system response tolerance. The values of bound for L_{1o}(s) by using (13) are shown in Table 2. The shape of the L_{1o}(s) will be obtained as shown in Figure 13. Note that vertical height of the universal high frequency bound (UHωB) for the nominal plant chosen as the maximum values of the uncertain plant is

$$B_h = 20 * log_{10}\frac{1.71}{30.14} = (-25\ dB)_{downward}. \quad (53)$$

The UHωB is also shown in Figure 13.
The nominal loop transmission function L_{1o}(s) is

$$L_{1o}(s) = \frac{2.8}{s} \frac{1}{\frac{s^2}{72900} + \frac{s}{270} + 1}, \tag{54}$$

and the compensator G_1(s) is

$$G_1(s) = \frac{2.8}{1.71} \frac{1}{\frac{s^2}{72900} + \frac{s}{270} + 1}. \tag{55}$$

(2) Loop 2 closure:
(2a) The maximum magnitudes of P_1(s) are selected as nominal plant. And choose nominal plant P_{2o}(s) as the maximum values of the uncertain plant, i.e., $P_{2o}(s) = \frac{13.58}{s}$, and nominal system response $|T_o|_{dB}$ as the maximum values of the system response tolerance, i.e., $|T_o|_{dB} = |T_1|_{dB}$. $P_2(s) = \frac{1.71}{s}$ and $|T|_{dB} = |T_2|_{dB}$ are chosen to achieve the maximum variations of uncertain plant as well as system response tolerance. By using (38), the bounds of L_{2o}(s) are shown in Table 3. The L_{2o}(s) can be shaped through the conventional QFT method (Horowitz and Sidi, 1972) as shown in Figure 14. Note that vertical height of the universal high frequency bound (UHωB) for the nominal plant P_{1o}(s) chosen as the maximum values of the uncertain plant is

$$B_h = 20 * log_{10} \frac{13.58}{1.71} = (18\ dB)_{upward}. \tag{56}$$

The UHωB is also shown in Figure 14.
The nominal loop transmission function L_{2o}(s) is

$$L_{2o}(s) = \frac{17}{s(\frac{s^2}{12100} + \frac{s}{110} + 1)(\frac{s}{1000} + 1)}, \tag{57}$$

the compensator G_2(s) is

$$G_2(s) = \frac{17}{35 * 13.58} \frac{\frac{s^3}{44100} + \frac{s^2}{210} + s + 35}{(\frac{s^2}{12100} + \frac{s}{110} + 1)(\frac{s}{1000} + 1)} \tag{58}$$

and the prefilter F(s) is

$$F(s) = \frac{(\frac{s}{5} + 1)(\frac{s}{9} + 1)}{(\frac{s}{2} + 1)(\frac{s}{2.5} + 1)(\frac{s}{4} + 1)}. \tag{59}$$

For the four extremes of the uncertain plant, the frequency responses all fall inside of the system bounds as shown in Figure 10 and the unit step responses also fall inside of the bounds as shown in Figure 11.
(2b) The minimum magnitudes of P_1(s) are selected as nominal plant. And choose nominal plant P_{2o}(s) as the maximum values of the uncertain plant, i.e., $P_{2o}(s) = \frac{13.58}{s}$, and nominal system response $|T_o|_{dB}$ as the maximum values of the system response tolerance, i.e., $|T_o|_{dB} = |T_1|_{dB}$. $P_2(s) = \frac{1.71}{s}$ and $|T|_{dB} = |T_2|_{dB}$ are chosen to achieve the maximum variations of uncertain plant as well as system response tolerance. By using (40), the bounds of L_{2o}(s) are shown in Table 4. The L_{2o}(s) can be shaped as shown in Figure 15. Note that vertical height of the universal high frequency bound (UHωB) for the nominal plant P_{1o}(s) chosen as the minimum values of the uncertain plant is

$$\begin{aligned} B_h &= (20 * log_{10} \frac{13.58}{1.71})\ and\ (20 * log_{10} \frac{1.71}{30.14}) \\ &= (18\ dB)_{upward}\ and\ (-25\ dB)_{downward}. \end{aligned} \tag{60}$$

The UHωB is also shown in Figure 15.
The nominal loop transmission function $L_{2o}(s)$ is

$$L_{2o}(s) = \frac{15(\frac{s}{18.5}+1)}{s(\frac{s}{5}+1)(\frac{s^2}{184900}+\frac{1.4s}{430}+1)(\frac{s}{20000}+1)}, \tag{61}$$

the compensator $G_2(s)$ is

$$G_2(s) = \frac{15}{2.8*13.58}\frac{(\frac{s}{18.5}+1)(\frac{s^3}{72900}+\frac{1.4s^2}{270}+s+2.8)}{(\frac{s}{5}+1)(\frac{s^2}{184900}+\frac{1.4s}{430}+1)(\frac{s}{20000}+1)} \tag{62}$$

and the prefilter F(s) is

$$F(s) = \frac{(\frac{s}{12}+1)}{(\frac{s}{2.5}+1)(\frac{s}{4}+1)}. \tag{63}$$

For the four extremes of the uncertain plant, the frequency responses all fall inside of the system bounds as shown in Figure 16 and the unit step responses also fall inside of the bounds as shown in Figure 17.

(3) Discussion:

The cost of feedback (COF) (Horowitz and Sidi, 1973) for a feedback system evaluated by the plant input with a sensor noise is derived as shown in Equations (1) and (2). The proposed design method improved the bandwidth propagation effect and decreased $|L_1|$ and $|L_2|$ vs. ω as quickly as possible as shown in Figure 12,14 and 13,15 respectively. The COFs $|\frac{X_1}{N_1}|$ and $|\frac{X_1}{N_2}|$ are demonstrated in the Bode Plot as shown in Figure 18,20 and 19,21 respectively. Results show that the proposed method which uses the variations of uncertain plant and system response tolerances can perform an alternative design method for uncertain cascaded multiple loops system.

6. Conclusion

The notion of equivalent external disturbance is introduced in this paper to provide an alternative approach for the design of uncertain cascaded multiple loops systems. Results show that the proposed approach will yield a design that meets all the specifications. Since the method is simple and effective, it may be concluded that this paper provides an alternative simple and effective frequency domain design methodology for the design of uncertain cascaded multiple loops systems.

References

Horowitz, I., and Sidi, M., 1972, "Synthesis of feedback systems with large plant ignorance for prescribed time-domain tolerances," *International Journal of Control*, vol. 16, no. 2, pp. 287–309.

Horowitz, I., and Sidi, M., 1973, "Synthesis of cascaded Multiple-loop feedback systems with large plant parameter ignorance," Automatica, vol. 9, pp. 589–600.

Horowitz, I. M., 1979, Quantitative synthesis of uncertain multiple input-output feedback system. *International Journal of Control*, Vol.30, No.1, pp.81–106.

Horowitz, I., and Wang, B. C., 1979, "Quantitative synthesis of uncertain cascade feedback system with plant modification," *International Journal of Control*, vol. 30, no. 5, pp. 837–862.

Jayasuriya, S., Franchek, M. A., 1991, "Frequency domain design for a maximum rejection of persistent bounded disturbance,"Journal of Dynamics Systems, Measurement and Control, 113, pp.195–205, 1991.

Wang, B. C., and Horowitz, I., 1988, "Quantitative synthesis of five-loop plant-modification control system," *International Journal of Control*, vol. 47, no. 6, pp. 1649–1664.

Table 1. Values of bound for P_1 uncertainty

ω	$\frac{T_o}{T}$	$\frac{P_{1o}}{P_1}$	L_{1o} (13)	$B(\omega) = \lvert\frac{1}{(1+L_{1o})}\rvert_{db}$
1	1.4804	17.6257	33.6106	-30.7842
2	2.2151	17.6257	12.6827	-22.7234
4	4.5267	17.6257	3.7143	-13.4683
7	11.7992	17.6257	0.5395	-3.7478
10	27.8905	17.6257	-0.3817	4.1764
15	97.7634	17.6257	-0.8282	15.2986

Table 2. Values of bound for P_1 uncertainty

ω	$\frac{T_o}{T}$	$\frac{P_{1o}}{P_1}$	L_{1o} (13)	$B(\omega) = \lvert\frac{1}{(1+L_{1o})}\rvert_{db}$
1	0.6755	0.0567	1.9069	-9.2686
2	0.4514	0.0567	0.7196	-4.7083
4	0.2209	0.0567	0.2107	-1.6610
7	0.0848	0.0567	0.0306	-0.2619
10	0.0359	0.0567	-0.0217	0.1902
15	0.0102	0.0567	-0.0470	0.4180

Table 3. Values of bound for P_2P_{1e} uncertainty

ω	$\frac{T_o}{T}$	$\frac{P_{2o}P_{1eo}}{P_2P_{1e}}$	L_{2o} (38)	$B(\omega) = \lvert\frac{1}{(1+L_{2o})}\rvert_{db}$
1	1.4804	8.8722	15.3880	-24.2950
2	2.2151	11.2052	7.3987	-18.4842
4	4.5267	17.6447	3.7197	-13.4782
7	11.7992	28.4525	1.5421	-8.1038
10	27.8905	39.3045	0.4245	-3.0730
15	97.7643	56.4629	-0.4268	4.8342
20	283.3826	71.9143	-0.7489	12.0021

Table 4. Values of bound for P_2 uncertainty

ω	$\frac{T_o}{T}$	$\frac{P_{2o}}{P_2}$	L_{2o} (38)	$B(\omega) = \lvert\frac{1}{(1+L_{2o})}\rvert_{db}$
1	1.4804	7.9415	13.4505	-23.1977
2	2.2151	7.9415	4.7127	-15.1369
4	4.5267	7.9415	0.9683	-5.8818
7	11.7992	7.9415	-0.3572	3.8387
10	27.8905	7.9415	-0.7419	11.7629
15	97.7643	7.9415	-0.9283	22.8851
20	283.3826	7.9415	-0.9754	32.1877

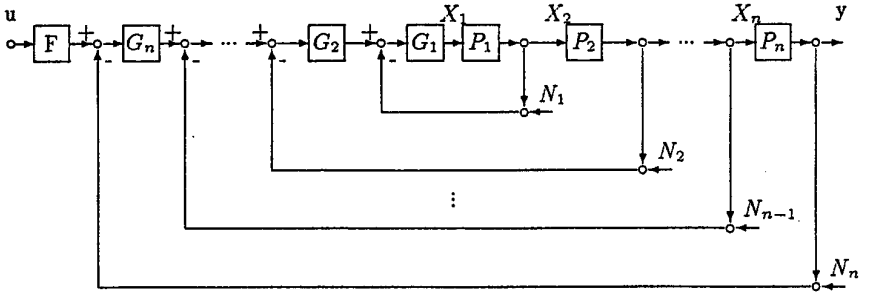

Figure 1. Uncertain cascaded multiple loops system

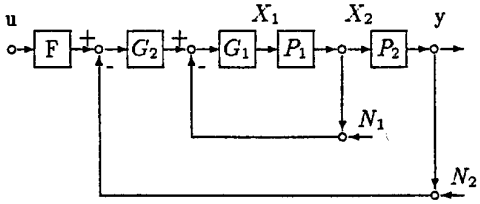

Figure 2. Uncertain cascaded two loops system

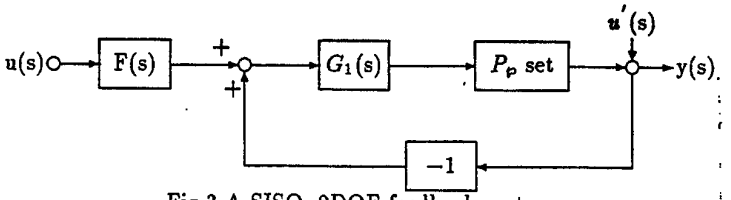

Fig.3 A SISO, 2DOF feedback system

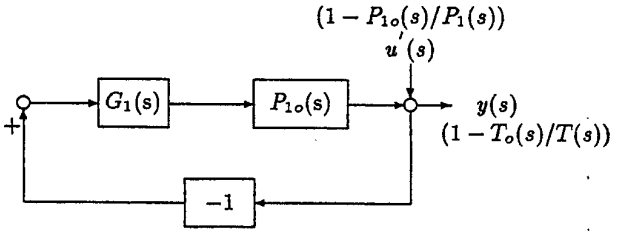

Fig.4 A equivalent external disturbance system

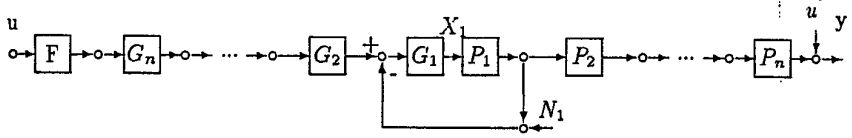

Figure 5. loop 1 closure

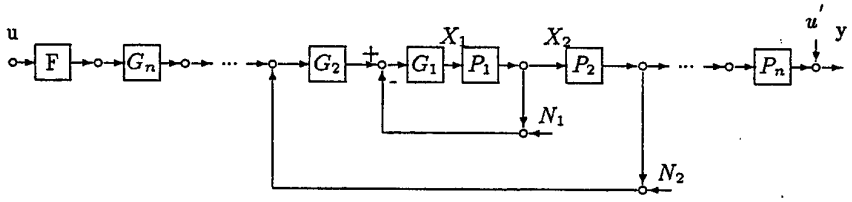

Figure 6. Loop 2 closure

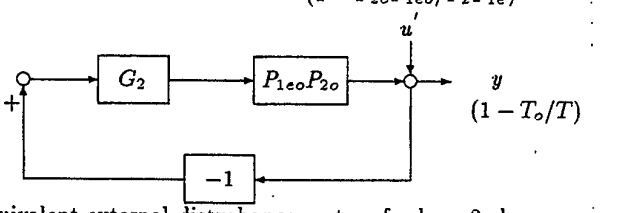

Fig.7 A equivalent external disturbance system for loop 2 closure

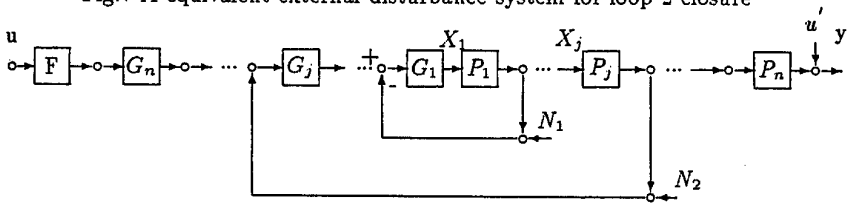

Figure 8. Loop j closure

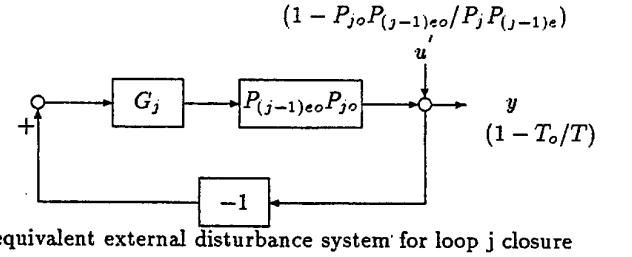

Fig.9 A equivalent external disturbance system for loop j closure

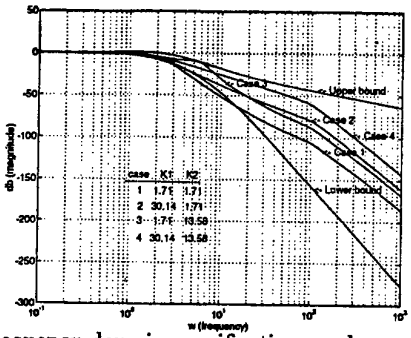

Figure 10. Frequency domain specifications and responses in Bode Plot

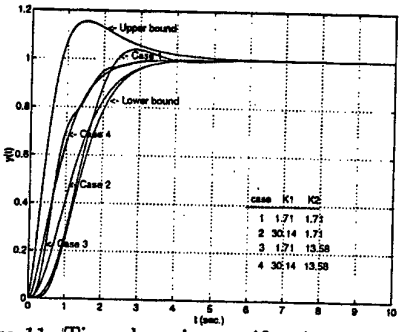

Figure 11. Time domain specifications and responses

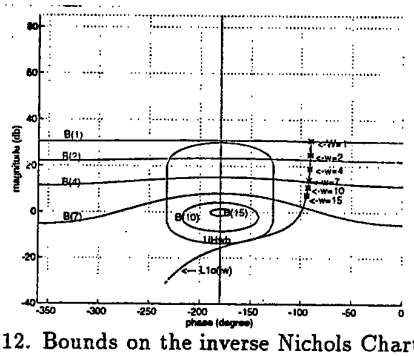

Figure 12. Bounds on the inverse Nichols Chart and

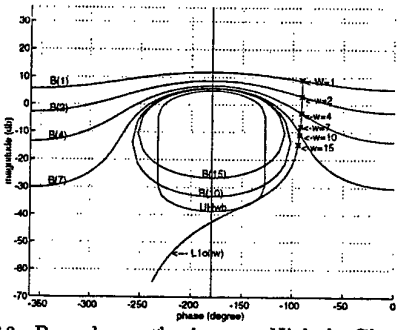

Figure 13. Bounds on the inverse Nichols Chart and L_{1o}(s)

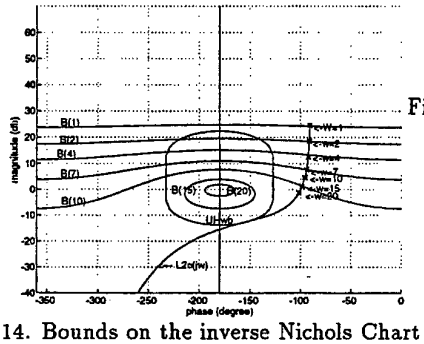

Figure 14. Bounds on the inverse Nichols Chart and L_{2o}(s)

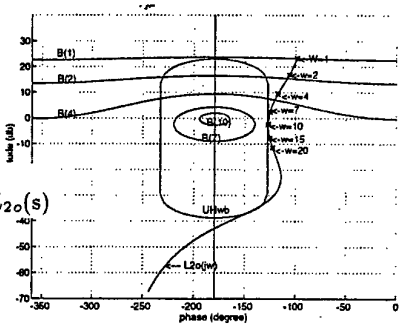

Figure 15. Bounds on the inverse Nichols Chart and L_{2o}(s)

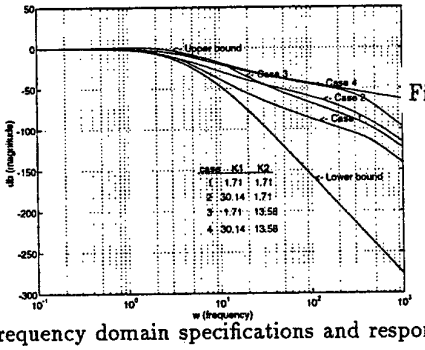

Figure 16. Frequency domain specifications and responses . in Bode Plot

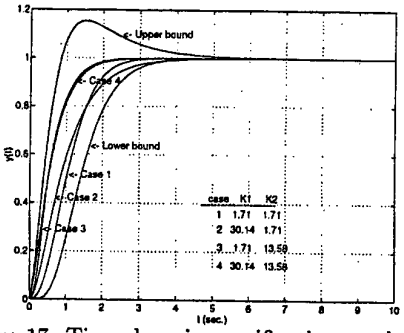

Figure 17. Time domain specifications and responses

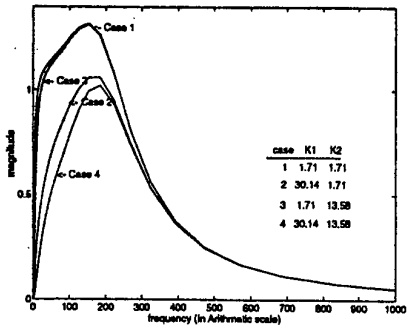

Figure 18. $|\frac{X_1}{N_1}|$

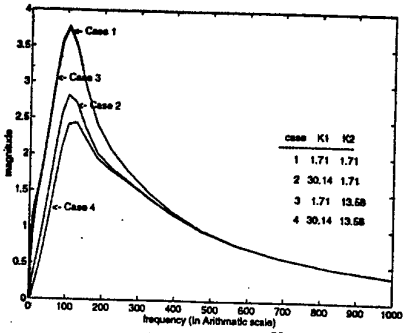

Figure 19. $|\frac{X_1}{N_2}|$

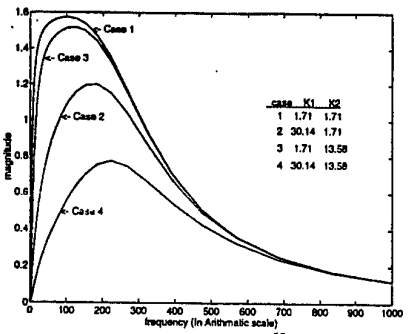

Figure 20. $|\frac{X_1}{N_1}|$

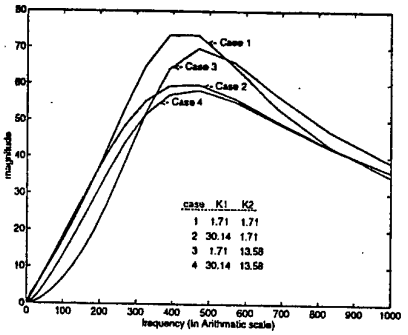

Figure 21. $|\frac{X_1}{N_2}|$

1999 International Symposium on
Quantitative Feedback Theory and Robust Frequency Domain Methods

CASCADED CONTROL FROM THE PERSPECTIVE OF LOAD SHARING CONTROL

Eduard Eitelberg
NOY Business
58 Baines Road, Durban 4001, South Africa

Abstract: *All systems, where at least one output depends on at least two inputs, are load sharing. In this paper, a popular multi-loop structure — that of cascaded feedback loops — is discussed from the perspective of the Load Sharing Control. In particular, the non plant modifying cascaded control system benefits and the inherent instability problem are analysed. Typical performance of cascaded control is demonstrated with an industrial superheater temperature control example. The material of this paper is adapted from the book "Load Sharing Control" by Eitelberg (1999 A).*

I Introduction to cascaded control loops

Cascaded plants are plants connected in series. Figure 1 shows relatively simple examples of two types of cascaded control structures for cascaded plants — *non plant modifying* and *plant modifying*, as defined by Horowitz (1993).

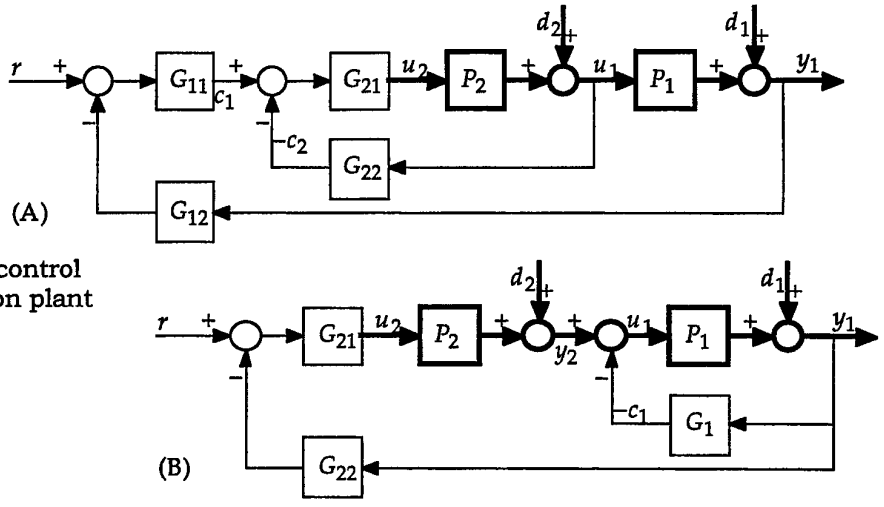

Figure 1: Cascaded control loop examples: (A) non plant modifying; (B) plant modifying.

An important difference between non plant modifying and plant modifying structures is the fact that, for any given system output, the plant signal levels are independent of the control system in the former case and they depend on the control system design or choice in the latter case. For example $U_2 = \left[(Y_1 - D_1)P_1^{-1} - D_2\right]P_2^{-1}$ in part (A) of Figure 1. However, in part (B) of Figure 1, the design or choice of G_1 modifies the

plant signal levels — in particular, $U_2 = \left[(Y_1 - D_1)P_1^{-1} - D_2 + Y_1 G_1\right]P_2^{-1}$. From the 'perspective' of load sharing, G_1 (and the associated actuator) is a supply 'plant' in part (B) and its design clearly affects the load distribution between y_2 and c_1.

A quantitative design procedure for plant modifying cascaded control systems, such as in Figure 1 (B), has been proposed by Horowitz and Wang (1979). A modified procedure, by utilising feed-forward into local loops, was proposed by Eitelberg (1991). The signals y_2 and c_1 share the load of regulating the disturbances d_1 and d_2 in an *independent load sharing control structure* — this type of system, among other load sharing structures, is thoroughly treated in the recent book by Eitelberg (1999 A).

In order to avoid huge supply *cross-sensitivities* (see Eitelberg, 1999), either G_1 or $G_{21}G_{22}P_2$ must have low gain — in the procedure of Horowitz and Wang (1979), G_1 is designed with as low gain as possible. Eitelberg (1991) used high gain in both loops, but transformed the structure into a co-ordinated control structure where cross-sensitivity is generally not a problem. At the time, it happened inadvertently — presently, this author would recommend co-ordinated control as the simpler option.

Plant modifying cascaded control is common in political and economic organisations, where often only the highest management levels have the necessary authority for 'plant modifying' injection of material, money, capital equipment or labour. It seems to be generally ignored in the control systems literature.

Presently, the non plant modifying cascaded control structure in Figure 1 (A) will be analysed further, because its primary control problem differs from the main emphasis of load sharing control. It is very present in industrial processes (such as flow or inlet temperature assisted outlet temperature control) and other applications (such as velocity gyro assisted position control on ships, in missiles, and others). In the academic and industrial control literature, it is generally introduced and explained with $G_{12} = G_{22} = 1$, although it is generally implemented with lead compensation and other terms in the respective return paths with $G_{12} \neq 1$ and $G_{22} \neq 1$.

II Non plant modifying cascaded control.

The signals c_1 and c_2 share the load of regulating the disturbances d_1 and d_2 in an independent load sharing control structure. The corresponding two *individual loop transfer functions*, with $G_{22} = 0$ or $G_{12} = 0$ respectively, are defined as

$$\begin{aligned} L_1(s) &= G_{11}(s)G_{12}(s)P_1(s)G_{21}(s)P_2(s) \\ L_2(s) &= G_{21}(s)G_{22}(s)P_2(s) \end{aligned} \qquad (1)$$

The combined loop transfer function $L = L_1 + L_2$ is important for judging the conditional stability and potential limit cycling of the main actuator at the input of P_2. However, here the primary control objective is related to the output y_1 of the plant P_1, where the following *conditional supply loop transfer function* (Eitelberg, 1999 A) determines the regulation performance:

$$L_{s1}(s) = \frac{L_1(s)}{1+L_2(s)} = L_1'(s)\frac{L_2(s)}{1+L_2(s)} \quad \text{with} \quad L_1'(s) = \frac{G_{11}(s)G_{12}(s)}{G_{22}(s)}P_1(s) \qquad (2)$$

With these definitions

$$Y_1 = \frac{L_{s1}}{1+L_{s1}}\frac{R}{G_{12}} + \frac{1}{1+L_{s1}}D_1 + \frac{P_1}{(1+L_{s1})(1+L_2)}D_2 \qquad (3)$$

It is important to recognise that the maximum gain cross-over frequency of the conditional and individual supply loop transfer functions, L_{s1} and L_1 respectively, are limited by the same non-minimum phase-lag of P_1P_2 independently of the design of L_2.

Therefore, having the inner loop L_2 is of no direct help in D_1 regulation. In fact, L_2 is counter-productive when, for example, L_2-failure tolerance dictates that L_1 must yield a stable closed-loop system. It will improve D_2 regulation by the factor $|1+L_2|$ in eq. (3), but this improvement may be unnecessary because L_{s1} regulates both, D_1 and P_1D_2, by the factor $|1+L_{s1}|$ in eq. (3)! The inner loop can be necessary when $|P_1D_2| >> |D_1|$.

In case of P_2 uncertainty, however, L_2 may improve D_1 regulation indirectly and very significantly. For example, when the stable L_2 bandwidth is sufficiently higher than that of L_{s1} then the uncertainty of P_2 can be removed from the design of $L_{s1} = (G_{11}G_{12}/G_{22})P_1 L_2/(1+L_2)$. With just enough gain in L_2, $L_{s1} \approx L_1' = (G_{11}G_{12}/G_{22})P_1$ — this will reduce the worst case stability margin over-design for L_{s1} and possibly increase its worst case low frequency gain. Horowitz (1993) uses this property of L_2 to reduce the required bandwidth of a 'pre-designed' minimum phase-lag conditional L_{s1}. From this L_{s1} and the uncertainty of P_2, he derives design boundaries for a relatively low-gain but high bandwidth L_2. It only appears as if L_2 was designed last — its characteristics are assumed during the effectively last design of L_{s1}.

The frequency domain effects of P_2 uncertainty are explained graphically in Figure 2. As long as the minimum magnitude of L_2 is above 0 dB, $L_2/(1 + L_2) \approx 1$ and the L_{s1} uncertainty is exclusively due to P_1. For this to be useful, the minimum gain cross-over frequency of L_2, ω_{gc2}, must be slightly greater than the maximum gain cross-over frequency of L_{s1}, ω_{gc1} — it is generally of little use to increase the minimum ω_{gc2} much beyond ω_{gc1}. In a single-loop structure, the lower values of the loop gain have to remain below those of the double loop by the entire uncertainty range of P_2 magnitude.

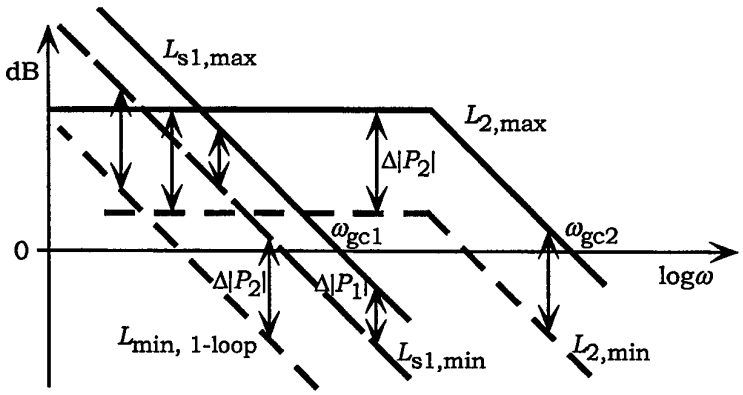

Figure 2: Effect of P_2 uncertainty for non plant modifying cascaded loops.

One of the most important recommendations for the design of general load sharing control systems (Eitelberg, 1999 A) *warns against designing or tuning slow loops last because of the resulting 'hidden' instability.* The procedure of Horowitz leads to an unstable closed loop L_1 — Figure 3 illustrates the reasons for this instability.

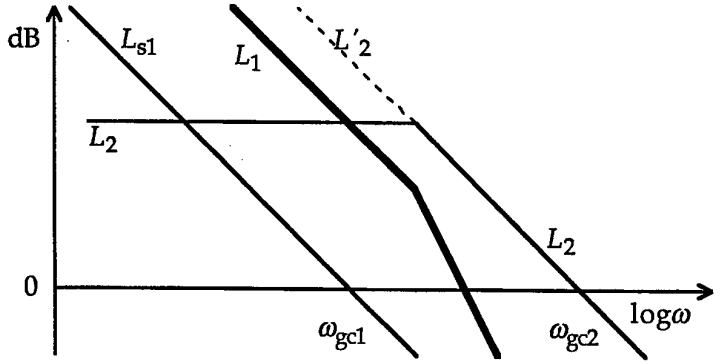

Figure 3: Design perspective for non plant modifying cascaded loops. ω_{gc} of L_1 is too high for stability when L_2 is not closed.

Industrial control literature instructs practitioners to tune a fast individual L_2 (to its maximum bandwidth) first and then tune the slow conditional L_{s1} (to its maximum bandwidth) — see for example the ISA Learning Module by Corripio (1990). This 'industry-standard' procedure too results in applications having unstable closed-loop L_1 — see Figure 3.

If integral mode is used in the inner loop then L_2 might look like L'_2 in Figure 4-3. Shinskey (1988, on p. 215) and McMillan (1990) recommend avoiding inner loop integral action whenever possible — in this case, the result might look something like L_2 in Figure 4-3. (Note that Shinskey (1988, on pages 217 and 224) argues that integral mode is necessary in the inner loop when the outer (primary) controller reset is protected against wind-up in a certain manner — this will be elaborated further ahead.) The resulting individual $L_1 = L_{s1}(1+L_2)$ is shown in Figure 3 for the case where neither the inner loop controller nor P_2 are integrating. Either way, the gain cross-over frequency of L_1 is above ω_{gc1} and its slope at the gain cross-over frequency is steeper than –40 dB/dec. Either one of these two conditions alone means instability for closed loop L_1.

The result is generally a limit cycling or completely inoperable system when L_2 saturates before the unstable L_1 is disabled — see Eitelberg (1999 A&B). Here, the actuator saturation is not dangerous, because it is common to L_1 and L_2. The danger comes from the range limitation of the inner loop sensor that measures u_1 in Figure 1. Many process instruments have an installed turn-down of not much higher than 3 or 5. Temperature sensors are often ranged for a very narrow operating span for sufficient resolution. There is no simple solution to this problem. Reducing L_{s1} bandwidth would decrease d_1 regulation below that of a single loop. Reducing L_2 bandwidth (and gain) would help only when it is no longer relevant.

A sensor range is obviously limited by the range of its primary physical effect and by the configured range of its transmitter. However, the measured variable itself can have 'surprising' limiting effects: such as two-phase flow temperature being a function of the pressure and not of the mass or energy content of the phases, completely independently of the sensor range — see the steam superheater example in the next section.

If performance requires the inner loop then the corresponding sensor must be absolutely reliable and ***the inner loop must be enabled whenever the outer loop is active***! This means that the cascaded control loops may have to be put on 'manual' or scheduled with different parameters for process start-up and shut-down.

Shinskey (1988, p. 217) recommends protecting the reset of the primary controller G_{11} of Figure 1 against wind-up by connecting it to u_1, (more or less) as is shown in Figure 4.

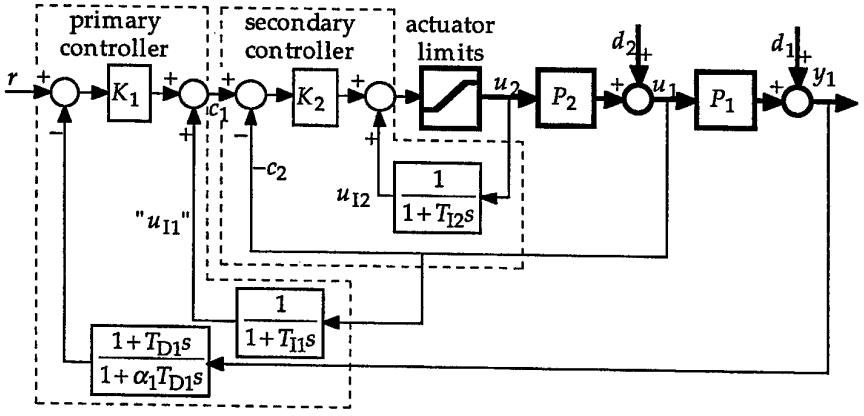

Figure 4: Cascaded PID controller 'implementation'. No lead-lag term is indicated in the inner loop, as it is seldom of much help — except for cancelling the sensor lag (not shown).

It is not known to the writer how this idea developed, but the following plausibility argument might have been involved. Suppose the inner loop has high gain from steady state up to much higher frequencies than the gain cross-over frequency of the outer loop and $d_2 = 0$. In this case, u_1 tracks the primary controller output c_1 in Figure 3 with virtually no delay and u_1 saturates 'exactly' when the P_2 actuator saturates. Therefore, u_1 is as good as a limiter output. A non-zero d_2 makes this saturation level uncertain and time-variable — it cannot be modelled in the primary controller without d_2 feed-forward.

Comparing to Figure 1, the following obvious association can be made for small signals (there are many equivalent ones):

$$G_{11}(s) = K_1 \qquad G_{12}(s) = \frac{1+T_{D1}s}{1+\alpha_1 T_{D1}s}$$
$$G_{21}(s) = K_2\left(1+\frac{1}{T_{I2}s}\right) \quad G_{22}(s) = \frac{1}{1+1/(T_{I1}s)} \tag{4}$$

Despite the apparent presence of the integral term in G_{21}, the inner loop does not have integral action any more. The effective G_{22} is high-pass, cancelling the integral action of G_{21}. The intended PI controller is approximated with a lag-lead term with the same gain for $\omega > 1/T_{I1}$:

$$L_2(s) = G_{21}(s)G_{22}(s)P_2(s) = \left(K_2\frac{T_{I1}}{T_{I2}}\right)\left(\frac{1+T_{I2}s}{1+T_{I1}s}\right)P_2(s) \tag{5}$$

The resulting L_2 will be similar to the one in Figure 3.

Despite the lack of an integral term in G_{11} or G_{12}, the master loop around P_1 does have integral action. From

$$L_1(s) = G_{11}(s)G_{12}(s)P_1(s)G_{21}(s)P_2(s) = \frac{G_{11}(s)G_{12}(s)}{G_{22}(s)}P_1(s)\,L_2(s) \tag{6}$$

we obtain for low frequency, where $|L_2| >> 1$,

$$L_{sl}(s) = \frac{L_1(s)}{1+L_2(s)} \approx \frac{G_{11}(s)G_{12}(s)}{G_{22}(s)}P_1(s) = K_1\left(1+\frac{1}{T_{I1}s}\right)\frac{1+T_{D1}s}{1+\alpha_1 T_{D1}s}P_1(s) \tag{7}$$

As Shinskey (1988, pages 217 and 224) has noted, the presence of the integral mode in the inner loop controller is generally required for the above trick to function as intended. A P (proportional) controller in the inner loop is equivalent to letting $T_{I2} \to \infty$ in Figure 4. The resulting $L_2(s) = P_2(s)K_2/(1+1/(T_{I1}s))$. If P_2 has finite steady-state gain then $L_2(0) = 0$ and at low frequency, the master loop around P_1 becomes $L_{sl}(s) \approx L_1(s) = K_1K_2\frac{1+T_{D1}s}{1+\alpha_1 T_{D1}s}P_1(s)P_2(s)$ — as if there was no inner loop at all.

This can be a useful cascaded control system — but don't expect integral action in the (master) control system. Some electrical power generation voltage control systems have a proportional controller in the master loop and a high-pass exciter voltage controller in the return path of the inner loop (see Glover and Sarma, 1989).

III A superheater cascaded temperature control example.

The following simplified superheater cascaded temperature control problem in Figure 5 is partially based on documentation and notes taken during a recovery boiler rebuilding project, after it was destroyed by an explosion of the smelt and leaked water 'mixture' in the furnace. The design and implementation of cascaded temperature control in power- and other boilers (of drum or once-through design) is similar. Boiler drum level control is another prominent example of cascaded loops, but this is more complex because of the steam flow feed forward and pressure change induced 'swell'.

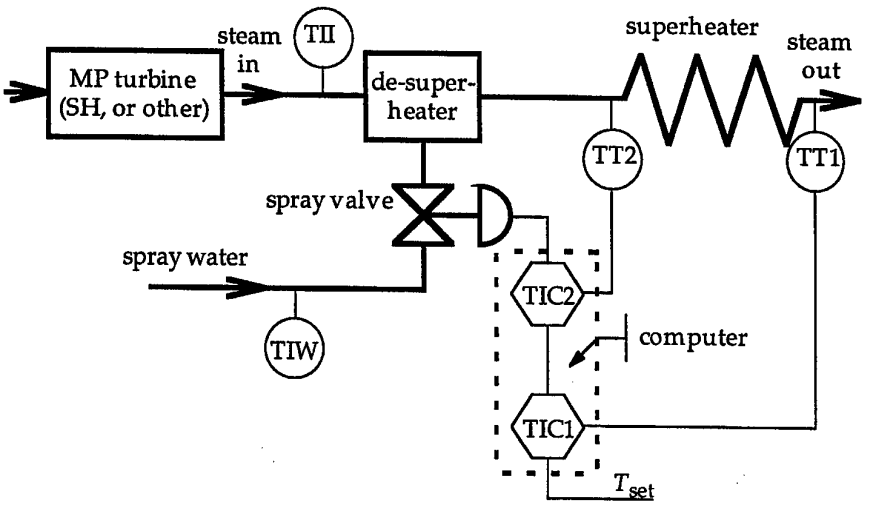

Figure 5: P&ID of a superheater cascaded temperature control system. (*Process & Instrument Drawing, Piping & Instrument Diagram, ...*)

Nomenclature:

- TII: temperature indicator — at de-superheater inlet;
- TT1: temperature transmitter — at superheater outlet;
- TIC1: temperature indicating controller — outer (master) loop;
- TT2: temperature transmitter — at superheater inlet;
- TIC2: temperature indicating controller — inner (slave) loop;
- T_{set}: reference temperature for T_1 at superheater outlet;
- TIW: spray water temperature indicator.

Approximate operating conditions:

- $\dot{m}_i = 60$ T/h steam into de-superheater;
- $p = 6$ MPa steam pressure;
- TII: $T_i = 300$°C;
- $T_{set} = 400$°C;
- TIW: $T_w = 50$°C.

The following data is for rough de-superheater modelling:

- $T_{sat} = 275$ °C, saturation temperature;
- $c'_p = 4.4$ kJ/(kg K), average specific heat capacity of water between 50°C and 275°C;
- $c''_p = 4.2$ kJ/(kg K), average specific heat capacity of steam between 275°C and 295°C;
- $\Delta h = 1600$ kJ/kg, latent heat (of evaporation/condensation).

The de-superheater heat energy flow balance is obtained by equating the energy flow rate that is taken from the (medium pressure) steam with the energy flow rate that is needed to heat the spray water to saturation temperature, evaporating it and then heating up to the final temperature. Heat exchange with the metal (pipes) is neglected. Dry steam condition is assumed throughout: meaning $T_2 > T_{sat}$. $T_1 > T_{sat}$ will follow then from the fact that the superheater is not a refrigerator.

$$\dot{m}_i c_p''(T_i - T_2) = \dot{m}_w\left[c_p'(T_{sat} - T_w) + \Delta h + c_p''(T_2 - T_{sat})\right] \tag{8}$$

Solving for T_2 yields

$$T_2 = \frac{\dot{m}_i T_i - \dot{m}_w\left[\Delta h/c_p'' + (c_p'/c_p'' - 1)T_{sat} - (c_p'/c_p'')T_w\right]}{\dot{m}_i + \dot{m}_w} \tag{9}$$

A highly simplified dynamic superheater model is given very approximately as

$$300\frac{dT_1(t)}{dt} = \frac{\dot{m}}{17}\left[T_2(t-60) - T_1(t)\right] + \Delta_q \tag{10}$$

where

- $\Delta_q \approx 110$: heating effect;
- t: time in [s];
- T_1 & T_2: temperature in [°C];
- $\dot{m} = \dot{m}_i + \dot{m}_w$: mass flow rate through superheater in [kg/s];
- $\dot{m}_w$: spray water flow rate ($0 \le \dot{m}_w \le 0.5$ kg/s).

The given model (10) only represents some aspects of superheaters, which are actually described by non-linear partial differential equations and interact with other boiler heat exchangers through the combustion chamber and flue gas duct thermal dynamics — see Lausterer, Franke and Eitelberg (1981 and 1983). For example, the effective dead-time of 60 seconds actually depends on the steam flow rate — this variability is ignored here. The TIC2 output $u(t)$ is in % — 0 corresponds to valve closed and 100 corresponds to valve fully open. Cooling down of hot steam with spray-water is thermodynamically inefficient — instead the combustion energy should be regulated. The de-superheater should do the fine regulation with small amounts of water or act against temporary large disturbances. The above given operating conditions lead to relatively small valve opening. The spray water control valve has a (slightly) *fast-opening* ***installed*** *characteristic* as is shown in Figure 6 — perhaps it is oversized or a nominally linear valve is installed in a long water pipe with significant pressure drop ...

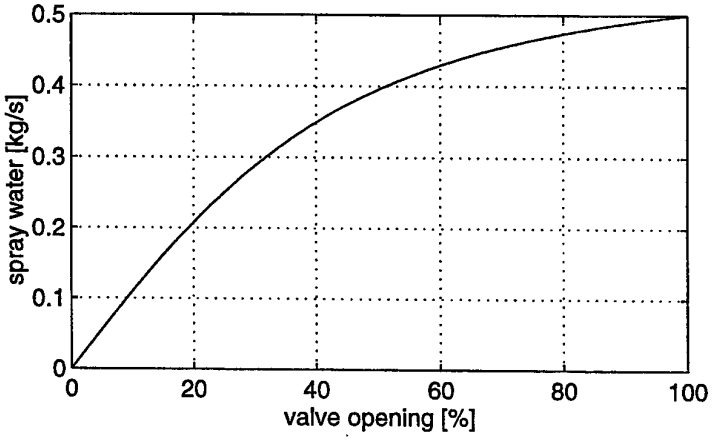

Figure 6: Installed spray water valve characteristic of eq. (11).

The equation for this valve characteristic is

$$\dot{m}_w = \frac{0.5}{\sqrt{1+0.2\left((100/u)^2-1\right)}} \text{ in [kg/s]} \tag{11}$$

The temperature measurement signals have a first order time-constant of 20 s. In good primary element installations, this time-constant should not be more than a few seconds.

The Matlab / Simulink diagram for the single-loop control is given in Figure 7.

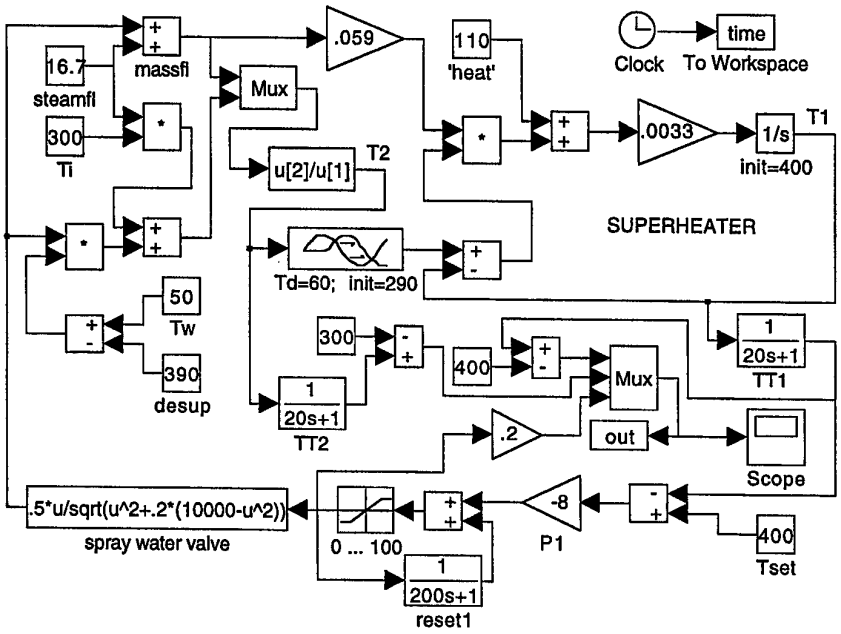

Figure 7: Simulink diagram of the single-loop temperature control system.

For single loop design or tuning, the worst case for stability is at small valve openings, where the loop gain is highest and the gain margin is lowest — all other non-linear effects are small in relation to the influence of the valve opening.

Generally, lead compensation of the temperature sensor's lag can be useful, because there is little noise — here the sensor/transmitter TT1 is relatively fast and lead compensation does not help to increase the loop bandwidth. The PI controller is tuned by using small steps of T_{set}. First, T_{I1} is set to a large value and the proportional gain K_1 is 'increased' to –20, leading to persistent oscillation in the loop. The period is about 250 s. Second, the gain is reduced to slightly less than half, $K_1 = -8$, and the integral time of 250 s is tried and then reduced to $T_{I1} = 200$. After confirming (unconditional) stability margins (lack of oscillations), at operating conditions that lead to large valve openings, this single-loop design is accepted as final.

The highest ('worst case') gain cross-over frequency of the final design should be about four or five sixths of the phase cross-over frequency of $2\pi/250 \approx 0.025$ rad/s.

The Matlab / Simulink diagram for the double-loop control is given in Figure 8.

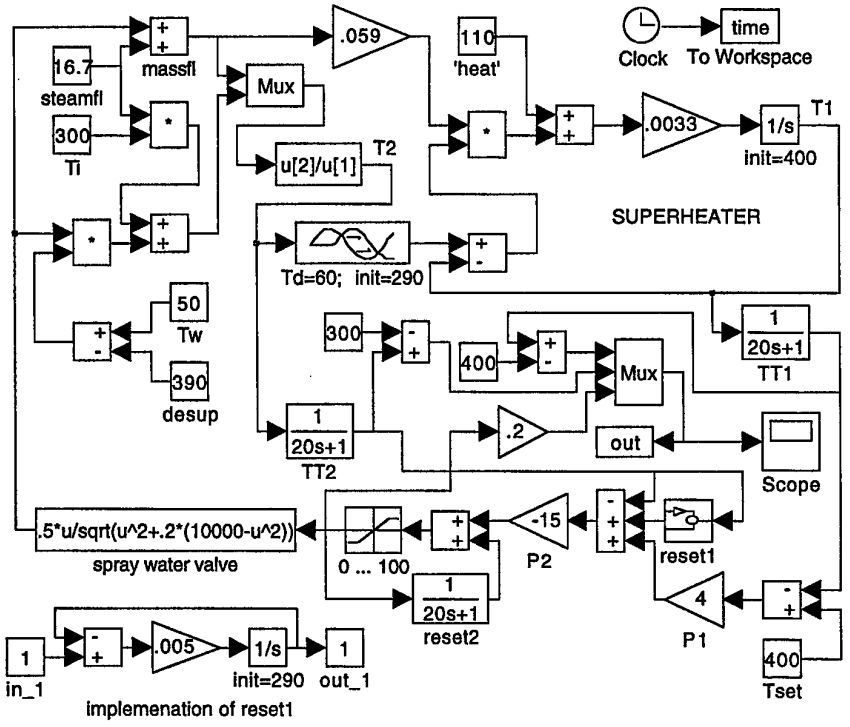

Figure 8: Simulink diagram of the double-loop cascaded temperature control system. The shown implementation of the outer loop's reset1 permits setting of non-zero initial conditions.

The cascaded loops are tuned from inside out — this is possible because of the open-loop plant stability. It is helpful to know from the single-loop design, that the outer loop phase cross-over frequency will be about 0.025 rad/s.

In order to eliminate the spray water valve gain uncertainty, the inner loop gain at this frequency should be about 3 = 10 dB or more for any plant gain — in particular for wide open valve. Assuming –30 dB/dec slope leads to the requirement that the inner loop gain cross-over frequency should be about 0.05 or more. Note that the temperature sensor corner frequency is given as 0.05 and the plant $P_2(s)$ is therefore close to algebraic up to this frequency. It follows, that the inner loop integral time of around T_{I2} = 20 seconds is adequate (in case the sensor time constant is greater, there will be more than 0.5π of phase lag between 0.05 rad/s and the smaller sensor corner frequency) and the gain should be tuned with the spray water valve almost open. The time constant of a small step response should be about 20 seconds or faster. The proportional gain $K_2 = -15$ is just adequate — much greater values are possible, provided that the sampling rate too is much higher than once every 10 seconds or so. In fact, infinitely many other combinations of gain and integral time will yield virtually identical performance in this example.

The outer loop, with much less varying gain, is tuned as the single loop before: this time, K_1 = 4 and T_{I1} = 200 are adequate.

The direct and indirect advantages of the cascaded control are demonstrated below. Figure 9 shows the effect of steam flow rate step changes from 15.2 to 16.2 kg/s and back at t = 30 and 40 minutes respectively. This disturbance can be caused by excess steam consumption for soot-blowing and it affects both, T_2 (output of P_2) and T_1 (output of P_1) directly. Hence, the inner loop regulates only a part of this disturbance.

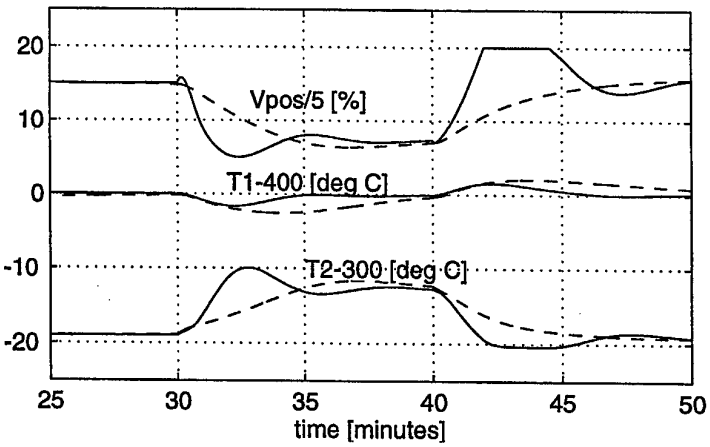

Figure 9: Steam flow rate step changes from 15.2 to 16.2 kg/s and back. Solid line: cascaded control; dashed line: single-loop control.

In this example, only the steam inlet temperature T_i and the spray water temperature T_w disturbances are 'enclosed' by the inner loop. Neither can generally change as suddenly as the steam massflow rate. Ignoring the reality of this example, Figure 10 demonstrates the inner loop's ability to regulate the effect of steam temperature step changes from 300 to 310 °C and back at t = 30 and 40 minutes respectively.

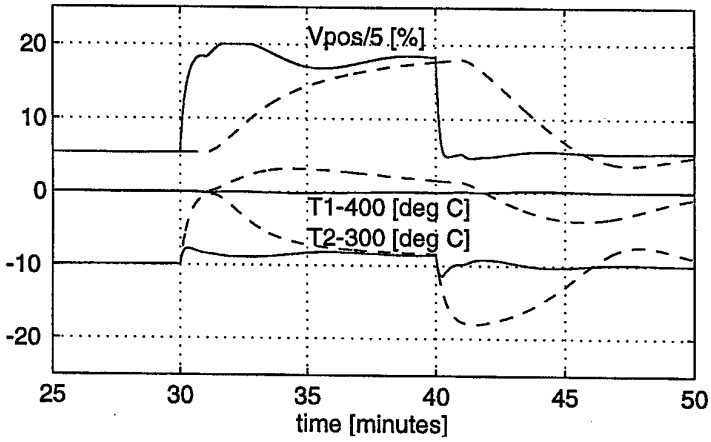

Figure 10: Steam temperature step changes from 300 to 310 °C and back. Solid line: cascaded control; dashed line: single-loop control.

The heating effect of approximately 110 degrees affects only the outer loop. Nevertheless, the valve gain uncertainty reduction by the inner loop improves the outer loop's performance significantly when the valve has to be opened wide. Figure 11 demonstrates overall performance improvement despite valve saturation.

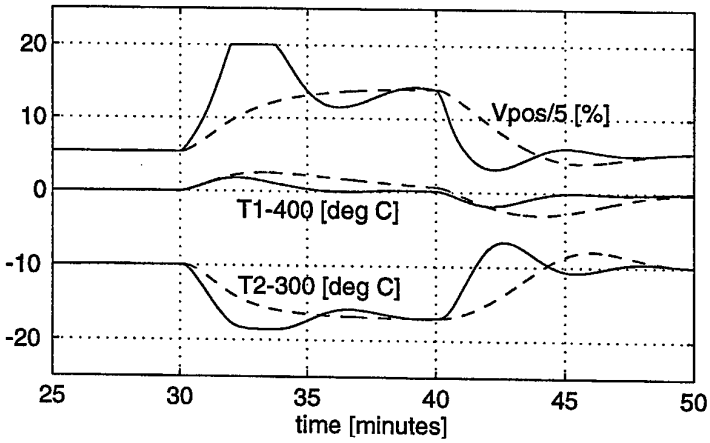

Figure 11: Heating effect step changes from 110 to 118 deg and back at 30 and 40 min respectively. Solid line: cascaded control; dashed line: single-loop control.

In industrial projects, there is economic need for standardisation. This means that management and maintenance staff like to have as few as possible different instruments. For example, identical transmitters could be purchased for TT1 and TT2. Suppose, in the present example, that TT1 and TT2 have identical ranges from 280 to 450 °C. For T_2 (and perhaps T_1) this is too wide — it leads to less than optimal resolution and precision.

More serious is the fact, that T_2 is too close to the lower limit of its transmitter's range — the writer has seen an embarrassed technician file off some carbon from a 'precision' calibration resistor in order to increase the range of such a temperature transmitter. Figure 12 demonstrates the destabilising effect of the slight sensor limitation during a temporary reduction of steam consumption: $\dot{m}_i$ goes from 14.5 kg/s to 13.5 kg/s and back at 20 and 40 minutes respectively. The (reduced) heating effect Δ_q = 100 degrees is kept constant.

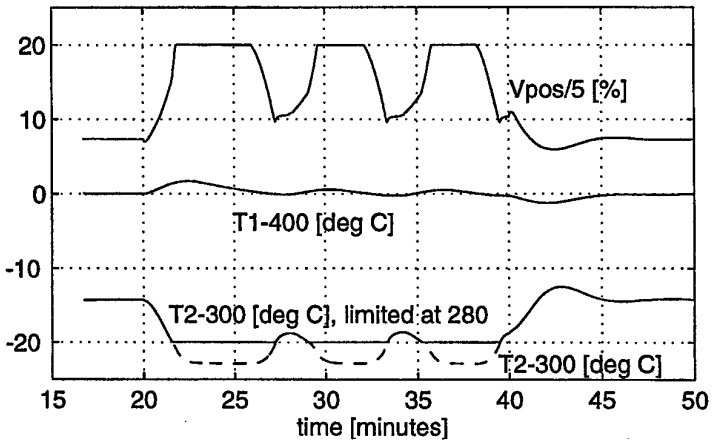

Figure 12: Destabilising effect of TT2 range limit at 280 °C in cascaded control. $\dot{m}_i$ changes from 14.5 kg/s to 13.5 kg/s and back at 20 and 40 min respectively. Δ_q = 100 deg. The actual (low-passed) T_2 is shown with dashed line.

The limit cycling extinguishes, here, immediately after increasing the steam flow rate because of the unconditionally stable design of $L=L_1+L_2$. This cannot be taken for granted, because the loop $L_{s2}=L_2/(1+L_1)$ around the temperature transmitter TT2 in Figure 5 is conditionally stable whenever the closed L_1 is unstable.

In this particular system, the ***inner loop will saturate and destabilise the cascaded system even with unlimited transmitter range.*** For example, if the boiler pressure is raised from the assumed 6 MPa to 6.5 MPa, then the saturation temperature will be 280 °C instead of the assumed 275 °C. The consequence is that the de-superheater outlet steam temperature T_2 cannot be cooled below 280 °C — instead, the steam will become wet.

There was a 100 MW power generating unit near Hannover, where one of the superheater temperature control systems had been on manual for years, because the plant operators had not realised that they were trying to cool saturated steam at the inlet of one of the superheaters. A single loop control system would have worked (according to some reasonably reduced expectations), because the steam became dry soon after entering the superheater pipes. The water content of the steam was actually not measured. Instead, very detailed dynamic calculations were carried out with a computer program that the writer had developed (see Franke, Eitelberg and others, 1979).

IV Conclusions

Plant modifying cascaded control systems are quite straight-forward *load sharing systems*, they are thoroughly treated in the recent book by Eitelberg (1999 A).

The non plant modifying cascaded control system too has a load sharing structure, but its primary control goal differs from the main emphasis of load sharing control.

The secondary (inner, slave) loop is useful for reducing disturbances that are 'enclosed' by it and for eliminating the uncertainty component of the enclosed plant section from the primary (outer, master) loop. However, it cannot make the primary loop gain cross-over frequency higher than that of a single loop control system.

A competently designed non plant modifying cascaded control system has a conditionally stable signal flow loop and will be unstable when the secondary loop saturates or is otherwise inactive. The writer is not aware of any applications where this is not the case and the inner loop is not a wasted, useless, confusing investment.

References

1. *Corripio, A. B.* (1990): "Tuning of Industrial Control Systems", (An Independent Learning Module from the Instrument Society of America), ISA.
2. *Eitelberg, Ed.* (1991): "Feedforward into local loops of plant modifying cascaded feedback systems", Int. J. Control, Vol. 53, No. 6, pp. 1467–1481.
3. *Eitelberg, Ed.* (1999 A): "Load Sharing Control", NOYB Press, Durban.
4. *Eitelberg, Ed.* (1999 B): "Performance of unstable control loops with limits", IFAC Contr. Eng. Practice, Vol. 7, Issue 4, pp. 517-522.
5. *Franke, J.; Eitelberg, Ed.; Kallina, G.; Weber, H. and Witte, U.* (1979): "Vorausberechnung des dynamischen Verhaltens eines Kraftwerksblockes", VGB Kraftwerkstechnik 59, Heft 2, pp. 124–128.
6. *Glover, J. D. and Sarma, M.* (1989): "Power System Analysis and Design", PWS-KENT.
7. *Horowitz, I.* (1993): "Quantitative Feedback Design Theory (QFT)", QFT Publications.
8. *Horowitz, I. and Wang, B.-C.* (1979): "Quantitative synthesis of uncertain cascade feedback systems with plant modification", Int. J. Control, Vol. 30, pp. 837–862.
9. *Lausterer, G. K.; Franke, J. and Eitelberg, Ed.* (1981): "A nonlinear model and control scheme for Benson boilers", the 8th IFAC World Congress, Kyoto, Japan, preprints Vol XX, pp. 72–77.
10. *Lausterer, G. K.; Franke, J. and Eitelberg, Ed.* (1983): "Modular modelling applied to a Benson boiler", IFAC Workshop on 'Modelling and Control of Power Plants', Como, Italy, pp. 11–19.
11. *McMillan, G. K.* (1990): "Tuning and Control Loop Performance", Second Edition, (A Practitioner's Guide), ISA.
12. *Shinskey, F. G.* (1988): "Process Control Systems", Third Edition, McGraw-Hill.

1999 International Symposium on
Quantitative Feedback Theory and Robust Frequency Domain Methods

Quantitative Digital Design of Crossfeed and Feedback Controllers for the UH-60 Black Hawk Helicopter †

Edward Boje
School of Electrical and Electronic Engineering
University of Natal, Durban, 4041, South Africa
email: boje@eng.und.ac.za

Abstract

This paper examines the use of quantitative crossfeed design followed by diagonal feedback design to decouple, stabilise and improve handling qualities of the UH-60 Black Hawk helicopter near hover. Linearised models of the helicopter are classified according to the likelihood of their occurrence in practice and this allows the performance for usual cases to be improved by a trade-off with reduced, but still quantitative, performance for less usual operating conditions. The Perron root of the interaction matrix is used as a measure of the level of triangularisation of uncertain multivariable plants and the crossfeed design seeks to reduce the interaction index before quantitative design of a diagonal feedback controller matrix is attempted. If the interaction index can be made less than unity by the design, stability of the diagonal loop designs guarantees stability of the closed loop multivariable system. The paper presents a w-domain based digital design for the helicopter control.

1. Introduction

In this paper we consider the two degree of freedom digital control system design for a 4-input, 4-output helicopter, illustrated as a Simulink block diagram in Figure 1. 24 linearised state space models of the UH-60 Black Hawk helicopter in near-hover flight were used in this design. The models were derived from linearisation about different flying conditions of the "Forecast" mathematical model discussed by Cheng, Tischler and Biezad (1995). The nominal flying condition is at hover and other models are obtained as the trim airspeed, rotor speed, aircraft weight, centre of gravity, turning rate, climb speed etc. are varied. The models are 33rd order and include gross body dynamics, rotor dynamics, and engine dynamics. The system inputs and outputs are defined in Table 1. The models were qualitatively classified into 3 subsets, {Most Probable}, {Less Probable} and {Least Probable} summarised in Table 2. This allows the performance for usual cases to be improved by a trade off with reduced but still quantitative performance for less usual operating conditions. Previous studies have determined that the frequency range of interest for piloted angle/rate commands (δ_a, δ_e, δ_r,) is 1.0 to 10.0 rad/s and for heave command (δ_c) is 0.2 to 2.0 rad/s. This paper will deal with the strictly technical aspects of the design but an important issue in satisfying handling qualities specifications is to correctly translate user requirements into feedback design specifications (bandwidth, phase lag and closed loop uncertainty). The final system performance would be evaluated against the ADS-33D that defines pilot assessed handling qualities for various Mission Task Elements (Hoh, and Mitchel 1996; Key, 1996; Yue and Postlethwaite, 1990; Hoh *et al*, 1993; Tischler, 1996; and Padfield, 1995, 1996)). The evaluation of the design presented here is discussed in Ukpai, Boje and Nwokah (1999?).

Input	Output
Aileron - lateral cyclic, δ_a	roll angle, ϕ
Elevator - longitudinal cyclic, δ_e	pitch angle, θ
Main rotor collective, δ_c	heave = vertical velocity, w
Tail rotor collective, δ_T	yaw rate, r

Table 1 - Input - output pairings for helicopter control

"most probable"	"less probable"	"least probable"
1,2,3,7,9	6,8,14,15	4,5,10,12,13,16,17,18,19,20,21,22,23,24,25

Table 2 - Classification of flight conditions

† This work was performed during a sabbatical visit to Osita D I Nwokah, Department of Mechanical Engineering, Southern Methodist University, Dallas. Dr Nwokah passed away on 26 April 1999.

In previous work, (Nwokah, Nordgren and Grewal, 1995 and Boje and Nwokah, 1997), the Perron root of the interaction matrix has been used as a measure of the level of triangularisation of uncertain multivariable plants. Forward loop pre-compensation (crossfeed) design seeks to reduce the interaction index before quantitative design of a diagonal feedback controller matrix is attempted. If the interaction index can be made less than unity by the design, stability of the diagonal loop designs guarantees stability of the closed loop multivariable system. This paper is an example of quantitative dynamic crossfeed design in contrast to the static crossfeed presented in Boje and Nwokah (1997). We also introduce differentiated specifications. Some level of open loop decoupling can be important for improving practical pilot handling qualities if the feedback loops are open.

Section 2 introduces the background Perron root theory including a stability theorem and an approach analogous to Gauss elimination for designing a unimodular dynamic crossfeed matrix. Section 3 details the design for the Black Hawk helicopter near hover, including digital design via use of the w-transform.

2. Quantitative design with decoupling crossfeed

For the feedback system shown in Figure 2, the tracking behaviour is given by,

$$\mathbf{T}_{Y/R} = (\mathbf{I}+\mathbf{PKG})^{-1}\mathbf{PKGF} \tag{1}$$

(All matrices in the helicopter example are 4×4.) We will consider the quantitative feedback design problem (Horowitz, 1979) of specifying a fully populated crossfeed matrix, **K**, with diagonal elements normalised to $k_{ii} = 1$, a diagonal feedback controller, **G**, and a pre-filter, **F**, to achieve certain tracking specifications,

$$\mathbf{A}_{ij}(\omega) \le \left|\mathbf{T}_{Y/R}(j\omega)\right|_{ij} \le \mathbf{B}_{ij}(\omega),\ i,j = 1, 2, \ldots, m$$

$\mathbf{A}_{ij}(\omega)$ and $\mathbf{B}_{ij}(\omega)$ are the client's desired specifications, for all plants, $\mathbf{P} \in \mathcal{P}$, where due to uncertainty, $\mathcal{P}$ is a set of all possible plants. In eq(1), $\hat{\mathbf{P}} = \mathbf{P}^{-1}$ and has elements $\hat{p}_{ij} = 1/q_{ij}$.

Our primary interest in this paper is to investigate the design of the off-diagonal elements of the crossfeed, **K**, to ease the subsequent task of designing the diagonal feedback controller, **G**. In a great number of applications, the regulating task is more important than tracking but the design approach is similar so we will focus on the latter.

2.1. Preliminary mathematics

Our investigation into the design will make use of the theory of non-negative matrices.

Definition 1: A matrix, $\mathbf{M} \in R^{n\times n}$ is an *M-matrix* if the diagonal elements of **M** are positive, the off diagonal elements of **M** are non positive, and the principal minors of **M** are non-negative.

Definition 2: Given a matrix $\mathbf{Z} \in C^{n\times n}$ the *comparison matrix* of **Z**, $M(\mathbf{Z})$, has elements,

$$M(\mathbf{Z})_{ij} = \begin{cases} |z_{ii}| & \text{(diagonal elements)} \\ -|z_{ij}| & i \neq j \end{cases}$$

Definition 3: A matrix, $\mathbf{Z} \in C^{n\times n}$ is *irreducible* if there does not exist a permutation, $\mathbf{P} \in C^{n\times n}$ such that

$$\mathbf{PZP}^{-1} = \left[\begin{array}{c|c} \mathbf{Z}_{11} & \mathbf{Z}_{12} \\ \hline 0 & \mathbf{Z}_{22} \end{array}\right], \text{ with square sub-matrices, } \mathbf{Z}_{11} \text{ and } \mathbf{Z}_{22}.$$

Definition 4: An irreducible matrix, $\mathbf{Z} \in C^{n\times n}$ is an *H-matrix* (Hadamard matrix) if $M(\mathbf{Z})$ is an *M*-matrix.

Definition 5: An *H*-matrix, $\mathbf{Z} \in C^{n\times n}$ is a *BH-matrix* if $\mathbf{Z}^{-1}$ is also an *H*-matrix.

Definition 6: A matrix, **Z** admits a *diagonal regular splitting* if it can be written as $\mathbf{Z} = \mathbf{D} + \mathbf{C}$, with $\mathbf{D} = \text{diag}\{\mathbf{Z}\}$ non-singular. (In some QFT design applications it may be more appropriate to form a triangular regular splitting.)

Definition 7: The *Perron root* of a matrix **M**, is the largest eigenvalue of the matrix formed from the absolute values of the elements of **M**.

$$\lambda_p(\mathbf{M}) = \max\{\lambda(\mathbf{M}_+)\} = \rho(\mathbf{M}_+)$$

$\rho(\mathbf{M}_+)$ is the spectral radius of $\mathbf{M}_+$. The absolute values are taken element-wise, $(\mathbf{M}_+)_{ij} = |\mathbf{M}_{ij}|$

The Perron root of an irreducible matrix is analytic and monotonic with respect to the elements of $\mathbf{M}_+$. The Perron root is an upper bound on the eigenvalues, $\lambda(\mathbf{M})$, and therefore the spectral radius, $\rho(\mathbf{M})$, of a matrix:

$$|\lambda(\mathbf{M})| \le \rho(\mathbf{M}) \le \lambda_p(\mathbf{M})$$

The spectral radius is a lower bound on all induced norms.

Definition 8: Given that $\mathbf{Z} \in C^{n\times n}$ admits the diagonal regular splitting,

$$\mathbf{Z} = \mathbf{D} + \mathbf{C} = (\mathbf{I} + \mathbf{C}\mathbf{D}^{-1})\mathbf{D} = (\mathbf{I} + \mathbf{M})^{-1}\mathbf{D}.$$

$\mathbf{M}$ is the *interaction matrix* and the *interaction index* of $\mathbf{Z}$ is the Perron root of the interaction matrix,

$$\gamma(\mathbf{Z}) = \lambda_P(\mathbf{M})$$

Considering the inverse of $\mathbf{Z}$, $\mathbf{Z}^{-1} = \hat{\mathbf{Z}}$, one sees the utility of the interaction index for feedback design: If $\mathbf{Z}$ is an *H-matrix*, $\mathbf{M}$ has spectral radius less than unity ($\rho(\mathbf{M}) \le \lambda_p(\mathbf{M}) < 1$, with $\gamma(\mathbf{Z}) \equiv \lambda_p(\mathbf{M})$) and, $(\mathbf{I}+\mathbf{M})^{-1} = \sum_{k=0}^{\infty} \mathbf{M}^k$ converges. In addition,

$$\gamma(\hat{\mathbf{Z}}) = \gamma\left(\mathbf{D}^{-1}(\mathbf{I}+\mathbf{M})^{-1}\right) = \lambda_P\left(\sum_{k=0}^{\infty}\mathbf{M}^k\right) \le \sum_{k=0}^{\infty}(\lambda_P(\mathbf{M}))^k = \frac{\gamma(\mathbf{Z})}{1-\gamma(\mathbf{Z})}. \quad (2)$$

Notice that if $\mathbf{Z}$ is row dominant, $|z_{ii}| > \sum_{k=1,k\neq i}^{n} |z_{ij}|$ for all i, $\gamma(\mathbf{Z}) < 1$, so that row (and column) dominance is a special case of requiring $\mathbf{Z}$ to be an *H-matrix*.

Theorem 1: An irreducible matrix, $\mathbf{Z} \in C^{n\times n}$ is a *BH-matrix* if $\min\{\gamma(\mathbf{Z}),\gamma(\hat{\mathbf{Z}})\} \le 0.5$

Proof: See Nwokah *et al*, 1995, or follows from eq(2) above.

Definition 9: An irreducible matrix $\mathbf{Z} \in C^{n\times n}$ is *almost decoupled* if $\max\{\gamma(\mathbf{Z}),\gamma(\hat{\mathbf{Z}})\} \le 0.5$. ($\mathbf{Z}$ almost decoupled $\Rightarrow$ $\mathbf{Z}$ is a *BH*-matrix - see below.)

Notice that the concept of almost decoupling is stronger that the requirements for $\mathbf{Z}$ to be a *BH*-matrix.

Theorem 2: An H matrix $\mathbf{Z} \in C^{n\times n}$ is almost decoupled, if $\gamma(\hat{\mathbf{Z}}) \le \frac{\gamma(\mathbf{Z})}{1-\gamma(\mathbf{Z})} \le 0.5$, requiring $\gamma(\mathbf{Z}) \le 1/3$.

Proof: See Nwokah *et al*, 1995, or follows from eq(2) above.

Corresponding to the Perron root are the right and left Perron eigenvectors, $\mathbf{x}$ and $\mathbf{y}^T$ respectively. They can be scaled so that their elements are all real and positive, with $\mathbf{y}^T\mathbf{x} = 1$. Examining the left and right Perron eigenvectors, one can assess the sensitivity of the Perron root to an individual element of a matrix via Theorem 2 below:

Theorem 3: Given a matrix, $\mathbf{M}$, with a simple (non-repeated) eigenvalue λ and the corresponding right and left eigenvectors, $\mathbf{x}$ and $\mathbf{y}^T$, scaled so that $\mathbf{y}^T\mathbf{x} = 1$, a perturbation of the (i,j) element of $\mathbf{M}$, $m_{ij}(\xi) = m_{ij} + \xi$, will perturb the eigenvalue with first order approximation,

$$\lambda(\xi) \approx \lambda + \xi y_i x_j. \quad (3)$$

In other words, eigenvalue differential sensitivity with respect to element (i,j) of $\mathbf{M}$, is

$$\frac{\partial\lambda}{\partial m_{ij}} = y_i x_j \quad (4)$$

As λ and m_{ij} are positive, the logarithmic differential sensitivity is,

$$\frac{\partial\log(\lambda)}{\partial\log(m_{ij})} = \frac{m_{ij}}{\lambda} y_i x_j \quad (5)$$

Proof: Follows from Lancaster and Tismenetsky, 1985, p.396.

2.2. Design approach for K using Gauss-elimination

The usual QFT approach if $\mathbf{P}$ is square and non-singular is to write the design eq(1) implicitly as,

$$(\hat{\mathbf{P}} + \mathbf{K}\mathbf{G})\mathbf{T}_{Y/R} = \mathbf{K}\mathbf{G}\mathbf{F} \quad (6)$$

or,

$$(\hat{\mathbf{K}}\hat{\mathbf{P}}+\mathbf{G})\mathbf{T}_{Y/R}=\mathbf{GF} \tag{7}$$

In eq(6) or eq(7), $\hat{\mathbf{P}}=\mathbf{P}^{-1}$, with elements $\hat{p}_{ij}=1/q_{ij}$. If the approach of Yaniv and Chait (1992) is used, thus pre-specifying **F**, or if the specifications can be converted to sensitivity specifications in some way (Boje, 1989) or if the plant is non-square, we can proceed by writing eq(6) without inversion as,

$$\mathbf{T}_{Y/R}\hat{\mathbf{F}}(\mathbf{PK}+\hat{\mathbf{G}})=\mathbf{PK} \tag{8}$$

As has been shown by Rosenbrock, 1970, any controller can be decomposed as a product of a permutation matrix, a unimodular matrix (a matrix with unity determinant formed from elementary operations) and a diagonal matrix. Yeung and Bryant (1992) have used Gauss elimination for stability analysis and design. For the design approach taken in this paper (Boje and Nwokah, 1999?), the diagonal matrix will be **G** and the unimodular matrix will be the **K** or $\hat{\mathbf{K}}$ in eq(7) or eq(8) respectively. **K** will be designed to reduce the interaction index, $\gamma=\lambda_P(\mathbf{M})$, as much as possible in the relevant frequency range. In order to apply single loop stability results (Section 2.4 below), it is sufficient to require $\lambda_P(\mathbf{M})<1$ i.e. an interaction index less than unity so that (**I**+**M**) is an *H*-matrix. To ensure that $(\mathbf{I}+\mathbf{M})^{-1}$ has low interaction index, we may apply the tougher constraint of requiring that (**I**+**M**) be a *BH*-matrix. This will ease over-design in the MIMO QFT method. Feedback benefits will be obtained by design of **G** as usual. Considering eq(7), we may write,

$$\hat{\mathbf{K}}=\hat{\mathbf{K}}^{[r]}\ldots\hat{\mathbf{K}}^{[2]}\hat{\mathbf{K}}^{[1]} \tag{9}$$

For each step, h, of the design (and corresponding i and j chosen by the designer for that step), $\hat{\mathbf{K}}^{[h]}=\mathbf{I}+\hat{k}_{ij}\mathbf{E}_{ij}$ with $\mathbf{E}_{ij}$ an elementary matrix having element (i,j) unity and all other elements zero. Define

$$\hat{\mathbf{P}}^{[h+1]}=\hat{\mathbf{K}}^{[h]}\hat{\mathbf{P}}^{[h]}=\left(\prod_{k=1}^{h}\hat{\mathbf{K}}^{[k]}\right)\hat{\mathbf{P}} \tag{10}$$

$\hat{\mathbf{K}}^{[h]}$ only affects the i^{th} row of $\hat{\mathbf{P}}^{[h+1]}$

$$\hat{p}_{ik}^{[h+1]}=\hat{p}_{ik}^{[h]}+k_{ij}\hat{p}_{jk}^{[h]}$$

Eq(1) is written implicitly as,

$$\left(\hat{\mathbf{P}}^{[h+1]}+\mathbf{G}\right)\mathbf{T}_{Y/R}=\left(\hat{\mathbf{K}}^{[h]}\hat{\mathbf{P}}^{[h]}+\mathbf{G}\right)\mathbf{T}_{Y/R}=\mathbf{GF} \tag{11}$$

Introduce the diagonal splitting,

$$\left(\hat{\mathbf{P}}^{[h+1]}+\mathbf{G}\right)=\left(\hat{\mathbf{P}}_D^{[h+1]}+\mathbf{G}\right)\left(\mathbf{I}+\mathbf{M}^{[h+1]}\right)$$

with interaction matrix, $\mathbf{M}^{[h+1]}=\left(\hat{\mathbf{P}}_D^{[h+1]}+\mathbf{G}\right)^{-1}\hat{\mathbf{P}}_O^{[h+1]}$, having individual elements,

$$m_{ik}^{[h+1]}=\frac{\hat{p}_{ik}^{[h+1]}}{\hat{p}_{ii}^{[h+1]}+g_i}=\frac{\hat{p}_{ik}^{[h]}+\hat{k}_{ij}\,\hat{p}_{jk}^{[h]}}{\hat{p}_{ii}^{[h]}+\hat{k}_{ij}\,\hat{p}_{ji}^{[h]}+g_i}$$

In step h, the interaction index is only changed as a result of changes in row i. We can therefore approximate the change in interaction index by,

$$\underset{\text{row i}}{\Delta}\log(\lambda^{[h+1]})\approx\sum_{\substack{k=1\\k\neq i}}^{m}\frac{\partial\log(\lambda)}{\partial\log(m_{ik})}\Delta\log(m_{ik})$$

$$\approx\log\left(\prod_{\substack{k=1\\k\neq i}}^{m}\left(\frac{\left(\hat{p}_{ik}^{[h]}+k_{ij}\hat{p}_{jk}^{[h]}\right)}{\left(\hat{p}_{ii}^{[h]}+k_{ij}\hat{p}_{ji}^{[h]}+g_i\right)}\frac{\left(\hat{p}_{ii}^{[h]}+g_i\right)}{\left(\hat{p}_{ik}^{[h]}\right)}\right)^{\frac{|m_{ik}^{[h]}|_{y_ix_k}}{\lambda^{[h]}}}\right) \tag{12}$$

If we follow a Gauss elimination approach, during forward elimination (lower triangular elements in $\hat{\mathbf{K}}$), the off-diagonal elements (i.e. with i≠k) in row i of $\hat{\mathbf{P}}$:

a) Should be small for k>j;
b) can be made small by subsequent steps for k<j;
c) should be made small for k=j, or;
d) may have relatively low contribution to the interaction index.

This justifies only examining the j^{th} element, giving,

$$\underset{\text{element ij}}{\Delta} \log(\lambda^{[h+1]}) \approx \Delta\log(m_{ij})\frac{\partial\log(\lambda)}{\partial\log(m_{ij})}$$

$$\approx \log\left(\frac{\left(\hat{p}_{ij}^{[h]}+k_{ij}\hat{p}_{jj}^{[h]}\right)}{\left(\hat{p}_{ii}^{[h]}+k_{ij}\hat{p}_{ji}^{[h]}+g_i\right)}\frac{\left(\hat{p}_{ii}^{[h]}+g_i\right)}{\left(\hat{p}_{ij}^{[h]}\right)}\right)^{\frac{|m_{ij}|y_ix_j}{\lambda^{[h]}}} \tag{13}$$

with $\ell_i = g_i/\hat{p}_{ii}$, and $\beta_{ij}^{[h]} = \left(\frac{\lambda_d^{[h+1]}}{\lambda^{[h]}}\right)^{\frac{\lambda^{[h]}}{|m_{ij}^{[h]}|(y_ix_j)^{[h]}}}$ an appropriate design task is to achieve,

$$\left|\frac{\hat{p}_{ij}^{[h]}+k_{ij}\hat{p}_{jj}^{[h]}}{\hat{p}_{ii}^{[h]}+k_{ij}\hat{p}_{ji}^{[h]}}\right| \le \beta_{ij}^{[h]}\left|\frac{\hat{p}_{ij}^{[h]}}{\hat{p}_{ii}^{[h]}}\right|\left|\frac{1+\ell_i^{[h+1]}}{1+\ell_i^{[h]}}\right|$$

Since the diagonal sensitivity depends on the specifications and changes in gain between $\hat{p}_{ii}^{[h]}$ and $\hat{p}_{ii}^{[h+1]}$ will be approximately compensated by changes in g_i, $\left|\frac{1+\ell_i^{[h+1]}}{1+\ell_i^{[h]}}\right| \approx 1$ and the design objective is:

$$\left|\frac{1+k_{ij}\hat{p}_{jj}^{[h]}/\hat{p}_{ij}^{[h]}}{1+k_{ij}\hat{p}_{ji}^{[h]}/\hat{p}_{ii}^{[h]}}\right| \le \beta_{ij}^{[h]} \tag{14}$$

Notes:

1) Eq(14) requires a reduction in the size of the off-diagonal element with respect to the diagonal element. This makes sense as high gain diagonal elements reduce the interaction and high gain off diagonal elements increase interaction.
2) If there were no uncertainty, we could satisfy ourselves with only lower triangular **K**. this would give perfect ℓ-dominance (Yeung and Bryant, 1992) and zero interaction. Because of uncertainty, we may need to perform a pseudo back-substitution step to reduce the interaction index further.
3) We could add phase specifications to the diagonal component, $q_{ii}^{[h+1]} = 1/\left(\hat{p}_{ii}^{[h]}+k_{ij}\hat{p}_{ji}^{[h]}\right)$, to ensure that as far as possible, the gain is minimum phase in the design frequency range. This is an area of further research.
4) At any stage, designing $\hat{\mathbf{K}}^{[h]}$ stable ensures that $\mathbf{K}^{[h]}$ is stable.
5) Yaniv and Chepovetsky (1995) have used a similar elementary matrix approach, with all elements in the i^{th} column of **K** specified at once and an LQ constraint.
6) A significant benefit of using this approach is that the compensated plant $\hat{\mathbf{K}}\hat{\mathbf{P}}$ or **PK** appears as a unit, preserving the benefit (in terms of ease of design) of having **G** diagonal in eq(7) or eq(8).
7) Designing **K** one element at a time does not necessarily lead to the minimum interaction index as it may be required to increase the interaction index, $\gamma(\hat{\mathbf{P}}^{[h]})$ at some stages in the formation of **K**.
8) The $\beta_{ij}^{[h]}$ in eq(14) can be calculated per plant element, allowing trade-off between high interaction and low interaction plants from the plant set.
9) (14) is a linear fractional mapping in k_{ij} for which standard CAD tools can be used (Borgesani, Chait and Yaniv, 1995).

2.3. Diagonal controller design

Once the cross-feed matrix has been designed, standard MIMO QFT may be used to design the diagonal controller, **G**. After the cross-feed design, it may be necessary to impose additional sensitivity specifications, $\left|\frac{1}{1+\ell_i}\right| \le \eta$, on the diagonal loops in order to achieve (if possible) the *H*-matrix condition on the interaction matrix, $\mathbf{M} = \left(\left\{\hat{\mathbf{K}}\hat{\mathbf{P}}\right\}_D + \mathbf{G}\right)^{-1}\left\{\hat{\mathbf{K}}\hat{\mathbf{P}}\right\}_O$, with, $m_{ij} = \begin{cases} \frac{q_{ii}^*/q_{ij}^*}{1+\ell_i} & i \ne j \\ 0 & i = j \end{cases}$ and $\hat{p}_{ij}^* = \left[\hat{\mathbf{K}}\hat{\mathbf{P}}\right]_{ij} = 1/q_{ij}^*$.

For feedback design, it is convenient to re-calculate eq(1) implicitly as,

$$(\hat{\mathbf{P}}^{*}+\mathbf{G})\mathbf{T}_{Y/R}=\mathbf{GF} \tag{15}$$

Reducing the individual off diagonal elements in $\hat{\mathbf{K}}\hat{\mathbf{P}}$ will ease the diagonal controller design significantly in many practical applications. The individual diagonal loops are, $\ell_i = g_{ii}q^{*}_{ii}$, and the i^{th} controller is designed via,

$$t_{ij}=\frac{f_{ij}\ell_i}{1+\ell_i}-\frac{1}{1+\ell_i}\left(\sum_{k=1,k\neq i}^{m}\frac{q^{*}_{ii}}{q^{*}_{ik}}t_{kj}\right)=\frac{f_{ij}\ell_i}{1+\ell_i}-\sum_{k=1,k\neq i}^{m}m_{ik}\,t_{kj} \tag{16}$$

for j = 1..m.

2.4. Stability result

The closed loop system after design of **K** and **G** must be internally stable, which means that the feedback controller must either stabilise an unstable plant or must not destabilise a stable one. We assume that the plant has no unstable hidden modes (i.e. no right hand plane (RHP) pole-zero cancellations in the plant).

Theorem: Given $\mathbf{P}\in\mathcal{P}$, square and invertible with no hidden unstable modes. The closed loop system in Fig. 2,

$$\begin{aligned}\mathbf{T}_{Y/R}&=(\mathbf{I}+\mathbf{PKG})^{-1}\mathbf{PKGF}\\&=(\mathbf{M}+\mathbf{I})^{-1}\left(\hat{\mathbf{G}}\left\{\hat{\mathbf{K}}\hat{\mathbf{P}}\right\}_D+\mathbf{I}\right)^{-1}\mathbf{F}\end{aligned} \tag{17}$$

is internally stable if

1. **F** is stable.
2. **K** is unimodular and stable.
3. $\lambda_P(\mathbf{M}(s)) < 1$ for all $s\in D$, the Nyquist contour covering the right hand plane.
4. $\left(\hat{\mathbf{G}}\left\{\hat{\mathbf{K}}\hat{\mathbf{P}}\right\}_D+\mathbf{I}\right)^{-1}=\mathrm{diag}\left\{\frac{g_i q^{*}_{ii}}{1+g_i q^{*}_{ii}}\right\}$, with $\left[\hat{\mathbf{K}}\hat{\mathbf{P}}\right]_{ij}=1/q^{*}_{ij}$, is designed to be internally stable, having the right hand plane closed loop poles and no right hand plane open loop pole-zero cancellations.

Proof: As **F** is stable, $\mathbf{T}_{Y/R}$ is only unstable if $(\mathbf{M}+\mathbf{I})^{-1}$ or $\left(\hat{\mathbf{G}}\left\{\hat{\mathbf{K}}\hat{\mathbf{P}}\right\}_D+\mathbf{I}\right)^{-1}$ is unstable. As **K** is unimodular, its poles and transmission zeros are co-incident and in the left half plane by design. (**K** may have non-minimum phase lag elements.) Therefore, no right hand plane pole-zero cancellations can be introduced in **PK**. Write $\mathbf{PK}(s)=\frac{1}{d(s)}\mathbf{N}(s)$, $\hat{\mathbf{K}}\hat{\mathbf{P}}(s)=\frac{d(s)}{\det(\mathbf{N}(s))}\mathrm{adj}(\mathbf{N}(s))=\frac{d_p}{n_p}\mathbf{A}$ and $g_i(s)=\frac{n_{gi}}{d_{gi}}$. By assumption (iv), each $\frac{g_i q^{*}_{ii}}{1+g_i q^{*}_{ii}}=\frac{n_{gi}\,n_p}{d_{gi}\,d_p\,A_{ii}+n_{gi}\,n_p}$ is designed to be internally stable. Therefore there are no right hand plane zeros in any $(d_{gi}\,d_p\,A_{ii}+n_{gi}\,n_p)$. Since $m_{ij}=\frac{q^{*}_{ii}/q^{*}_{ij}}{1+g_i q^{*}_{ii}}=\frac{d_{gI}\,d_p\,A_{ij}}{d_{gi}\,d_p\,A_{ii}+n_{gi}\,n_p}$, $i\neq j$, (I+M) has no right hand plane poles. By assumption (iii), $\lambda_P(\mathbf{M}(s)) < 1\ \forall\ s\in D$, so $\Delta\arg\{\det(\mathbf{I}+\mathbf{M})\}=0$ around this contour. By the principle of argument, (I+M) therefore has no right hand plane zeros. This completes the proof.

Comments

1) It is impractical and unnecessary to require $\lambda_P(\mathbf{M}) < 1$ for all frequencies. At frequencies where the spectral radius, $\rho(\mathbf{PKG})<1$, $(\mathbf{I}+\mathbf{PKG})$ cannot have right hand plane zeros, which means that the only unstable poles are high frequency unstable poles in **P** that have not been cancelled by feedback action (and cannot be unless the gain is increased). The results of the theorem above could be modified for a Nyquist path that covers the relevant portion of the right hand plane.
2) Achievement of $\lambda_P(\mathbf{M})$ specifications assume that the specifications on outer loop $|1/(1+\ell_j)|$'s are achieved and the $\lambda_P(\mathbf{M})$ specifications are required for this latter design to be valid.

3) Notice that the stability result only requires that $\lambda_P(\mathbf{M}) < 1$ for $(\mathbf{I}+\mathbf{PKG}) \in H$. We may specify the stronger condition $\lambda_P(\mathbf{M})<0.5$ to obtain $\lambda_P\left((\mathbf{I}+\mathbf{PKG})^{-1}\right)<1$, i.e. higher level of decoupling to get $(\mathbf{I}+\mathbf{PKG})^{-1} \in H$ or even, $\lambda_P(\mathbf{M})<1/3$ (almost decoupling condition) to get $\lambda_P\left((\mathbf{I}+\mathbf{PKG})^{-1}\right)<0.5$.
4) For stability alone it is sufficient to ensure that a single plant in a connected plant set is stable and deduce stability for the remaining elements of the plant set from the continuity of poles with respect to parameters of linear transfer functions.
5) Requiring the $\gamma < 1$ at some frequency for a 2×2 system is equivalent to requiring the compensated system, $\mathbf{P}^* = \mathbf{KP}$ to have $p^*_{11}\, p^*_{22} > p^*_{21}\, p^*_{12}$. Similar results may be derived for larger systems.

2.5. Pre-filter design

Once the feedback loop design has been fixed, the tracking response can be enhanced by means of a pre-filter matrix, **F**. Generally in QFT design for basically non-interacting specifications, the feedback controller would be designed (with sufficiently high gain at the relevant frequencies) to achieve specified reduction in uncertainty of the diagonal closed loop elements and sufficiently small off-diagonal elements. The pre-filter would then have only diagonal elements, (**F** = diag{f_{ii}}) designed to match the compensated diagonal elements to the client's specifications. In our approach, if it is possible to obtain a low open loop interaction index, we are only assured of generalised triangular behaviour. If there are no non-minimum phase or plant input constraints, it is then possible to design the diagonal controller matrix, **G**, with high enough gain at all frequencies to achieve arbitrary tracking performance. In practical designs this will seldom be the case. Suppose that $\mathbf{T} = (\mathbf{I}+\mathbf{L})^{-1}\mathbf{L}$ is almost lower triangular or can be made almost lower triangular by row and column swapping. By "almost lower triangular", we mean that the elements above the diagonal are significantly smaller than the other elements. If the uncertainty in off-diagonal elements of $(\mathbf{I}+\mathbf{L})^{-1}\mathbf{L}$ is not too large, it may be possible to reduce interaction in the off diagonal tracking behaviour ($\mathbf{T}_{Y/R} = \mathbf{TF}$) by designing off-diagonal elements in **F** in a straightforward manner as discussed by Boje and Nwokah, 1997.

3. Digital controller design for the UH-60 Black Hawk helicopter

3.1 Digital design in the w-domain

In this and many other control problems, design for digital implementation has often been based on somehow discretising a continuous time design. The difficulty with this approach is that sampling effects at high frequency are not properly taken into account. We prefer to design in the w-domain directly. As the s- and w- domains are nearly equivalent at low frequency, there is almost no approximation error in simply using the s-domain specifications. This enables an exact design to be carried out provided the specifications are in the w-domain. The w-domain correctly captures high frequency sampling effects. As the client has fixed the sampling rate, Ts=15ms, we get directly to the w-domain via the z-transform:

$$\begin{aligned}\mathbf{P}(w) &= \mathbf{P}_z(z)\Big|_{z=\frac{1+wT/2}{1-wT/2}} = \left(\mathbf{C}(\mathbf{I}z-\mathbf{A}_D)\mathbf{B}_D\right)\Big|_{z=\frac{1+wT/2}{1-wT/2}} \\ &\approx \mathbf{P}_s(w)(1-wT/2)\end{aligned}. \qquad (18)$$

(See Eitelberg, 1988, Boje, 1990 and Eitelberg and Boje, 1991.) $\mathbf{A}_D = e^{\mathbf{A}T_S}$ and for zero order hold, $\mathbf{B}_D = \int_0^{T_S} e^{\mathbf{A}\tau}\, d\tau\, \mathbf{B}$. $\left[\begin{array}{c:c}\mathbf{A} & \mathbf{B} \\ \hdashline \mathbf{C} & \mathbf{0}\end{array}\right]$ is the state space system for the design model which includes the plant, actuators and sensor effects. Computational delay, $z^{-1} = \dfrac{1-wT/2}{1+wT/2}$ is added after discretisation. The rotor delay is included in the continuous time model, sampling effects are taken care of in the s → w domain transformation and computation delay is explicitly included. Continuous time sensor and actuator models are inclided in the plant dynamics before discretisation.

3.2 Crossfeed design

This section will examine the application of pseudo-Gauss elimination to a single cross-feed element of the helicopter. The cross-feed selected is the (4,3) element, from measured heave controller output to tail rotor collective input. This has been found to have the most significant effect on the interaction over the set of given models.

To illustrate the use of differentiated specifications, we will apply different constraints to two model subsets by specifying improved performance in the more probable cases ({More Probable} = {Most Probable} ∪ {Less Probable}) at the expense of lower but still acceptable performance in the least probable cases. A final feedback design also requires consideration of actuator and sensor dynamics. These do not affect the interaction index as they are diagonal matrices but may affect the cross-feed design if phase lag constraints (mentioned in Section 2) are included.

The (4,3) cross-feed design has the following structure.

$$\hat{\mathbf{K}}^{[h]}\hat{\mathbf{P}}^{[h]} = \hat{\mathbf{P}}^{[h+1]}$$

$$\begin{pmatrix} 1 & 0 & 0 & 0 \\ 0 & 1 & 0 & 0 \\ 0 & 0 & 1 & 0 \\ 0 & 0 & \hat{k}_{43} & 1 \end{pmatrix}\begin{pmatrix} \hat{p}_{11} & \hat{p}_{12} & \hat{p}_{13} & \hat{p}_{14} \\ \hat{p}_{21} & \hat{p}_{22} & \hat{p}_{23} & \hat{p}_{24} \\ \hat{p}_{31} & \hat{p}_{32} & \hat{p}_{33} & \hat{p}_{34} \\ \hat{p}_{41} & \hat{p}_{42} & \hat{p}_{43} & \hat{p}_{44} \end{pmatrix} = \begin{pmatrix} \hat{p}_{11} & \hat{p}_{12} & \hat{p}_{13} & \hat{p}_{14} \\ \hat{p}_{21} & \hat{p}_{22} & \hat{p}_{23} & \hat{p}_{24} \\ \hat{p}_{31} & \hat{p}_{32} & \hat{p}_{33} & \hat{p}_{34} \\ \hat{p}_{41}+\hat{k}_{43}\hat{p}_{31} & \hat{p}_{42}+\hat{k}_{43}\hat{p}_{32} & \hat{p}_{43}+\hat{k}_{43}\hat{p}_{33} & \hat{p}_{44}+\hat{k}_{43}\hat{p}_{34} \end{pmatrix}$$

Figure 3 illustrates the interaction index for the uncompensated plant, **P**. It is expected that either through the action of the pilot or diagonal controller (auto-pilot), acceptable performance can be obtained at frequencies below 1 rad/s. Decoupling by means of cross-feed is therefore required in the gain cross-over region, from 1 to 10 rad/s. Figure 4b shows the detail of the worst (maximum) cases for {More Probable}, and {Least Probable} subsets in this design region. Fig 4 shows the following hypothetical client specifications for interaction reduction:

a) {More Probable} : $\lambda_{spec} \le \min\{0.9, 0.8\times\lambda\}$

b) {Least Probable} : $\lambda_{spec} \le \min\{1.2, 0.8\times\lambda\}$, $\lambda_{spec} \le 1.4$ for $\omega \le 1.25$

Of course knowledge about what is achievable and the extent of trade-off permissible between the plant sub-sets is embedded in these specifications.

Using these values, the design in eq(14) becomes,

$$\left|\frac{1+\hat{k}_{43}\,\hat{p}_{33}/\hat{p}_{43}}{1+\hat{k}_{43}\,\hat{p}_{34}/\hat{p}_{44}}\right| \le \beta_{43} \text{ with } \beta_{43} = \left(\frac{\lambda_{spec}}{\lambda}\right)^{\frac{\lambda}{|m_{43}|(y_4x_3)}} . \tag{19}$$

The (4,3) cross-feed provides tail rotor collective to compensate for the change in yawing torque caused by change main rotor collective in the heave channel. This makes physical sense. Figure 5 shows the minimum product of interaction index sensitivity and **M** matrix element, $|m_{ij}|(y_i x_j)$, for the off-diagonal elements of $\hat{\mathbf{P}}$ to partially (as the minimum may not represent the worst case) illustrate why the (4,3) element is a good candidate from the point of view of the model data. Small values for other channels would result in large exponents in the calculation of the corresponding β_{ij} in eq(14) and this means that cross-feed in those channels will achieve very modest reduction of the interaction index.

The log-polar plane (modified Nichols Chart) in Figure 6 shows the design bounds on $\hat{k}_{43}$ at ω=2 for the entire plant set. If a single specification had been used for all the elements of the plant set, each subset would have generated a small feasible region, and the intersection of these feasible regions would have no intersection. As shown in Figure 6, the specifications have been made so tight that the intersection is very small. This intersection is shown as a shaded region in Figure 7 (which has a different scale). Figure 7 shows the intersection of bounds for the {More Probable} and {Least Probable} subset specifications independently at the design frequencies, ω = [1,1.5,2,3,4,6,8,10] rad/s. Figure 7 also shows the cross-feed design given by the stable but not minimum phase lag,

$$k_{43} = \frac{-0.125(-w/2+1)(w/1.75+1)}{(w/2.4)^2+0.8w/2.4+1} \tag{20}$$

This design satisfies the {More Probable} specifications but as the intersection of the specification bounds is empty at most frequencies, cannot satisfy simultaneously the {More Probable} and {Least Probable} specifications. Clearly, a final design would need to relax the specifications until the feasible region is large enough to enable a design. The trade off between the specifications for different plant subsets, the resulting size of the feasible region and resulting controller complexity requires engineering skill.

Figure 8 shows the reduction in worst case interaction index for the three cases. As expected from Figure 7, the specifications for the {Least Probable} set have not been met. There are also less serious violations of the specifications for the {More Probable} cases that can be attributed to the fact that the specification of β_{43} was based on differential sensitivity considerations.

The only remaining cross-feed element that results in a useful reduction in interaction is the (1,4) element where the design is,

$$k_{14} = \frac{2.3(w/0.36+1)}{w/0.07+1} \tag{21}$$

Although direct comparison is unfair because of different design objectives, the interaction index of the compensated plant compares favourably with the design in Cheng, Tischler and Biezad (1995) (their crossfeed is more densely populated, using 7 out of a possible 12 elements). Their crossfeed design produces somewhat lower interaction over the {More Probable} plant set at the expense of slightly higher worst case interaction.

3.3. Feedback design

Because of the very large uncertainty, especially at low frequency, as a first cut, we design controllers to give high bandwidth with adequate margins and moderate gains. Our experience with QFT design is that the approach of over-bounding design equations with the specifications, thereby neglecting phase information and the effects of ordering amongst plant cases, often leads to designs requiring unrealistic or unachievable bandwidth to meet the user's requirements. A first cut at the design gives good information (i.e. insight) about likely phase and gain of channels for which a refined design is still to be performed. The controllers here are a seat-of-the-pants design for illustration. For the pitch and roll axis, designs are P-D type, corresponding to attitude-command, attitude-hold type of performance and rate signals could be used to obtain the derivative action. The designs roll off at high frequency, and this may be implemented as sensor filtering or in the forward path. The heave and yaw axes are rate-command, rate-hold systems and the controllers are P-I type, where the integral term may obtained from measured height and yaw angle or from integration in the controllers. Much more sophisticated controllers may designed or tuned using the insight obtained from applying the QFT philosophy of Horowitz (1979, 1982, 1991, 1992) rigorously. As the interaction index is less than unity from 1 to 15 rad/s for the {More Probable} plant cases (and in a more restricted range for the entire plant set), single loop designs are justifiable around these mid frequencies. The initial designs were performed based only on robustness margins for the sensitivity and complementary sensitivity only. Level sets on the nominal plant were obtained over the entire plant set for $|1/(1+\ell_i)| \le \gamma_S$, $|\ell_i/(1+\ell_i)| \le \gamma_C$. 0 and 6 dB sets were used for convenience but more detailed specifications such as minimum and maximum tracking specifications, input constraints, etc. could be added. A good reason for not taking this initial design too seriously is provided by Tischler, *et al* (1990): The roll rate gain was reduced from 6.0 (initial simulation) to 2.4 (final design) to 1.3 (flight-tested) – a reduction of 13dB!

None of the other authors who have worked on this problem seem to have explained how to start the feedback design! As a result of varying number of open loop, right hand plane poles in the system, it is not obvious how to choose a controller that stabilises all the plants simultaneously. The culprit is a crowd of body modes near the origin. The design produced here is closed-loop stable for the whole plant set. As these modes are the result of linearisation etc, it probably does not matter much whether they are in the left or right hand plane as they will cause slow drift away from the trim position in the real system. A reasonable approach is to make the "stability" assessment boundary include a semi-circle of radius say 1/60 (i.e. 1 minute time constant) into the right hand plane at the origin. Any slow instabilities can easily be controlled by the pilot or may vanish (be stable) in the actual non-linear, uncertain, time varying system.

The first-cut controllers below are illustrated in Figure 9.

roll angle	$g_1 = \frac{3(w/5+1)}{(w/30)^2+2\times0.4\times(w/30)+1}$	heave	$g_3 = \frac{-0.7(w/2+1)}{w(w/20+1)}$
pitch angle	$g_2 = \frac{10(w/2+1)}{(w/30)^2+2\times0.5\times(w/30)+1}$	yaw rate	$g_4 = \frac{0.75(w/0.1+1)}{w(w/30+1)}$

3.4 Pre-filter elements

In the design presented in Ukpai, Boje and Nwokah (1999?), off-diagonal pre-filter elements are used to reduce coupling in the tracking behaviour. For this paper, we will use only diagonal pre-filter elements to roughly satisfy the tracking specifications used by Cheng, Tischler and Biezad (1995). The following basic pre-filters achieve the results illustrated in Figures 10 and 11:

roll angle command	$f_{11} = \frac{w/1.5+1}{(w/2.5)^2+2\times0.75\times(w/2.5)+1}$	heave command	$f_{33} = \frac{(w/1.3)^2+2\times0.6\times(w/1.3)+1}{(w/0.9)^2+2\times0.7\times(w/0.9)+1}$
pitch angle command	$f_{22} = \frac{1}{w/1.5+1}$	yaw rate command	$f_{22} = \frac{1}{w/50+1}$

3.5 Simulated response

Of course, the real test of system design is through piloted simulation, prototyping and implementation. Our controller designs have been tested more modestly by simulation for conformance with some flying quality specifications of ADS33D in Ukpai, Boje and Nwokah (1999?). Due to space constraints, only one test is illustrated in Figure 12. This is a pulse input in the roll angle channel. ADS33D, Specification 3.2.6 expects: "For a pulse actuator input the pitch and roll attitudes must return to within ±10% of the peak excursion in less than 10 seconds".

4. Conclusion

This paper has shown the use of the Perron root interaction index as a measure of the level of coupling in the linear model of the UH 60 helicopter. A dynamic crossfeed has been designed to reduce the interaction. This eases the feedback loop design by reducing overdesign and justifying single loop at a time methods. If the crossfeed is used when the feedback connection is open, the pilot workload should still be reduced. In the absence of client specifications, a full QFT design following standard practice has not been attempted. The design would be somewhat complicated (and tedious) because of the high level of coupling at low frequency, non-minimum phase lag constraints, fair dimension and high (client) expectations. A first cut design was presented that is comparable to previously published results.

6. Acknowledgments

The financial assistance of the National Research Foundation, the University of Natal and NASA Ames Research Centre is acknowledged.

References

Boje E and Nwokah ODI; "Quantitative Feedback Design Using Forward Path Decoupling" *Symposium on Quantitative Feedback Theory and Other Frequency Domain Methods* University of Strathclyde, 21-22 August 1997, pp185-191.

Boje E and Nwokah ODI; "Quantitative Multivariable Feedback Design for a Turbofan Engine with Forward Path Decoupling" *Symposium on Quantitative Feedback Theory and Other Frequency Domain Methods* University of Strathclyde, 21-22 August 1997, pp192-208.

Boje E and Nwokah, O. D. I, "Non-diagonal controllers in MIMO Quantitative Feedback Design", submitted to *International Journal of Control.*

Boje E; "Further results on Eitelberg's sampling rate design based on (1-sT/2)", *International Journal of Control,* Vol. 51, No 5, 1990, pp1155-1158.

Boje E; "Multivariable quantitative feedback designs with plant input specifications", *IEEE International Conference on Control and Applications,* ICCON 89, Jerusalem, Israel, 3-6 April 1989, Session WP-2.

Borgesani C, Chait, Y and Yaniv, O, "Matlab™ Quantitative Feedback Theory Toolbox", The Mathworks Inc., 1995.

Catapang, D, Tischler, M. B, and D. J. Biezad, "Robust Crossfeed Design for Hovering Rotorcraft", Proceedings of the Quantitative Feedback Theory Symposium, USAF Document WL-TR-92-3036, Wright-Patterson AFT, Ohio, Aug. 1992, pp 190-211.

Cheng RP, Tischler MB and Biezad DJ, "Rotorcraft Flight Control design using Quantitative Feedback Theory and Dynamic Crossfeeds", *Quantitative and Parametric Feedback Theory Symposium*, Purdue University, Indiana, pp23-39, August 1995

Eitelberg E and Boje E; "Feedback controller design for plants with modes and disturbances above the sampling frequency", *International Journal of System Science,* Vol. 22, No 9, pp1553-1562, 1991.

Eitelberg E, "Sampling rate design based on (1-sT/2)", *International Journal of Control*, 1988, vol. 48, No. 4, 1423 – 1432.

Hoh, R et al, "Military Standard – Rotorcraft Flight and Ground Handling Qualities, General Requirements for US Army Aviation and Troop Command", MIL-STD-XXXX, Nov. 24th 1993 (draft).

Hoh, R. H., and Mitchel D. G, "Handling Qualities Specification – a Fundamental requirement for the Flight Control System", *Advances in Aircraft Flight Control*, Tischer M. B. (ed.), Taylor and Francis, 1996.

Horowitz I, "Improved technique for uncertain MIMO systems", International *Journal of Control*, vol. 36, pp977-988, 1982.

Horowitz I, "QFT for uncertain MIMO systems", *International Journal of Control*, vol. 30, pp81-106, 1979.

Horowitz I, "Survey of Quantitative Feedback Theory (QFT)", *International Journal of Control*, Vol. 53, No. 2, pp. 255-291, 1991.

Horowitz, I, "Quantitative Feedback Theory (QFT), Vol. 1", *QFT Publications*, Boulder Colorado, 80303, 1992

Lancaster P and Tismenetsky M, *The Theory of Matrices* (Second Edition), Academic Press, 1985.

Nwokah O D I, Nordgren R E and Grewal G S, "Inverse Nyquist Array: A quantitative theory", *IEE Proc. - Control theory Appl*, Vol. 142, No. 1, January 1995, pp23-30.

Padfield, G. D., "Objective Assessment and Criteria Development," *Helicopter Flight Dynamics: The Theory and Application of Flying Qualities and Simulation Modelling*, AIAA Education Series, Washington, 1995

Padfield, GD, *Helicopter Flight Dynamics: The Theory and Application of Flying Qualities and Simulation Modeling*, AIAA /Blackwell Science, Oxford, 1996

Rosenbrock HH, *State Space and Multivariable Theory*, Nelson, 1970.

Tischler MB, *Advances in Aircraft Flight Control*, Taylor and Francis, London, 1996.

Tischler MB, Fletcher JW, Morris PM and Tucker GE, "Flying Quanlity Analysis and Flight Evaluation of a Highly Augmented Combat Rotorcraft", *AIAA Journal of* Guidance, Vol. 14, no. 5, 1990.

Ukpai UI, Boje E and Nwokah ODI "Quantitative Crossfeed and Feedback Design of a Helicopter Near Hover Flight", submitted to *AIAA.*

Yaniv O and Chait Y, "A simplified multi-input multi-output formulation for the Quantitative Feedback Theory", *Trans. ASME, Journal of Dynamic Systems, Measurement and Control*, Vol. 114, pp. 179-185, June 1992.

Yaniv O and Chepovetsky, "Robust control of MIMO plants: Non-diagonal QFT design", *Quantitative and Parametric Feedback Theory Symposium*, Purdue University, August 1995, pp69-78

Yeung LF and Bryant GF, "New dominance concepts for multivariable control system design", *International Journal of Control*, Col.55, No. 4, 969-988, 1992.

Yue A and Postlethwaite I, "Improvement of Helicopter Handling Qualities using H_∞ Optimisation", *IEEE Proceedings* v137 pt D, N0 3, May 1990.

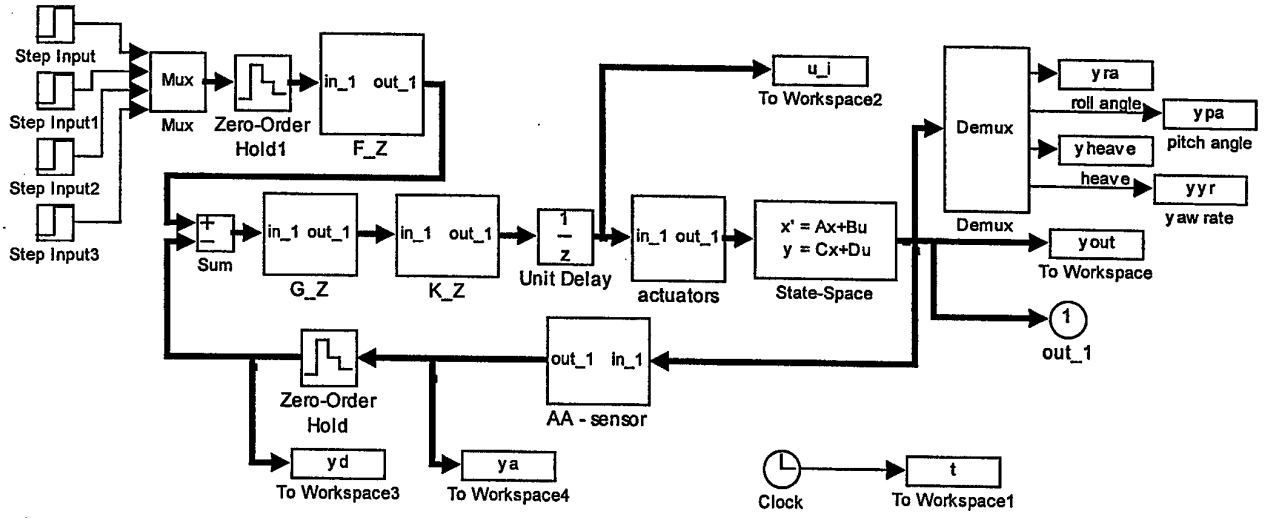

Figure 1 – Simulink model of helicopter and digital control system

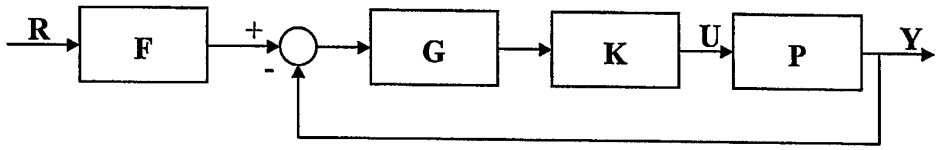

Figure 2 – Two-degree-of-freedom feedback structure

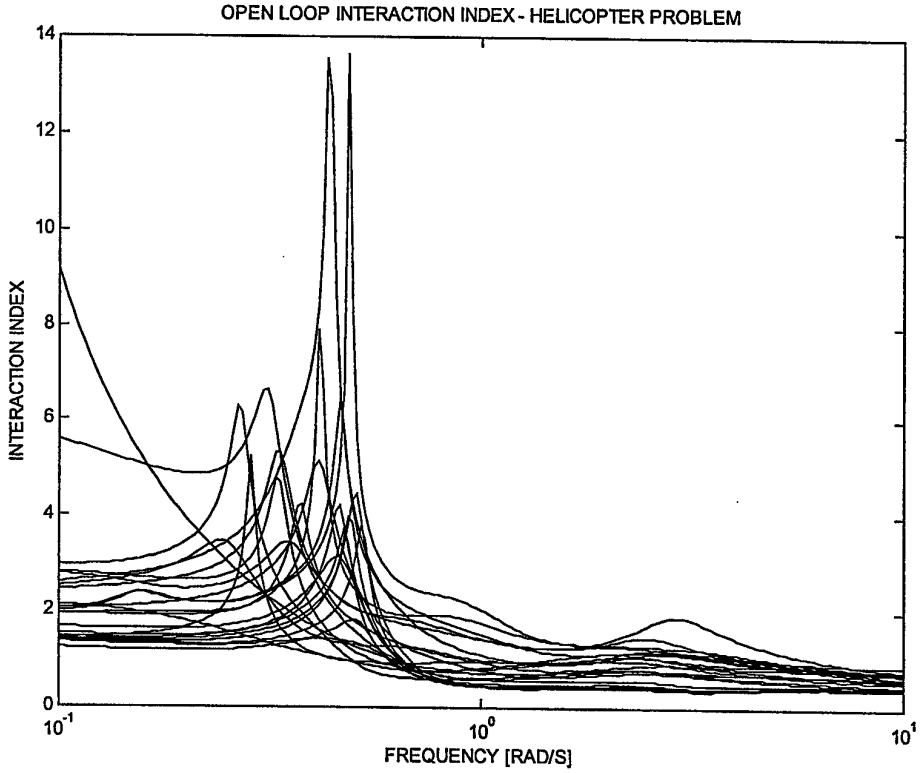

Figure 3 – Open loop interaction index for the helicopter problem

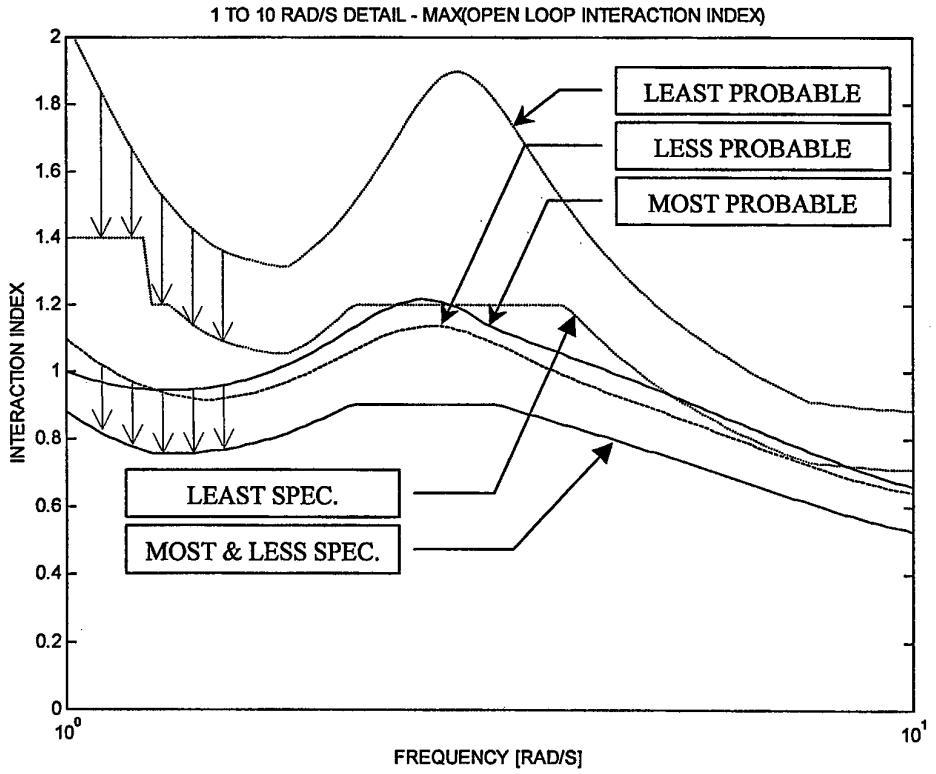

Figure 4 – Worst cases of open loop interaction index and specifications in [1, 10] rad/s. Solid – "Most Probable"; dashed – "Less Probable"; dotted – "Least Probable"

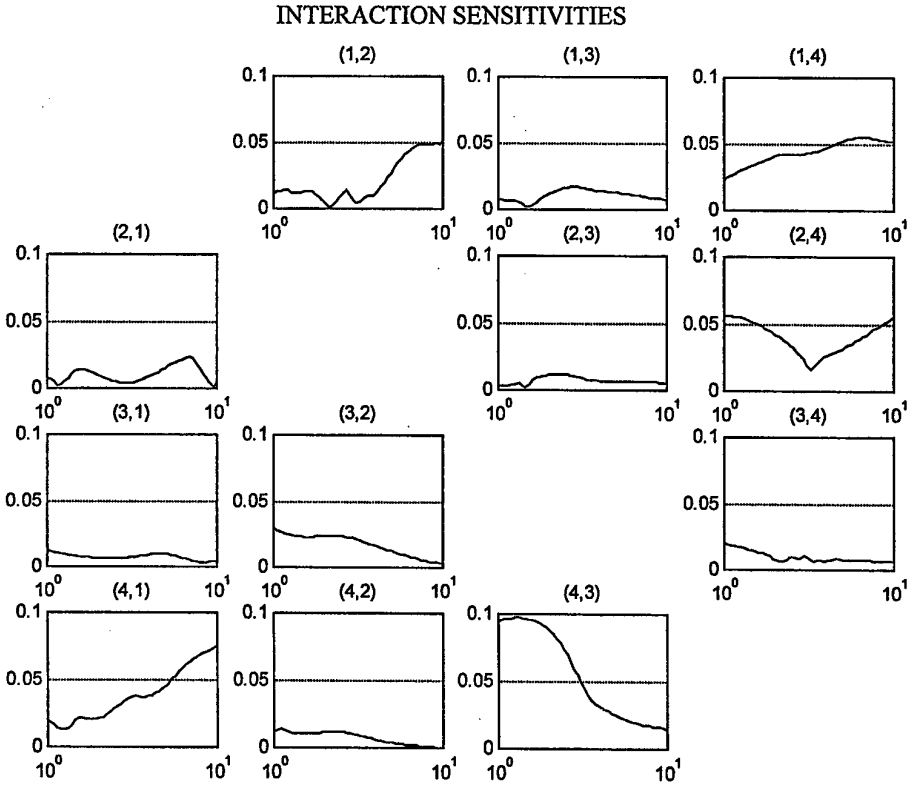

Figure 5 – Minimum product of interaction index sensitivity and M matrix element, $|m_{ij}|(y_i x_j)$

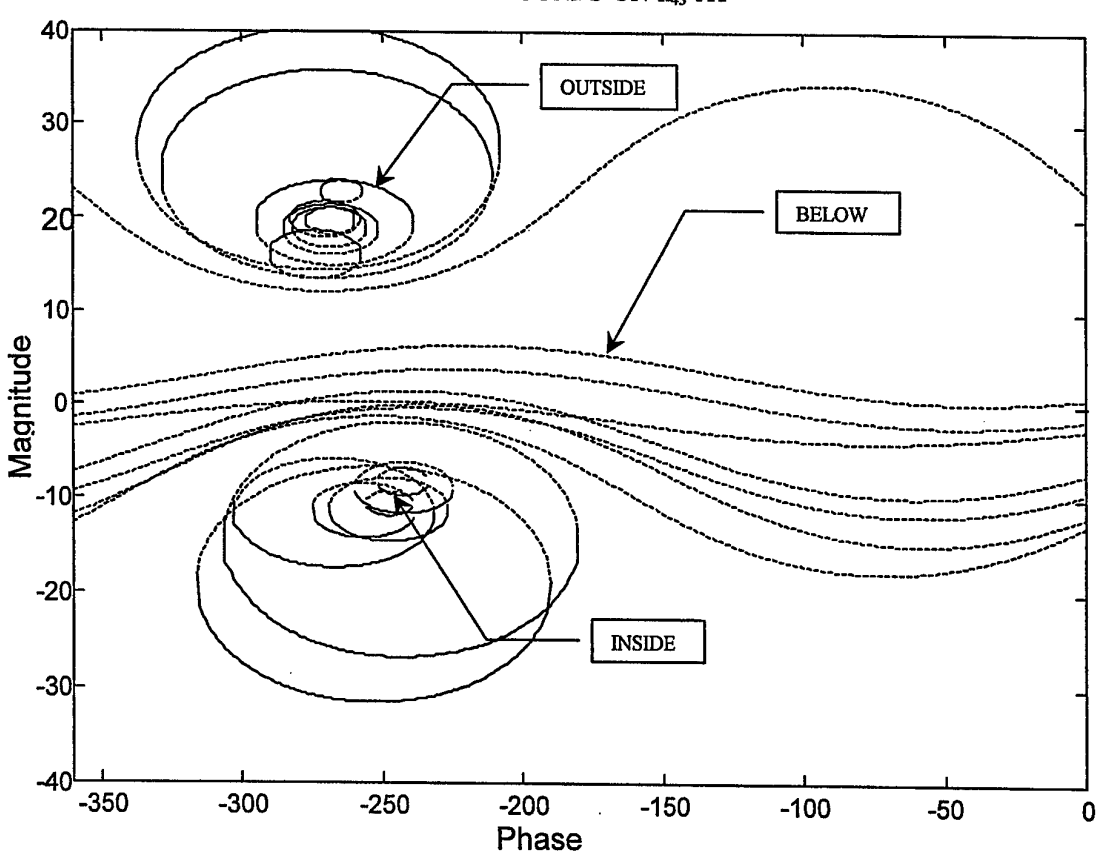

Figure 6 – Bounds on k_{43} at $\omega = 2$ for all plant cases. Final design must be in the intersection indicated by "INSIDE" to satisfy the specifications

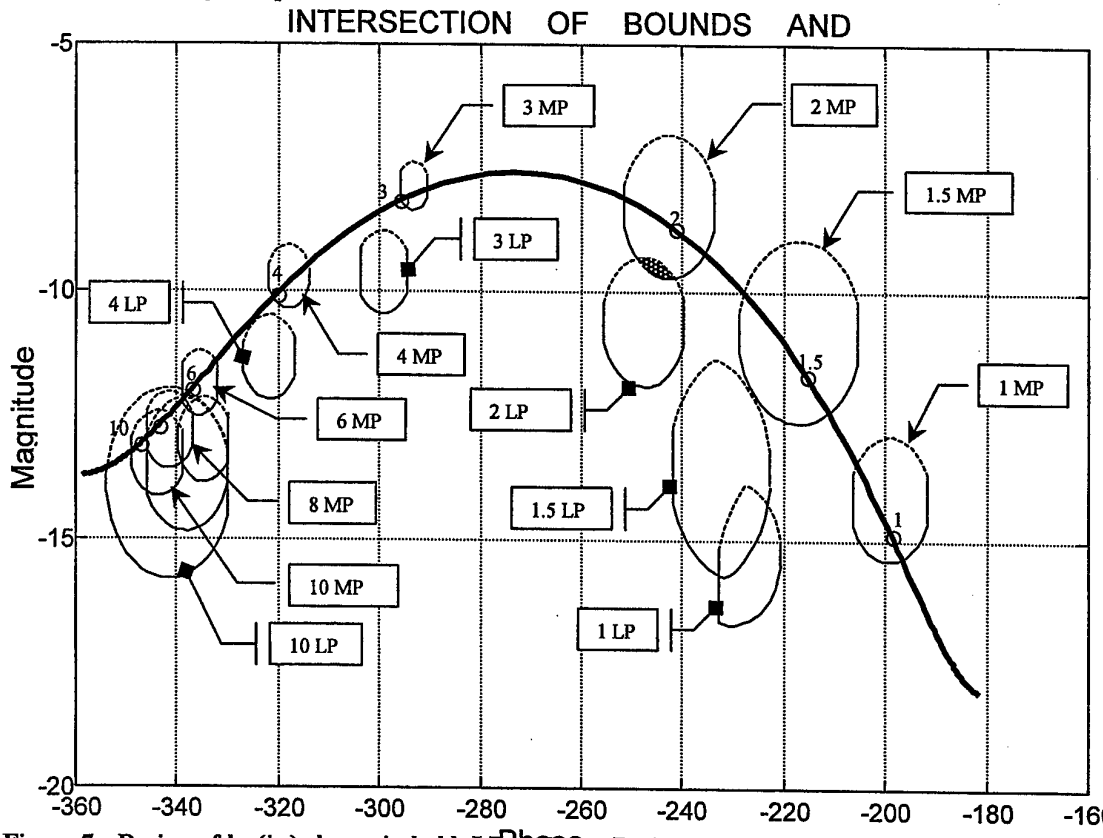

Figure 7 - Design of $k_{43}(j\omega)$ shown in bold. LP = "Least Probable" specifications, MP = "Most Probable" and "Less Probable" specifications.

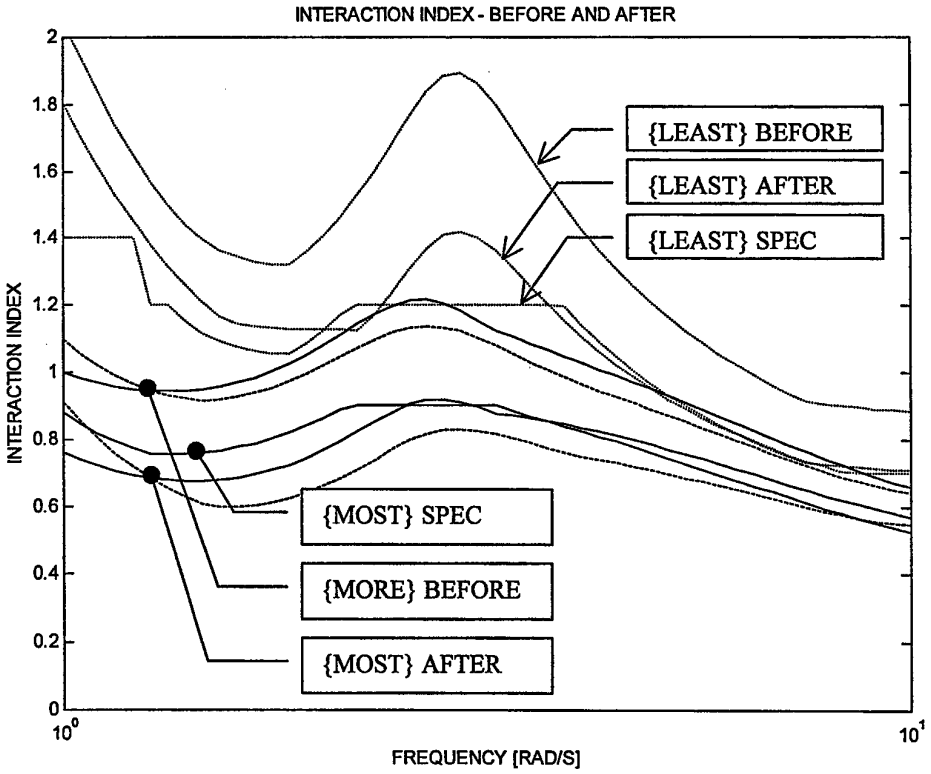

Figure 8 – Reduction in interaction index by k_{43} design

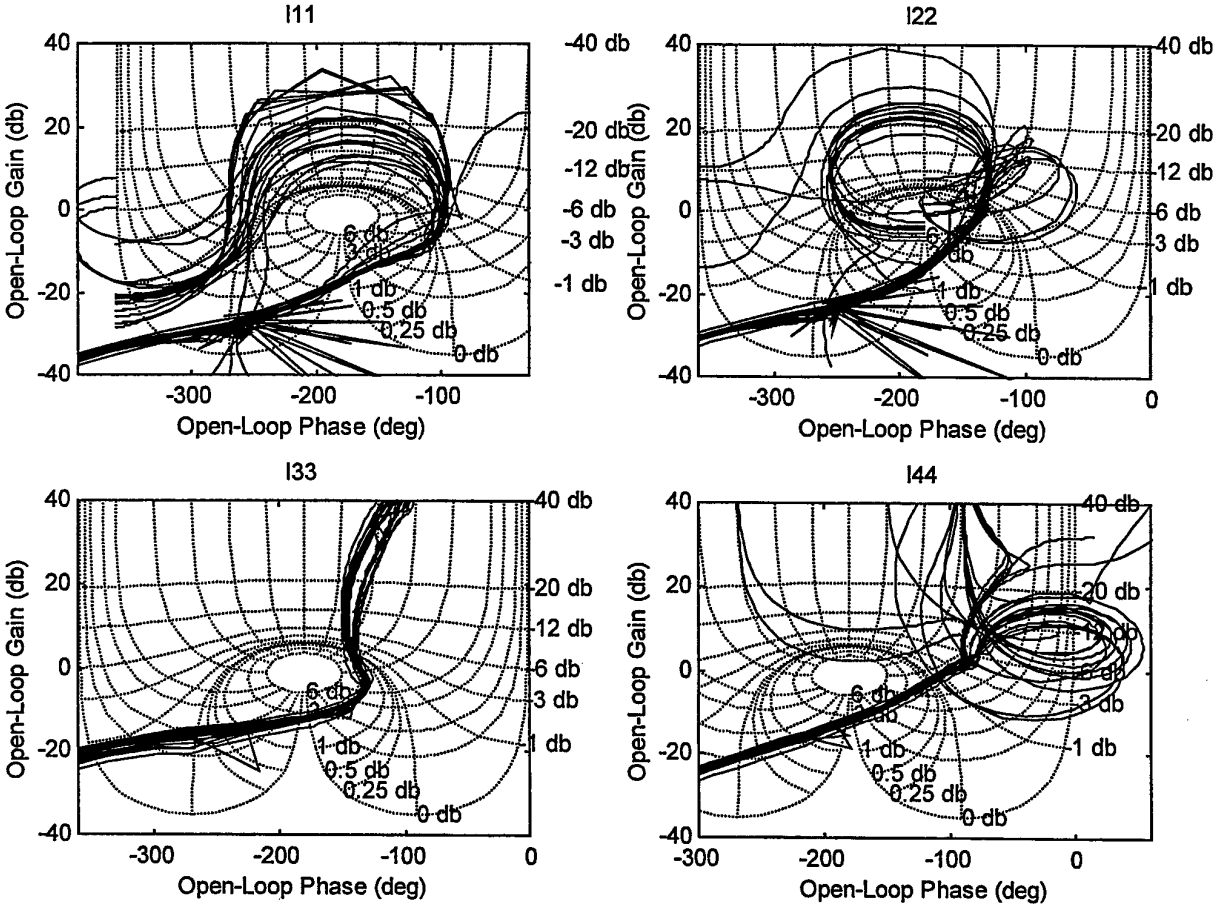

Figure 9 – Inverse Nichols charts of individual loop designs

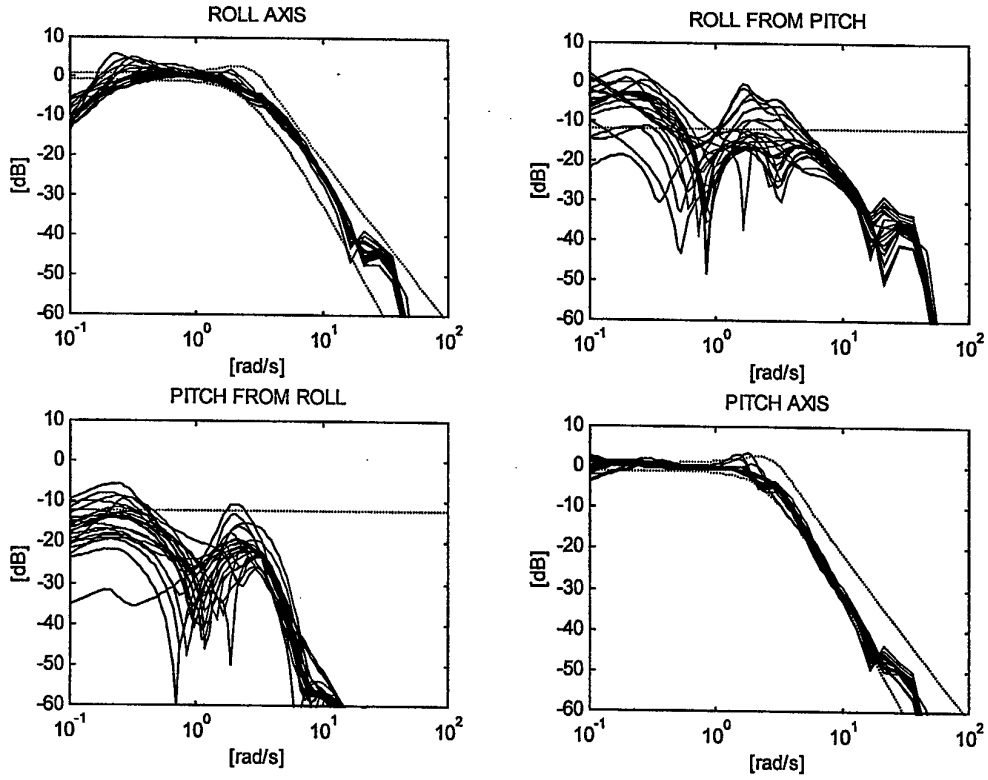

Figure 10 - Pitch and roll axis response and coupling

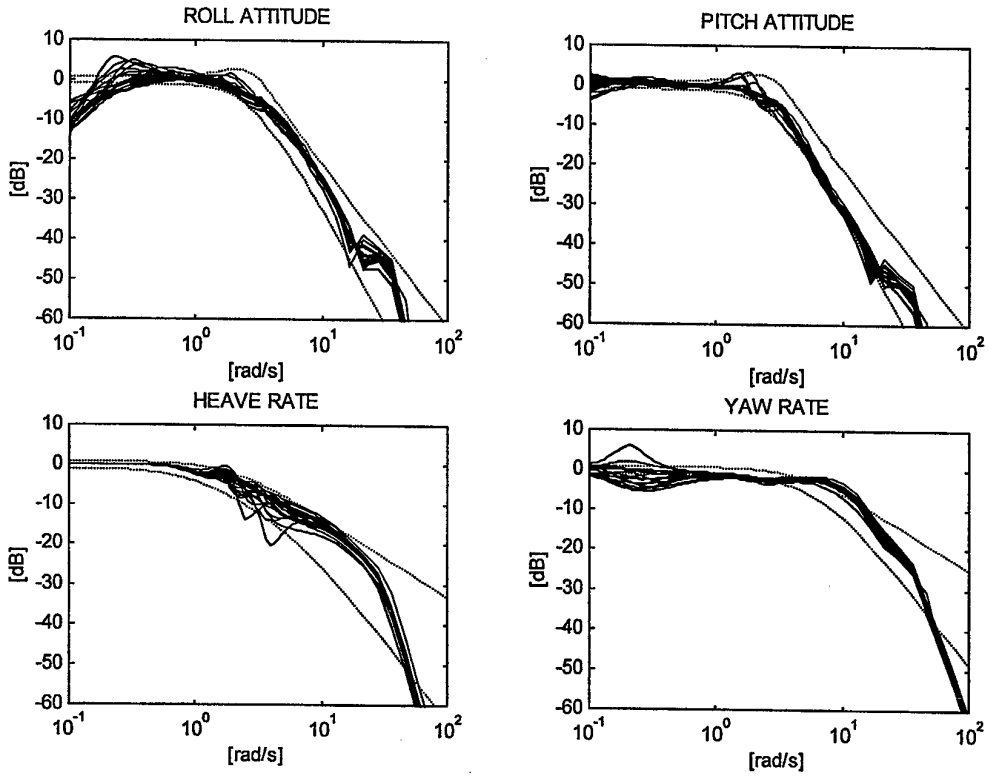

Figure 11 – On-axis responses.
(Dotted lines in Fig. 10 and 11 are specifications used in Cheng, Tischler and Biezad, 1995 for [1, 10] rad/s in the rotating axes and [0.2, 2] rad/s in heave. These specifications were not used explicitly in our design and are for information only.)

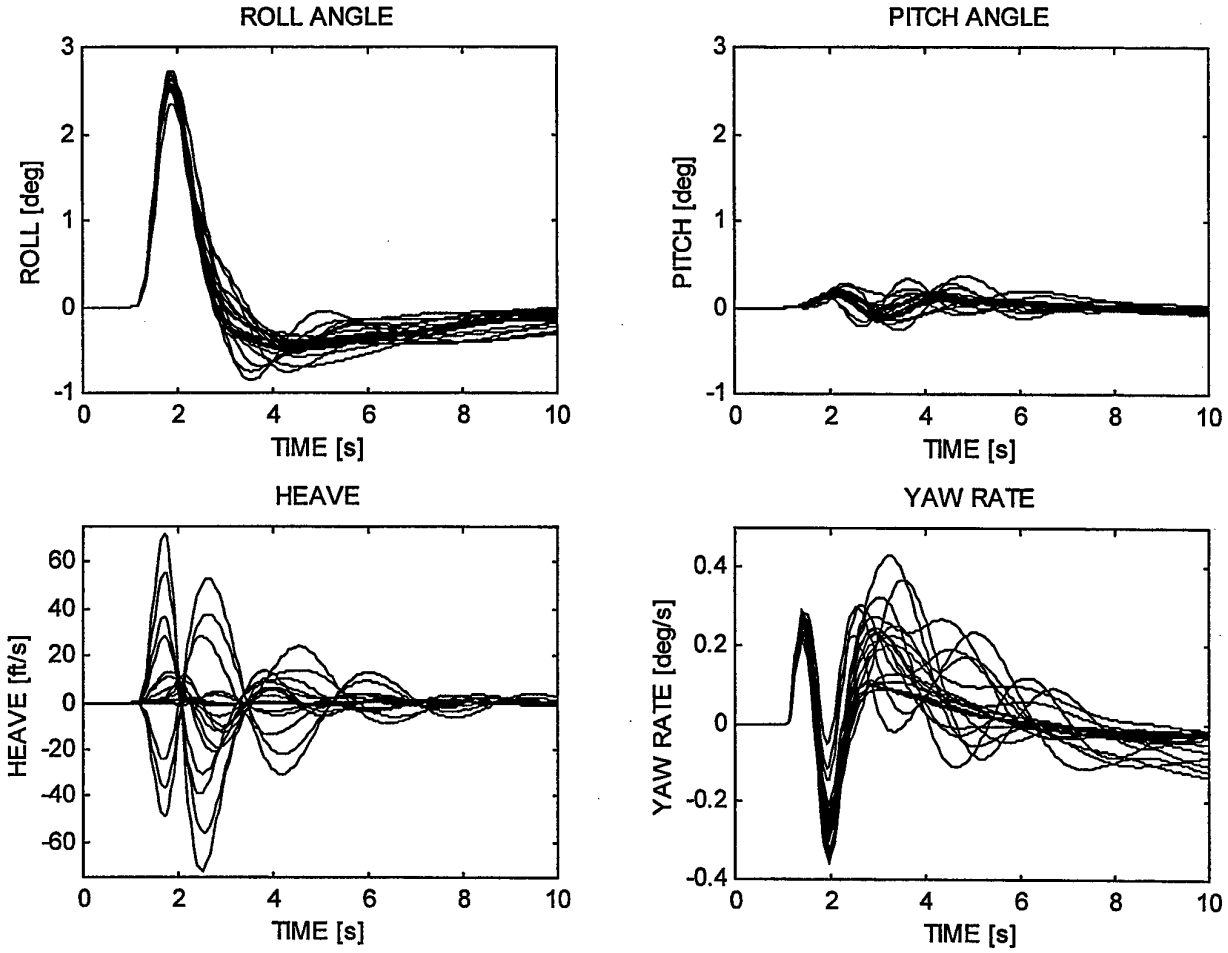

Figure 12 – Response to a 5°, 0.5s pulse applied to the roll angle reference at t=1s.

1999 International Symposium on
Quantitative Feedback Theory and Robust Frequency Domain Methods

μ-Synthesis of Flight Control System

Karin Ståhl Gunnarsson
SAAB AB
Linköping, Sweden
E-mail: Karin.Stahl-Gunnarsson@saab.se

Abstract

A longitudinal axis controller is designed for the HIRM benchmark problem using μ-synthesis. Special effort is spent on how integrator action should be included in the controller in order to achieve desirable properties. Results from linear and non-linear simulations are also presented.

Introduction

GARTEUR is a European organisation that aims at stimulating and coordinating cooperation between research establishments and industries in the areas of aerodynamics, flight mechanics, helicopters, structures, materials, and propulsion technology. Joint research work is performed in Action Groups specifically established for different fields.

In 1995 an Action Group on Robust Flight Control was formed. About 20 organisations from different European countries participated. Sweden was represented by SAAB AB and the Automatic Control Group at Linköping University. One of the objectives of this Action Group was to demonstrate the application of robust control techniques to aircraft control law design problems. In order to achieve this, a robust flight control benchmark problem was defined for the aircraft model HIRM (High Incidence Research Model), [1]. In [1] different solutions to the design problem are presented. The design methods used included LQ methods, H_∞ Loop Shaping, μ-Synthesis, Nonlinear Dynamic Inversion and the Robust Inverse Dynamics Estimation approach. SAAB AB contributed with a controller designed using μ-synthesis.

μ-synthesis is a design method that have been successfully applied to flight control problems, [2], [3], [4] and [5]. In some applications, μ-synthesis have been used in combination with Nonlinear Dynamic Inversion, [4], [5]. There are several reasons for choosing μ-synthesis as design method. Traditionally, handling qualities are expressed in terms of low order transfer functions. Requirements formulated this way are suitable to handle within the μ framework. Furthermore, the design method is a multivariable method that can handle simultaneous requirements on different signals to be controlled by use of several control effectors. Finally the level of control activity and robustness issues can be taken into account.

In a flight control system for the longitudinal dynamics it is desirable to include integrator action, usually referred to as trim. In the contribution by SAAB AB in [1], integrator action was forced into the controller by using weighting functions with very high low frequency gain. However, since one of the drawbacks with controllers designed by μ-synthesis is the lack of structure of the controllers, the integrator is not visible to the designer. In order to be able to use antiwindup methods in case of control saturation, the integrator must be visible in the controller. It is possible to extract the integrators from a μ-controller, but in this paper a different

approach is used. The integrator is kept visible by feeding the output from the integrator to the μ-controller.

Problem formulation

The HIRM model represents a typical modern twin engined combat aircraft. However, it is basically stable. Considering only the longitudinal motion, the pilot commands are longitudinal stick deflection and throttle lever. Available control signals are taileron, canard and left and right throttle. However, the engines are supposed to operate symmetrically.
According to the specifications the longitudinal stick deflection shall control pitch rate while the throttle lever should control air speed.
The design envelope is Mach 0.15 to 0.5, 100 to 20000 ft altitude and -10 to 30 degrees angle of attack. Within this envelope, the Flight Control System (FCS) shall give good handling qualities and provide robustness. The handling qualities are expressed as requirements on the pitch rate and pitch attitude responses. It is desirable to design a fixed-gain FCS that avoids traditional gain-scheduling, which implies that the FCS must be robust to the variations in aircraft dynamics in the considered flight envelope.

When there are several control effectors, these must be used in an efficient way, such that they do not counteract each other. Here, the taileron is the most efficient control surface, while the canard gives a minimum-phase response. Thus it was decided to use both control surfaces for manoeuvring, while only use taileron for trim.

Controller structure

The chosen controller structure is shown in Figure 1. It consists of a linear part, designed by μ-synthesis, providing robustness and handling qualities. Longitudinal stick deflection and throttle position are transformed to pitch rate and air speed commands respectively. The μ-controller uses pitch rate, q, and air speed, V, as feed-back signals. The pitch rate command is filtered through a response model, and the error between desired response and pitch rate is integrated and fed to the linear controller. The controller employs a generalized aerodynamic control signal and throttle position. The aerodynamic control signal is then fed to the taileron, δ_{TS} and the high-pass filtered control signal is fed to the canard δ_{CS}. This construction gives the controller the desired property only to use taileron for trim. The throttle command is fed to the right and left throttle positions δ_{TH1} and δ_{TH2}. In order to take care of the variations in dynamic pressure, which affects the control surface effectiveness, the controller demands are scaled with dynamic pressure before being fed to the actuators.

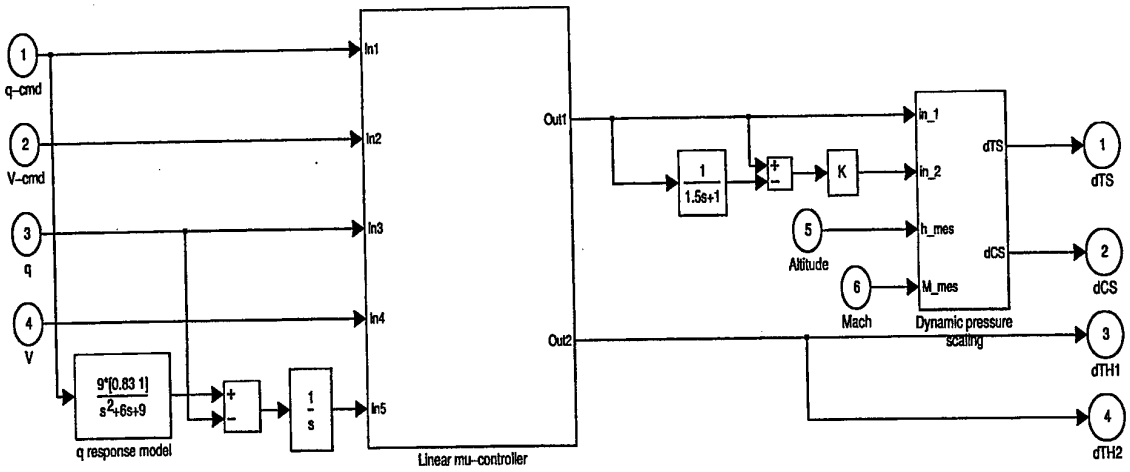

Figure 1: Controller structure

The interconnection structure

Within the μ framework, robustness and performance design criteria are taken care of by means of augmenting the open loop dynamics, here the aircraft model, with transfer functions that reflect the requirements. The augmented system is usually referred to as the interconnection structure. The interconnection structure for this problem is shown in Figure 2 and consists of the aircraft model augmented by uncertainty models, ideal response models and weighting functions. In the interconnection structure the disturbances signals, control signals, error signals and measurement signals are defined. Below the different components of the interconnection structure are described shortly.

The approach was to carry out the design for a flight case in the middle of the flight envelope. By making the controller robust and scaling the control signals with dynamic pressure, one fixed-gain controller could be used in the considered flight envelope. As design flight case, Mach 0.3 at 5000 ft altitude was chosen. The aircraft model in the interconnection structure is the linearized longitudinal dynamics at the design flight case. The model includes engine dynamics. The model states are air speed , angle of attack, pitch rate and two engine states. Since only symmetric throttle positions will be considered, the effect of the two engines are added.

In the design it was not found necessary to include actuator dynamics, while the time delay in the sensors was significant. It was thus decided to approximate the sensor dynamics with a first order Pade approximation corresponding to a time delay of 50 ms.

The different disturbance signals, i.e. axial and vertical wind gusts, pilot commands and measurement noise, are all weighted with transfer functions that reflect the magnitude and frequency content of the different signals. Note that measurement noise is also added to the integrated error signal.

A structured complex multiplicative uncertainty at the input of the aircraft model, results in small control surface deflections and also introduce stability margins.

Handling qualities are achieved by introducing tracking-error signals. The tracking error is the difference between the ideal response model and the actual signal. The pitch rate ideal response model is given by using [6] according which the handling qualities at the design flight case should be equivalent with a second order system with a natural frequency of 3 rad/s and damping ratio greater than 0.35. Here a damping ratio of 0.8 was chosen. Furthermore, in

order to get desired properties, a zero at -1.2 is introduced. The air speed ideal model was chosen as a first order transfer function with time constant 1s, which corresponds to the requirements in [1]. Then a pitch rate error signal and an air speed error signal are created. The errors are weighted and the inverse of the weight indicates how big steady-state tracking errors due to command input or gust disturbance are allowed.

In order to achieve a controller that fulfils the requirements, some of the transfer functions mentioned above are used as design parameters. By adjusting the noise weighting transfer functions of the different feedback signals, the amount of pitch rate, air speed and integrated pitch rate error that are used by the controller can be affected. This was used in order to achieve the desired property that the integrator should work that fast, that the effect of the integrator is included in the dynamic response. Furthermore the transfer functions weighting the pitch rate error and air speed error are adjusted until a reasonable level of tracking is achieved.

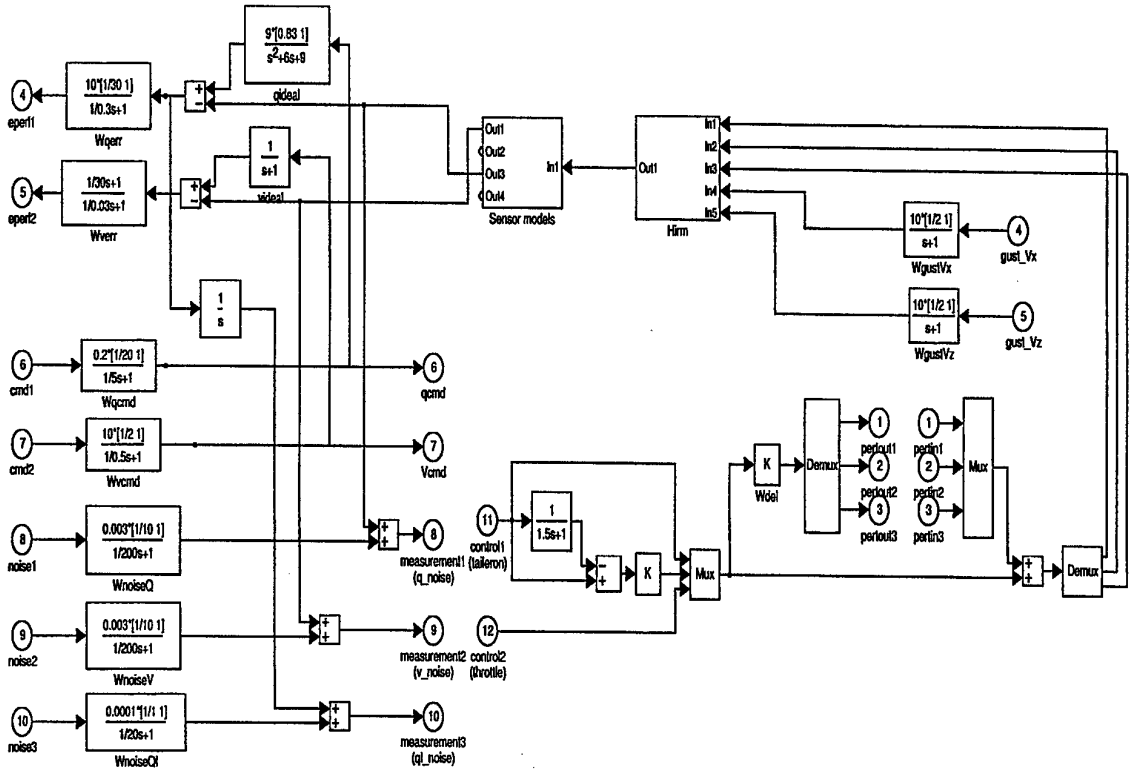

Figure 2: Interconnection structure

Controller design

From the interconnection structure presented in the previous section, the open-loop design model was derived. The design model had 22 states, 10 outputs and 12 inputs.

A controller, K, was designed using the D-K-iteration procedure. The first step in D-K iteration involves H_∞ controller design in which a controller that minimizes the infinity norm of the closed-loop system is found. The second step in D-K-iteration consists of μ-analysis of the closed-loop system. Transfer functions are fitted to the frequency dependent scaling variables that are produced in the analysis. The original open-loop design model is augmented with

these transfer functions, and used in the next iteration. After three iterations the design had converged. The final γ, i.e. the infinity norm of the closed-loop system, achieved was 0.73, which implied that the performance requirements were achieved. Here constant transfer functions were fitted to the scaling variables, so the D-K iteration procedure did not increase the order of the design model and the resulting controller was also of order 22. The controller order was reduced using a model reduction technique. The final controller achieved after model reduction was of order 8. The controller was stable and all poles are well damped. For a more detailed description of μ-synthesis, D-K iteration and model reduction, see [7].

Analysis of the controller

The properties of the controller were analysed using linear and non-linear simulations.

In the linear simulations environment actuator dynamics were added. The simulations of a step command in pitch rate of 5 deg/s resulted in responses that were almost identical within the considered flight envelope. The simulations were carried out at Mach 0.3 and 1500 m (dashed), Mach 0.4 and 3000 m (dash-dotted) and at Mach 0.5 and 4500 m (dotted). The control surface deflections and rates were small, and the desired use of control surfaces was achieved. From the simulations it is found that the integrator is fast enough such that the effect of the integrator is well included in the dynamic response.

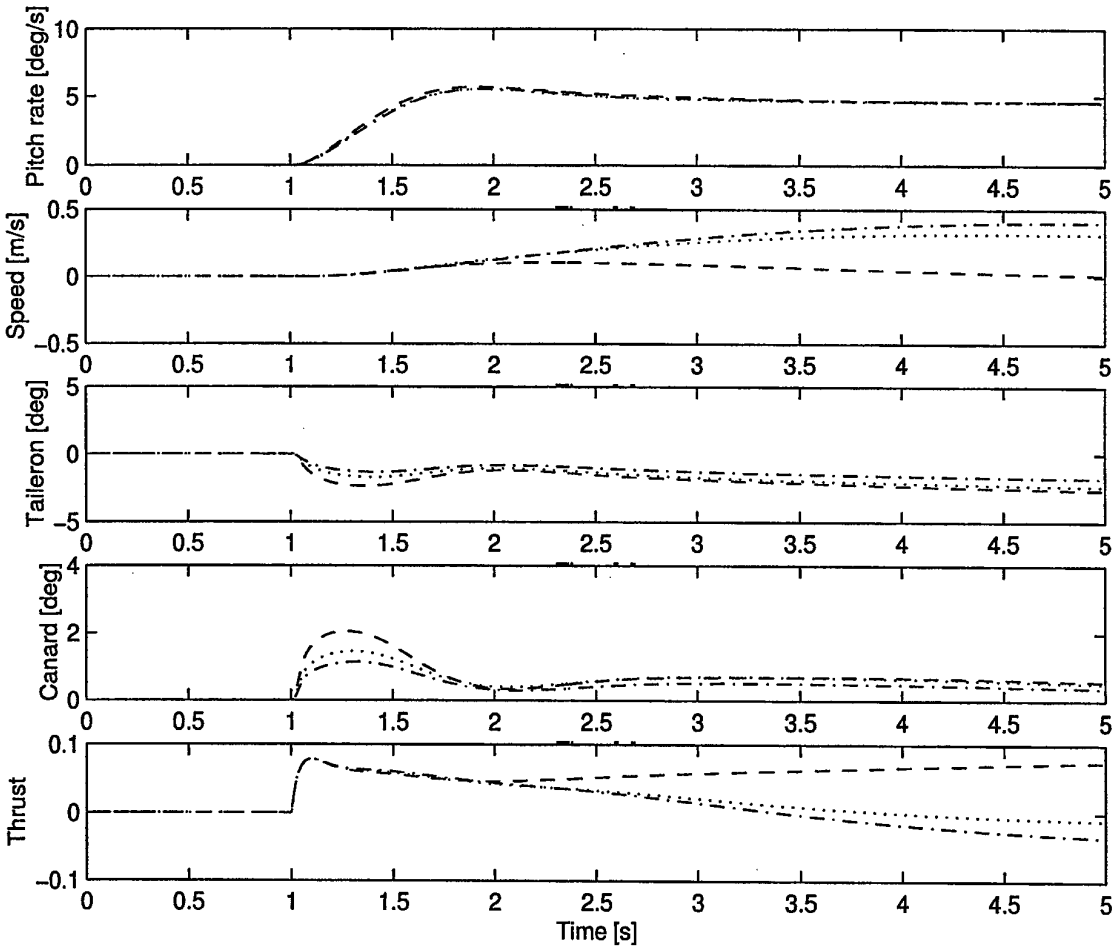

Figure 3: Responses to pitch rate command in linear simulations

Nonlinear simulations were carried out using a 6-degree-of-freedom Fortran model, integrated with Simulink. The model included sensor and actuator models according to [1]. A pitch rate command of 5 deg/s was applied at the flight cases that were studied by linear simulations, and the responses are shown in figure 4. The controller shows very similar pitch response for the different flight cases.

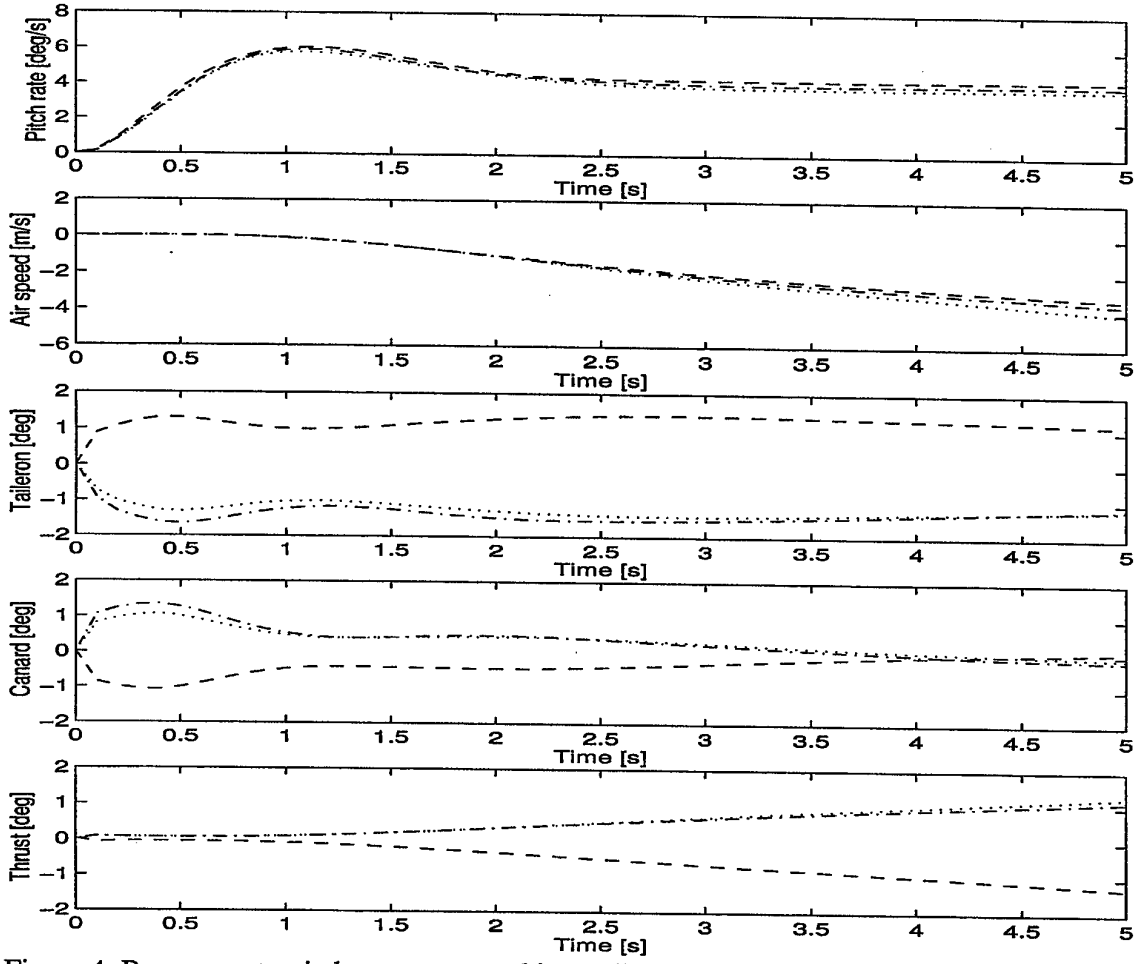

Figure 4: Responses to pitch rate command in nonlinear simulations.

Conclusions

A longitudinal controller was designed using μ-synthesis. μ-synthesis was found to be a suitable method to design controllers for flight applications due to the easy way handling qualities requirements and robustness considerations can be handled in the design. One drawback however, is that the controller order is sometimes high, and the "black-box" structure of the controllers. In the design presented here, an effort to make the integrator action visible was done. The chosen controller structure included integrator action in a way that antiwindup schemes could be applied. Furthermore the controller fulfilled the objectives on control surfaces usage.

The controller performed well within the design envelope considered. This was verified using linear and nonlinear simulations.

References

[1] Robust Flight Control, A Design Challenge, Lecture Notes in Control and Information Sciences 224, Magni, Bennani, Terlouw (Eds), 1997, Springer.

[2] Balas, Reiner, Garrard, *Design of a flight control system for a highly maneuverable aircraft using μ-synthesis*, Proc. AIAA Guidance, Navigation and Control Conf., AIAA Paper No. 93-3774, Monterey, CA, 9-11 August 1993.

[3] Balas, Packard, Renfrow, Mullaney, M'Closkey, *Control of the F-14 Aircraft Lateral-directional Axis During Powered Approach*, Journal of Guidance, Control and Dynamics, Vol. 21, No. 6, November-December 1998.

[4] Buffington, Adams, Banda, *Robust, nonlinear, high angle-of-attack control design for a supermaneuverable vehicle,* Proc. AIAA Guidance, Navigation and Control Conf., AIAA Paper No. 93-3774, Monterey, CA, 9-11 August 1993.

[5] Reiner, Balas, Garrard, *Flight Control Design Using Robust Dynamic Inversion and Time-scale Separation,* Automatica, Vol. 32, No. 11, pp. 1493-1504, 1996.

[6] MIL-F-8785C, Military Specification, Flying qualities of piloted airplanes, 1991.

[7] Balas, Doyle, Glover, Packard, Smith, *The μ-Analysis and Synthesis Toolbox*, MYSYN and MathWorks, Natick, MA, Nov. 1995.

1999 International Symposium on
Quantitative Feedback Theory and Robust Frequency Domain Methods

Quantitative Non-Diagonal MIMO Controller Design for Uncertain Systems

I.Egaña, M.García-Sanz

Depart. Automática y Computación, Universidad Pública de Navarra, Campus de Arrosadía. 31006 Pamplona, Spain. Tel: +34 948 169387. Fax: +34 948 169281. Email: mgsanz@upna.es

Abstract

A very crucial problem for real MIMO systems is the loop interaction reduction under the presence of uncertainty. In this paper, we analyse the role played by the non-diagonal elements, in order to study the use of fully populated controller matrices to achieve robust performance and loop decoupling. So that, the definition of a new coupling matrix comes in useful to quantify the amount of loop coupling. This yields a criterion that permits us to propose a sequential design methodology. Finally, a simple numerical example is included to show the practical use of this technique.

1. Introduction

Consider a $n \times n$ linear multivariable system, as shown in Fig. 1, composed by a plant $\boldsymbol{P}$, a non-diagonal controller $\boldsymbol{G}$, and a prefilter $\boldsymbol{F}$, where $P \in \boldsymbol{P}$ and $\boldsymbol{P}$ is a set of possible plants due to uncertainty.

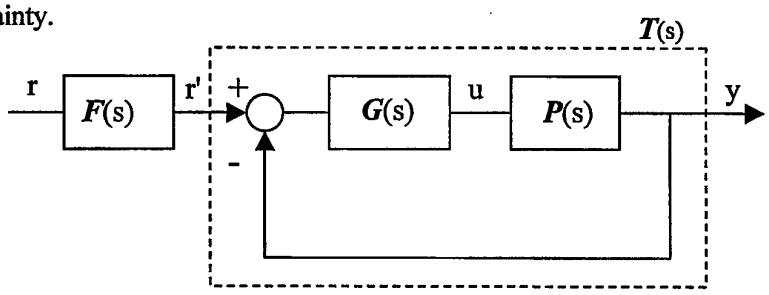

Fig. 1 Control structure of a 2 DOF system

The transfer function matrix of the system can be written as,

$$y = [I + \boldsymbol{P} \cdot \boldsymbol{G}]^{-1} \cdot \boldsymbol{P} \cdot \boldsymbol{G} \cdot \boldsymbol{F} \cdot r = \boldsymbol{T} \cdot \boldsymbol{F} \cdot r = T_{Y/R} \cdot r \qquad (1)$$

where all the matrices are $n \times n$.

Let us consider the quantitative feedback design problem [1] of specifying a fully populated controller $\boldsymbol{G}$, and a prefilter $\boldsymbol{F}$, to achieve certain tracking specifications $\boldsymbol{A}(\omega) = \{a_{ij}(\omega)\}$ and $\boldsymbol{B}(\omega) = \{b_{ij}(\omega)\}$ for the function $T_{Y/R} = \{t_{ij}^{Y/R}\}$,

$$a_{ij}(\omega) \le \left| t_{ij}^{Y/R}(j\omega) \right| \le b_{ij}(\omega) \qquad (2)$$

For a system defined as above, the different roles of $\boldsymbol{F}$ and $\boldsymbol{G}$ must be emphasized. As well as the feedback controller $\boldsymbol{G}$ guarantees the robust performance –as regards stability, uncertain and coupling influence reduction, and disturbance rejection-, the prefilter $\boldsymbol{F}$ shapes the closed-loop system performance to fit the tracking specifications.

In the last decades, many papers that deal with the design of controllers for uncertain systems have appeared: the Inverse Nyquist Array [2], the Direct Nyquist Array [3], the Perron-Frobenius root

method [4], the Individiual Channel Analysis and Design -ICAD- [5], etc. In the QFT frame, Horowitz [1] started to use Schauder's fixed point theory to analyse and design MIMO controllers.

Anagously to the gamma function of ICAD, this work studies the coupling. However, here it is included the effect of the controller non-diagonal elements on the transfer function matrix of the system in order to state a design criterion to reduce the coupling influence. This leads to the development of a design methodology for non-diagonal controllers.

The arrangement of this paper is the following. In Section 2 the theoretical principles used by Horowitz [1] are explained, making up the starting point of the present paper. In Section 3, some hypotheses are suggested to simplify the study of the coupling taking into account the action of the controller non-diagonal elements, and the effect of plant uncertainty. A new matrix that represents the coupling, can be used to find a design criterion for these non-diagonal elements of the controller. This yields an optimum non-diagonal controller element for decoupling. In Section 4, a non-diagonal controller design technique based on the above is described, and a simple example is included to show the proposed methodology. Section 5 concludes the paper highlighting the most relevant ideas.

2. Theoretical principles

As we can see in Eq. (1), there are n^2 transfer functions of $\boldsymbol{G}$ and another n^2 transfer functions of $\boldsymbol{F}$ to accomplish the n^2 tracking specifications defined by $\boldsymbol{A}(\omega)$ and $\boldsymbol{B}(\omega)$ in Eq. (2). However, each element $t_{ij}^{Y/R}$ of $\boldsymbol{T}_{Y/R}$ depends on every controller element g_{ij}. These expressions of $t_{ij}^{Y/R}$ are very complex to analyse. So, taking them into account we cannot study the effect of the non-diagonal elements g_{ij} ($i \neq j$). Therefore, it is necessary to transform somehow the $n \times n$ multivariable system to get a simpler analysis.

The study realised in this paper about the controller non-diagonal elements is based on the reduction of the MIMO system of Eq. (1) into n^2 equivalent SISO systems. This technique was previously justified by Horowitz -[1] and [6]-.

Such a reduction is solved anagously to Horowitz *et al.* -[6] and [7]-, and it takes the expression of $\boldsymbol{T}$ deduced from Eq. (1) as the starting point to write,

$$\boldsymbol{T}\cdot r' = \left(\boldsymbol{I} + \left(\hat{\boldsymbol{P}}_d\right)^{-1}\cdot \boldsymbol{G}_d\right)^{-1}\cdot\left(\hat{\boldsymbol{P}}_d\right)^{-1}\cdot\left[\boldsymbol{G}_d\cdot r' + \left(\boldsymbol{G}_b\cdot r' - \left(\hat{\boldsymbol{P}}_b + \boldsymbol{G}_b\right)\cdot\boldsymbol{T}\cdot r'\right)\right] \tag{3}$$

where $\hat{\boldsymbol{P}}$ is the plant inverse, and $\hat{\boldsymbol{P}}_d$, $\hat{\boldsymbol{P}}_b$, $\boldsymbol{G}_d$ and $\boldsymbol{G}_b$ the diagonal part -subscript d- and non-diagonal part -subscript b- of $\hat{\boldsymbol{P}}$ and $\boldsymbol{G}$ respectively.

In order to design the controller $\boldsymbol{G}$, a set of acceptable complementary sensitivity functions $= \{\tau_{ij}\}$ is defined from the tracking specifications $\boldsymbol{A}(\omega)$ and $\boldsymbol{B}(\omega)$, as in [8].

Horowitz -[1] and [6]- proposed the Schauder's fixed point theory to develop a synthesis technique suitable for MIMO systems. To do so, he defined a mapping $\boldsymbol{T}=\boldsymbol{Y}(\boldsymbol{T}_i)$ from Eq. (3), based upon a unit impulse input, so that,

$$\boldsymbol{Y}(\boldsymbol{T}_i) = \left(\boldsymbol{I} + \left(\hat{\boldsymbol{P}}_d\right)^{-1}\cdot \boldsymbol{G}_d\right)^{-1}\cdot\left(\hat{\boldsymbol{P}}_d\right)^{-1}\cdot\left[\boldsymbol{G}_d + \left(\boldsymbol{G}_b - \left(\hat{\boldsymbol{P}}_b + \boldsymbol{G}_b\right)\cdot\boldsymbol{T}_i\right)\right] \tag{4}$$

where $\boldsymbol{T}_i \in \boldsymbol{T}$.

Now, looking at Eq. (4), we can see two different terms:

i. On the one hand,

$$\boldsymbol{Y}_{\mathrm{d}}(\boldsymbol{T}_{\mathrm{i}})=\left(\boldsymbol{I}+\left(\hat{\boldsymbol{P}}_{\mathrm{d}}\right)^{-1}\cdot\boldsymbol{G}_{\mathrm{d}}\right)^{-1}\cdot\left(\hat{\boldsymbol{P}}_{\mathrm{d}}\right)^{-1}\cdot\boldsymbol{G}_{\mathrm{d}} \tag{5}$$

is a completely diagonal structure. It is equivalent to a reference tracking MIMO system of a plant equal to $\left(\hat{\boldsymbol{P}}_{\mathrm{d}}\right)^{-1}$ controlled by a diagonal $\boldsymbol{G}_{\mathrm{d}}$ with unity feedback. It is also equivalent to n SISO systems, as in Fig. 2.

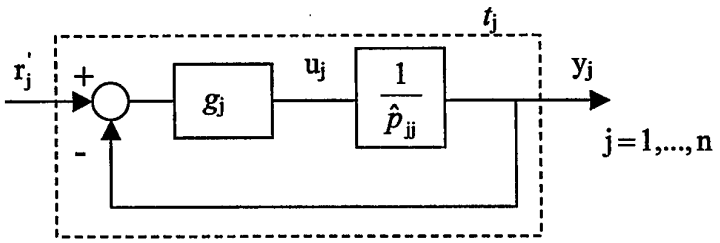

Fig. 2 j-th equivalent SISO system

ii. On the other hand,

$$\boldsymbol{Y}_{\mathrm{b}}(\boldsymbol{T}_{\mathrm{i}})=\left(\boldsymbol{I}+\left(\hat{\boldsymbol{P}}_{\mathrm{d}}\right)^{-1}\cdot\boldsymbol{G}_{\mathrm{d}}\right)^{-1}\cdot\left(\hat{\boldsymbol{P}}_{\mathrm{d}}\right)^{-1}\cdot\left[\boldsymbol{G}_{\mathrm{b}}-\left(\hat{\boldsymbol{P}}_{\mathrm{b}}+\boldsymbol{G}_{\mathrm{b}}\right)\cdot\boldsymbol{T}_{\mathrm{i}}\right]=\left(\boldsymbol{I}+\left(\hat{\boldsymbol{P}}_{\mathrm{d}}\right)^{-1}\cdot\boldsymbol{G}_{\mathrm{d}}\right)^{-1}\cdot\left(\hat{\boldsymbol{P}}_{\mathrm{d}}\right)^{-1}\cdot\boldsymbol{C} \tag{6}$$

is a non-diagonal structure. It is equivalent to the same previous diagonal MIMO system but working as a regulator -reference=0-, with disturbances at plant output, represented by the matrix $\boldsymbol{C}=\{c_{ij}\}$. It also can be considered as n^2 SISO regulator systems with disturbances c_{ij} at plant output, as in Fig. 3.

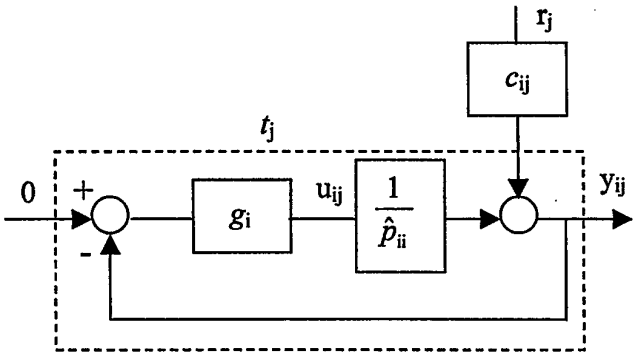

Fig. 3 Equivalent SISO system of i-th row and j-th column

In Eq. (6), the matrix $\boldsymbol{C}$ is the only element dependent on the non-diagonal parts, $\boldsymbol{G}_{\mathrm{b}}$ and $\hat{\boldsymbol{P}}_{\mathrm{b}}$. So, it is possible to say that such a matrix $\boldsymbol{C}$ represents the system coupling. It will be named as the *matrix of the diagonal equivalent system coupling*,

$$\boldsymbol{C}=\boldsymbol{G}_{\mathrm{b}}-\left(\hat{\boldsymbol{P}}_{\mathrm{b}}+\boldsymbol{G}_{\mathrm{b}}\right)\cdot\boldsymbol{T}_{\mathrm{i}} \tag{7}$$

3. Coupling analysis

The perfect understanding of the influence on the coupling of both the non-diagonal elements g_{ij} and the plant uncertainty, will ease the design of controllers that achieve robust performance specifications -including loop interaction reduction-.

Accordingly, we first analyse the coupling matrix $\boldsymbol{C}$ to determine the role played by the non-diagonal elements g_{ij}. Then we find a general optimum controller to reduce loop interaction. Secondly, we study the effect of the plant uncertainty on the loop interaction to choose the nominal

plant that specifies the above controller to improve the decoupling. Finally, based on this study , we propose a criterion to design non-diagonal controllers.

3.1. Coupling quantification

Eq. (7) is the starting point to study the coupling. Each one of the coupling matrix elements c_{ij} obeys,

$$c_{ij} = g_{ij} - \sum_{k=1}^{n} t_{kj} \cdot (\hat{p}_{ik} + g_{ik}) \cdot (1 - \delta_{ik}), \ \forall i \neq j, \tag{8}$$

where δ_{ki} is the delta of Kronecker, defined as, $\delta_{ki} \begin{cases} \delta_{ki} = 1 \Leftrightarrow k = i \\ \delta_{ki} = 0 \Leftrightarrow k \neq i \end{cases}$

To analyse the coupling elements c_{ij}, it is necessary to state two previous hypotheses to help to simplify Eq. (8):

Hypothesis H1 The plant $\boldsymbol{P}$ is not 'ill-conditioned' for any of the whole set of possible plants $\mathcal{P}$.

This hypothesis is included to guarantee the robustness of the analysis and the later design. It is very difficult to control an 'ill-conditioned' plant $\boldsymbol{P}$ [9], which shows a large condition number and a RGA matrix [10] that yields large elements.

Hypothesis H2 Diagonal elements t_{jj} are much larger than the non-diagonals $t_{ij}, \forall i \neq j$,

$$t_{jj} >> t_{ij}, i \neq j \tag{9}$$

This hypothesis H2 previously supposes the fulfilment of H1 in order to state the closed-loop system decoupling as an achievable design objetive.

These two hypotheses H1 and H2 allow us to use two simplifications in Eq. (8) to facilitate the disturbance quantification due to coupling elements c_{ij}:

Simplification S1 Starting from Hypothesis H2, the terms $(\hat{p}_{ik} + g_{ik})$ of Eq. (8) multiplied by $t_{ij}, \forall i \neq j$, can be neglected against those multiplied by t_{jj}. Thus, Eq. (8) can be rewritten as,

$$c_{ij} = g_{ij} - t_{jj} \cdot (\hat{p}_{ij} + g_{ij}) \tag{10}$$

Simplification S2 Based on Hypothesis H2, the elements t_{jj} can be computed from the diagonal equivalent system derived from Eq. (4), so that,

$$t_{jj} = \frac{g_{jj} \cdot \hat{p}_{jj}^{-1}}{1 + g_{jj} \cdot \hat{p}_{jj}^{-1}} \tag{11}$$

Due to Simplifications S1 and S2, the disturbance c_{ij} can be written as,

$$c_{ij} = g_{ij} - \frac{g_{jj} \cdot \hat{p}_{jj}^{-1}}{1 + g_{jj} \cdot \hat{p}_{jj}^{-1}} \cdot (\hat{p}_{ij} + g_{ij}), \quad i \neq j \tag{12}$$

Using this expression it is possible to compute the disturbance magnitude at plant output that influences on the equivalent systems defined in Eq. (6).

3.2. Optimum controller

We propose the use of the non-diagonal elements g_{ij} to minimise the coupling c_{ij}. To do so, we use Eq. (12), not placing closed-loop RHP poles. However, for this purpose, it is necessary to impose the following Hypothesis,

Hypothesis H3 The plant $\boldsymbol{P}$ and its inverse $\hat{\boldsymbol{P}}$ are stable and have no hidden unstable modes.

Therefore, making the expression of the coupling c_{ij} -Eq. (12)- equal to zero, for any two plants of the uncertainty $\hat{p}_{ij} = \hat{p}_{ij}^0$ $(i \neq j)$ and $\hat{p}_{jj} = \hat{p}_{jj}^0$, the following optimum controller is obtained,

$$g_{ij} = g_{jj} \cdot \frac{\hat{p}_{ij}^0}{\hat{p}_{jj}^0}, i \neq j \tag{13}$$

3.3. The effect of uncertainty

On the one hand, the effect of uncertainty of $\hat{p}_{jj}^{-1}$ and $\hat{p}_{ij}^{-1}$ must be reduced in Eq. (12) in order to achieve the robust performance specifications. Looking at this expression, it is easy to see that the design of the non-diagonal element g_{ij} cannot do so. The only way to minimise the influence of plant uncertainty on the coupling is by the diagonal element g_{jj}.

On the other hand, before to try to cancel the coupling c_{ij} out of Eq. (12), the uncertainty influence of $\hat{p}_{ij}$ and $\hat{p}_{jj}$ must be taken into account. So, it is necessary to determine which one of the possible couplings is to be cancelled out. For the moment it is supposed that $\hat{p}_{ij} = \hat{p}_{ij}^0$ $(i \neq j)$ and $\hat{p}_{jj} = \hat{p}_{jj}^0$, where $\hat{p}_{ij}^0$ and $\hat{p}_{jj}^0$ are two any elements within the possible uncertainty for $\hat{p}_{ij}$ and $\hat{p}_{jj}$.

Lemma L1 A non-diagonal controller element like $g_{ij} = g_{jj} \cdot \frac{\hat{p}_{ij}^0}{\hat{p}_{jj}^0}, i \neq j$, designed for the elements $\hat{p}_{ij} = \hat{p}_{ij}^0$ $(i \neq j)$ and $\hat{p}_{jj} = \hat{p}_{jj}^0$ that minimise $\left|\hat{p}_{ij} - \hat{p}_{ij}^0\right|$ and $\left|\hat{p}_{jj} - \hat{p}_{jj}^0\right|$, maximises the achievable decoupling for all the possible uncertain $\hat{p}_{ij}$ and $\hat{p}_{jj}$.

The demonstration is included in Appendix A1.

Based on the Lemma L1, we propose the following definition,

Definition D1 The *nominal plant* $\hat{p}_{ij}^N$ $(i = 1,...,n, j = 1,...n)$ of all the possible uncertain plants of $\hat{p}_{ij}$ minimises the non-parametric uncertainty radius $\Delta\hat{p}_{ij}$.

Therefore, the *nominal optimum controller* that gets the maximum achievable decoupling is,

$$g_{ij}^* = g_{jj} \cdot \frac{\hat{p}_{ij}^N}{\hat{p}_{jj}^N}, i \neq j \tag{14}$$

This is the proposed non-diagonal element for the controller. Note that if no uncertainty is present, (the uncertainty radii are $\Delta\hat{p}_{ij} = 0$ and $\Delta\hat{p}_{jj} = 0$), by definition, the coupling c_{ij} computed as in Eq. (12) with Eq. (14) is null.

The nominal optimum controller yields the minimum achievable coupling, substituting Eq. (14) into Eq. (12), and taking into account the uncertainty radii $\Delta\hat{p}_{ij}$ and $\Delta\hat{p}_{jj}$, we obtain,

$$\left|c_{ij}\right|_{min} = \left| \frac{g_{jj} \cdot \frac{\hat{p}_{ij}^{N}}{\hat{p}_{jj}^{N}}}{1 + g_{jj} \cdot \frac{1}{\hat{p}_{jj}^{N} \cdot \left(1 + \Delta\hat{p}_{jj}\right)}} \cdot \left[\frac{\Delta\hat{p}_{jj} + \Delta\hat{p}_{ij}}{1 + \Delta\hat{p}_{jj}} \right] \right|, \; i \neq j \tag{15}$$

This is very useful in order to state a decoupling level that cannot be exceeded.

Furthermore, in the same way we can obtain the coupling c_{ij} without any non-diagonal controller, -with g_{ij}=0-, so that,

$$\left|c_{ij}\right| = \left| \frac{g_{jj} \cdot \frac{\hat{p}_{ij}^{N}}{\hat{p}_{jj}^{N}}}{1 + g_{jj} \cdot \frac{1}{\hat{p}_{jj}^{N} \cdot \left(1 + \Delta\hat{p}_{jj}\right)}} \cdot \left[\frac{1 + \Delta\hat{p}_{ij}}{1 + \Delta\hat{p}_{jj}} \right] \right|, \; i \neq j \tag{16}$$

Note that if $\Delta\hat{p}_{ij}$ is much larger than $\Delta\hat{p}_{jj}$ and than 1, it is almost worth for nothing the use of the non-diagonal g_{ij}.

3.3. Criterion to design non-diagonal controller elements

Based on the above, we propose a design criterion for the non-diagonal elements of the controller:

- If the uncertainty radius $\Delta\hat{p}_{ij}$ is much larger than $\Delta\hat{p}_{jj}$ and than 1, then there is no need of g_{ij}.
- If not, the nominal optimum controller of Eq. (14) is considered in order to achieve a satisfactory level of loop decoupling, trying to minimise c_{ij} of Eq. (12).

4. Design methodology

First, we present the proposed design method, based on a technique that sequentially closes the loops. Later an example is shown to demonstrate its practical use.

4.1. Method

We use the above criterion expounded in Section 3 to design the controller non-diagonal elements g_{ij} in a parallel way to the MQFT [11], and to the technique proposed by M.A.Franchek *et al.* [12] to regulate a MIMO system.

The main characteristic that differs the method proposed in this paper and MQFT is that ours include the non-diagonal elements of the controller in order to reduce the loop coupling. Besides, the two differences with the proposed technique by Franchek *et al.* is that our objective is reference tracking instead of regulation, and that our method does not distinguish the upper triangular elements from the lower triangular elements of the controller ***G***.

To be able to use this methodology, it is necessary to suppose as true the Hypotheses H1, H2 and H3. Then, the process begins pairing inputs and outputs by the RGA technique [10]. Later, the

sequential controller design is composed of n stages (n loops) with the following two steps (for loop k):

P1. Design of the diagonal controller g_{kk} for the equivalent plant p_{kk}^{e}. The design of the diagonal element g_{kk} is searched through standard loop-shaping in order to achieve robust stability and robust performance specifications. The equivalent plant p_{kk}^{e} is the inverse of $[\hat{p}_{kk}]_{k\text{-th interaction}}$, that is the equivalent element of the plant inverse $\hat{\boldsymbol{P}}$ for the loop k as proposed by M.A.Franchek *et al.* [8].

P2: Design of the (n-1) non-diagonal elements g_{ik} of the k-th controller column, searching for the minimisation of c_{ik} -Eq. (12)-. To achieve this goal, the nominal optimum controller must be taken into account -Eq. (14)-.

The closed-loop stability of the system is guaranteed if the previous hypotheses H1, H2 and H3 are fulfiled [12].

Finally, the design of the prefilter $\boldsymbol{F}$ is a trivial problem and does not present any difficulty, if the complementary sensitivity function is almost decoupled. Therefore, the prefilter $\boldsymbol{F}$ can be diagonal.

4.2. Numerical design example

In this subsection, a numerical design of a 2×2 MIMO system presents the practical use of this method.

Let us consider the linear multivariable system,

$$\mathrm{P}=\left\{\boldsymbol{P}=\begin{bmatrix} p_{11} & p_{12} \\ p_{21} & p_{22} \end{bmatrix}=\begin{bmatrix} \dfrac{10ab}{2s+b} & \dfrac{-4b}{s+b} \\ \dfrac{2ac}{s+c} & \dfrac{3ac}{0.5s+c} \end{bmatrix};a\in[0.8;1.2];\ b\in[8;10];\ c\in[5;6]\right\} \tag{17}$$

The performance tolerances are:

1. Achieve the robust stability specification for each loop,

$$\left|\frac{p_{ii}^{e}\cdot g_{ii}}{1+p_{ii}^{e}\cdot g_{ii}}\right|\le 1.4 \tag{18}$$

where p_{ii}^{e} is the i-th plant transfer function when the other loop is closed.

2. Achieve a tracking specification for each loop as,

$$\left|T_{11}^{L}(s)\right|=\left|\frac{4^2}{\left(s^2+2\cdot 0.9\cdot 4\cdot s+4^2\right)\cdot(s/10+1)}\right|\le\left|t_{11}^{Y/R}\right|\le\left|\frac{4^2\cdot(s/15+1)}{s^2+2\cdot 0.6\cdot 4\cdot s+4^2}\right|=\left|T_{11}^{U}(s)\right| \tag{19}$$

$$\left|T_{22}^{L}(s)\right|=\left|\frac{10^2}{\left(s^2+2\cdot 0.8\cdot 10\cdot s+10^2\right)\cdot(s/20+1)}\right|\le\left|t_{22}^{Y/R}\right|\le\left|\frac{10^2\cdot(s/25+1)}{s^2+2\cdot 0.7\cdot 10\cdot s+10^2}\right|=\left|T_{22}^{U}(s)\right| \tag{20}$$

that is equivalent to impose the variation of the diagonal elements of $\boldsymbol{T}$ to be,

$$|\Delta t_{11}(s)| \le |T_{11}^{U}(s)| - |T_{11}^{L}(s)| \tag{21}$$

$$|\Delta t_{22}(s)| \le |T_{22}^{U}(s)| - |T_{22}^{L}(s)| \tag{22}$$

with a diagonal prefilter $\boldsymbol{F}$. In this example we focus on the design of the feedback controller $\boldsymbol{G}$.

3. Reduce the coupling effects, $t_{12}^{Y/R}$ and $t_{21}^{Y/R}$.

The controller design is composed of the following steps:

Previous

The RGA matrix of the plant is,

$$\Lambda = \begin{bmatrix} e & 1-e \\ 1-e & e \end{bmatrix}, \quad \text{where } e \in [0.75;0.818] \text{ due to the uncertainty.} \tag{23}$$

So that, the input 1 will control the output 1, and the input 2 the output 2.

The p_{11} is chosen to be the first loop to close because it has the lowest bandwith compared to p_{22} [11].

Step 1

Through a standard loop-shaping a controller is found to achieve robust stability and tracking specifications. The controller for p_{11} is,

$$g_{11} = \frac{0.6496}{s/0.8556 + 1} \tag{24}$$

Step 2

The nominal optimum controller element g_{21}^{*} is taken into account,

$$g_{21}^{*} = -0.433 \frac{\left(\frac{s}{11}+1\right)}{\left(\frac{s}{0.8556}+1\right)\cdot\left(\frac{s}{5.5}+1\right)} \tag{25}$$

The proposed element g_{21} is simpler than the optimum -Eq. (25)- but it is enough to reduce the coupling c_{21},

$$g_{21} = \frac{-0.43}{\left(\frac{s}{0.8556}+1\right)} \tag{26}$$

Step 3

The loop-shaping of g_{22} searchs for a controller to be able to achieve robust equivalent plant p_{22}^{e},

$$p_{22}^{e} = p_{22} - \frac{(p_{22}\cdot g_{21} + p_{21}\cdot g_{11})\cdot p_{12}}{1 + p_{12}\cdot g_{21} + p_{11}\cdot g_{11}} \tag{27}$$

The controller g_{22}, that achieves the robust stability and tracking specifications is,

$$g_{22} = \frac{1.197}{\left(\frac{s}{47.66}+1\right)} \tag{28}$$

Step 4

Analogously to Step 3, the nominal optimum controller g_{12}^{*} to take into account is,

$$g_{12}^{*} = 0.479\frac{\left(\frac{s}{4.5}+1\right)}{\left(\frac{s}{9}+1\right)\cdot\left(\frac{s}{47.66}+1\right)} \tag{29}$$

and the proposed element,

$$g_{12} = \frac{0.48}{\left(\frac{s}{47}+1\right)} \tag{30}$$

The system with the full controller $\boldsymbol{G}$ presents a more decoupled complementary sensitivity function $\boldsymbol{T}$ than working only with the diagonal $\boldsymbol{G}_d = diag\{g_{11}, g_{22}\}$, as shown in Fig. 4 and 5.

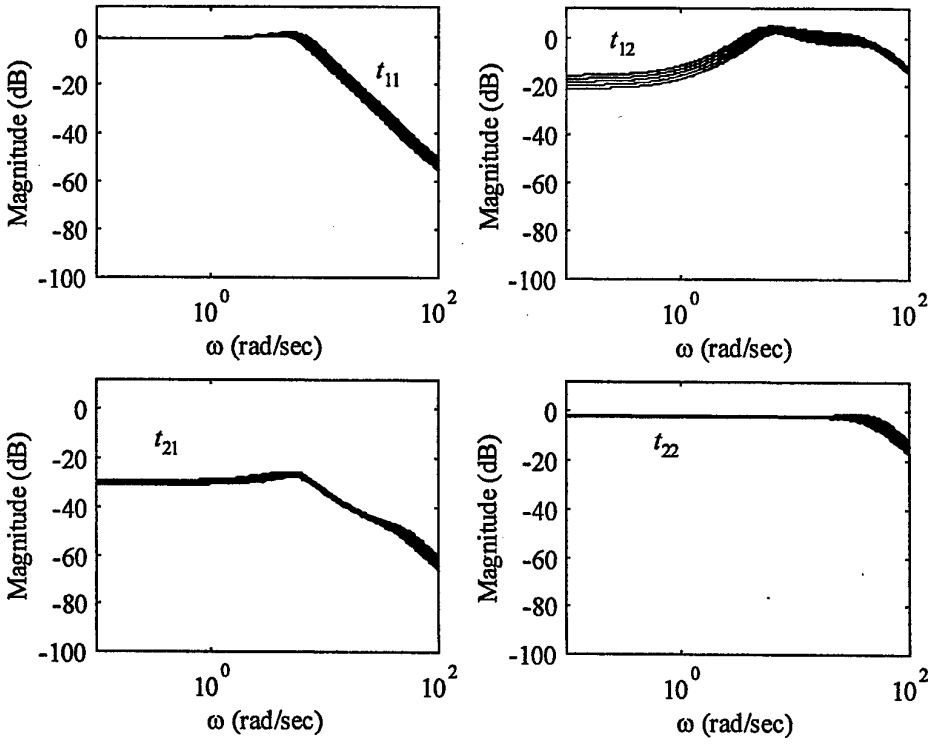

Fig. 4 Complementary sensitivity function $\boldsymbol{T}$ *with the diagonal controller* $\boldsymbol{G}_d$=diag$\{g_{11},g_{22}\}$

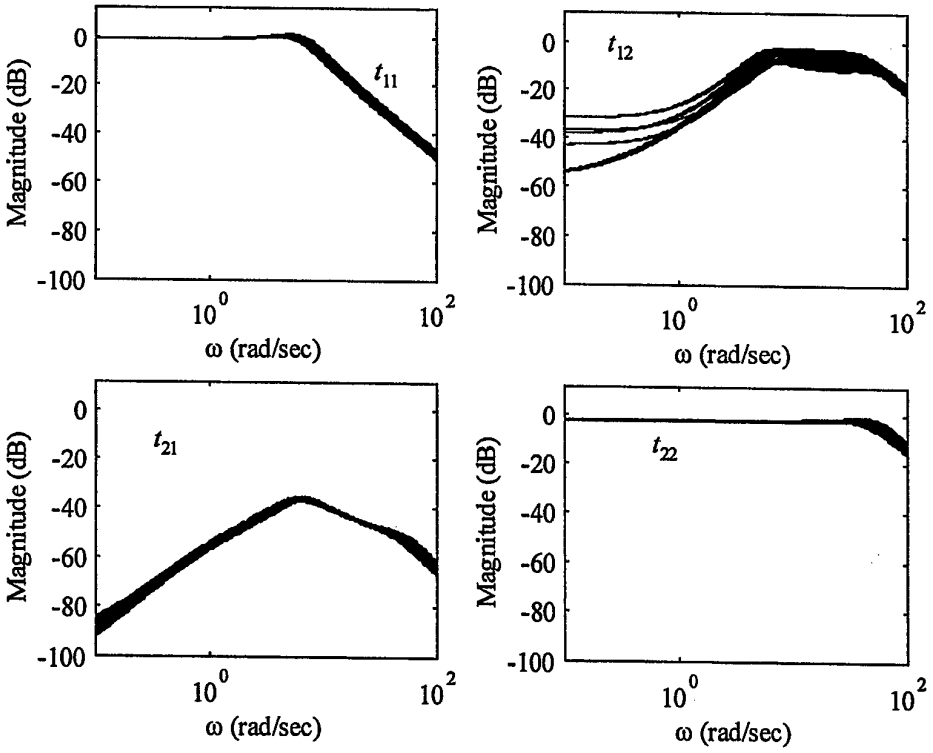

Fig. 5 Complementarty sensitivity function $\boldsymbol{T}$ *with the full controller* $\boldsymbol{G}$

5. Conclusions

In this paper we present a quantification of the loop coupling for uncertain MIMO systems. From the analysis of this effect, some important characteristics are deduced that help to find the best of all possible decoupling elements g_{ij}.

The study of the coupling effect shows that the non-diagonal elements g_{ij} of the controller are worth for the minimisation of the loop coupling, but not for the reduction of the uncertainty influence. So, the only achievable objective for these elements is the loop interaction reduction.

As well as the non-diagonal controller element problem is trivial for a system with no uncertainty - it can be seen as a feedforward controller-, under the presence of uncertainty it is necessary to design a controller that achieves the minimum loop interaction for the whole uncertain plant set. The quantification of the loop coupling makes possible to propose a nominal optimum controller to minimise the loop interaction. However, to apply the proposed non-diagonal controller, it is necessary that the plant $\boldsymbol{P}$ and its inverse $\hat{\boldsymbol{P}}$ are stable, and have no hidden unstable modes.

This optimum non-diagonal controller yields the minimum achievable interaction. This states a bound that cannot be exceeded, and it is a reference to evaluate the quality of a design.

This last boundary also can be compared to the coupling effect without any non-diagonal controller. Therefore, it is possible to decide whether it is worth to design that element. In general, for very large uncertainty of non-diagonal plant elements, it is not worth the effort of designing the non-diagonal controllers.

Furthermore, the coupling quantification can be used to determine the magnitudes of loop interactions that the diagonal elements g_{ij} have to reject.

Finally, based on the above, we propose a new methodology to design robust multivariable controllers for stable systems with stable plant inverse and non 'ill-conditioned', with a high coupling level. This methodology formulation is based on a sequential design of each controller column. This technique makes possible to find non-diagonal controllers in order to reduce the loop interaction.

Appendix A1

The coupling c_{ij}, with a controller g_{ij} like (12), can be written as,

$$c_{ij} = g_{ij} - \frac{g_{jj}\cdot\hat{p}_{jj}^{-1}}{1+g_{jj}\cdot\hat{p}_{jj}^{-1}}\cdot\left(\hat{p}_{ij}+g_{ij}\right) = g_{jj}\cdot\frac{\hat{p}_{ij}^{0}}{\hat{p}_{jj}^{0}} - \frac{g_{jj}\cdot\hat{p}_{jj}^{-1}}{1+g_{jj}\cdot\hat{p}_{jj}^{-1}}\cdot\left(\hat{p}_{ij}+g_{jj}\cdot\frac{\hat{p}_{ij}^{0}}{\hat{p}_{jj}^{0}}\right) =$$

$$= \frac{g_{jj}}{1+g_{jj}\cdot\hat{p}_{jj}^{-1}}\cdot\left(\frac{\hat{p}_{ij}^{0}}{\hat{p}_{jj}^{0}} - \frac{\hat{p}_{ij}}{\hat{p}_{jj}}\right) = \frac{g_{jj}}{1+g_{jj}\cdot\hat{p}_{jj}^{-1}}\cdot\left(\frac{\hat{p}_{ij}^{N}\cdot\left(1+\Delta\hat{p}_{ij}^{0}\right)}{\hat{p}_{jj}^{N}\cdot\left(1+\Delta\hat{p}_{jj}^{0}\right)} - \frac{\hat{p}_{ij}^{N}\cdot\left(1+\Delta\hat{p}_{ij}\right)}{\hat{p}_{jj}^{N}\cdot\left(1+\Delta\hat{p}_{jj}\right)}\right) =$$

$$= \frac{g_{jj}}{1+g_{jj}\cdot\hat{p}_{jj}^{-1}}\cdot\frac{\hat{p}_{ij}^{N}}{\hat{p}_{jj}^{N}}\left(\frac{\left(1+\Delta\hat{p}_{ij}^{0}\right)\cdot\left(1+\Delta\hat{p}_{jj}\right) - \left(1+\Delta\hat{p}_{jj}^{0}\right)\cdot\left(1+\Delta\hat{p}_{ij}\right)}{\left(1+\Delta\hat{p}_{jj}^{0}\right)\cdot\left(1+\Delta\hat{p}_{jj}\right)}\right) =$$

$$= \frac{g_{jj}}{1+g_{jj}\cdot\hat{p}_{jj}^{-1}}\cdot\frac{\hat{p}_{ij}^{N}}{\hat{p}_{jj}^{N}}\left(\frac{\left(\Delta\hat{p}_{ij}^{0}-\Delta\hat{p}_{ij}\right)+\left(\Delta\hat{p}_{jj}-\Delta\hat{p}_{jj}^{0}\right)+\left(\Delta\hat{p}_{ij}^{0}\cdot\Delta\hat{p}_{jj}-\Delta\hat{p}_{jj}^{0}\cdot\Delta\hat{p}_{ij}\right)}{\left(1+\Delta\hat{p}_{jj}^{0}\right)\cdot\left(1+\Delta\hat{p}_{jj}\right)}\right) =$$

As non-parametric uncertainty radii obey that,

$$\Delta\hat{p}_{ij} = \frac{\hat{p}_{ij}}{\hat{p}_{ij}^{N}} - 1; \qquad \Delta\hat{p}_{ij}^{0} = \frac{\hat{p}_{ij}^{0}}{\hat{p}_{ij}^{N}} - 1$$

$$\Delta\hat{p}_{jj} = \frac{\hat{p}_{jj}}{\hat{p}_{jj}^{N}} - 1 \qquad \Delta\hat{p}_{jj}^{0} = \frac{\hat{p}_{jj}^{0}}{\hat{p}_{jj}^{N}} - 1$$

then,

$$= \frac{g_{jj}}{1+g_{jj}\cdot\hat{p}_{jj}^{-1}}\cdot\frac{\hat{p}_{ij}^{N}}{\hat{p}_{jj}^{N}}\left(\frac{\left(\frac{\hat{p}_{ij}^{0}-\hat{p}_{ij}}{\hat{p}_{ij}^{N}}\right)+\left(\frac{\hat{p}_{jj}-\hat{p}_{jj}^{0}}{\hat{p}_{jj}^{N}}\right)+\left(\left(\frac{\hat{p}_{ij}^{0}}{\hat{p}_{ij}^{N}}-1\right)\cdot\left(\frac{\hat{p}_{jj}}{\hat{p}_{jj}^{N}}-1\right)-\left(\frac{\hat{p}_{jj}^{0}}{\hat{p}_{jj}^{N}}-1\right)\cdot\left(\frac{\hat{p}_{ij}}{\hat{p}_{ij}^{N}}-1\right)\right)}{\left(1+\Delta\hat{p}_{jj}^{0}\right)\cdot\left(1+\Delta\hat{p}_{jj}\right)}\right) =$$

$$= \frac{g_{jj}}{1+g_{jj}\cdot\hat{p}_{jj}^{-1}}\cdot\frac{\hat{p}_{ij}^{N}}{\hat{p}_{jj}^{N}}\left(\frac{\left(\frac{\hat{p}_{ij}^{0}-\hat{p}_{ij}}{\hat{p}_{ij}^{N}}\right)+\left(\frac{\hat{p}_{jj}-\hat{p}_{jj}^{0}}{\hat{p}_{jj}^{N}}\right)+\frac{\left(\hat{p}_{ij}^{0}-\hat{p}_{ij}^{N}\right)\cdot r_{jj}-\left(\hat{p}_{jj}^{0}-\hat{p}_{jj}^{N}\right)\cdot r_{ij}}{\hat{p}_{ij}^{N}\cdot\hat{p}_{jj}^{N}}}{\left(1+\Delta\hat{p}_{jj}^{0}\right)\cdot\left(1+\Delta\hat{p}_{jj}\right)}\right)$$

In this equation, if $\left|\hat{p}_{ij}^{0}-\hat{p}_{ij}^{N}\right|$ and $\left|\hat{p}_{jj}^{0}-\hat{p}_{jj}^{N}\right|$ are minimum, then, the coupling c_{ij} is minimum too.

Acknowledgement

The authors gratefully appreciate the support given by the Spanish 'Comisión Interministerial de Ciencia y Tecnología' (CICYT) under grant TAP'97-0471.

References

[1] I.Horowitz, "Quantitative synthesis of uncertain multiple input-output feedback system", *International Journal of Control*, 1979, vol. 30, no. 1, pp. 81-106.

[2] H.H.Rosenbrock, "State-space and multivariable theory", 1970, *John Wiley*, New York.

[3] J.M.Maciejowski, "Multivariable feedback design", 1989, *Addison Wesley*, Harlow, United Kingdom.

[4] E.Boje, and O.D.I.Nwokah, "Quantitative feedback design using forward path decoupling", *Proceedings of the International Symposium on Quantitative Feedback Theory and Other Frequency Domain Methods and Applications*, 1997, University of Strathclyde, Glasgow, United Kingdom, pp. 185-191.

[5] J.O'Reilly, and W.E.Leithead, "Multivariable control by 'individual channel design'", *International Journal of Control*, 1991, vol. 54, no. 1, pp. 1-46.

[6] I.Horowitz, "A synthesis for linear time-varying feedback systems with plant uncertainty", *Transactions on Automatic Control*, 1975, vol. 20, no. 4, pp. 454-463.

[7] I.Horowitz, and M.Sidi, "Practical design of feedback systems with uncertain multivariable plants", *International Journal of Systems Science*, 1980, vol. 11, no. 7, pp. 851-875.

[8] J.J.D'Azzo, and C.H.Houpis, *Linear Control System Analysis and Design: Conventional and Modern*, 1995, McGraw-Hill, New York, pp. 580-635.

[9] S.Skogestad, and K.Havre, "The use of RGA and condition number as robustness measures", *Proceedings of the European Symposium on Computer-Aided Process Engineering*, 1996, Rodhes, Greece.

[10] E.H.Bristol, "On a new measure of interactions for multivariable process control", *IEEE Transactions on Automatic Control*, 1966, vol. 11, pp. 133-134.

[11] O.Yaniv, and I.M.Horowitz, "A quantitative design method for MIMO linear feedback systems having uncertain plants", *International Journal of Control*, 1986, vol. 43, no. 2, pp. 401-421.

[12] M.A.Franchek, P.Herman, and O.D.I.Nwokah, "Robust nondiagonal controller design for uncertain multivariable regulating systems", *ASME Journal of Dynamic Systems, Measurement, and Control*, 1997, vol. 119, pp. 80-85.

1999 International Symposium on
Quantitative Feedback Theory and Robust Frequency Domain Methods

Nonlinear Prototype for Forcing Functions in Second Order Systems

A.C. Burston and Dr B. Wigdorowitz

Department of Electrical Engineering
University of the Witwatersrand
Private Bag 3, Wits 2050
South Africa
Burston@ledge.co.za
B.Wigdorowitz@ee.wits.ac.za
Fax: +27 11 403 1929

Abstract

A nonlinear prototype for modelling average value bias in forced oscillatory systems has been developed. Several important requirements for improved operation in forced oscillatory systems were identified in order to guide the development process. The prototype has been placed in context with respect to system analysis and control design. An example illustrating how the prototype could be fitted to a nonlinear equation is also given.

1 Introduction

With the development and implementation of optimal multi-variable control in chemical industries around the world, companies are increasingly looking towards ways of getting more out of their existing processes. While much can be done to improve productivity by reducing down-time and operating closer to system limitations, this process eventually brings one to a point where expensive physical modifications of the plant are required to further improve production. One possible way of getting the best out of existing equipment is to explore the possibility of recurrent steady state operation besides the standard fixed point steady state operation [2].

This paper discusses an important part in the development of a methodology for analyzing a nonlinear system which can be used to determine if any benefits exist in operating the process in a nonlinear recurrent mode of operation. The part of the methodology discussed here is the development of a general second order nonlinear prototype. The prototype must exhibit the behaviour required to model many different nonlinear systems at and around their equilibrium point.

This paper outlines the ideas and background philosophy in approaching this nonlinear problem. It also gives some simulation results that reveal several prerequisites for benefits in nonlinear

recurrent steady state operation. A practical method for fitting this prototype to chemical reaction systems is the subject of another paper.

2 Background

Firstly, it is important to place the prototype within the the context of how it can be used to solve nonlinear control problems. This involves two steps:

1. Showing the progression of ideas within this area of research which led to the concepts presented in this paper.
2. Explaining how the prototype is used within a broader methodology which can be used to solve nonlinear control problems.

The origin of this research is process control in the field of chemical engineering. The works cited in this paper come mainly from that background. Modelling of chemical processes is a very well established field and nonlinear modelling of chemically reacting systems has been an active area of research in chemical engineering for several decades as can be seen from a sampling of papers dealing with CSTR reactor dynamics [10] [8] [1] [6].

The idea of using nonlinear dynamics to improve performance was already being discussed in 1966 [5] and possibly earlier. The idea was that "under certain circumstances an oscillator will have a performance greater than expected than for a fixed point steady state design"[4]. Douglas [4] developed an analytical solution to the problem of calculating the average value for a particular CSTR problem. This was later extended to encompass more complex problems [3]. The problem with this approach is that it is very inflexible. Trying to solve the problem analytically for an arbitrary system is a tedious task which could be impossible to automate.

Experimental studies were done on Catalytic Ammonia Synthesis in the early 1980's [7]. This work confirmed what had been theoretically postulated and provided a practical example of how forced operation can result in improved reactor performance. More recently (with the appearance of inexpensive powerful computers), several different numerical methods have been proposed for solving the problem of optimizing reactor performance [9]. The approach in the literature cited has been completely from a chemical engineering perspective.

The aim of this research is to approach the problem from a control engineering perspective and develop nonlinear tools similar to those used in linear control methodologies. It is important at this point to outline the methodology that could be used with the prototype discussed in this paper. This will be done via a comparison to an existing approach.

A common methodology that is employed in many control engineering problems (often implicitly) is as follows:

1. Obtain a nonlinear ordinary differential equation model of the system to be controlled.
2. Linearize the system at the equilibrium point (for fixed point steady state operation).
3. Transform the linearized system into a form appropriate for analysis and control design (for example the controllability form).

4. Use results obtained to fit an existing prototype (for example the second order prototype).

5. Design and verify the operation of the controller iteratively by making use of the chosen prototype.

This methodology may not represent all design approaches, but it is often used where models are obtained from experimental data (in that case the first step falls away). Prototypes provide a generalized model which can be fitted to many different types of systems.

The prototype described in this paper can be used for a system which can be forced to operate in a steady state oscillatory mode by using a forcing function. Once it has been fitted to the process via linearization, at and around the equilibrium point, it can be used for both analysis and control design. Due to the fact that the prototype is simpler than the original system, it is easier to develop general results and methods which can be used to solve control problems. These results will then be automatically applicable to different systems which can be approximated via the prototype. Hence one can see the importance of having the correct prototype for the problem at hand and why the prototype is the heart of building a nonlinear control methodology.

3 Prototype

A prototype is a very useful tool in analyzing and predicting behaviour. It reduces the amount of time required to gain an understanding of the behaviour of a system. There are several linear prototypes which already exist and are used in every facet of modelling for control and control system design. We need to develop a prototype that can be used to analyze and predict the effects of steady state oscillatory behaviour. A good place to start for second order systems is the linear second order prototype shown in state space form in (1).

$$\dot{\mathrm{z}} = \begin{bmatrix} 0 & 1 \\ \alpha & \beta \end{bmatrix} \mathrm{z} \tag{1}$$

The approach adopted in the methodology is to construct a nonlinear prototype which has the structure of (1) and then to transform actual nonlinear systems into this prototype structure. For a nonlinear prototype with structure (1), α and β are in general nonlinear functions of z_1, z_2 of which there are an infinite number to choose from. The problem at hand helps us to select an appropriate function.

To review, the problem to be solved is to determine whether a system can be operated in a steady state oscillatory mode of operation to achieve improved performance. This manifests itself in the average value of the system output being higher or lower than the equilibrium value for fixed point steady state operation.

This problem immediately places several restrictions upon the prototype to be developed:

- The prototype must be stable at the equilibrium point and for a reasonable neighbourhood around it.

- The prototype must have only one equilibrium point in the region of operation.

Once these limitations have been defined, we are free to suggest several different prototypes which could fulfill the role for this system. To decide on the most appropriate solution we should first more clearly define the problem we are trying to solve.

The idea of increasing system performance by making use of oscillation is a well established phenomenon used in many devices. Some of the most obvious examples are musical instruments which make use of resonant frequencies to increase the amplitude of the vibrations within the instrument. Due to the nonlinear relationship between the power of a sinusoidal signal and its amplitude, that is, the root mean square value, the increased amplitude of the signal translates into a louder sound. This concept can be used in other areas of engineering to achieve similar results where the benefits of oscillatory operation may be less obvious.

What the discussion has so far revealed, is that for any benefits to occur, an increase in the gain of the system must occur at a particular frequency. In most situations this frequency is known as the resonant frequency. Here one comes across another important limitation which needs to be placed on the prototype. The system gain at the resonant frequency must be appreciably higher than the fixed point steady state gain of the system. Only systems which exhibit this property can have a chance of producing the effect we desire.

Another way of stating the resonant frequency gain requirement is to say that the linearized system at the equilibrium point must have complex conjugate poles, that is poles which are not on the real axis. In phase-plane terminology this is known as a focus (an equilibrium point with non-real poles). This results in α and β satisfying the linear model conditions given by equations (2)–(7).

$$\dot{z} = \begin{bmatrix} 0 & 1 \\ \alpha & \beta \end{bmatrix} z \tag{2}$$

$$H(s) = \frac{1}{det\,(sI - A)} \tag{3}$$

$$H(s) = \frac{1}{(s^2 - \beta s - \alpha)} \tag{4}$$

$$p_1, p_2 = \frac{1}{2}\left(\beta + \left[\beta^2 + 4\alpha\right]^{0.5}\right) \tag{5}$$

$$\beta < 0 \tag{6}$$

$$\alpha < -\frac{1}{4}\beta^2 \tag{7}$$

Equations (6) and (7) define the linear restrictions for the prototype. The next step is to determine the nonlinearities that must be added to cause a bias in the average value away from zero when a forcing function is applied.

A first step is to determine which term, α or β, should be made nonlinear to achieve a bias in the average value. This can be done by setting up a linear example which fulfills the requirements laid down in (6) and (7). One can then simulate the system for α and β made functions of z_1 and z_2. The function one can initially choose is a step function with the discontinuity at zero.

α	β	$\bar{z}_1$	$\bar{z}_2$
$-2u(z_1)-1$	$-0,5$	-15%	$-0,3\%$
$-2u(z_2)-1$	$-0,5$	$-1,6\%$	$-0,3\%$
-3	$-0,5u(z_1)-0,5$	$0,2\%$	$-0,2\%$
-3	$-0,5u(z_2)-0,5$	$2,3\%$	$-0,2\%$

Table 1: Simulation results

The step functions that need to be tested ($u(t)$ represents a unit step) can be reduced by doing simulations for different choices of functions $\alpha(z_1)$, $\alpha(z_2)$, $\beta(z_1)$ and $\beta(z_2)$. It was found by simulation (Table 1)that the function which had the greatest impact on the average value was $\alpha(z_1)$. The bias in each case was calculated using (8).

$$\text{bias} = \frac{\text{average}}{\text{maximum} - \text{minimum}} \tag{8}$$

Table 1 was generated by applying a forcing function of $0,4\sin t$ to the $\dot{z}_2$ term of (1). The simulations used an Euler's method with a fixed step size of 0.1 seconds and a total simulation time of 200 seconds. The initial conditions of the system were

$$z = \begin{bmatrix} 0 \\ 0 \end{bmatrix}$$

4 Example

An example is used to illustrate a possible approach to fitting the prototype to a nonlinear system. There may be more efficient ways of doing this, but the method presented can be seen as a first approximation. Several issues pertinent to this example are also discussed.

Consider a system described by (9). Linearizing (9) at the equilibrium point (which is at the origin) results in (11). This gives a system with a resonant frequency of $\omega_0 = 0,97$ rad/s and a resonant frequency gain of $G_{\omega_0} = 2$. If we make the forcing function frequency equal to the resonant frequency, we can use G_{ω_0} to calculate an approximate value for A, the amplitude of the forcing function. We do this by choosing a variation in x_1 which is acceptable (in this case assume x_1 may vary by 1 either up or down). A can then be calculated using (13) to be $0,5$. Hence we have a simple method for deciding on the value of A, which could be used in the design of a periodically forced system.

$$\begin{bmatrix} \dot{x}_1 \\ \dot{x}_2 \end{bmatrix} = \begin{bmatrix} 0 & 1 \\ -e^{x_1} & -0,5 \end{bmatrix} \begin{bmatrix} x_1 \\ x_2 \end{bmatrix} + \begin{bmatrix} 0 \\ 1 \end{bmatrix} A\sin\omega t \tag{9}$$

(10)

α	β	$\bar{x}_1$	$\bar{x}_2$
$-e^{x_1}$	$-0,5$	$-19,2\%$	0%
$-(e-e^{-1})u(t)-e^{-1}$	$-0,5$	$-27,7\%$	0%

Table 2: Example average bias

$$\begin{bmatrix} \dot{x}_1 \\ \dot{x}_2 \end{bmatrix} = \begin{bmatrix} 0 & 1 \\ -1 & -0,5 \end{bmatrix} \begin{bmatrix} x_1 \\ x_2 \end{bmatrix} + \begin{bmatrix} 0 \\ 1 \end{bmatrix} A \sin \omega t \tag{11}$$

$$\tag{12}$$

$$A = \frac{\Delta x_1}{G_{\omega_1}} \tag{13}$$

The next step is to fit the prototype to the system. This is done by substituting the extreme values of x_1 into (9). Since (9) already has the same structure as (2) (the prototype), no transformations are necessary. The step function for the prototype becomes

$$\alpha = -(e-e^{-1})u(t)-e^{-1}$$

Using this result and doing simulations for the actual system as well as the prototype, Table 2 shows the difference in the biased average values and Figure 1 shows a comparison between the two systems output responses. The systems are sufficiently similar to justify using the prototype as a means of approximating the system for control design.

There are several important reasons why the prototype is a better system to use when doing the control design:

- It is a simpler system than the original system and although an approximation, it sufficiently models the system in the region of operation.
- General results for the prototype can be applied to the design which could not be used with the original system.
- It is partially analytically tractable, whereas the original system has a high probability of being analytically intractable.

An important issue that comes to mind during this exercise, is the place of control design in forced periodic systems. With the requirement for resonance being so important for oscillatory operation to be beneficial, comes a possibility that in nonlinear systems which do not experience resonance, resonance could be introduced using control. This would have to be done via the β term of the prototype to actually make a contribution to the benefits (introducing it via the α term would mean that you should rather operate the plant in fixed point steady state operation for best performance). This issue will be investigated in future work.

5 Conclusion

The prototype development revealed some important information about forced second order nonlinear systems:

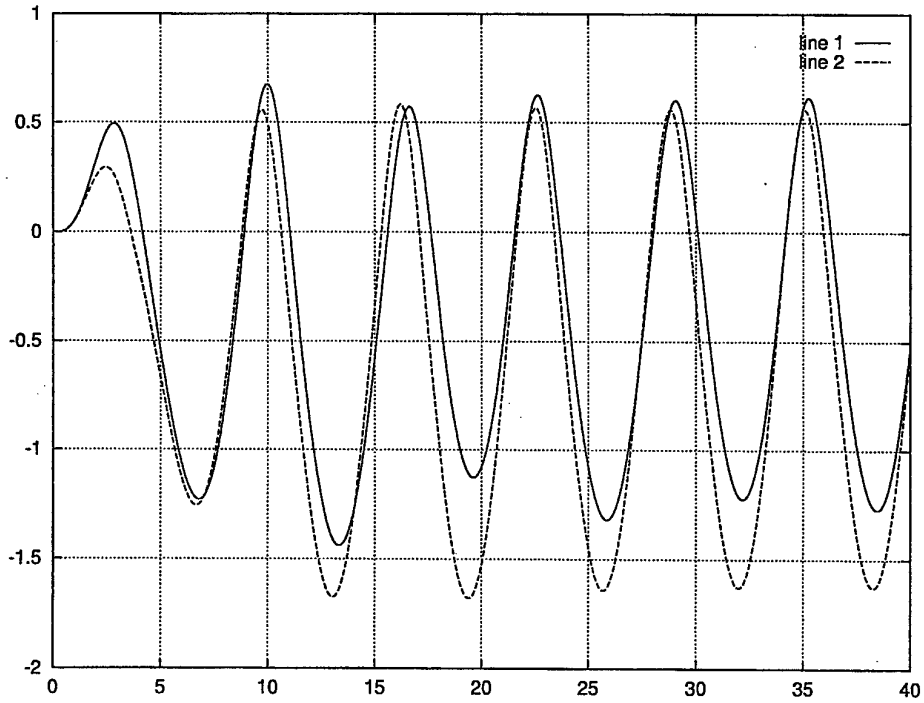

Figure 1: Example/prototype comparison (upper trace is original system)

- Only systems with a single stable equilibrium point within the region of operation can be analyzed using the prototype proposed.
- The behaviour at and around the equilibrium point must exhibit a large gain at a certain resonant frequency (non-real poles/focus).
- For the greatest bias in the average value, the function $\alpha(z_1)$ should be highly nonlinear and non-symmetrical around the origin within the boundaries of stability.

These requirements can be refined into a better prototype and combined with a methodology for transforming nonlinear models to provide a practically useful way of solving this class of nonlinear problem. This is the subject of a future paper.

Nomenclature

A	Amplitude of the forcing function.
α	Cross term in the nonlinear prototype.
β	Diagonal term in the nonlinear prototype.
G_{ω_0}	System gain at the resonant freqency.
H(s)	System transfer function.
ω	Frequency in radians per second.
ω_0	Resonant frequency in radians per second.

References

[1] Chien-Chong Chen, Chun-Chong Fu, and Chong-Hung Tsai. Stabilized chaotic dynamics of coupled nonisothermal cstrs. *Chemical Engineering Science*, 51, 1996.

[2] Chien-Chong Chen and Chyi Hwang. Optimal periodic forcing of nonlinear chemical processes for performance improvements. *The Canadian Journal of Chemical Engineering*, 72, August 1994.

[3] T. G. Dorawala and J. M. Douglas. Complex reactions in oscillating reactors. *AIChe Journal*, 17 No 4, July 1971.

[4] J. M. Douglas and N. Y. Gaitonde. Analytical estimates of the performance of chemical oscillators. *I&EC Fundamentals*, 6 No 2, May 1967.

[5] J. M. Douglas and D. W. T. Ripin. *Chemical Engineering Science*, 21, 1966.

[6] Razon L et al. Multiplicities and instabilities in chemically reacting systems — a review. *Chemical Engineering Science*, 42, 1987.

[7] A. K. Jain, R. R. Hudgins, and P. L. Silveston. Part i - effect of cycling parameters and mean composition. *The Canadian Journal of Chemical Engineering*, 61, December 1983.

[8] I. G. Kevrekidis, L. D. Schmidt, and R. Aris. Some common features of periodically forced reacting systems. *Chemical Engineering Science*, 41, 1986.

[9] F. Ozgulsen, R. A. Adomaitis, and A. Cinar. A numerical method for determining optimal parameter values in forced periodic operation. *Chemical Engineering Science*, 47 No 3, 1992.

[10] A. Uppal, W. H. Ray, and A. B. Poore. On the dynamic behaviour of continuous stirred tank reactors. *Chemical Engineering Science*, 29, 1974.

1999 International Symposium on
Quantitative Feedback Theory and Robust Frequency Domain Methods

SMALL FLOW CONTROL BY USING NONLINEAR QFT

A. Arenas*, A. Baños**, L. Victoria*, and J. Abellán*

*Dep. Física Aplicada, Univ. Murcia, Campus Espinardo, 30071 Murcia, Spain
**Facultad de Informática, Univ. Murcia, Campus Espinardo, 30071, Murcia, Spain

Abstract: The control of small flows using a cheap actuator, that is a ball valve actuated by a stepping motor, is considered under the framework of QFT. The basic problem comes from the fact that the ball has a nonlinear characteristic, which may be time varying as a function of a disturbance. In addition, the motor imposes intrinsic limitations on the bandwidth of the controller. The nonlinear control problem is translated in a linear equivalent control problem for a range of reference values. The resulting linear problem is relatively single, since the valve is modeled as an uncertain gain. After designing the controller using linear QFT, different experiments are done in order to validate the design.

1 Introduction

Flow control is of great practical importance in chemical and food industry, where the goal is to keep regulated the flow through some load, independently of possible variations over the conditions of the flow source. Here our objective is to design a control system that gives a constant flow using a cheap actuator, for different values of the setpoint.

The main difficulty of the control problem is due to the fact that the actuator, a ball valve actuated by a stepping motor, has a nonlinear behavior that may also depends on the pressure of the flow source. The rest of the plant exhibits a linear and time invariant dynamics. For slow variations of the flow source, the disturbance in the rest of the paper, the nonlinear behavior of the valve can be modeled with an uncertain nonlinear static characteristic.

The problem of regulating the output flow for several setpoints, and with some time-domain tolerances, is reformulated as a nonlinear regulation problem for which the nonlinear QFT technique ([2,3]) can be applied. The basic idea is to translate the uncertain nonlinear plant to a set of equivalent linear plants. With some assumptions, a valid design for the equivalent linear set is also valid for the original nonlinear problem.

The rest of the paper is organized as follows. In Section 2, the control problem is presented with some detail. Section 3 gives a QFT solution to the problem, and finally Section 4 include some experimental results.

2 The control problem

The control problem consists of designing a robust compensator for regulating the flow passing through a streamer, for different values of the setpoint between 10 and 60 ml/s. The main difficulty relies upon the fact that the actuator, a ball valve, has a relatively strong nonlinear behavior.

The valve is operated through a stepping motor that limits the bandwidth of the control signal to 100 Hz. The dynamics of the motor and the valve is very fast compared to other parts of the system, thus it is considered static. In particular, the flow sensor has a constant time of 10 s, which is the slowest subsystem. In addition, for a given valve angle, the valve output flow may depend on the differential pressure between the net and the load.

The characterization of the valve has been made through experimentation, given the results of Fig. 1, where the output flow is given as a function of the valve angle (in number of pulses, 1 pulse = 0.03°) for different pressures between 1 and 3.2 atmospheres. The differential pressure between the net and the load will be considered as a disturbance in the control problem, and will be referred to as d in the rest of the paper.

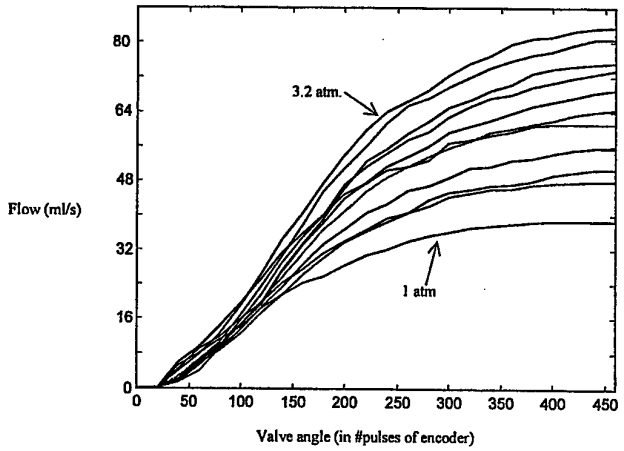

Fig. 1: Experimental data of the valve, in terms of output flow versus valve angle, for $d = 1,1.2,1.4,...,3.2$ at.

The valve output is connected to a streamer, which represents a load. Its output is measured by a sensor developed by some of the authors ([1]), specially designed for the measure of small flows. The dynamics of the load and the sensor is given by $H(s)$, and after identification, is given by

$$H(s) = \frac{1}{(0.01s^2 + 0.12s + 1)(10s + 1)}$$

Fig. 2 represents the plant, embedded in a two degrees of freedom control structure. The control problem is to design compensators F and G for the flow at the valve output to be regulated for values in the interval [10, 60] ml/s, with a 2% tolerance error.

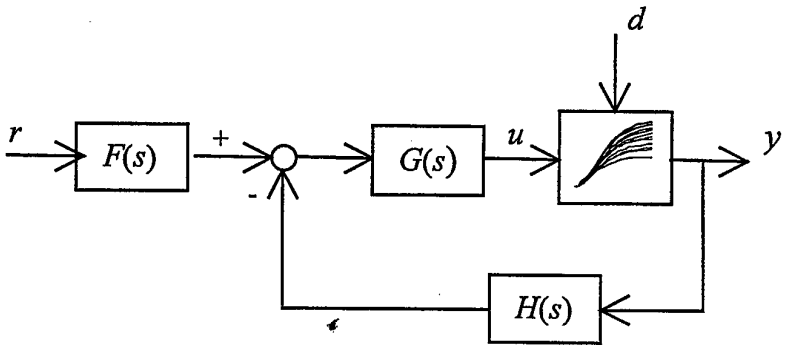

Fig. 2: Control System: F and G are the compensators, $H(s)$ gives the dynamics of the streamer and the sensor

3 QFT design

The nonlinear characteristic of the valve, including its behavior depending on the perturbation *d*, results in a control problem suitable for nonlinear QFT synthesis ([2-4]). Assuming that the perturbation varies slowly compared to the rest of closed loop signals, the valve can be substituted by an equivalent set of linear time-invariant systems (usually referred to as the equivalent linear family, ELF, in the QFT literature).

Design specifications are given in the frequency domain. The closed loop system is considered to behave as a transfer function, for references between 10 and 60 ml/s, with frequency response bounded in magnitude as given in Fig. 3. Since the output is to be regulated between 10 and 60 ml/s, and the valve is considered static, the computation of the ELF is rather simple in this case. From the data represented in Fig.1, it is possible to obtain valve angles corresponding to specified output flows, for different values of the disturbance. Taking the minimum and maximum values of the quotient between the output and the input, the resulting ELF is an uncertain gain K given by $K \in [0.74,4.29]$.

Shaping compensators $G(s)$ and $F(s)$ for the uncertain linear equivalent problem, using linear QFT [3], completes the design. Fig.4 shows boundaries for the linear equivalent problem for the specifications given in Fig. 3. In addition a relative stability restriction is included.

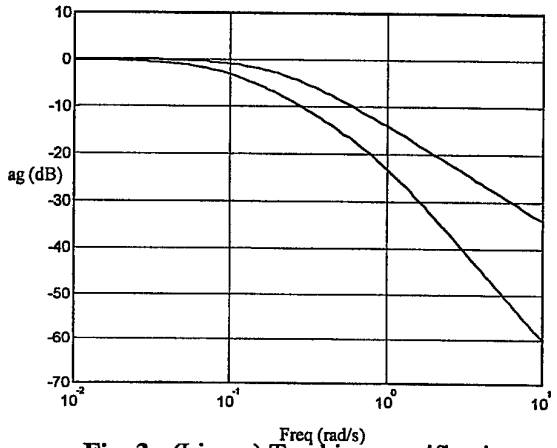

Fig. 3: (Linear) Tracking specification

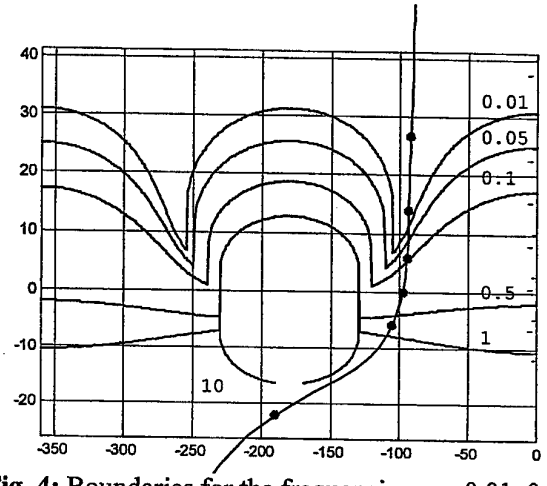

Fig. 4: Boundaries for the frequencies $\omega = 0.01$, 0.05, 0.1, 1, 5, and 10 rad/s, and loop shaping

Fig. 4 also shows a tentative shaping for the nominal open loop gain. One of the goals has been to obtain a low order compensator, with a restriction of 100 Hz bandwidth. The result is given by:

$$G(s) = 0.4\frac{(1+\frac{s}{0.1})}{s(1+\frac{s}{50})}$$

Simulation of the resulting nonlinear closed loop system performs well for the different disturbance values and for the different setpoints. Simulation results are omitted. Here we are mainly interested in showing experimental results, which are presented in next Section.

4 Experimental results

The QFT controller has been implemented in a digital form (using a sample time of 0.5 s). Experimental results are given in Fig. 5 to 8. Fig. 5 shows closed loop outputs y for setpoints between 10 and 60 ml/s, and Fig. 6 measured values of the output flow y in response to a variable setpoint. All of these experiments have been made for a constant value of the net pressure, meaning a constant disturbance d after some transitory period.

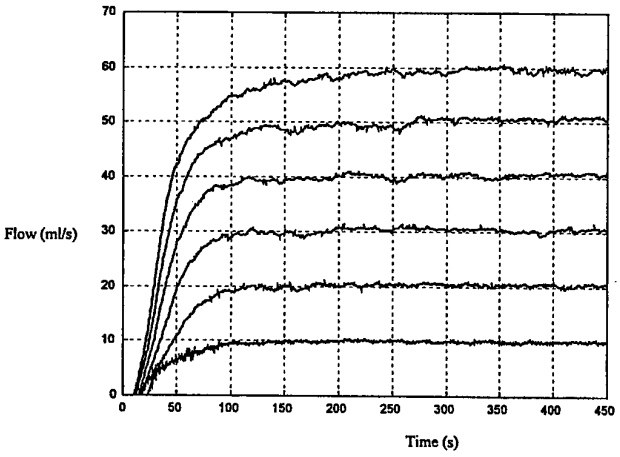

Fig. 5: Output flow for setpoints 10, 20,..,60 ml/s, showing measured outputs of the control system

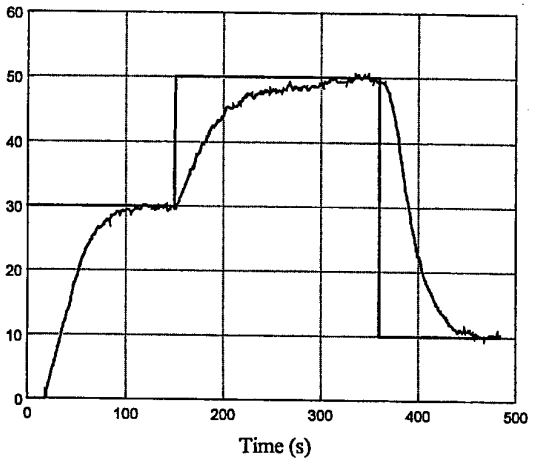

Fig. 6: Measured flow in ml/s, showing tracking for different output values

Finally, Fig. 7 and 8 show closed loop output and control input respectively, for a regulation experiment about 30 ml/s, and with a periodic disturbance (period = 60 s) varying between 2 and 2.6 atmospheres. Although the system performs relatively well for this case, it has been noted by simulation that it increasingly degrades for faster disturbances, which can be considered as interesting practical cases. At this point, some redesign will be needed to improve the performance.

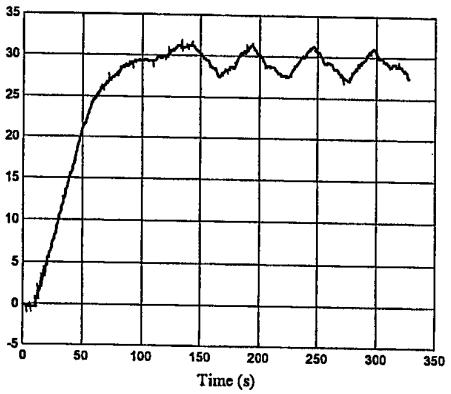

Fig 7: Closed-loop output flow for a reference of 30 ml/s, and with a periodic disturbance

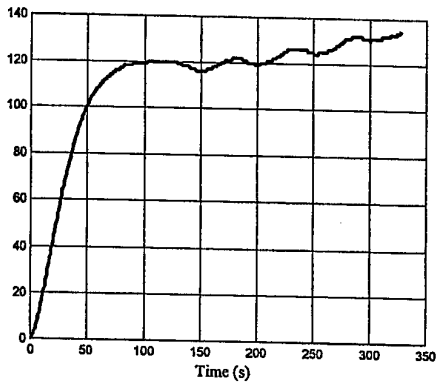

Fig. 8: Closed-loop valve angle for the same conditions of Fig. 6

Conclusions

In a flow control problem appears the problem of designing a compensator for a nonlinear time-varying system. Using nonlinear QFT ideas, at least for slow perturbations, the nonlinear subsystem can be viewed as an uncertain gain, which allows formulating a rather simple linear equivalent problem. This problem has been solved using linear QFT. An experimental validation of the technique has been done, resulting in good results for very slow disturbances. A design that allows faster disturbances deserves more consideration.

References

1. A. Arenas, L. Victoria, and T. Luna, "A digital circuit for measuring small flow", *Am. J. Phys.*, vol. 57, no. 12, pp. 1153-1154, 1989.
2. Horowitz, "Synthesis of feedback systems with nonlinear and time-varying uncertain plants to satisfy quantitative performance specifications", *Proc. IEEE*, vol. 64, pp. 123-130, 1976.
3. I. Horowitz, *Quantitative Feedback Theory (vol. 1)*, QFT Publications, Boulder, Colorado, 1993.
4. A. Baños, and F. N. Bailey, "Design and validation of linear robust controllers for nonlinear plants", *Int. Journal of Robust and Nonlinear Control,* vol. 8, pp. 803-816, 1998.

1999 International Symposium on
Quantitative Feedback Theory and Robust Frequency Domain Methods

Robust Nonlinear Control of a Two Link Robotic Manipulator

Wen-Hua Chen and Donald J. Ballance
Centre for Systems & Control and Department of Mechanical Engineering
University of Glasgow, Glasgow, G12 8QQ, Scotland, UK.
wchen@mech.gla.ac.uk, D.Ballance@mech.gla.ac.uk, Fax: 0141 330 4343

Abstract

Robust nonlinear control of a two link manipulator with large variations of tip load is addressed in this paper. A robust nonlinear control scheme which combines nonlinear Dynamic Inversion Control (DIC) and multivariable Quantitative Feedback Theory (QFT) is developed. In the inner loop Dynamic Inversion Control cancels most of the kinematic nonlinearities of the robot. The outer loop QFT controller is designed to achieve performance specifications against large uncertainties in loads using a multivariable QFT design. It is shown the integration of a nonlinear control technique and QFT combines the strengths of both techniques and eliminates some of the problems associated with using only one of the design methods. The cancellation of the majority of the kinematic nonlinearities of the system ensures that the size of the templates that QFT has to deal with are significantly reduced, thus making the QFT design easier. The introduction of the outer control loop greatly enhances the robustness of the Dynamic Inversion Control against large variations of parameters.

1 Introduction

Dynamic Inversion Control is a widely used design method for exact linearisation of nonlinear systems. It is known as Computed Torque Control in robotics. The basic idea is to cancel nonlinearities and add the desired linear dynamics to the plant. The performance of Dynamic Inversion Control is dependent upon the assumption that the model and the parameters are known exactly. When there are uncertainties in the model and parameters the cancellation of the nonlinearities is not exact and the resultant performance can be very sensitive to variations of parameters.

Since it was developed by Horowitz [3, 4], Quantitative Feedback Theory (QFT) has found many successful applications in control engineering. The underlying principle of QFT is to transform plant uncertainties and closed-loop design specifications into robust stability and then open-loop performance bounds. This way a robust controller can be designed using simple gain-phase loop shaping techniques with the nominal system. The most important feature of QFT is that it is able to tackle design problems concerning complicated uncertain plants. When QFT is applied to design a robust controller for an uncertain nonlinear system, the nonlinear system is represented by a set of Linear Time Invariant (LTI) plants within specified ranges of signal. Then the design can be performed using the standard QFT design technique. Using Schauder's fixed point theorem, Horowitz has shown that if the resultant QFT controller can work for the set of equivalent LTI plants, it also works for the original nonlinear system. For example, Kelemen and Bagchi [5] designed a QFT controller for a flexible arm of a robot to achieve the prescribed frequency-domain tolerances. However when the nonlinear plant has strong nonlinearity and large uncertainties, the equivalent LTI plant set is too large and the resulting plant templates are also large. This, in turn, results in a difficult loop shaping problem and a high gain controller [4]. Snell and Stout [9] show that when the conventional QFT is used to design a control law for the unstable, nonlinear, short-period dynamics of the F-16 aircraft, large templates result from using a set of LTI equivalent models to accurately represent the nonlinear aircraft dynamics over a wide operating envelope. A high gain controller results. By using a variable gain before the QFT design, the size of these templates can be reduced.

Design of a controller for an uncertain nonlinear system to achieve the desired performance specifications is a challenging problem. A promising way to this difficult problem is to integrate existing approaches in nonlinear control and robust control. For aircraft operating over large ranges of angle of attack, Dynamic Inversion Control and the structured singular value μ design method were integrated in [6] to design flight controllers.

The inner loop controller, designed by DIC, is used to linearise the aircraft dynamics. The outer loop controller is then designed by μ synthesis to enhance the robustness. Snell and Stout [8, 10] integrate Dynamic Inversion Control with QFT for flight control system design. It is pointed out that the integration of these two methods strengthens both methods. All of them are based on SISO QFT design technique.

This paper focuses on design of a robust nonlinear controller for a manipulator with large variation of loads. In general, the tip mass or the load of a manipulator changes within a prescribed range in the operating period and a poor performance robustness may result if this is not taken into consideration when designing controllers. This paper develops a methodology which integrates Dynamic Inversion Control and multivariable QFT. A robust nonlinear controller for the manipulator is designed by this methodology to achieve prescribed specifications when the tip load changes within a given range.

2 Two Link Manipulator

The manipulator considered in this paper consists of two links. Each link is independently directly driven by a D.C. motor. The displacement and the velocity of each link are measured by potentiometers and tachometers respectively. The dynamics of the two-link arms are represented by [7]

$$J_1(\theta)\ddot{\theta} + G_1(\theta, \dot{\theta}) = f(t) \tag{1}$$

where θ and F are the displacement of the links and the input torque vectors respectively, given by

$$\theta = \begin{bmatrix} \theta_1 \\ \theta_2 \end{bmatrix}, \qquad f = \begin{bmatrix} f_1 \\ f_2 \end{bmatrix} \tag{2}$$

It is reasonable to ignore the inertia and the induction of the motor in modelling the manipulator [5, 7]. The dynamic model of the voltage controlled D.C. motors is given by [7]

$$u_i = \frac{r_i}{k_{fi}} f_i + k_{di}\dot{\theta}_i, \; i = 1, 2 \tag{3}$$

where k_{fi}, k_{di} and r_i are the motor torque constant, voltage constant and armature resistance respectively and u_i is the motor input voltage. The model of the two link manipulator consisting of the dynamics of the links (1) and the D.C. motor (3) can be written as

$$J(\theta)\ddot{\theta} + G(\theta, \dot{\theta}) = u \tag{4}$$

where

$$u = \begin{bmatrix} u_1 \\ u_2 \end{bmatrix}; J(\theta) = \begin{bmatrix} \frac{r_1}{k_{f1}} & 0 \\ 0 & \frac{r_2}{k_{f2}} \end{bmatrix} J_1(\theta)$$

and

$$G(\theta, \dot{\theta}) = \begin{bmatrix} \frac{r_1}{k_{f1}} & 0 \\ 0 & \frac{r_2}{k_{f2}} \end{bmatrix} G_1(\theta) + \begin{bmatrix} k_{d1}\theta_1 \\ k_{d2}\theta_2 \end{bmatrix}$$

3 Dynamic Inversion Control

Dynamic Inversion Control (DIC) is a technique in which feedback is used to linearise the system to be controlled and to provide a desired response. When all the parameters of the two link manipulator are exactly known, let

$$u(t) = J(\theta)v(t) + G(\theta, \dot{\theta}) \tag{5}$$

where v determines the desired dynamic response. Substituting the DIC (5) into the model of the manipulator (4) yields

$$\ddot{\theta}(t) = v(t) \tag{6}$$

which, in general, is given by

$$v(t) = \ddot{\theta}_d(t) + K_v(\dot{\theta}_d(t) - \dot{\theta}(t)) + K_p(\theta_d(t) - \theta(t)) \tag{7}$$

When $\ddot{\theta}_d(t)$ and $\dot{\theta}_d(t)$ are not available, $v(t)$ becomes

$$v(t) = -K_v\dot{\theta} + K_p(\theta_d(t) - \theta(t)) \tag{8}$$

where K_v and K_p are velocity and position feedback gain matrices, which specify the desired response. The closed-loop transfer function from the reference signal θ_d to the link position is given by

$$\frac{\theta_{di}}{\theta_i} = \frac{K_{pi}}{s^2 + K_{vi}s + K_{pi}}, \; i = 1, 2 \tag{9}$$

4 Problem Formulation

Figure 1 shows a schematic diagram of the combined Dynamic Inversion Control and Quantitative Feedback Theory controller.

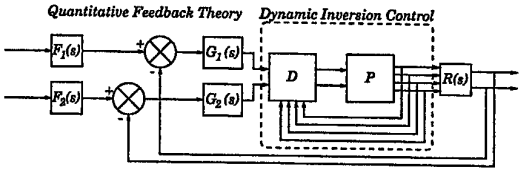

Figure 1: Nonlinear Controller Structure

4.1 Performance Specifications

The task of the controller in robotic manipulators is to track a reference trajectory given by the path planning according to the work task. A tip trajectory is coordinated and divided into a reference to each link. The performance specification for control system design in robotic manipulators is based on the non-interaction rule. That is, each link is designed to track its command signal given by the path planning without coupling from other links. According to the limitation of the motors and the robotic manipulator in our lab, the tracking performance of each link is specified in term of the frequency domain step tracking performance bounds which are given in Figure 2.

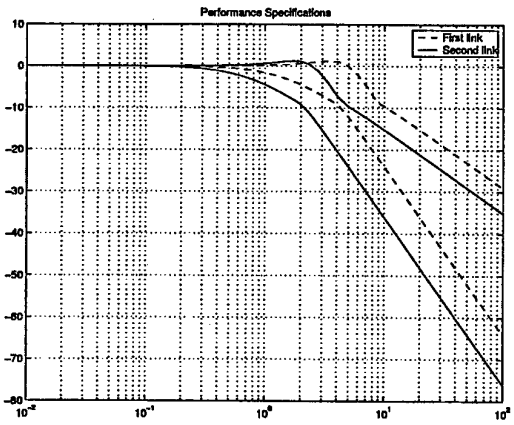

Figure 2: Performance Specification for the Two Links

It includes the responses of a number of first order and second order plants. Following the physical properties of robotic manipulators, the movement of the second link has little effect on the first link. The main coupling between the first and the second links is that the movement of the first link has significant effect on the second link. The requirement for the coupling between each link is to be less than 10%. That is, when the second link's command is zero, the output of the second link should be less than 10% of the first link's command signal.

4.2 Template Generation

After the inner loop controller is designed by DIC, if there is no uncertainty it cancels all kinematic nonlinearies of the robotic manipulator and introduces the desired linear dynamics. The interaction between the two links is eliminated totally. However, due to uncertainties, Dynamic Inversion Control only cancels most of the kinematic nonlinearities. In the design of QFT controllers, the whole robotic manipulator under DIC is considered as the plant. This is an uncertain multivariable nonlinear control problem.

The way to design a controller for a nonlinear plant in QFT is to replace the nonlinear plant with a set of equivalent linear time invariant plants (LTI). It is expected that, due to the introduction of DIC in the inner loop, the size of the templates of the controlled plant are much smaller than that of the original since the most of the nonlinearities have been cancelled. As a result, this greatly reduces the difficulties of the design of QFT controllers [4]. In general, when the templates of an uncertain plant are large, in order to achieve the desired performance response, a high gain control is required.

The set of the equivalent LTI plants are obtained as follows: for each link, first a second order or first order model, which is called as a reference model, is used to produce the desired tracking responses from a step input signal. Then a high gain controller is designed for each link as in Figure 3 such that the real output of the each link accurately tracks the output of the reference model. The equivalent plant can be identified from the input and output data pair of the robot. This is a problem of identifying a rational transfer function from a set of input and output data. Several identification methods are tested. Among them we find Golubev and Horowitz method [2] is the best one. Two criteria are adopted to select the identification methods. One criterion is that after the equivalent transfer function is identified, the previous input data is imposed on both the identified model and the plant to be identified. The outputs from the identified model and the real plant are compared. The other criterion is that for a known linear plant, the frequency response of the identified model is compared with that of the real plant. In both these two aspects, the Golubev and Horowitz method exhibits good performance. The order of the identified plant is determined according to the fitness error. That is, the order of the model is increased until the fitness error is not further reduced significantly.

High gain controllers for links one and two are designed on the basis that the closed loop system is stable and the manipulator's output closely follows the output of the reference model. In this paper, the high gain controller for link one and

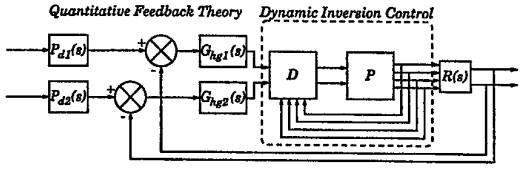

Figure 3: High-gain Controller for Temperate Generation

two are designed as

$$G_{hg1}(s) = \frac{800(s+3)}{s+10}$$

and

$$G_{hg2}(s) = \frac{800(s+1)}{s+10}$$

respectively.

Since the manipulator under DIC is nonlinear when there are uncertainties, it is well known that the magnitude of the input signal affects the dynamics of the plant and therefore the equivalent LTI plants. Step inputs with the magnitude 1.57 rad (180°), 1.0 rad (57.5°) and 0.5 rad (28.8°) are used. The result shows that the amplitude only has a small effect on the LTI plants for this manipulator. This is justified based on the comparison of the frequency responses of the plants under the different amplitudes of the input signals. Hence in this paper the amplitude of the step input for identification is chosen as 1.0 rad.

By changing the reference models such that the whole range of the performance specification is covered, a set of LTI plants for the first link and the second link are found for a specific tip mass. Calculating such a set of LTI plant for typical values of the load within a prescribed range gives the whole set of the LTI plants for the robot under tip mass variation within the specified range. The maximum load is chosen as 0.3 kg in this paper. Three values of the tip mass are chosen: 0.0 kg, 0.1 kg, and 0.3 kg. The procedure for identifying the LTI plants for the transfer function between the first link and the second link is the same as above.

It should be noted the high gain controllers are only designed to identify the equivalent (LTI) plants for the nonlinear plant.

4.3 The Choice of Controller Parameters in DIC

The choice of the controller parameters in Dynamic Inversion Control has a significant effect on the equivalent set of LTI plants and hence the size of the templates. For example when only a very simple dynamic inversion with

$$v(t) = \theta_d(t)$$

is used, the ideal plant after the Dynamic Inversion Control is $1/s^2$. A small perturbation in the parameters of the robot will result in a large variation in the low frequency characteristics of the equivalent linear plant. Consequently it complicates the design of the subsequent QFT design. When the nonlinear Dynamic Inversion Control law is designed such that the desired linear plant is $25/(s^2+10s+25)$, the equivalent templates for the first and second links are given in Figures 4–5 where P_{ij}, $i,j = 1,2$ denote the equivalent transfer function form the jth input to the ith output. Similarly the equivalent template of P_{12} also can be generated by this way. As will be shown in later, it will be used to calculate the equivalent disturbance bound.

When the desired linear dynamics are chosen as $(2.5s+25)/(s^2+10s+25)$, as shown in Figure 6, the size of the equivalent plant templates of the second link can be further reduced.

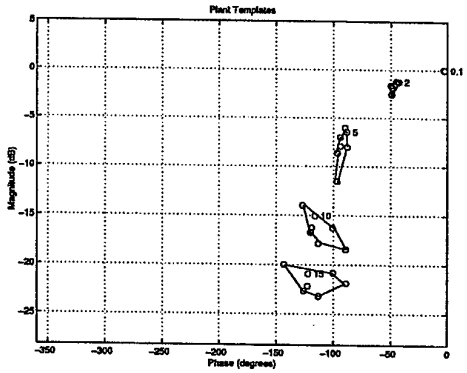

Figure 4: Plant Template P_{11} for First Link after Dynamic Inversion Control

5 Design of Outer Loop QFT Controllers

5.1 First Link

In QFT a multivariable system design problem is divided into several Multiple Input and Single Output (MISO) system design problems. Although a two link manipulator is a multivariable uncertain nonlinear system, analysis indicates that the second link has little influence on the first link. Thus when designing the controller

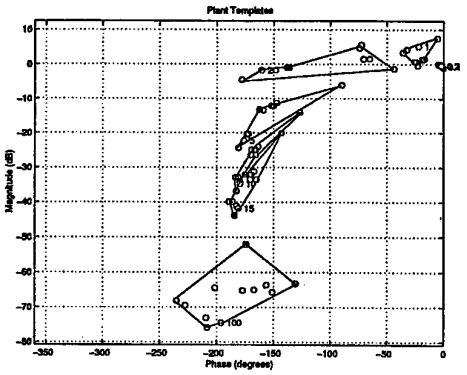

Figure 5: Plant Template P_{22} for Second Link after Dynamic Inversion Control

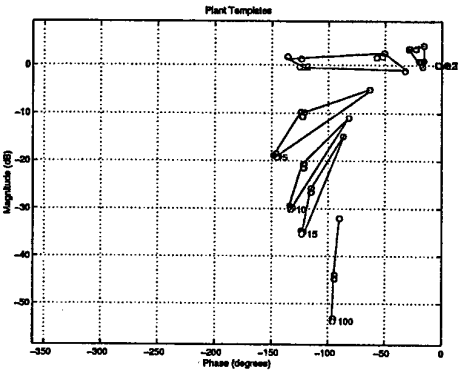

Figure 6: Plant Template for Coupling after Dynamic Inversion Control

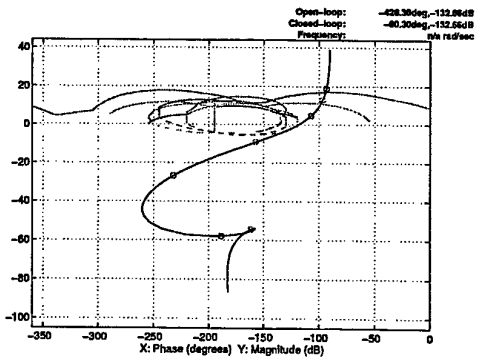

Figure 7: Loop Shaping for the Control of the First Link

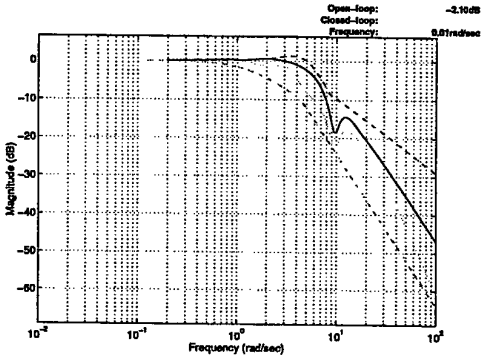

Figure 8: Loop Shaping for the Filter of the First Link

for the first link, the influence of the second link is ignored. According to the performance specification in Section 4.1 and the plant template generated in Section 4.2, following the standard QFT SISO system design procedure, the QFT controller for the first link is given by

$$G_1(s) = \frac{0.883(s^2/9.61^2 + 2 \times 0.0846s/9.61 + 1)}{s(s/6.91 + 1)(s/10.9 + 1)} = \frac{9.557e-3s^2 + 1.555e-2s + 0.8828}{0.015s^3 + 0.2555s^2 + s}$$

In the design of QFT controller G_1, to reduce the steady state tracking error, an integrator is embedded in it. In fact one can find G_1 has a PID-like structure. The loop shaping depicted in Figure 7 shows that all stability and performance QFT bounds are satisfied.

The filter for the first link is designed as

$$F_1(s) = \frac{s^2/1.4^2 + 2 \times 0.61s/1.4 + 1}{0.01s^2 + 0.06s + 1}$$

and the loop shaping result is shown in Figure 8.

5.2 Second Link

Let

$$P = \begin{bmatrix} P_{11} & P_{12} \\ P_{21} & P_{22} \end{bmatrix}$$

denote the equivalent transfer function matrix for the manipulator under DIC. The movement of the first link has significant influence on the second link. This is due to the coupling between these two links. This coupling term can be considered as a disturbance. Following the multivariable QFT design method in [4, 1] and noting $P_{12} = 0$, the disturbance can be calculated by

$$D_{21}(s) = \frac{L_1}{1 + L_1} \frac{F_1}{P_{12}} r_1(s) \qquad (10)$$

where

$$P'_{12} = P_{21}P_{11}^{-1}P_{22}^{-1}$$

and L_1 and r_1 are the nominal loop transmission and the command signal of the first link.

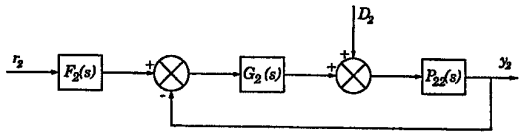

Figure 9: QFT Design Block Diagram for the Second Link

From Figure 9, the output of the second link caused by the disturbance is given by

$$y_{21} = \frac{P_{22}}{1+L_2}D_{21}(s)$$

Therefore, the equivalent disturbance attenuation problem can be written as

$$y_{21}D_{21}^{-1} = \frac{P_{22}}{1+L_2}$$

In this paper t_{21} is required to be less 0.1, that is

$$|t_{21}(j\omega)| = \frac{y_{21}}{r_1} \leq 0.1$$

The disturbance bound can calculated by

$$W_3(\omega) = \min_{P_{21},P_{22},P_{11}} y_{21}D_{21}^{-1}$$

$$= 0.1\left(\frac{L_1 f_1}{1+L_1}\min_{P_{21},P_{22},P_{11}}\frac{P_{11}P_{22}}{P_{21}}\right)^{-1}$$

The disturbance attenuation problem becomes

$$\left|\frac{P_{22}}{1+L_2}\right| \leq W_3(\omega)$$

Hence in the design of the controller G_2 for the second link, in additional to the tracking performance specification, the above disturbance attenuation specification also must be satisfied. Finally, similar to the controller for the first link, the resultant controller G_2 also is a PID controller, given by

$$G = \frac{5.454(s^2/0.3522^2 + 2\times 0.2366s/0.3522 + 1)}{s(s/10.25+1)(s/363.1+1)}$$

$$= \frac{(43.968s^2 + 7.3277s + 5.454)}{s(0.000287s^2 + 0.01s + 1)}$$

] and the prefilter is designed as

$$F_2(s) = \frac{s/9.8+1}{1/2.032^2s^2 + 1.1414/2.032s + 1}$$

The loop shaping results for the controller G_2 and the prefilter F_2 are drawn in Figures 10 and 11.

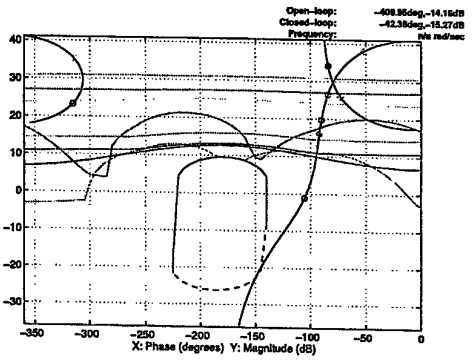

Figure 10: Loop Shaping for the Control of the Second Link

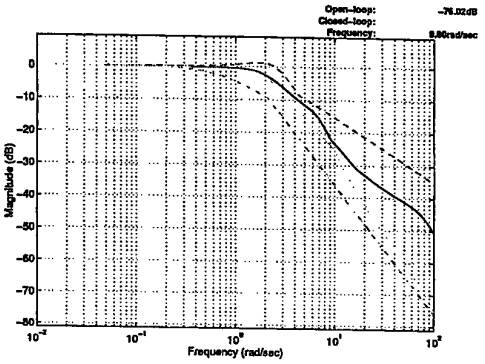

Figure 11: Plant Template for Coupling after Dynamic Inversion Control

6 Simulation Results

6.1 Performance under DIC

In the simulation, first the performance under the Dynamic Inversion Control is investigated. The DIC is designed on the assumption of no tip load. When this control law is applied to the manipulator with no tip mass, Figures 12 and 13 show that a good performance is achieved. In Figure 12, the first link has an unit step command signal and the second link has no command. The opposite input signals are imposed in Figure 13. However when the plant has 0.3 kg load, as shown in Figures 14 and 15, poor performance results. When there is a step reference in the first link and no command on the second link, although the first link still has a good response, the large coupling effect results in a poor transient in the second link. When there is a step reference in the

second link and no command on the first link, a poor step response appears in the second link.

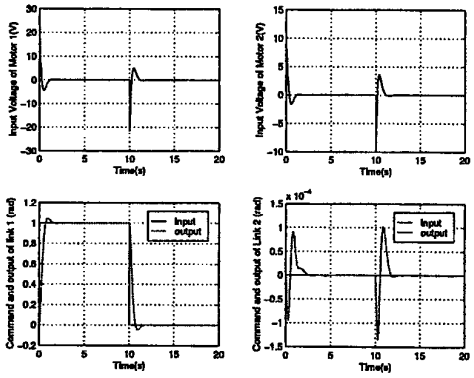

Figure 12: Control and Response for Dynamic Inversion Control under First Link Input: No Load

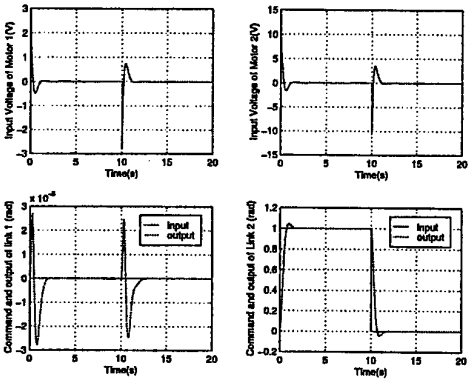

Figure 13: Control and Response for Dynamic Inversion Control under Second Link Input: no load

6.2 Performance using Robust Nonlinear Control

Now the performance of the manipulator under the robust nonlinear controller developed in this paper is investigated. As shown in Figures 16–19, the outer loop QFT controllers greatly enhance the robustness of the DIC. Satisfactory responses under the tip mass varying from 0.0 kg to 0.3 kg are obtained. At the nominal case, no load, the performance of the nonlinear robust controller is almost the same as the DIC. That is, it retains the advantage of the DIC—good tracking performance for each link reference and decoupling ability. When the manipulator has the load 0.3 kg,

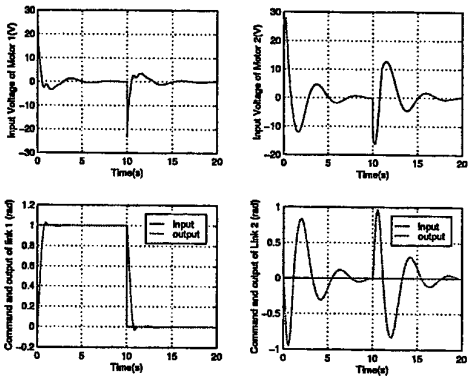

Figure 14: Control and Response for Dynamic Inversion Control under First Link Input: Load 0.3 kg

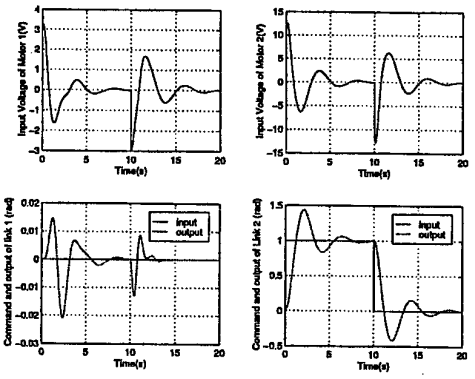

Figure 15: Control and Response for Dynamic Inversion Control under Second Link Input: Load 0.3 kg

Figures 18–19 shows that the coupling effect is greatly reduced and the tracking performance is significantly improved.

6.3 Robustness against Modelling Errors

To further test the robustness of the design nonlinear robust controller, several factors including the friction and the variations of motor resistance are considered. The motor resistance varies with the temperature of the motor. In the following simulation it is supposed that the resistance of both motors changes by 20% of their values. Results for two cases are given in Figures 20 and 21 where Figure 20 is for no tip load and Figure 21 for a tip load of 0.3 kg. Comparison with the response in Figures 17 and 18 respectively shows

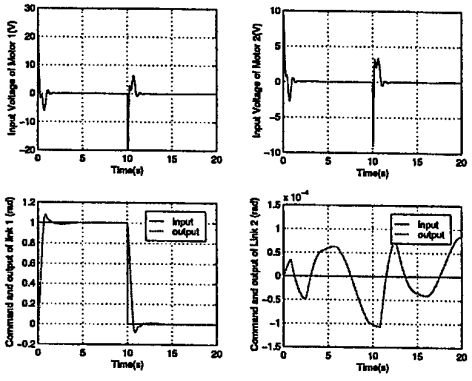

Figure 16: Control and Response for Robust Nonlinear Control under First Link Input: No Load

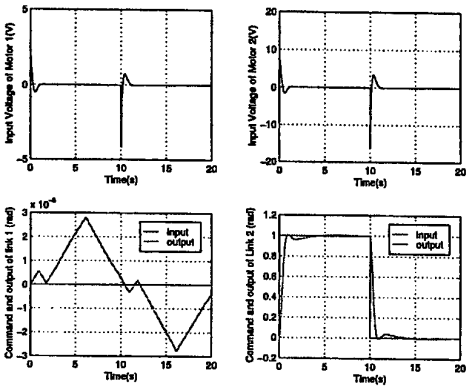

Figure 17: Control and Response for Robust Nonlinear Control under Second Link Input: No Load

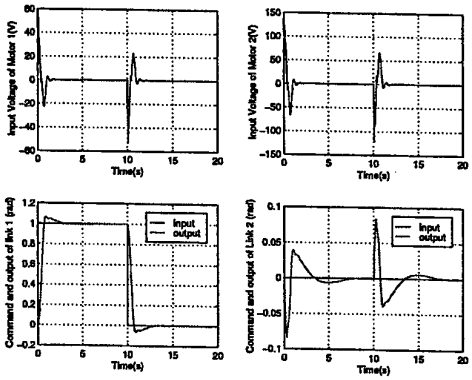

Figure 18: Control and Response for Robust Nonlinear Control under First Link Input: Load 0.3 kg

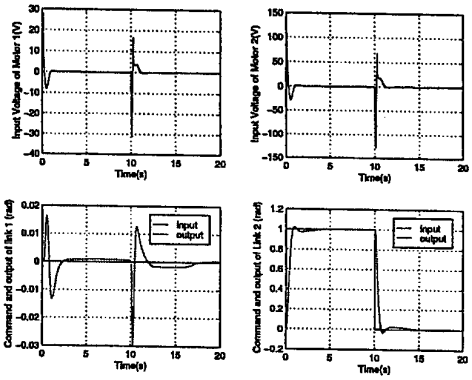

Figure 19: Control and Response for Robust Nonlinear Control for Second Link Input: Load 0.3 kg

little variation in performance.

A similar result is also obtained for friction. The nonlinear robust control exhibits good robustness against uncertainties. One of the reasons is that an integrator is embedded in design of the QFT controllers.

7 Conclusion

Design of a controller for a nonlinear uncertain multivariable system to achieve prescribed specifications is a challenging problem for control engineering. To this end, this paper developed a new methodology which integrates DIC in nonlinear control theory and and QFT in robust control. The design procedure is illustrated by a two link manipulator with large variations of the load. The simulation result shows that the result is encouraging. Further work is continuing to implement the proposed control scheme on the lab manipulator.

References

[1] C. M. Chen, B. C. Wang, and I. M. Horowitz. An alternative method for design of mimo systems with large plant uncertainty. *Control-Theory and Advanced Technology*, 9(4):955–969, 1993.

[2] B. Golubev and I. Horowitz. Plant rational transfer approximation from input-output data. *International Journal of Control*, 36(4):711–723, 1982.

[3] I. M. Horowitz. Optimum loop transfer function in single-loop minimum-phase feedback systems. *Int. J. Control*, 18:97–113, 1973.

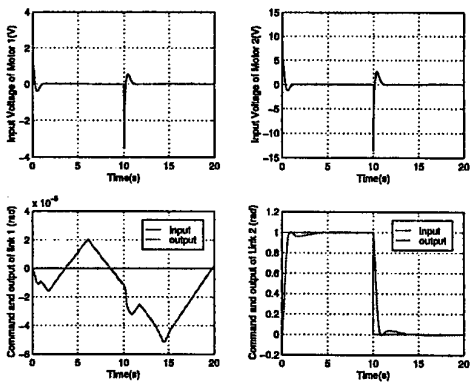

Figure 20: Control and Response for Robust Nonlinear Control with 20% Motor Resistance Variation: No Load

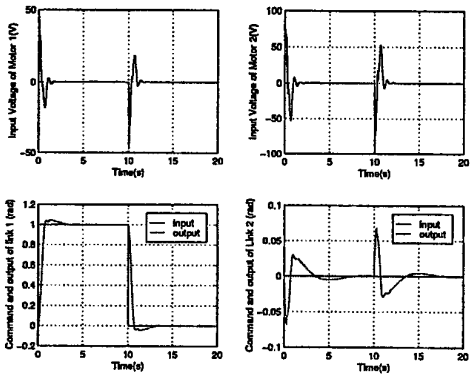

Figure 21: Control and Response for Robust Nonlinear Control with Motor 20% Resistance Variation: Load 0.3 kg

[4] I. M. Horowitz. *Quantitative Feedback Design Theory (QFT)*, volume 1. QFT Publications, 4470 Grinnel Ave., Boulder, Colorado 80303, USA, 1992.

[5] M. Kelemen and A. Bagchi. Modeling and feedback control of a flexible arm of a robot for prescribed frequency-domain tolerances. *Automatica*, 29(4):899–909, 1993.

[6] J. Reiner, G. J. Balas, and W. L. Garrard. Robust dynamic inversion for control of highly maneuverable aircraft. *Journal of Guidance, Control and Dynamics*, 18(1):18–24, 1995.

[7] D. W. Roberts. *Bond Graph Model Based Control of Robotic Manipulators.* Ph.D. Thesis, Glasgow University, Faculty of Engineering, 1993. Supervised by P. J. Gawthrop.

[8] S. A. Snell and P. W. Stout. Full envelope longitudinal flight control law using a nonlinear controller combined with quantitative feedback theory. In *American Society of Mechanical Engineers, Dynamic Systems and Control Division (Publication) DSC*, volume 57-1, pages 265–273, 1995.

[9] S. A. Snell and P. W. Stout. Quantitative feedback theory with a scheduled gain for full envelope longitudinal control. *Journal of Guidance, Control, and Dynamics*, 19(5):1095–1101, 1996.

[10] S. A. Snell and P. W. Stout. Robust longitudinal control design using dynamic inversion and quantitative feedback theory. *Journal of Guidance, Control, and Dynamics*, 20(5):933–940, 1997.

1999 International Symposium on
Quantitative Feedback Theory and Robust Frequency Domain Methods

QFT Control of an Autonomous Path-Tracking Robot

D. Paszkiewicz - Pascault
{didier.pascault@wanadoo.fr}

Institut Universitaire de Technologie d'Amiens
avenue des Facultés
80 025 Amiens, France

SUMMARY

The problem of motion control of a path-tracking autonomous robot is considered in this paper.
While modeling of mobile robots has attracted growing interest recently (see [1], [2] for instance) it has been shown that these nonholonomic systems are neither stabilizable by means of smooth time invariant laws nor linearizable by static feedback laws when Global Control is needed. Complex dynamic state feedback or discontinuous state feedback laws (see [3]) have been proposed and simulated.
However, these methods do not take into account inherent uncertainties due to nonlinearities of actuators, sensor uncertainty or slippery conditions and hence, could not be applied to a real path-tracking robot.
Following the analysis of problems we have encountered when trying to apply the above proposed methods, we present the development of a linearized model, plant templates and tracking bounds from experimental data and theoretical models.
Then, using the method by Chen and Ballance [4], [5] we have designed and tested a QFT Local Controller for this unstable system. The robustness of the overall design has been proved on a real robot.

1. INTRODUCTION

The problem of motion control of mobile robots, either on wheels or tracked, has been studied extensively during last years.
Many challenging applications have been presented in the literature : armored personnel carrier used as an autonomous vehicle [8] or an unmanned underground mining vehicle : a so called 'load, haul and dump truck'. While the 'Pathfinder' for Mars exploration has attracted a lot of interest within the general public there is an enormous, economically motivated need for mobile unmanned robots in agriculture, for search and rescue tasks as well as for general factory and office purposes like cleaning or transportation.

A. BACKGROUND.

Even if different mobile platforms are used in practice, the problem of motion control of mobile robots is a generic one. Obstacle avoidance, self-localization, self-adaptation are common keywords.

The motion of a mobile robot, or more precisely : the motion of a coordinate system R_1 attached to the mobile robot with respect to an inertial coordinate system R, will be described on a *Oxy* plane by :

$$\begin{aligned} dx/dt &= -\, v(t)\ sin(\theta) \\ dy/dt &= \ \ v(t)\ cos(\theta) \\ d\theta/dt &= \ \omega(t) \end{aligned} \qquad (1)$$

where : v is the linear velocity of the robot, here : v is in the direction of y_1 axis of the R_1 coordinate system ;

θ is the heading angle, here with respect to y axis of the R coordinate system

and ω is the angular velocity around the z axis of the R coordinate system.

The triple (x, y, θ) forms the configuration of the robot.

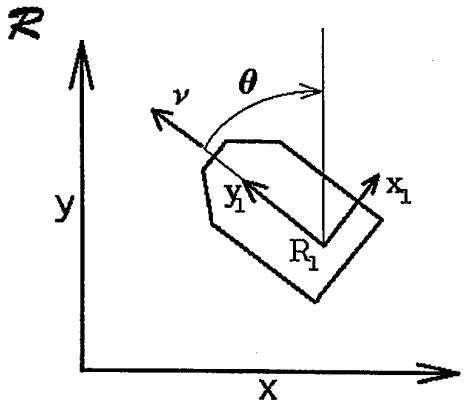

Fig. 1 Coordinate systems for motion control of a mobile robot

B. TWO METHODS OF MOBILE ROBOT CONTROL

Now, two different approaches can be considered for the design of a control law to steer the robot on the plane *Oxy* :

to the Reference Final Configuration. (a)
via Path (or : Line or : Trajectory) tracking (b)

The Method (a) consists in designing a Global control law (i.e. $v(t)$ and $\omega(t)$ as functions of configuration variables (x, y, θ)) if from any initial configuration (x_0, y_0, θ_0) the robot is to move to the Final Configuration : (x_f, y_f, θ_f). (not necessarily to (0,0,0) !).
Even if such control laws have been proposed (for example [3]), it has also been proved (see [1] for some details) that there exists no smooth, time invariant feedback law capable of stabilizing the Final Configuration. Complex discontinuous or time varying control laws result in a very erratic motion of a robot even in computer simulations. No input delay or parameter uncertainty could be introduced in any of these very high gain control laws. All this makes these laws quite difficult to use in practice .

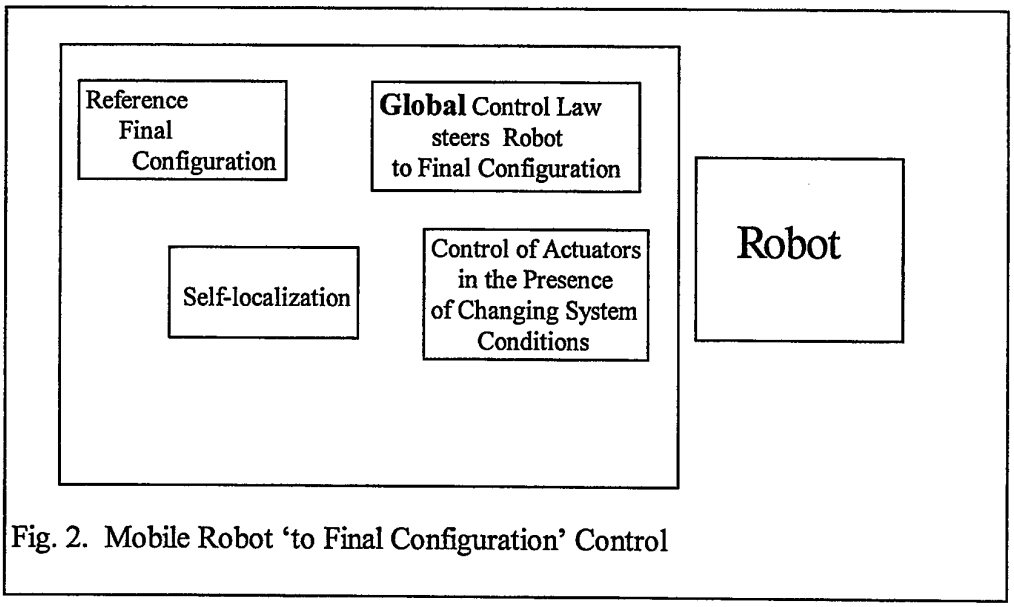

Fig. 2. Mobile Robot 'to Final Configuration' Control

The Method (b) consists in generating a path between an initial configuration and the final one ; or from the actual configuration to the reference trajectory, and subsequently steering the robot along this path. The Local control law which steers the robot is now $v(t)$ and $\omega(t)$ as functions of the robot position and orientation with respect to the path.
The design and analysis of a QFT Local control law for a general mobile platform will be presented in this paper.

C. CHAINED STRUCTURE OF A MOBILE ROBOT CONTROL SYSTEM

The overall structure for these two control systems as well as problems one must solve are the same. Self-localization of the robot will be done using sonar, odometric or laser sensors or cameras (for recent ideas see [9],[10]).

Then, it is also necessary to take into account the particular dynamic models of a robot. Different configurations of wheels (see [1]) will result in different models. For tracked vehicles see Reference [2].
The set of equations describing robot dynamics will be added to the motion equations (1). However, it is possible to make these two sets of equations independent.

Ground traction force, motor characteristics as well some other system parameters may change during the robot operation. This set of equations with previous ones forms the overall model of the system. (for some recent ideas see [11]). But it is once more possible (at least in normal conditions) to organize local control loops to servo $v(t)$ and $\omega(t)$ to reference values given by the motion model (1).

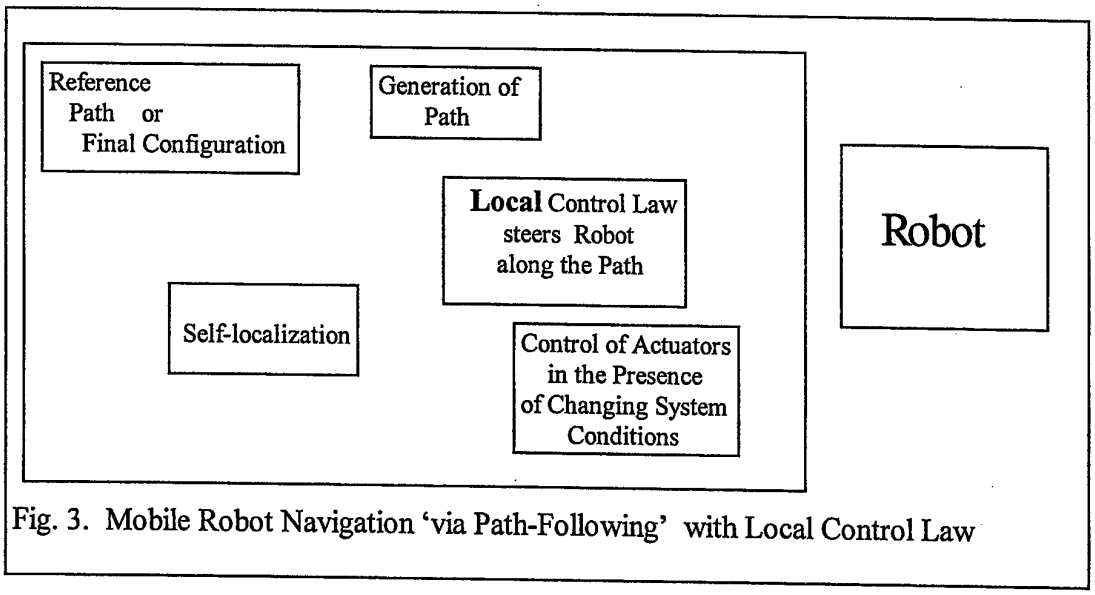

Fig. 3. Mobile Robot Navigation 'via Path-Following' with Local Control Law

C. MODEL OF MOTION FOR PATH TRACKING

As we have seen, one of the important tasks of robot navigating within the Method (b) is to keep the robot on the path.
Directly from the Fig. 4. or from the motion model (1) we write down nonlinear models of motion along the path.

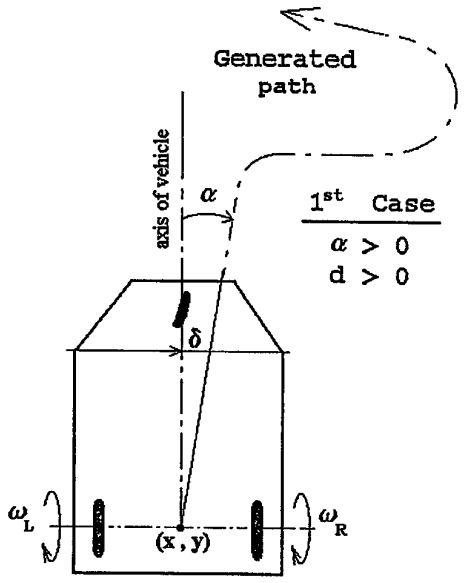

Fig. 4. Path tracking robot

The model of a two wheels robot writes down:

$$d\,\delta / dt = \omega_m(t)\, R\, tan(\alpha)$$
$$d\,\alpha / dt = (R/H)\, \omega(t) \qquad (2)$$

where :

δ	distance from the axis of the robot to the path [in meters]
α	orientation angle between the axis of robot and the path [in radians]
$\omega_m(t)$	instantaneous speed of both wheels (mean value of them) [radians / sec]
$\omega(t)$	rotation speed of the robot around perpendicular axis [radians / sec] proportional to the difference of rotation speeds of the left $\omega_L(t)$ and right $\omega_R(t)$ wheels
R and H	radius of the driving wheels and the width of the robot [meters]

We have tested several platforms : tracked and on wheels. The model of motion along the path (2) presented here for this particular robot is quite straightforward but for most other robots only geometric parameters will differ.

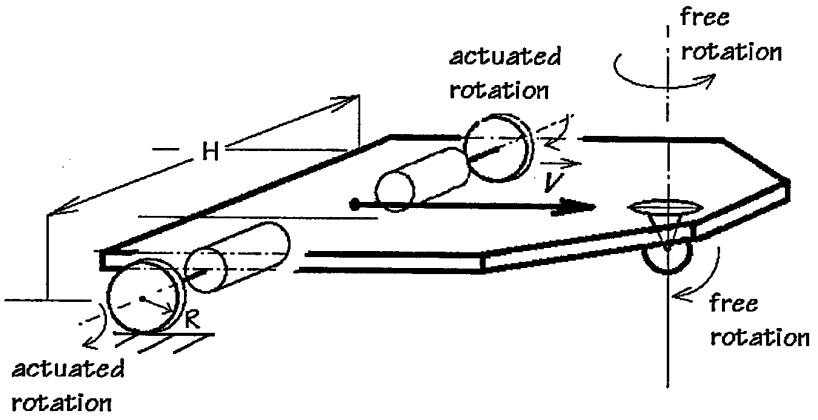

Fig. 5. Two wheels robot platform

However, it is worth noting that model (2) must incorporate orientation angle α as four different operating conditions must be taken into account: 1) $\alpha, \delta > 0$, 2) $\alpha > 0, \delta < 0$, 3) $\alpha, \delta < 0$ and 4) $\alpha < 0$, $\delta > 0$. Developing in Taylor series the nonlinear part of the model equation $tan(\alpha)$ and taking into account the chained structure of the control problem, where changing conditions introduce input delay θ only, we get the transfer function of the system analyzed:

$$G(s) = \delta(s) / \omega(s) = (\omega_m (R^2/H)\,(1 - s(\theta/2))/(s^2(1 + s(\theta/2))) \qquad (3)$$

where : input variable is the difference of rotation speeds $\omega(t) = \omega_L(t) - \omega_R(t)$ and the output of the system is the distance $\delta(t)$ from the axis of the robot to the path.

2. QFT LOCAL CONTROL LAW

From the above presented discussion it is clear that QFT can design robust Local Control Laws for mobile robots and suits well for this task. While geometric parameters R and H are constant, ω_m and θ are not. However, it is relatively easy to understand the bounds of these variables.

From the analysis of operating conditions we got 4 [radians/sec] $< \omega_m <$ 8 [radians/sec] and 0.2 [sec] $< \theta <$ 0.8 [sec]. In our case H= 0.4 [m] and R = 0.1[m].

We can re-write now the transfer function (3) :

$$G(s) = (-k(s-b))/(s^2(s+b)) \quad (4)$$

with :

$$2.5 < b < 10$$
$$0.1 < k < 0.2$$

The control law is applied from computer with sampling period of 0.1 seconds [100 ms].

A. TRACKING SPECIFICATIONS

Tracking bounds : upper and lower have been selected using standard M_p : Maximum peak overshoot, and t_s : settling time analysis.

$$T_{RU}(s) = -0.3 / (s^2 + 1.1\,s + 0.3)$$
$$T_{RL}(s) = -(0.6s + 0.5) / (s^2 + 1.1\,s + 0.5) \quad (5)$$

For Robust Stability margin of a Closed Loop system with L(s) = C(s)G(s)

$$|L(s)/(1+L(s)| < M_p = 0.1 \text{ dB}$$

and settling time of 8 seconds maximum. The maximum peak overshoot condition must be very stringent in this case while settling time is relatively long.

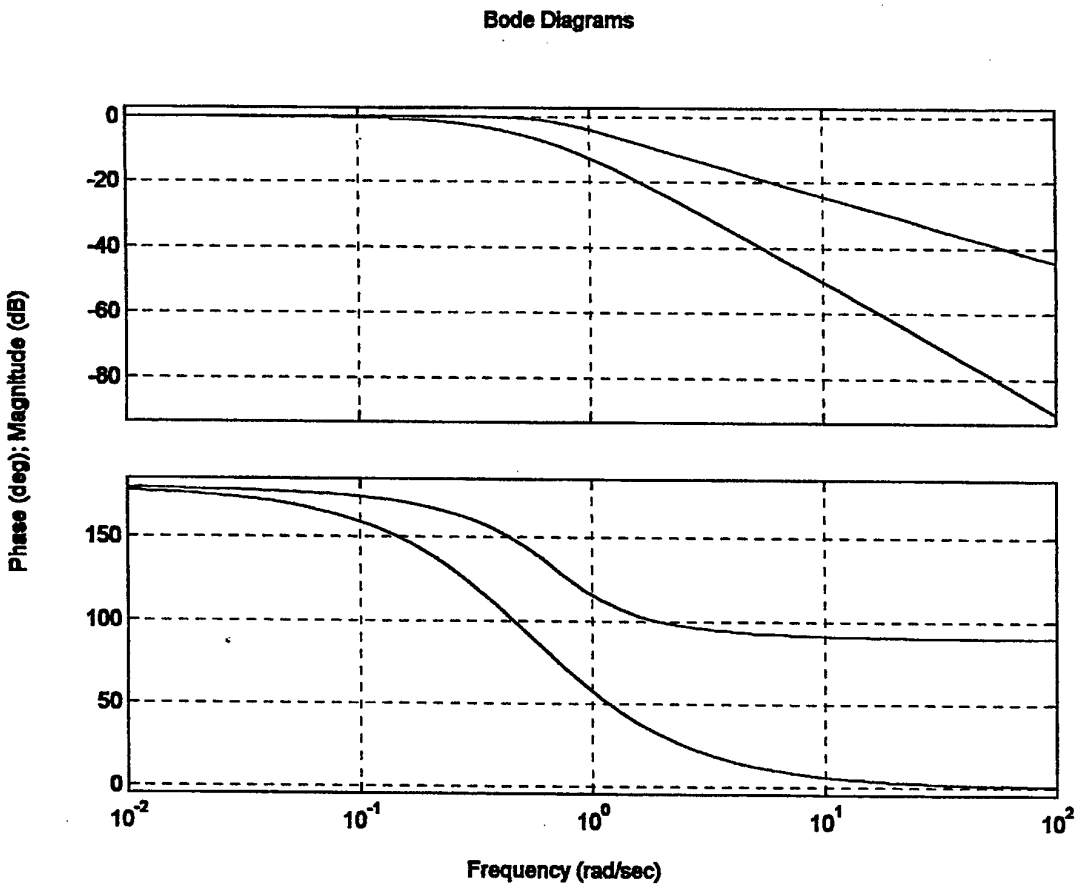

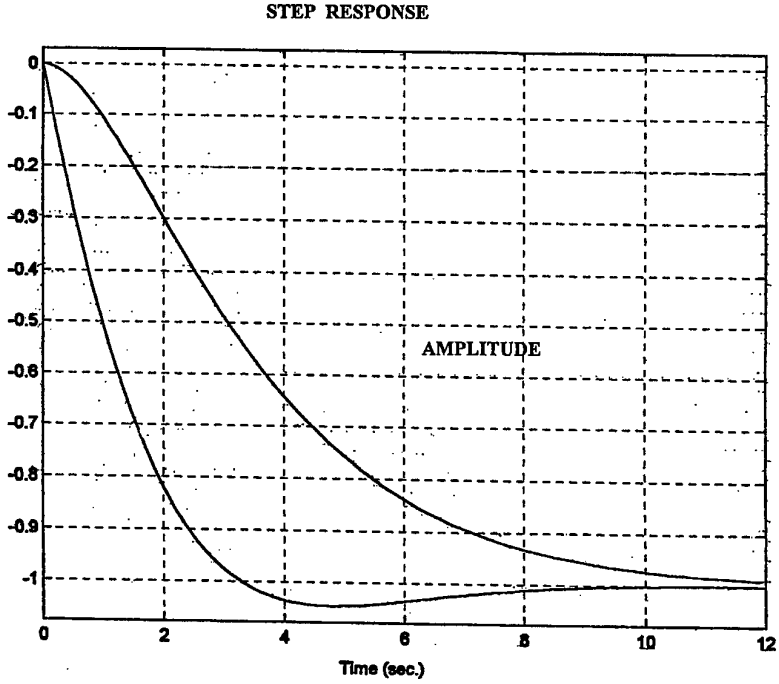

Tracking functions specifications in frequency and time domains

B. NOMINAL PLANT SELECTION AND PLANT TEMPLATES GENERATION

The system we have to stabilize here is non-minimum phase and unstable. According to the systematic procedure in [4] and [5] we select now a nominal $G_0(s)$ plant :

$$G_0(s) = 0.1\,(0.4s + 1)/(s^2(s + 0.1)) \tag{6}$$

The uncertain plant must be enlarged now:

$$G(s) = k\,(0.4s + 1)(1-bs) / (s^2(s + \theta/2)(1+bs)) \tag{7}$$

with $0 < b < 0.4$
$0.1 < k < 0.2$
$0.1 < \theta/2 < 0.4$

Plant templates for this enlarged uncertain plant have been generated using MATLAB package

C. CONTROLLER AND PREFILTER DESIGN

Controller and Prefilter have been designed using MATLAB package with respect to the frequencies : ω = [0.01 0.03 0.1 0.3 1 3 10 100] radians / sec.

The discrete in time version of this controller for 0.1 seconds sampling period gives :

$$Cd[z] = (0.020\,z^2 + 0.0294\,z - 0.0493) / (z^2 - 1.98\,z + 0.9802)$$

C. CONTROLLER VALIDATION AND REAL ROBOT TESTS

Checking on the Nyquist Plot under the resulting Controller gives a stable Closed Loop system.

This controller has been implemented in C on a real time, multitask operating system. Series of tests have been conducted on a platform from Fig. 5. (DC 12 Volts motors, IR light sensitive and sonar (Siemens Bero) sensors.

1) Several reference trajectories :
Straight line
U-Turns radius 2 meters
Circles radius 2 meters
have been driven with no noticeable difference in robot behavior.

2) Tests for $\omega_m = 2*\pi$ radians per second

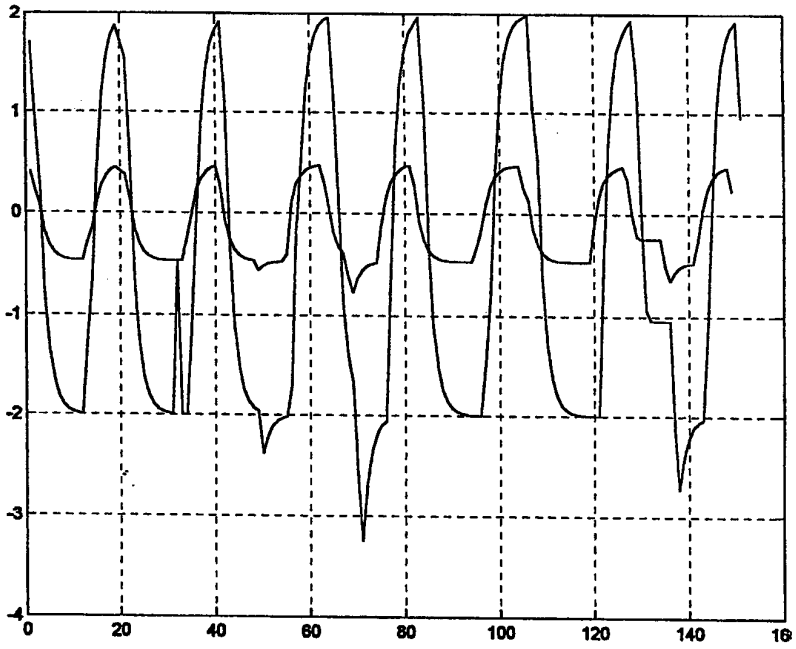

x axis: time in seconds * 0.2, **y axis** : small curve -u in radians per second
big curve δ in millimeters / 10

Tests for $\omega_m = 8$ radians per second

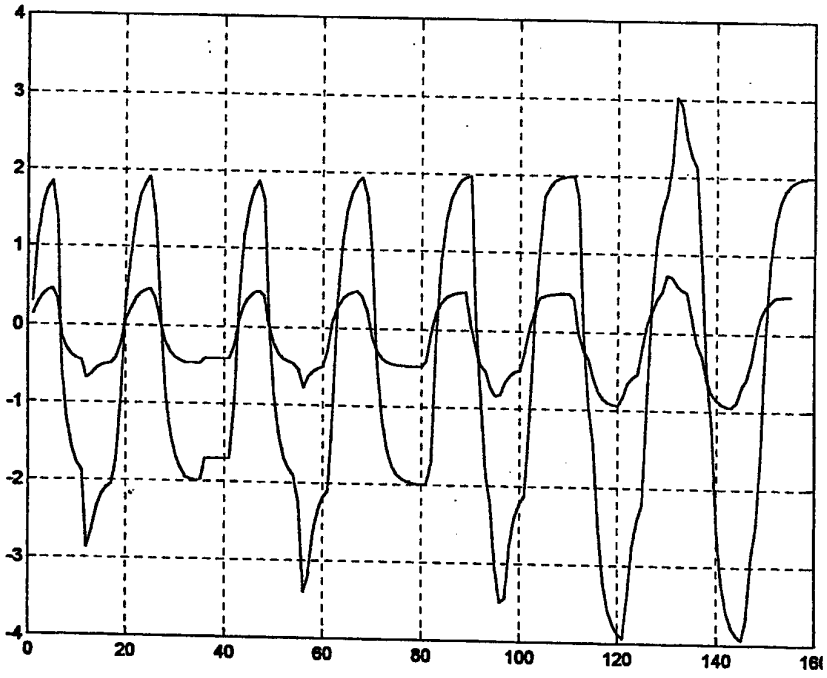

x axis: time in seconds * 0.2, **y axis** : small curve -u in radians per second
big curve δ in millimeters / 10

3. CONCLUSIONS

Modeling and theoretical analysis of dynamic behavior of mobile robots allowed us to implement robust and efficient control loops.
The QFT methods have been used to design a Local Controller for a path tracking robot.
Some novel and rigorous QFT methods of design for a non minimum phase, unstable systems have been successfully applied.

Very good behavior of the overall control system have been demonstrated on a real robot.

4. REFERENCES

[1] B. Thuilot,B. D'Andréa-Novel, and A. Miccaelli, 'Modeling and Feedback Control of Mobile Robots equipped with several Steering Wheels ', *IEEE Trans. Robot. Automat.*, vol 12, no. 3, pp. 375- 390, June 1996.

[2] P.Lu and K-Ch.Lin, 'Nonlinear Control of an Autonomous tracked Vehicle', *Trans. Inst. MC*, vol. 16, no. 4, pp. 214-220, 1994.

[3] J.-B. Pomet, B. Thuilot, G. Bastin and G. Campion, 'A Hybrid Strategy for the Feedback Stabilization of Nonholonomic Mobile Robots ', in *Proc. ICRA 1992*, Nice, France.

[4] W. Chen and D. Ballance, 'QFT Design for Uncertain Nonminimum Phase and Unstable Plants' *in Proc. ACC*, 1998.

[5] W. Chen and D. Ballance, 'On Choice of the Nominal Plant in Quantitative Feedback Theory', *preprint*, 1997.

[6] I. Horowitz and M. Sidi, 'Optimum synthesis of non-minimum phase feedback systems with plant uncertainty', *Int. J. Contr.*, vol. 27, no. 3, pp. 361 - 386, 1978.

[7] C. Canudas de Wit and O.J. Sordalen, 'Exponential Stabilization of Mobile Robots with Nonholonomic Constraints', *IEEE Trans. Automat. Contr.*, vol. 37, no. 11, pp. 1791-1797, November 1992.

[8] G.G. Wang, I. Horowitz, S.H. Wang, and C.W. Chen, 'A Control Design for a Tracked Vehicle with Implicit Nonlinearities Using Quantitative Feedback Theory', in *Proc. IEEE 27th CDC*, pp. 2416 - 2418, 1988.

[9] G. Borghi and V. Caglioti, 'Minimum Uncertainty Explorations in the Self-Localization of Mobile Robots', *IEEE Trans. Robot. Automat.*, vol. 14, no. 6, pp. 902 - 911, December 1998.

[10] L. Jetto, S. Longhi, and G. Venturini, 'Development and Experimental Validation of an Adaptive Extended Kalman Filter for Localization of Mobile Robots', *IEEE Trans. Robot. Automat.*, vol. 15, no. 2, pp. 219 - 229, April 1999.

[11] M.D. Adams, 'Adaptive Motor Control to Aid Mobile Robot Trajectory Execution in the Presence of changing System Parameters', *IEEE Trans. Robot. Automat.*, vol 14, no. 12, pp. 894 - 902, December 1998.

International Symposium on
Quantitative Feedback Theory and Robust Frequency Domain Methods

FREQUENCY RESPONSE IN CONTROL

Isaac Horowitz
Prof. Emeritus, Weizmann Institute of Science, and Univ. of California, Davis

If we are to discuss frequency response in Linear Feedback Control, we must also talk about its rival, State Space. Obviously, one important difference between them is in the Mathematical tools, first discussed. But an overlooked important difference is in the Motivation and Problem Definition. For that, we need the Historical Background that is responsible for the huge differences between the two.

What is the advantage of replacing an nth order LTI differential equation by n first order equations. It seems to me that a much better perspective is s available from the former, especially if it is in factored Transfer Function form., even more so from its graphical frequency response. I read in a Pure Maths book that the state-space form was convenient for Existence theorems. So the State Space passion then seemed to me part of the snobbish Mathematics fad. Our business as Engineers is primarily to build systems, not to prove Existence theorems, although inevitably on the way it is useful to do so. Part of the State Space justification was its greater generality for MIMO and Nonlinear systems. But in a $n \times n$ MIMO of order M, why use M×n equations when n suffice. Also, if a system is LTI, I want to exploit this and expose it in its most transparent form, rather than its most opaque form. The Operational tool, first revealed and marvelously used by Oliver Heaviside in the late 19th Century, is a gift from Heaven. Why obscure it, demean it, ignore its tremendous insights, and try to shame one away from it. Finally, in Feedback Control, State Space has led to concentration on non-problems [1] such as controllability, and thereby, the miseducation of several generations of Engineers, which persists to this day. But to explain this I must turn to...

HISTORICAL BACKGROUND

The earliest systematic research in Feedback Theory was in Feedback Amplifiers. by H. W. Bode [2] of Bell Labs. It is important to contrast his work, with that of the MIT Servo Lab. on Radar design during World War 2. Bode was motivated by the Long Distance Telephone line, where hundreds of Amplifiers (Repeaters) are needed along the line. One wants to maximize the number of channels on the line: Let B_{min} be the minimum Bandwidth needed per channel. The tolerance U_c over B_{min} must be very small, since it is multiplied by the large number of repeater stations. Hence feedback must be used. The maximum "Plant" Uncertainty U_p is ascertained; minimum Loop Gain needed over B_{min}, is (U_p/U_c). The objective is to maximize the available Repeater Bandwidth B_t, because the maximum number of useable channels is B_t/B_{min}.

Bode showed that the ultimate constraint on B_t, is due to the Plant high-frequency parasitics. (Fig. 1 - The High - ω Asymptote, beyond which the Plant model is not trustworthy).

1) What is the best one can do for a given high-ω asymptote?
2) Given an unlimited supply of basic amplifier elements, with its high-frequency parasitics, what is the optimum layout and number of elements to use in a repeater, to maximize its high-w asymptote?

Bode solved both problems. His result became known as the "ideal Bode Cut-Off", although he emphasized it was only a reasonable, practical compromise. In the process, Bode created a

scientific theory of feedback, which is still unknown, 60 years later, to the vast majority of modern Feedback Control researchers. interesting Bode was a Mathematician, not an Engineer, but he never sacrificed practicality and fundamental constraints, for the sake of an elegant Mathematical publication.

It is worth noting that it was Bode who invented the Sensitivity function, $S = \Delta T(s)/T(s)/\Delta P(s)/P(s)$, with P(s), T(s) the open-loop Plant and closed-loop System transfer functions. BUT he used the Loop Transmission L for detailed design. There are very good reasons why S is a very poor tool for transparent, practical design. One is shown in (Fig. 2: The Sensitivity Function is very INSENSITIVE to Sensor Noise Effect), which is a major Cost of Feedback.

At about the same time, Feedback Control (Servo Theory) was developed at the MIT Servo Lab, primarily for the Radar problem. Its model has only 1^oF (Fig. 3 - One-degree-of-freedom) with S =1-T. Hence, one must compromise between the system response function (T) and its sensitivity (S) to Plant Uncertainty. In fact, in any practical case (Fig. 4), there is an important ω-range in which the Sensitivity of a feedback implementation of a desired T(s), is worse (i.e. $|S| > 1$) than open-loop design. In Fig. 4, $T(s) = (\omega_n^2)/[s^2+2(\zeta\omega_n)s+\omega_n^2]$. For ζ=1, .707, .5, $|S| > 1$ for w/Bandwidth > 1.1, 1.0, .791. The MIT CLASSICAL design theory was a reasonable compromise, because in those "classical olden days", the customer demanded functioning radar systems, not mathematical research papers of dubious practical relevancy.

PHASE 2 OF FEEDBACK CONTROL RESEARCH 1946 - 1955

It is unfortunate that the MIT Servo people did not spell out the above structural conflict.. It is hardly believable but Academic Feedback Control research persisted with this wretched one degree of freedom constraint, despite its non-existence for the vast majority of practical SISO feedback control systems. **The primary OBJECTIVE of Academic research during this period, was to "obtain a desired system input-output relation, under the constraint of an imbedded fixed (not uncertain) Plant".** No wonder that it became a very arid subject, despite temporary relief by topics such as Root-Locus, Digital Control, Weiner filter theory, MIMO systems. **The genuine Feedback problem, that of "Coping with Plant Uncertainty" was totally overlooked.**

The ADAPTIVE Phase. In those days, in Flight Control at WPAFB, it seems that "Scheduling" was used for Jet A/C, to cope with the large Plant parameter changes due to Mach and Altitude changes. The latter two variables are measured on-line, look-up tables give the parameter changes, and the compensations automatically accordingly adjusted. . There was a crash, attributed to the complexity of the Scheduling system, which apparently tried to compensate at every point in the flight control equations where Mach and Altitude appeared. Lt. Gregory of the Flight Control Lab. at WPAFB suggested (~1955), that an ADAPTIVE system be used instead, based on the Plant output, thus launching the Adaptive Era, with pilgrimages to the generous Air Force Money Fountain.

Lt. Gregory was in fact suggesting traditional Feedback Control to cope with the Plant Sensitivity problem. Academia should therefore have responded by examining the long-neglected Sensitivity problem, and would have been led to need for two-degree-of-freedom (2^oF) design. In fact, there then appeared John Truxal's "Control System Synthesis", which became very popular. It had a chapter on "achieving simultaneously a desired nominal system

transfer function, and a desired nominal disturbance attenuation function", so used a 2°F structure. He did not consider Plant Uncertainty and Cost of Feedback. Unfortunately, he used the current s-plane pole-zero fad, giving a very opaque procedure (but still more general than the later state-space eigenvalue fad). Frequency Response solves the more general problem of "Disturbance Attenuation under Plant Uncertainty" much easier and with much greater transparency. But he was the first that had at least the important point of 2°F synthesis, which was not picked up at all by himself or the Adaptive workers, as a means of coping with Plant Uncertainty.

Instead, Adaptive researchers turned to NONLINEAR FEEDBACK to deal with Plant Uncertainty. Ordinary, i.e. LTI feedback was not admitted into the ADAPTIVE CLUB. At best, it was called PASSIVE ADAPTIVE. Some felt the need to justify the abandonment of linear feedback. The following by Kalman was typical: ".... It is generally taken for granted that the dynamic characteristics of the process will change only slightly under any operating conditions encountered during the lifetime of the control system. Such slight changes are foreseen and are usually counteracted by using feedback. Should the changes become large, the control equipment as originally designed may to meet performance specifications...."

Of course, the Adaptive (Nonlinear) work of that period led to hardly any practical or theoretical value. The most successful was the Oscillating Adaptive system of Minneapolis Honeywell (M-H), which had some success on the X15 problem (1000 to 1 uncertainty), because it is in effect a quasilinear technique. M-H never did produce a systematic design theory, and dropped it after a crash in which a veteran X-15 test pilot was killed. I began QFT at about this time. Its main ingredients were and remain that Feedback in Control is mandatory ONLY DUE TO PLANT UNCERTAINTY, a minimum of 2°F are needed, and most important, QUANTITATIVE DESIGN IS ESSENTIAL In order to vividly disprove Kalman and the Adaptive Community, I applied the first somewhat primitive QFT technique to the 1000 to 1 X15 problem, giving in less than a week, a simple satisfactory design with reasonable compensator bandwidth. Typically, Academia ignored this work, but it did earn me the enmity of the Air Force, which persists by some of them to this day.. Ironically, later, my students and I considered the Oscillating Adaptive System as a bridge between Linear and Nonlinear Feedback, and we developed systematic QFT design theories for several important versions. In fact, I had challenged Adaptive enthusiasts [3], o provide adaptive problems which could not be solved by LINEAR feedback, but which they could solve by their Adaptive design. There was no response to this challenge. We later answered our challenge, for a class of nonminimum-phase plants, by means of an Oscillating design [4].

STATE SPACE: PHASE 1. LYAPUNOV STABILITY, OPTIMAL CONTROL

In any case, this Adaptive phase was a temporary fad, before the great State Space deluge of Modern Control theory which persists to this day. I was present at what I consider its birth, at the First Joint Conference of Electrical, Mechanical and Chemical Control Engineers in Dallas, in 1959, in which Kalman and I were Plenary speakers. I gave the first paper on Quantitative Feedback theory that included a significant Plant Uncertainty design. Kalman introduced State Space via Lyapunov Stability theory. We all know which won out. The latter provided many Doctorates for the next few years, and then Optimal Control theory via State Space dominated Academic Control. Of course, it was primarily Mathematics, not Control, because Uncertainty was not considered, nor the sensitivity of the optimal control law to small Plant uncertainty. Even a giant like Pontryagin had this popular naive faith that the mere use of a feedback structure automatically gave an implementation less sensitive to Plant uncertainty, than an open-loop implementation. Some years later, it was proven that both

implementations have identical first order sensitivity.

The, State Space notation became very popular, and Kalman's Controllability- Observability became holy canons, despite the impracticality of the former (uncontrollable outputs pass the Kalman test [5, part V]). The Control Community was so sick of Classical Control, so voraciously hungry for something new, for new Course & research opportunities, that there was uncritical examination of the new merchandise. **But aside from Lyapunov stability and Optimal Control, the central problem in Feedback Control did not change at all.** It remained the realization of a desired input-output relation under the constraint of a fixed, perfectly known Plant. But instead of describing this desired input-output relation in frequency response or pole-zero terms, "eigenvalues" were used, which of course ignores the important role of system zeros. The heart of the problem, PLANT UNCERTAINTY, continued to be ignored.

I persisted in development of QFT, but was isolated. Frequency Response as a tool was derided. I felt that either I was blind or the rest of the gang was blind, so deliberately taught State Space and Optimal Control three times, but concluded that these were highly impractical tools for the Feedback Control problem of "quantitative coping with Plant Uncertainty".

The next development was LINEAR QUADRATIC REGULATOR (LQR) theory, which led to constant gain (infinite bandwidth) compensators, one for each state. Eventually, it was realized, even by its enthusiasts, that such implementation is difficult (it is really impossible) and expensive. This led to Observer theory, and its various offshoots LTR etc. Also, the need for sensor per state led to Model Truncation followed by eventual Model "Restoration". Hundreds of Theses subjects thereby became available to Academia starving for theses topics. But all this time, the heart of the feedback problem, Plant Uncertainty, remained ignored. Several generations of students were thus mis-educated. **How ironic that QFT, whose motivation, objectives and results, are totally different from Classical feedback control theory, should be denigrated as Classical, because it uses the same mathematical TOOL as Classical theory. Whereas, Modern Feedback Control theory, whose objectives and results, are POORER versions of Classical theory, should be honored as up-to-date, enlightened MODERN because it used the much more impractical, but so-called Modern tool of State-Space.**

Progress since 1980's

It was not until the 1980s that Modern Control theory considered Plant Uncertainty, at first with Singular Value theory and later H_∞ and its variations. . These seem to ignore the Cost of Feedback, because they often emerge with infinite bandwidth compensators. This does not bother Academia in the least. But, It is my duty to expose some resulting travesties.

The first is depicted in Fig. 5, with its four infinite bandwidth (75 dB gain compensators, and poorly damped step responses, of an H_∞ / Structured Singular Value design. This paper, without any simulation results, was published in IEEE-AC Trans. and received its Best Practical Paper Award. Prof. Oded Yaniv made the simulations and the indicated QFT design in Fig. 5, using only two practical compensators of about 10-rps cut-off, and much superior simulation results. His paper was rejected by the same Journal.

In the second example the same model was used, but Prof. Limebeer of Imperial College, made it much more difficult by including Plant Uncertainty and imposing severe

QUANTITATIVE performance specs.. He issued it as a Design Challenge Problem.
The responses (all H_∞ type) were far from satisfying the specs. We found that the best of them was unstable when the Plant time delay of one minute was correctly modelled, rather than approximated by a rational function. At the Conference, the Session Chairman refused to allow Prof. Yaniv to participate, stating that QFT was not a legitimate Synthesis technique. No one supported Prof. Yaniv. In any case, to the best of my knowledge, **the only design which has satisfied the stringent specs., is the one I did with QFT,** which is detailed in [1, Sec. 14.5.1) .

COMMENTS ON QFT

The balance of this address is devoted to QFT. First, I want to correct a serious error sometimes encountered that the QFT time-varying, nonlinear technique is "without mathematical rigor". There are, in fact, two such techniques and both are mathematically rigorous. The confusion may be due to QFT use of LTI Plant Sets which are EQUIVALENT to the Nonlinear Plant sets, only with respect to the Desired Output sets. QFT is proud of this distinction. That is precisely why it is a sound Engineering technique. It would be very wasteful ii a flight control problem, to have a LTI equivalent valid for high-fi audio inputs. While there have been gratifying increase in QFT applications, It seems that in the last 10 years there have been hardly any QFT breakthroughs into new areas. So I would like to draw attention to QFT topics on which promising initial work has been done, and which are ripe for significant follow-up.

NONDIAGONAL PREFILTERS and LOOP COMPENSATORS

There are so far two approaches to nondiagonal loop compensators. One uses a sort of global, matrix approach. It has been briefly noted in [1;14.3.7] ; but Boje and Nwokah appear to be the first who have seriously worked on this approach. [9, 10]. The second [6] approach deals directly with the individual matrix elements. Let H be a nondiagonal loop matrix in the return path, M a prefilter matrix. (Of course, any canonic 2^oF structure can be used).. In QFT language, t11, t21 for a 3 by 3 system, are: (li=giqii, vij=1/qij):

$$(1+l_1)\, t_{11} = q_{11}(m_{11}) - q_{11}\,[(v_{12}+h_{12})t_{21} + (v_{13}+h_{13})t_{31}]$$
$$(1+l_2)\, t_{21} = q_{22}(m_{21}) - q_{22}[(v_{21}+h_{21})t_{11} + ((v_{23}+h_{23})t_{31}]$$

Thus each "equivalent disturbance v_{ij} term" for $i \neq j$, has its off-diagonal h_{ij}, for partial cancellation if a h_{ij} can be found for reduction of the set $\{v_{ij}+h_{ij}\}$. The advantage is that unlike the Matrix method, such h_{ij} is chosen independently of the others.

SINGULAR COMPENSATION FOR SISO & MIMO SYSTEMS

The QFT arsenal was enlarged when confronted with the X29 2x2 flight control pitch-acceleration problem, over a range of Mach-Altitude flight conditions. The Plant determinant had a right half-plane dipole at each flight condition. Both Grumman and Minneapolis Honeywell correctly found that even a separate design for each case gave terrible stability margins -- at best a fraction of a degree and dB. This was at the heyday of Modern Singular value theory, which M-H touted for solving the problem, and received a lucrative Government Contract for this purpose. This theory was of no use whatsoever for this problem, so they changed the problem into one of pitch-flight path outputs. This new problem is easily handled.

However, we found a Singular Compensation technique, applied it in a Master thesis, in which use of a singular MIMO loop compensator G (det(G) identically zero), permits a single design for all flight conditions, to give excellent stability margins over the entire Plant

uncertainty range. Scheduling of the prefilter outside the loops gave individual desired t_{ij}.

Of greater interest, we found a method to apply this technique to SISO Plants with highly uncertain right half-plane poles and zeros, even dipoles, by converting the SISO into a MIMO for its stability property. This is done by two or more independent samplings of the SISO output, with independent compensations of each such sampling. The Singular Compensator technique is then applied to this equivalent MIMO system, with similar results of excellent stability margins over the entire Plant range. However, the trouble is that the high sensitivity which such a system normally has to the Uncertain Plant, is now transferred to the much less uncertain compensation, so the latter must have very small Uncertainty for the technique to work. I suggest that it is worthwhile to investigate further such Linear Time Varying Systems, which form a bridge between Linear and Nonlinear systems.

The General Internal Variable MIMO Feedback System

Assume a MIMO Plant with an arbitrary, finite number of internal variables that can be sensed and used for feedback purposes. We know from our work in SISO systems, that such internal variables can be used to tremendously reduce the Cost of Feedback. And we have done enough specific examples that this is also so, for MIMO systems. Prof. Yaniv developed as his Doctorate, a systematic QFT technique for this purpose, for the special Cascade MIMO structure. But there is important research just waiting to be done for the general case.

We have shown [6] that the general n×n internal variable MIMO can be transformed into n equivalent general internal variable SISO feedback structures, plus n^2 prefilters. Just as in the simpler MIMO output feedback case, "equivalent" disturbances represent the interchannel effect. The solution of this collection of SISO problems is guaranteed to work for the original general MIMO problem. So it is simply a matter of developing a QFT synthesis technique for the general SISO internal variable feedback problem. I believe that the work previously done for several such special structures, points the way to the solution of the general SISO problem. This hint should suffice for the ambitious researcher.

Parallel Plant Feedback and Load Sharing

Many years ago I was privileged to hear a talk by H. W. Bode [2b], in which he remarked that it took him only a few years to find the fundamental limitations and cost-benefit relations for single-loop feedback, and then he spent many years unsuccessfully trying to "beat the game", which was done finally by a colleague, Brockway MacMillan. I rushed to see his Reference, and realized it involved an important structural change -- a FAMILY of Plants, in which there could be feedback within the family, as if protecting its members from the outside world. Indeed, for certain applications, instead of 120^o lag giving a |L| decrease rate of 8 dB/octave, one could have, for n parallel plants, effectively 8n dB/octave decrease. This is a fascinating idea. It was explained in my 1963 book in detail, only briefly in [1, p. 456].

But there has been no follow-up at all by the QFT research community. There is lacking a detailed design procedure for exploiting this idea, its extension to multiple-loop systems etc, etc. This class of Plants is related to the Load Sharing ideas and work of Prof. Eduard Eitelberg, whose recent new book [7], is a goldmine of important research ideas, for this very large and very important class of feedback systems, which is virtually virgin territory to QFT.

Plant Modification Systems

This, too, is a very important problem class, wherein feedback to internal variables is allowed,

thereby affecting the signal levels within the Plant - hence the term Plant Modification. We know that use of internal sensors can greatly reduce the Cost of Feedback [1]. But the reduction can be very much greater if feedback is used to internal variables, as well as from internal variables. It is limited only by the resulting increase in the internal variable signal level, which must therefore be constrained. This work was pioneered by Dr. B. C. Wang [8], who remains the pioneer and almost sole researcher in a most important area. For it includes Economic systems, Organizational systems, all systems involving living creatures. There are so many areas to explore, nonlinear plants, MIMO systems. I urge Dr. Wang be given some friendly competition.

REFERENCES

1. I. Horowitz, Quantitative Feedback Design Theory, QFT Pubs., 660 S. Monaco Pkwy, Denver, CO 80224; O132012@aol.com; p.26.
2. a) H. W. Bode, Network Analysis and Feedback Amplifier Design, Van Nostrand, 1945; b) Feedback -- History of an Idea, Proc. Symp. Active Networks & Feedback Systems, Microwave Research Institute 1961, pp. 1-21.
3. I. Horowitz, Plant adaptive systems vs ordinary feedback systems, Trans. IRE, AC-7, Jan. 1962, 48-56.
4. O. Yaniv, I. Horowitz, S. Oldak, Disturbance Attenuation in single-loop dithered adaptive systems. Int. J. Control, 1988, 48, 179-192.
5. I. Horowitz, U. Shaked, Superiority of transfer function over state-variable methods in LTI feedback system design, IEEE trans. AC-20, 1975, 84-97.
6. I. Horowitz, Uncertain MIMO systems with internal variable feedback, Int. J. Control, 36 1982, 989-1010.
7. E. Eitelberg, Load Sharing Control, NOYB Press, 58 Baines Rd., Durban 4001, S. Africa, 1999.
8. B.C. Wang, I. Horowitz, Quantitative synthesis of a 5-loop plant modification control system, Int. J. Control, 47, 1988, 1649-64; Quantitative synthesis of uncertain cascad systems with plant modification, ibid, 30, 1979, 837-62; R. Chu, B. C. Wang, J. L. Lai, 1992, Proc. First QFT Symp., 334-54.
9. E. Boje, O. Nwokah, Non-diagonal controllers in MIMO quantitative feedback design, submitted.
10. Ibid, Quantitative feedback design using forward path decoupling, submitted.